

*In-situ* Health Monitoring for Wind Turbine Blade Using  
Acoustic Wireless Sensor Networks at Low Sampling  
Rates

---

A thesis submitted to Newcastle University in candidature for the degree of  
Doctor of Philosophy.

**Omar Mabrok Bouzid**



School of Electrical and Electronic Engineering  
Newcastle University

September 2013

**CERTIFICATE OF ORIGINALITY**

I declare that this thesis is my own work and it has not been previously submitted by me or by anyone else, for a degree or diploma at any educational institute, School or University. To the best of my knowledge, this thesis does not contain any previously published work, except where another person's work used has been cited and included in the list of references.

..... (Signed)

..... (Candidate)

## Abstract

The development of *in-situ* structural health monitoring (SHM) techniques represents a challenge for offshore wind turbines (OWTs) in order to reduce the cost of the operation and maintenance (O&M) of safety-critical components and systems. This thesis proposes an *in-situ* wireless SHM system based on acoustic emission (AE) techniques. The proposed wireless system of AE sensor networks is not without its own challenges amongst which are requirements of high sampling rates, limitations in the communication bandwidth, memory space, and power resources. This work is part of the HEMOW-FP7 Project, ‘The Health Monitoring of Offshore Wind Farms’.

The present study investigates solutions relevant to the abovementioned challenges. Two related topics have been considered: to implement a novel *in-situ* wireless SHM technique for wind turbine blades (WTBs); and to develop an appropriate signal processing algorithm to detect, localise, and classify different AE events. The major contributions of this study can be summarised as follows: 1) investigating the possibility of employing low sampling rates lower than the Nyquist rate in the data acquisition operation and content-based feature (envelope and time-frequency data analysis) for data analysis; 2) proposing techniques to overcome drawbacks associated with lowering sampling rates, such as information loss and low spatial resolution; 3) showing that the time-frequency domain is an effective domain for analysing the aliased signals, and an envelope-based wavelet transform cross-correlation algorithm, developed in the course of this study, can enhance the estimation accuracy of wireless acoustic source localisation; 4) investigating the implementation of a novel *in-situ* wireless SHM technique with field deployment on the WTB structure, and developing a constraint model and approaches for localisation of AE sources and environmental monitoring respectively.

Finally, the system has been experimentally evaluated with the consideration of the localisation and classification of different AE events as well as changes of environmental conditions. The study concludes that the *in-situ* wireless SHM platform developed in the course of this research represents a promising technique for reliable SHM for OWTBs in which solutions for major challenges, e.g., employing low sampling rates lower than the Nyquist rate in the acquisition operation and resource constraints of WSNs in terms of communication bandwidth and memory space are presented.

# Acknowledgements

In the Name of Allah, the most Gracious, the most Merciful, say: ‘Truly, my prayer and my service of sacrifice, my life and my death, are (all) for Allah, the Cherisher of the worlds’ (Qur’an, Al-An`am 6:162). First and foremost, all praise and deep thanks are due to Allah (the creator), who helped and guided me through the challenges of my study. Glory be to Allah who has given me the strength, patience and knowledge to continue and finish my PhD journey.

This thesis represents the closing stages of a four-year journey to achieve my PhD degree. During this journey, I have been accompanied and supported by many people who deserve to be acknowledged.

From the depths of my heart, I would like to express my sincere gratitude to my supervisor, Professor Gui Yun Tian, of Sensor Technologies, for his guidance, intellectual advice and patience throughout the study process. I owe him heartfelt thanks for his time and effort that assisted me throughout my study. My humble acknowledgments and gratitude go also to my co-supervisor, Mr Jeffrey Neasham for his guidance and support during my study journey. I wish you all the best and further success and achievements in your life.

It is unfair to just say thank you to those who have made many sacrifices to help me: my parents who, after Allah, were my greatest supporters. They provided me with love, guidance, prayer, endless support and wisdom. These are things I will never be able to repay. The only thing I can say to you is that your dream to see me become a scientist will soon be realised. I love you from the bottom of my heart.

Grateful thanks to my wife, Nagwa, and children, Rayan, Yones, Raihan, and Genan, who had lived this journey with me, in times of happiness and hardship. Thank you very much for being the motivational factor in my life, supporting me in every possible way and giving me hope after hope to complete this work successfully. Please forgive me for my shortcomings, which were many, through this journey.

My brothers, sister Zohra, and my family in law: thank you very much for your prayers and encouragement. My whole team and my friends: thank you very much for what you have done for me. In fact, I do not need to list your names because I am sure that you know who you are. I also thank the Electrical and Mechanical Workshop staff, Mr Jack, Stuart, Allan, Stephen, Stephen Robson, Graham and Jeffrey. I thank you all for your help during the period of my project implementation.

Special appreciation goes to the 'Health Monitoring of Offshore Wind Farms' (FP7-PEOPLE-2010-IRSES, 269202) project and the School of Electrical and Electronic Engineering, Newcastle University, for providing me with this opportunity to conduct my research.

I would also like to express special thanks to my home country (LIBYA) for providing a scholarship for my study. Finally, I dedicate this research to the soul of my mother and the souls of the 17<sup>th</sup> February martyrs of the Libyan revolution.

---

---

# Contents

CHAPTER 1: INTRODUCTION	1
1.1 Background	3
1.1.1 Problems for Wind Turbines	4
1.1.2 Importance of SHM in the Wind Turbine Industry	6
1.2 State-of-the-Art Inspection Techniques used in SHM for WTBs	7
1.3 Challenges of Applying SHM and Relevant NDT Methods to OWTBs	8
1.3.1 Difficulties in Offshore Monitoring	8
1.3.2 Challenges of Proposed Wireless SHM Method	10
1.4 Aim and Objectives	11
1.5 Scope of the Work	13
1.6 Research Contributions	13
1.7 Publications Arising from this Thesis	15
1.8 Thesis Outline	16
CHAPTER 2: LITERATURE REVIEW ON WTB HEALTH MONITORING	20
2.1 Background to Wind Power Systems	20
2.1.1 Nacelle and Tower	21
2.1.2 Rotor and Blades	22
2.2 Failure Models for Wind Turbine Blades	23
2.2.1 Impact Damage	24
2.2.2 Delamination	25
2.2.3 Fatigue Crack	26

---

2.3	State-of-the-Art Techniques for SHM of WTBs	27
2.3.1	Ultrasonic Technique	30
2.3.2	Acoustic Emission	33
2.3.3	Fibre Optic Method	34
2.3.4	Thermography Technique	35
2.3.5	Radiographic Inspection	36
2.3.6	Relevant Work on <i>in-situ</i> SHM Systems for WTBs	37
2.3.7	Comparison of NDT Methods used in SHM for WTBs	40
2.3.8	Choice of Appropriate NDT Technique for SHM for OWTBs	41
2.4	WSNs and Data Acquisition Techniques	44
2.4.1	Data-driven Approaches and WSNs	45
2.4.2	Feature Extraction under the Use of Low Sampling Rates	49
2.5	Summary and Problem Formulation	50
CHAPTER 3: SYSTEMATIC APPROACH AND SAMPLING RATE REQUIREMENTS FOR WIRELESS SENSOR NETWORKS		53
3.1	Research Methodology	54
3.2	Requirements of Low Sampling Rates	56
3.2.1	Compressive Sensing Theory	56
3.2.2	Uniform Low Sampling Rates Concept	58
3.2.3	Conditions for the Utilisation of Uniform Low Sampling Rates	60
3.3	Acoustic Source Localisation Using Low Sampled Data	60
3.3.1	Time Delay Estimation Using Microphone Arrays	61
3.3.2	Selection of Appropriate Analysis Method for Low Sampled Data	63
3.4	Experimental Setup for TDE at Low Sampling Rates	66
3.5	Results and Discussion	67
3.6	Summary	72

---

CHAPTER 4: EXPERIMENTAL VALIDATION OF SOUND LOCALISATION USING AWSNs AT LOW SAMPLING RATES	74
4.1 Background	75
4.2 Signal Processing Strategy under the Use of Low Sampling Rates	75
4.3 Proposed Localisation Method	76
4.3.1 Envelope Fitting for Smoothing Shape Feature	77
4.3.2 Wavelet Transform	77
4.4 Shannon Entropy based EWT for TDE	85
4.4.1 Shannon Entropy Criterion for Optimum Scale Selection	85
4.4.2 Problem of Applying SE and CWT	86
4.5 Experimental Setup for ASL Using AWSNs	88
4.5.1 Configuration of the Experimental AWSNs	89
4.5.2 Realisation of Synchronised Data Acquisition in AWSNs	93
4.6 Results and Discussion	96
4.6.1 Synchronised Data Acquisition Process	96
4.6.2 Wireless ASL at Low Sampling Rates	98
4.7 Summary	105
CHAPTER 5: WIRELESS SHM CASE STUDY I: SOUND LOCALISATION ON WTBs AT LOW SAMPLING RATES	106
5.1 <i>In-situ</i> Wireless SHM System Setup for WTBs	106
5.1.1 AWSN Model and Hardware Requirements	107
5.1.2 Integration of Wireless System and AE Technique	108
5.1.3 Acoustic Emission Technique	110
5.1.4 System Setup and Implementation	112
5.2 Software Setup and Sensing Considerations	113
5.2.1 AE Sensing for Field Study	114
5.2.2 Event Based Transmission Strategy for Field Study	114



---

5.2.3	On-Board AE Feature Extraction Algorithm for Field Study	115
5.3	Validation of AE Source Localisation on WTBs	118
5.3.1	Line-of-Sight AE Source Localisation on WTB	118
5.3.2	Zonal Localisation for Active Blade Identification	120
5.3.3	Constraint Geometrical Point Localisation of AE Sources	120
5.4	Results and Discussion	122
5.4.1	Line-of-Sight Localisation of AE Events	122
5.4.2	Active Blade Identification	123
5.4.3	Constraint Geometrical Point Localisation of AE Events	126
5.5	Summary	127
CHAPTER 6: WIRELESS SHM CASE STUDY II: AE EVENT AND ENVIRONMENTAL MONITORING		129
6.1	Introduction	129
6.2	Extraction and Fusion of AE Features	131
6.2.1	Pre-processing of Aliased AE Signals	131
6.2.2	Principal Component Analysis-Based Features	131
6.2.3	Wavelet Transform-Based Features	133
6.2.4	Wavelet Transform-Principal Component Analysis Based Features	135
6.3	System Validation Using Emulated Impact Damage and Environmental Monitoring	136
6.4	Validation Results and Discussion	136
6.4.1	AE Event and Environmental Monitoring	137
6.4.2	Discrimination and Classification of Emulated Impact Damage	143
6.5	Summary	148
CHAPTER 7: CONCLUSIONS AND FURTHER WORK		150
7.1	Research Summary	150
7.2	Main Contributions of the Research	153

---

7.3	Limitations of the Research	154
7.4	Suggestions for Future Work	155
7.5	Research Implications for Practice	157
	References	159
	Appendix A: MICAz Specifications	176
	Appendix B: Wind Turbine Specifications	178

---

---

## List of Acronyms

AE	Acoustic Emission
AET	Acoustic Emission Technique
ANN	Artificial Neural Networks
ASL	Acoustic Source Localisation
AVG	Average
AWI	Acoustic Wave-Field Imaging
AWSN	Acoustic Wireless Sensor Network
BCC	Basic Cross Correlation
COTS	Low-Cost Commercial Off-The-Shelf
CPSD	Cross-Power Spectral Density
CS	Compressive Sensing
CSLDV	Continuous-Scan Laser Doppler Vibrometry
AVP	Acoustic Vector Property
CWT	Continuous Wavelet Transform
DAQ	Data Acquisition
DWT	Discrete Wavelet Transform
EGPS	Envelope Generalised Phase Spectrum
EWT-CC	Envelope-Based WT Cross-Correlation
FRCW	Frequency Modulated Continuous Wave

---

GPS	Generalised Phase Spectrum
GUI	Graphical User Interface
HEH	Hardware Event Handler
HEMOW	Health Monitoring of Offshore Wind Farms
IITM	Indian Institute of Technology Madras
LDS	laser Displacement Sensor
MEMS	Micro-Electro-Mechanical Systems
NAREC	National Renewable Energy Centre
NDE	Non-Destructive Evaluation
NDT	Non-Destructive Testing
NREL	National Renewable Energy Laboratory
NUAA	Nanjing University of Aeronautics and Astronautics
O&M	Operation and Maintenance
OWTBs	Offshore Wind Turbine Blades
OWTs	Offshore Wind Turbines
PCA	Principal Component Analysis
PCs	Principal Components
PEC	Pulsed Eddy Current
PPD	Propagation Path Difference
RF	Radio Frequency
RMS	Root Mean Square
SCADA	Supervisory Control And Data Acquisition
SEM	Scanning Electron Microscopy
SEWCs	Shannon Entropy of Wavelet Coefficients

---

SHM	Structural Health Monitoring
SNL	Sandia National Laboratory
SSE	Synchronisation Sensing Error
STD	Standard Deviation
SVM	Support Vector Machine
TDE	Time Delay Estimation
UNEW	Newcastle University
UT	Ultrasonic Technique
WPs	Work Packages
WSNs	Wireless Sensor Networks
WT	Wavelet Transform
WTBs	Wind Turbine Blades
XR-CT	X-Ray Computed Tomography
ZU	Zhejiang University
ZUT	West Pomeranian University of Technology

---

---

## List of Figures

Figure 1: HEMOW project diagram. ....	2
Figure 2: Annual installation of wind turbines onshore and offshore in Europe. ....	4
Figure 3: Recorded wind turbine accidents since 1996. ....	5
Figure 4: Main objectives of SHM in the OWT industry. ....	7
Figure 5: Example of harsh environment of OWTs. ....	9
Figure 6: Layout of wireless sensor networks. ....	11
Figure 7: Key parts of a wind turbine. ....	21
Figure 8: Cross section of a WTB showing its main parts and their variable thicknesses. ....	23
Figure 9: Failure causes and models of WTB and inspection techniques. ....	24
Figure 10: SEM images of failure modes on twelve-layer GFRPs laminates: (a) Matrix micro-cracking and macro-cracking, (b) Delamination (c) Fibre-matrix interface debonding (d) Fibre breakage. ....	25
Figure 11: Delamination damage to WTB driven by a buckling load. ....	26
Figure 12: A block-diagram of a smart structural health monitoring system. ....	28
Figure 13: Wind farm SCADA system. ....	29
Figure 14: Active and passive techniques. ....	30
Figure 15: <i>In-situ</i> tests: a, b) AET, c) Laser vibrometer and d) Robot inspector. ....	38
Figure 16: Taxonomy of approaches to energy saving in sensor networks. ....	45
Figure 17: Taxonomy of data-driven approaches to energy conservation. ....	46
Figure 18: Taxonomy of energy-efficient DAQ approaches with the new data reduction method. ....	48
Figure 19: Block diagram of the research methodology. ....	55
Figure 20: The principle of utilising low sampling rates at: a) wireless node, b) central unit. ....	59

---

Figure 21: Geometrical relationship of three microphones and a sound source. $R$ is the shortest path between sound source $S$ and $M_2$ .....	62
Figure 22: Selection of the cut-off frequencies $\omega_0$ , $\omega_1$ , and frequency bandwidth $\Delta\omega$ . .....	65
Figure 23: Schematic representation of the wired experimental setup for the ASL. ....	67
Figure 24: Wave forms of sound sources and their spectrum used as test signals: left, pulse signal, and right male speech ‘acoustic camera’. ....	67
Figure 25: Comparison results of TDE algorithms using: a) pulse, b) speech signals, for a delay of 40 samples. ....	69
Figure 26: Comparison results of TDE algorithms using: a) pulse, b) speech signals, for a delay of 30 samples. ....	70
Figure 27: Comparison results of TDE algorithms using: a) pulse, b) speech signals, for a delay of 10 samples. ....	72
Figure 28: Detailed block diagram of the proposed TDE algorithm EWT-CC. ....	77
Figure 29: Comparative plot of correlation coefficients with various wavelet filters for the signals under investigation. ....	80
Figure 30: Curve-fitting interpolation using three points. ....	84
Figure 31: Detailed block diagram of the modified TDE algorithm, SE-EWT. ....	85
Figure 32: Redundancy of CWT coefficient (Zoom-In) of an acoustic pulse: a) matrix $A$ , b) matrix $B$ and c) difference ( $A-B$ ).....	87
Figure 33: Shannon entropy of wavelet coefficients, SEWCs, vs. scales.....	88
Figure 34: The schematic structure of a wireless sensing unit.....	90
Figure 35: Wireless experimental setup and the triangular configuration of wireless units-sound source for the localisation where $P_i$ represents wireless unit position and $R$ is the shortest path between sound source $S$ and the wireless unit located at $P_2$ . $R$ varies between 1 and 2.5m.....	91
Figure 36: Connection of KEITHLEY 3390 function generator with MICAz as a trigger node. ....	92
Figure 37: The first 200 envelope samples of captured acoustic signals using a) HEH mode and b) task mode. ....	97
Figure 38: Repeatability measurements of Task and HEH modes. ....	98

---

Figure 39: The first 200 samples of captured signals by wireless units one, two, and three at 4.8KHz: a) Aliased acoustic signals b) Their envelopes.....	99
Figure 40: Zoom-In output of CC and EWTCC with and without parabolic fit interpolation. ....	100
Figure 41: RMS errors for CC, EWT-CC and EWT-CC-Fitting algorithm. ....	102
Figure 42: First example for using the SEWCs to select the optimum scale value (58) which delivers the PPD (20.59cm), where the actual PPD 21cm was. ....	103
Figure 43: Second example for using the SEWCs to select the optimum scale value (59) which delivers the PPD (35.50cm), where the actual PPD 36cm was. ....	104
Figure 44: a) Illustration of a monitoring network with the wind turbine. ....	108
Figure 45: Hardware components: wireless unit (WU) and gateway. ....	108
Figure 46: Wireless unit installation: a) photograph of WSN node inside the nose, b) photograph of AE sensors fixed on the blades, c) Diagram of AE sensors fixed on the blades.....	109
Figure 47: Key features of an aliased AE signal.....	111
Figure 48: System installation: a) WT installation on the school's roof, b) Gateway fixed to the WT tower, c) Control unit.....	112
Figure 49: Screenshot of the GUI of the wireless demonstration system.....	113
Figure 50: Schematic diagram of synchronised sensing and transmission operations. ....	114
Figure 51: On-board feature extraction algorithm. ....	116
Figure 52: Aliased AE signals with its envelope. ....	117
Figure 53: Linear localisation of AE events. ....	118
Figure 54: Proposed configuration of acoustic wireless units, $x$ and $y$ are the unknown coordinates of AE source, $t_i$ is the arrival time of AE signal at AE sensor $S_i$ .....	121
Figure 55: Proposed 2D localisation model. ....	122
Figure 56: Aliased AE signals received from the wireless units as a consequence of hitting the three blades individually a) one, b) two, and c) three.....	125
Figure 57: Active blade identification based on peak value features of AE events shown in Figure 56. ....	126
Figure 58: AE events detection and classification strategy. ....	130
Figure 59: Block diagram of SWT.....	135
Figure 60: Wind condition waveform detected.....	137



---

Figure 61: <i>Rainfall condition</i> waveform detected.....	138
Figure 62: <i>Rainfall</i> and <i>wind condition</i> waveform detected. ....	138
Figure 63: Emulated impact damage waveform. ....	139
Figure 64: Emulated impact damage and rain condition waveform detected.....	140
Figure 65: AE events received at three wireless units (WU), a) for rain, b) rain and hit measurements.....	140
Figure 66: Classification of received events under different environment conditions using time domain features. ....	141
Figure 67: Classification of received events under different environment conditions using the integration of time domain and PCA features. ....	142
Figure 68: Emulated impact damage setup. ....	143
Figure 69: Aliased AE signals caused by the emulated impact damages by the three balls; a) LB, b) MB, and c) SB.....	145
Figure 70: Discrimination between impact signals caused by the three balls.....	146
Figure 71: Discrimination between impact signals caused by the three balls using SWT-based features. ....	146
Figure 72: The principal component analysis of the WT coefficients to discrimination between impact signals caused by the three balls. ....	147
Figure 73: Third principal component correlates with normalised average power parameter of aliased AE signals for the three impact cases. ....	147
Figure 74: Combination of the proposed <i>in-situ</i> wireless SHM system and vehicular climbing robots. ....	158

---

---

## List of Tables

Table 1: List of WPs HEMOW-FP7 Project.....	3
Table 2: Comparison of NDT techniques used in SHM for WTBs. ....	40
Table 3: Important selection criteria of NDT method for SHM for OWTBs. ....	43
Table 4: Basic mathematical expressions for BCC and GCC.....	64
Table 5: Commonly used weighting functions in the GCC method. ....	64
Table 6: Waveforms of some selected mother wavelet. ....	81
Table 7: Computational complexity comparison of both TDE algorithms.....	89
Table 8: AVGs and STDs of estimated PPDs for 15 experiments using CC, EWT-CC, and EWT-CC Fitting. ....	101
Table 9: Comparison between EWT-CC and SE-EWT algorithms.....	104
Table 10: Line-of-sight results of AE events localisation based on AVPs.....	123
Table 11: Estimation results of constraint geometrical point localisation. ....	127
Table 12: Waveform descriptions of the AE event and environmental conditions. ....	148

# CHAPTER 1: INTRODUCTION

Demand for the harvesting of wind energy has increased recently due to the current energy crisis and environmental pollution not only in the UK but also worldwide. As a result, wind turbines have become physically larger and more wind farms are placed in remote areas in order to increase efficiency and levels of power generated [1]. One consequence of this is that maintenance and repair work becomes more difficult and challenging. For instance, the cost of the operation and maintenance (O&M) of offshore wind turbines (OWTs) has become significantly higher due to access difficulties, particularly during extreme weather conditions, where special landing boats may be needed [2].

These and many other challenges have made the development of structural health monitoring (SHM) systems for OWTs an important research topic. Many scientific institutions and wind turbine manufacturers are trying to develop novel techniques for monitoring the health of these structures [3-6]. The HEMOW-FP7 Project, ‘The Health Monitoring of Offshore Wind Farms’, is one such funded wind-power research study which concentrated initially on the *in-situ* monitoring of offshore wind turbine blades (OWTBs), gearbox and generator systems for both existing and new topologies that will be developed in the future [7]. This project aims to support a development of smart SHM systems in order to contribute to a cost-optimised O&M particularly for offshore wind farms, where faults cause long downtimes. This will be achieved by addressing the following challenges [7]:

1. Smart sensors for wind turbines systems.
2. Gearbox NDE, generator and condition monitoring.
3. Hierarchical communication, signal processing and data management.
4. ICT tools for information fusion and wind farm maintenance management.

5. Build a sustainable platform for international collaborative research, networking and knowledge transfer.

The HEMOW project is coordinated at Newcastle University (UNEW), UK, other partners are West Pomeranian University of Technology (ZUT), Poland, Nanjing University of Aeronautics and Astronautics (NUAA), China, Zhejiang University (ZU), China and Indian Institute of Technology Madras (IITM), India. The project is divided into 6 work packages (WPs), as shown in Figure 1, while WP6 is management and dissemination and it is not shown in this figure. The list of these WPs is given in Table 1.

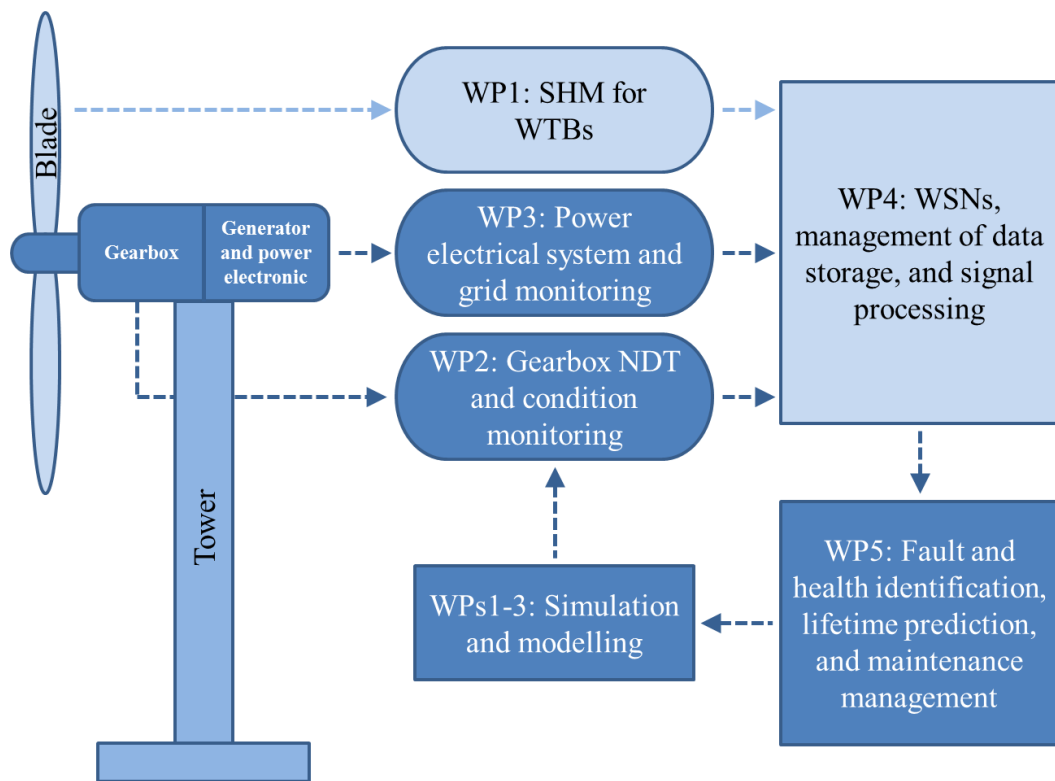


Figure 1: HEMOW project diagram.

As part of Newcastle University contributions to the HEMOW-FP7 Project, the focus of this research involves the investigation of several non-destructive testing (NDT) and condition monitoring techniques in order to develop a suitable SHM technique for wind turbine blades (WTBs). To achieve this goal, a research project is being carried out to investigate the employment of wireless sensor networks (WSNs) in conjunction with acoustic emission (AE) to build *in-situ* long-term health monitoring systems for OWTBs. This research also involves the development of approaches to reduce levels of the transfer of sensing data by lowering sampling rates and the local pre-processing of

raw data on-board on wireless units so that only the results of evaluation and other meaningful information need to be transmitted to the remote control room.

Table 1: List of WPs HEMOW-FP7 Project.

WP No.	Work Package Title	Lead Partner Organisation
1	Turbine blade health monitoring	NUAA, IITM, UNEW
2	Gearbox NDE and condition monitoring	ZUT
3	Power electrical system and grid monitoring	ZU
4	WSNs, management of data storage, and signal processing	UNEW, NUAA
5	Fault and health identification, lifetime prediction, and maintenance management	UNEW, ZUT
6	Management and dissemination	UNEW

This chapter is organised as follows. A brief background is given on the increased demand for wind energy, in the UK and worldwide, and the challenges associated with meeting this demand as well as the importance of SHM in the wind power industry. After that state-of-the-art inspection techniques used for monitoring the structural health of WTBs are briefly reviewed, followed by the challenges associated with these methods and the methods which have been proposed for this application. A synopsis of the present research objectives is then provided and the scope of the work discussed. The major contributions of the research are presented and finally an outline of the thesis is laid out.

## 1.1 Background

Wind energy is one of the main renewable energy sources that, in recent decades, has gained much attention not only in the UK but also worldwide due to energy crises and environmental pollution [1]. Figure 2 shows the annual installations in both onshore and offshore wind sectors for the period from 2000 and projected till 2030 [8]. Investment in the onshore sector rises steadily until it is expected to reach a peak at 17.8GW in 2020 and then starts to decrease due to movement towards offshore wind power. In contrast, offshore investment continues to grow due to better wind speeds there, and it is project-

ed to reach almost 14GW in 2030 [8].

In addition, the US Department of Energy has reported that, in 2030, wind power will contribute 20% to the total US electrical supply [9], whereas 30% of the UK’s electricity supply in 2020 will be delivered by the wind energy [10]. Therefore, it is expected that over the next decade the offshore wind sector will grow particularly rapidly in the UK, in order to profit from the more favourable wind conditions at sea which will contribute towards the fulfilment of UK energy requirements. This, however, necessitates significant investigation particularly to minimise the production and maintenance costs of OWT as well as improving reliability via the health monitoring of wind turbine structures.

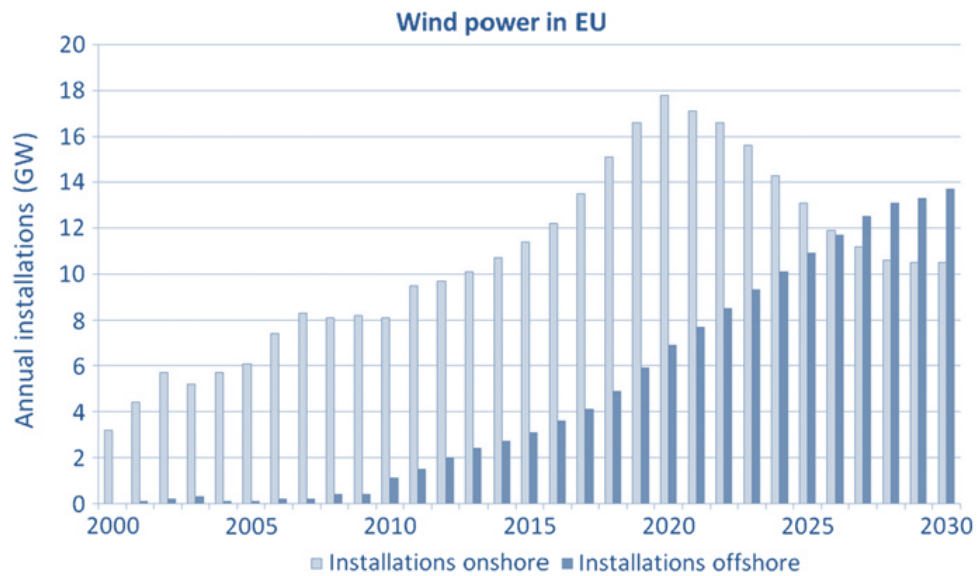


Figure 2: Annual installation of wind turbines onshore and offshore in Europe [8].

To reach this goal and to increase the offshore wind turbine efficiency and consequently capacity, significant investments are being made in wind turbine technology. This has led manufactures to develop more complex wind turbines with physically larger size and longer as well as lighter blades [11]. However, as a result of the increasing size of wind turbine structures, more difficulties follow in installation, maintenance and repair work.

### 1.1.1 Problems for Wind Turbines

Unfortunately, as more turbines are installed and their size increases to fulfil demand, more frequent accidents and disasters related to wind turbines have been documented.

This has been confirmed by the Caithness Windfarm Information Forum [12], which reported that the average number of wind turbine incidents in the UK increased from six per year from 1992-6 to 140 per year from 2009-12 as shown in Figure 3.

In addition to that, the Daily Telegraph stated that RenewableUK [13] revealed in December 2011 that the number of wind turbine accidents and incidents (e.g., blade failure) had reached 1500 in the UK alone in the period between 2006 and 2011. This general trend is expected to accelerate as wind turbines and their blades increase further in size and length respectively, unless their structural health can be monitored [1].

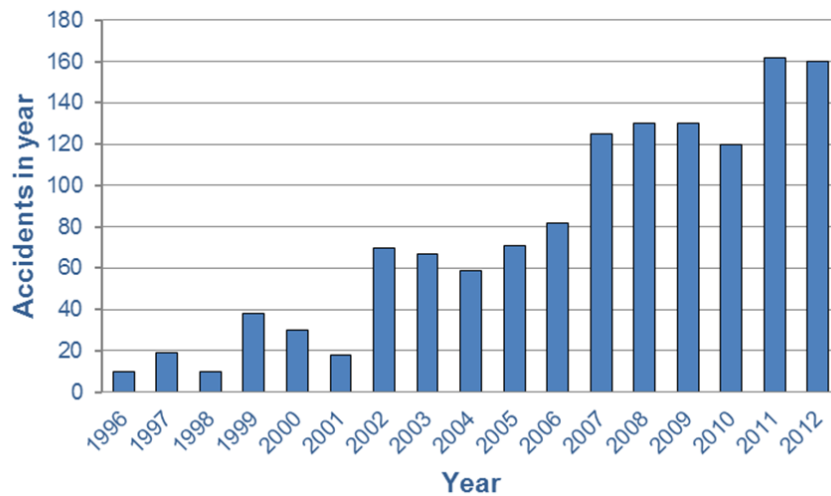


Figure 3: Recorded wind turbine accidents since 1996 [12].

A WTB is one of the most dangerous parts of the wind turbine structure due to its large size and rotation speed. The Caithness Windfarm Information Forum stated that the highest proportion of documented incidents were as a consequence of blade failure. Blade accidents can be caused by different factors, which can lead the whole wind turbine to break down or where either complete blades or parts of them are detached and thrown over long distances. Such blade catastrophes risk not only damaging other wind turbines in the wind farm but also affecting surrounding residential areas. These factors have led this study to focus on the development and implementation of SHM algorithms for WTBs.

Due to the developments described above, an increasingly scientific approach is now being taken to the design and development of SHM techniques for the wind turbine industry. SHM is typically a strategy of monitoring engineering structures by utilising

permanent sensors in order to detect damage and to characterise the condition of these structures [3, 14]. Such techniques can provide information about the status of the wind turbine components or structure, without affecting their current or future performance. SHM should therefore be an essential part of the wind turbine industry, particularly for offshore turbines, in order to overcome challenges facing them as discussed in the next sections.

### *1.1.2 Importance of SHM in the Wind Turbine Industry*

The large structures of wind turbines and their long blades can not only cause serious accidents and catastrophes but also lead to them being massively hard to install and maintain. This is particularly true for OWTs which are sited in remote areas. This necessitates that OWTs should incorporate SHM systems in order to collect quantitative as well as qualitative information about the wind turbine status. This can be achieved by collecting continuous online feedback which will also help in predicting the remaining lifetime of the OWTs. It also will minimise O&M costs as well as giving operators or inspectors the ability to inspect these structures from offsite, while securely maintaining the wind turbine [3, 15, 16].

The overall significance of SHM for the OWT industry can be summarised in the following points [1, 3, 17] which are also illustrated in Figure 4:

- Minimising the O&M costs of wind turbine structures.
- Prediction and evaluation of remaining lifetime as well as the prevention of early collapse, including alerting to the need for product replacement and maintenance requirements in the early stages.
- Fault/failure prediction, inspection, detection, assessment, and identification.
- Safety monitoring of wind turbines offsite.
- Gathering information and collecting data for future design and optimisation calculations.
- Performance improvement.

In addition, the importance of SHM is also represented by the monitoring of OWTs immediately after natural hazards and man-made disasters as well as extreme weather conditions, which will then reduce the impact of such disasters in both economic and



social terms. This requires appropriate SHM techniques to be integrated into these structures. The following sections review state-of-the-art inspection methods in brief, particularly for WTBs, whereas more detailed reviews of different SHM systems are provided in Chapter 2, along with some relevant non-destructive testing (NDT) techniques.

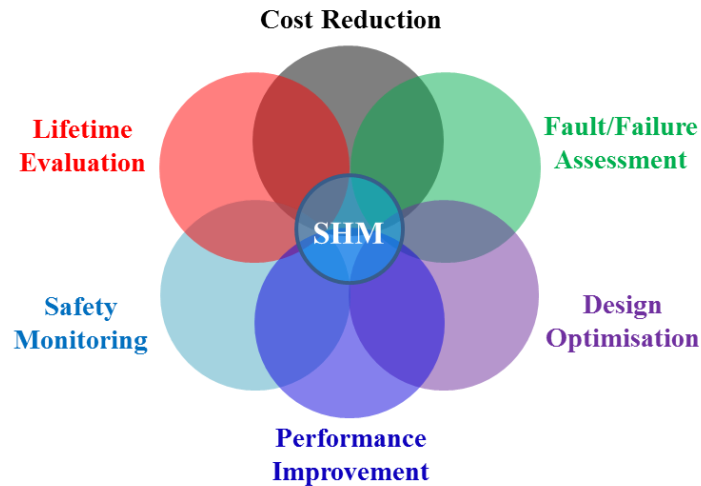


Figure 4: Main objectives of SHM in the OWT industry.

### 1.2 State-of-the-Art Inspection Techniques used in SHM for WTBs

The blade (see Section 2.1) is an essential component of the wind turbine system and one of the most expensive to maintain, representing 15-20% of the overall cost. This is because failure of the blade can cause damage to the overall wind turbine structure as a result of rotational imbalance [1, 18, 19]. This has motivated many researchers to develop new approaches to monitoring the health of these structures [3-6].

The majority of blade health inspection techniques are classified as certification tests and they specify that laboratory testing must be conducted for the purpose of postproduction inspection prior to blade fitting [1, 3, 15, 19-21]. Such widely utilised techniques include, for example, ultrasonic [22, 23] and AE [24], thermography [25], shearography [26, 27], and computed tomography (XR-CT) [28].

In contrast, fewer researchers have attempted to develop in-field (*in-situ*) SHM approaches with wind turbine blades. Such approaches are either stationary or dynamic in-service methods. Stationary testing means that the inspection process is completed while the blades are static [5, 24, 29], whereas in dynamic testing the inspection process is realised as the blades rotate while in-service [30].

However, the abovementioned techniques are unfortunately incapable of providing a robust continuous online SHM system, particularly for OWTBs. This is because they are costly and/or time-consuming, and may rely on regular inspection. In addition, most of these approaches apart from the AE technique are active, and need to be used under the supervision of operators which represents a big challenge for their utilisation in the SHM of OWTBs. Further discussion of these issues is presented in Chapter 2.

In this research, the main focus of study is the development of a robust wireless inspection system for OWTBs based on the AE technique in conjunction with WSNs. This is because AE is a passive technique which can be applied to the blade structure with limited access, and allows the investigation of defects in the structure under wind load while the wind turbine is in-service, as discussed in Chapters 2 and 5. In addition, most types of blade failures cause detectable AE waves, including crack initiation and growth, crack opening as well as closure, and others [31]. The WSNs also provide a perfect means for sending wirelessly the AE sensing data to the remote control unit. The integration of these two technologies in this application, however, faces several challenges which are summarised in the next section.

### **1.3 Challenges of Applying SHM and Relevant NDT Methods to OWTBs**

Although there are many advanced SHM and relevant NDT techniques that can be utilised for the inspection of WTBs in laboratory environment, and although there have been some attempts to develop *in-situ* blade SHM systems, as stated above, significant challenges are still faced. This section briefly outlines these challenges. Firstly, the challenges that face the implementation of existing SHM methods with OWTBs are listed, and then the problems with the proposed dynamic in-service monitoring approach when applied to OWTBs are discussed.

#### ***1.3.1 Difficulties in Offshore Monitoring***

OWTBs are located in remote areas which could involve extremely harsh environments, for example due to weather conditions. If current SHM methods are applied to these OWTBs, the following challenges will be encountered:

- The offshore wind energy market is rapidly expanding. The Offshore Wind Infrastructure Application Lab ([www.owi-lab.be](http://www.owi-lab.be)) stated that in “*the coming 4*

years 12GW will be installed offshore; this is 3 times the amount of what has been realized over the last 20 years.” This means that the size and the length of WTBs will increase. Blade structure will be more complex which poses additional monitoring challenges.

- Offshore wind turbines are placed in remote areas, as shown in Figure 5. This leads to access difficulties, particularly during extreme weather conditions. Access to large blades requires the use of means such as ropes or others which may expose inspectors to risk. Special landing boats may even be needed to gain access to wind turbines. The inspection process may be a lengthy procedure, and for all these reasons inspection costs will increase.



Figure 5: Example of harsh environment of OWTs [32, 33].

- Problems of access may limit visual inspections to only surface defects and not interior anomalies [34]. The direct adoption of traditional NDT techniques such as tap tests and ultrasonic testing, including A-scan, B-scan, or C-scan, to OWTBs in order to achieve full *in-situ* inspection may also be limited. This is because these techniques require active excitation units and their operation needs to be supervised by inspectors. Full coverage of a blade could be achieved, however, if more advanced approaches such as thermography [25] or shearography [26] were used. However, the limited portability of these methods makes them unsuitable for offshore *in-situ* inspection applications.
- Finally, current SHM techniques are wire-based methods. This represents another

er challenge if they are applied in the long-term offshore monitoring of OWTBs with continuous online feedback. This has stimulated the proposal of the development of smart wireless sensing with advanced hierarchical communication and signal processing for information fusion as well as data aggregation techniques to collect, process, and manage huge amounts of collected data. The challenges associated with this proposal are presented below.

### ***1.3.2 Challenges of Proposed Wireless SHM Method***

The integration of AE techniques with WSNs makes the combination of these technologies an attractive alternative in developing a robust SHM for OWTBs. This is because WSN technology can provide a robust, scalable, reliable, efficient, and economical approach for such applications. Nevertheless, WSNs have some technical limitations and challenges which need to be tackled before they can be integrated into SHM techniques for offshore blades. Some of these challenges are discussed below, following an overview of WSNs technology.

WSNs comprise a group of small wireless units known as sensor nodes (wireless units). Each has a microcontroller, a wireless interface, and one or more sensors. These nodes can be arranged in single- or multi-hop WSNs and they can work collaboratively to monitor an area or execute a certain task. They can also interact with a remote control unit or other units via a gateway, as shown in Figure 6. Such wireless networks can be either centralised or distributed WSNs. The former approach requires that data be transferred from wireless units to a centralised control unit to be globally analysed and where advanced signal processing techniques can be applied, as described in Chapter 4. In the latter approach, data is locally processed on-board the wireless units and only meaningful information is sent to the control unit. However, this is subject to the condition that only simple signal processing techniques are used, as elaborated in Chapter 5. This is due to the limitations of wireless units which are as follows [35-38]:

- Power resources; where in some applications batteries cannot be replaced or even recharged.
- Processing and memory capabilities.
- Computational capacity.
- Transmission range and throughput.

- Bandwidth for data transmission.

This means that the proposed SHM technique must work under severe resource constraints, which represent one of the foremost challenges. Typically, SHM systems generate huge amounts of sensing data so that high processing and memory capabilities as well as computational capacity are required. This is because the large size of OWTBs necessitates having a considerable number of sensors in a complete SHM system in order to achieve full blade coverage. In addition, it is necessary that the SHM techniques used should be able to sense the condition of blade structures at all times in order to give continuous online feedback for the long-term monitoring system.

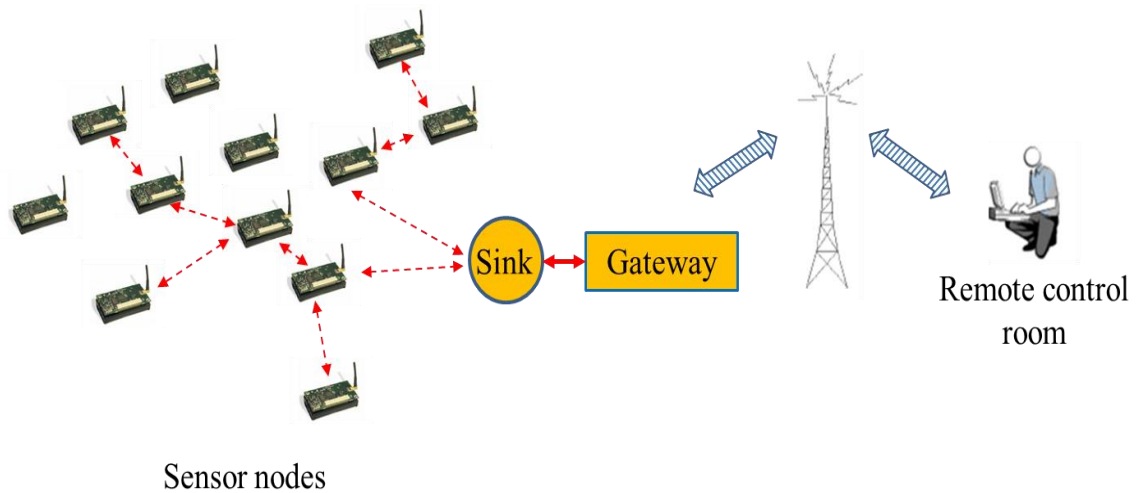


Figure 6: Layout of wireless sensor networks.

Furthermore, the AE technique integrated with WSNs could be very costly due to the high sampling rates required [39]. The consequent generation of enormous amounts of data may overload the mechanisms of storage, data management, data transmission, and data processing as well as power resources in the WSNs.

Therefore, the reduction of the amounts of sensing data acquired will play a significant role in tackling such SHM problems. This is achieved in this study by deployment of low sampling rates in acquiring acoustic signals as seen in the coming sections.

#### 1.4 Aim and Objectives

In the emerging cross-disciplinary field of research into the SHM of OWTs, and as part

of the HEMOW-FP7 Project, the main aim of this research is to design and develop an *in-situ* wireless SHM system for OWTBs in conjunction with the AE technique. It is expected that this will increase the consistency and efficiency of these techniques and make them more valuable when applied not only with OWTs but also in aerospace, and other engineering applications.

The proposed *in-situ* SHM system includes the sensor configuration, data acquisition and processing, feature extraction and fusion for impact detection and classification.

The objectives of this research are summarised as follows:

- To undertake a comprehensive literature survey that explores current SHM techniques and relevant NDT techniques for WTBs and the usage of WSNs in conjunction with one of these techniques to be used for monitoring the structural health of OWTBs.
- To investigate the requirements of acoustic wireless sensor networks (AWSNs) for SHM systems by studying the constraints of acquisition sampling frequency under the use of low sampling rates in order to specify an appropriate signal domain of analysis.
- To develop a prototype wireless system for conducting acoustic source localisation measurements using low sampling rates well below the Nyquist rate in acquiring acoustic signals.
- To propose/utilise new techniques in signal processing for solving the problems encountered when working with low acquisition sampling rates, such as the low spatial resolution for acoustic source localisation.
- To develop feature extraction algorithms based on the use of low sampled data for defect detection and classification in order to achieve the highest possible levels of system performance even at low sampling rates.
- To develop and implement an advanced wireless system for a continuous SHM system which will be used to evaluate and test the proposed SHM system. This will be done by building a real *in-situ* prototype system on the roof of the School of Electrical and Electronic Engineering at Newcastle University incorporating a small wind turbine unit, an AWSN, and a user-friendly graphical user interface

(GUI).

### **1.5 Scope of the Work**

The research involves extensive experimentation in combination with theoretical studies into the strengths and weaknesses of selected methods which may be used to make WSNs more valuable and efficient if they are applied to SHM applications. This is realised via investigating the requirements of utilising low sampling rates below the Nyquist rate in acquiring acoustic signals using AWSNs. This is particularly useful if this technology is integrated with AE techniques in conjunction with the use of low sampling rate approach for SHM applications.

Following this investigation, the development of signal processing techniques are introduced to work with low sampling rates and achieve good wireless localisation results using data received from AWSN. Tests are carried out with a lab-based wireless acoustic source localisation (ASL) system to validate the techniques established and study the underlying theory behind the techniques developed.

Next, issues involved in implementing an *in-situ* wireless SHM system for OWTBs are discussed to provide in field wireless AE measurements based on distributed AWSNs. This is accomplished by having a 300W wind turbine installed on the School roof with an acoustic wireless sensing system on the top of it which is composed of a distributed WSN and an AE technique. AE sensing data will be locally processed on-board and only vectors carrying common AE features extracted named ‘acoustic vector properties’ (AVPs) will be sent to the remote control unit. The AVPs will be then used to assess blades health and to localise as well as classify AE events and environmental monitoring respectively under different environmental conditions.

### **1.6 Research Contributions**

As part of the HEMOW-FP7 Project, this study makes a number of contributions to the body of knowledge about SHM. In fact, the major contribution is the development of the *in-situ* wireless SHM system with field deployment on the WTB structure which is intended for use in monitoring the structural health of OWTBs. Other main contributions include showing the use of low sampling rates in the sensing process and identifying its potential and limitations as well as specifying how these limitations could be

overcome. These contributions are described in more detail below.

- A thorough review has been undertaken of different SHM systems with relevant non-destructive testing and evaluation techniques in conjunction with WSNs as well as the potential for their integration.
- Through a comparative study in conjunction with the use of different time delay estimation algorithms, it has been shown that the utilisation of low sampling rates overcomes the challenges posed by the limitations of data transmission over WSNs for ASL. This original contribution will be important in terms of data reduction and power savings in the design and development of the proposed offshore wind turbine SHM technique based on AWSNs.
- Through the investigation of a novel combination of the wavelet transform, envelope fitting, cross-correlation and the Shannon entropy criterion, the utilisation of ASL using AWSNs with the setting of sampling frequency lower than the commonly required Nyquist frequency has been validated. These results contribute to the reduction of the amount of sensing data, level of power consumption, and communication bandwidth required and is therefore beneficial for AWSN applications.
- Through the implementation of an *in-situ* SHM system on the top of a 300W wind turbine installed on the School roof composed of the developed WSN and an AE technique, the proposed data reduction technique has been evaluated in a field environment. In addition, signal processing techniques for the extraction of local AE features from the aliased AE signals have been used to monitor and assess the structural health of WTBs. This contributes to solving the problems of limited power and bandwidth for data transmission in WSNs, which could enhance the performance of the developed *in-situ* wireless SHM for OWTBs.
- The *in-situ* wireless SHM has also been experimentally evaluated based on the utilisation of low sampling rates the consideration given to the detection, monitoring, and classification of different AE events emulating impact damage and audible cracks as well as changes in environmental conditions. Furthermore, through a combination of zonal and constraint geometrical point localisation techniques, a localisation model has been developed and precise source localisa-



tion results were achieved for the complex structure of WTBs. Such a model is a potential candidate for large scale WTBs to provide precise estimation results for AE source localisation.

- Several aspects of the research have been the subject of publications in refereed journals, conference papers, and posters.

### 1.7 Publications Arising from this Thesis

#### Journal Papers

- J1. O. M. Bouzid, G. Y. Tian, J. Neasham, and B. Sharif, "Investigation of sampling frequency requirements for acoustic source localisation using wireless sensor networks," *Journal of Applied Acoustics*, vol. 74, pp. 269-274, 2013.
- J2. O. M. Bouzid, G. Y. Tian, J. Neasham, and B. Sharif, "Envelope and wavelet transform for sound localisation at low sampling rates in wireless sensor networks," *Journal of Sensors*, vol. 2012, 9 pp., 2012.
- J3. P. Wang, Y. Yan, G. Y. Tian, O. M. Bouzid, and Z. Ding, "Investigation of wireless sensor networks for structural health monitoring," *Journal of Sensors*, vol. 2012, 7 pp., 2012.
- J4. O. M. Bouzid, G. Y. Tian, J. Neasham, and K. Cumanan, "Sound localisation using WSNs for SHM of wind turbine blades at Low Sampling Rates," submitted to *Journal of Structural Health Monitoring*, 2013.

#### Conference Papers

- C1. O. M. Bouzid, G. Y. Tian, J. Neasham and B. Sharif, "Acoustic source localisation using wireless sensor network at low sampling frequency for structural integrity assessment," ESIA11, International Conference on Engineering Structural Integrity Assessment, Manchester, UK, 2011.
- C2. G. Y. Tian, F. Abugchem, L. Cheng, and O. M. Bouzid, "Health monitoring of offshore wind farms," ESIA11, International Conference on Engineering Structural Integrity Assessment, Manchester, UK, 2011.
- C3. O. Bunting, J. Stammers, D. Chesmore, O. M. Bouzid, G. Y. Tian, C. Karatsovis, and S. Dyne, "Instrument for soundscape recognition, identification and evaluation (ISRIE): technology and practical uses," Euronoise 2009, Edin-

burgh, UK, Oct. 2009.

### Posters

- P1. O. M. Bouzid, G. Y. Tian, J. Neasham and B. Sharif, “Acoustic wireless sensor network for structural health monitoring,” Post Graduate Conference 2010, Newcastle University, Jan. 2010.
- P2. O. M. Bouzid, G. Y. Tian, J. Neasham and B. Sharif, “Wireless condition monitoring of wind turbine blade using low rate acoustic sampling,” Products and Processes Postgraduate Research Awareness Event, Newcastle University, Mar. 2012.
- P3. O. M. Bouzid, K. J. Li, G. Y. Tian and A. Al-Qubaa, “Integration of acoustic emission and wireless sensor networks for intelligent wind turbine blade structural health monitoring,” Sustainable Control of Offshore Wind Turbines Workshop, Hull University, Sep. 2012.
- P4. O. M. Bouzid, L. Cheng, and G. Y. Tian, “Intelligent AE and PECT based structural health monitoring system for wind power systems,” 6th European Workshop on Structural Health Monitoring, July 2012.

### 1.8 Thesis Outline

This thesis consists of seven chapters. Chapter 2 provides an extensive literature review of SHM methods. Chapters 3 to 6 represent the main contributions of this study, while Chapter 7 concludes the research and outlines future work. The following sections summarise each chapter.

Chapter 1 presents the research background which shows the significance of SHM for the offshore wind turbine industry in general and WTBs in particular. A brief review of current inspection techniques combined with their associated challenges is given. The chapter also outlines the aim and objectives, scope of the work and the general achievements of this study.

Chapter 2 presents the literature survey conducted in this research, starting with an introduction to wind power systems and their most important parts, with more attention given to the WTB. The types of failure modelling for WTBs are reviewed along with the state-of-the-art health inspection techniques for WTBs. The strength and weaknesses

of the relevant techniques are discussed with an emphasis on those which show potential for integration with WSNs.

Based on the comparison study conducted in this chapter, the AE technique was found to be an effective method of detecting such failures, since most of these are related to stress waves; therefore, special attention is paid to this technique in the literature survey, with an emphasis on its integration with WSNs. The major challenges of this combination are discussed and the utilisation of low sampling rates method is described for making WSNs more valuable and efficient in the intended SHM application. Finally a summary of the problem is presented, outlining the need for the integration of AE technique with WSNs in conjunction with low sampling rates to provide an appropriate SHM approach for the assessment of OWTBs.

Chapter 3 presents the theoretical background of the compressive sensing approach with an emphasis on how this method differs from in this study proposed method so that the acoustic signals captured can be processed under the use of low sampling rates to perform source localisation or feature extraction based on the aliased versions of acoustic signals without the need to reconstruct the original signals. A general overview of TDE algorithms in the time, frequency, and time-frequency domains is then elaborated. These domains are investigated in this research in order to derive guidelines for working under the low sampling rates and to specify the appropriate domain of analysis for the estimation algorithms if WSN is involved.

Next, a comparative experimental investigation of the TDE methods is detailed and the results are discussed. These confirm the possibility of relaxing the Nyquist rate and utilising sampling rates much below this criterion in the proposed application, provided that the time-frequency domain is used. The material of this chapter is the basis of a paper published in the Journal of Applied Acoustics and International Conference on Engineering Structural Integrity Assessment, [J1 and C1 in Section 1.7].

Chapter 4 reports the wireless experimental setup as well as validation results for locating a sound source using data received from AWSNs in conjunction with low sampling rates method. It starts with an introduction to the theoretical background of the wavelet transform (WT) and the complementary TDE algorithm developed based on the recommendations made in previous chapters. Two TDE algorithms proposed for central-

ised wireless work are discussed and compared. Ways of selecting the optimum scale value in continuous WT in addition to methods for enhancing the TDE accuracy are then explained, and the results of the continual wireless experimental assessments of system performance are reported.

Issues related to the realisation of synchronised sensing operations among wireless units are analysed and discussed. Finally, the test results show that the proposed methods can provide good capabilities in overcoming the challenges of working under the employment of low sampling rates and in providing good localisation results. The material of this chapter is the basis of a paper published in the Journal of Sensors [J2 in Section 1.7].

Chapter 5 describes the implementation of an *in-situ* wireless SHM technique with its field deployment on the wind turbine blade structure. The chapter starts with a background which covers the most relevant work to development of SHM for WTBs, followed by the discussion of the installation challenges with an emphasis on hardware and software considerations. A brief review of the AE technique is also presented in this chapter, followed by an elaboration of the feature extraction algorithms and their use in AE event detection and localisation.

The feasibility of this system in hardware and software perspectives has been validated by conducting several zonal and constraint geometrical point localisations. The experimental wireless measurements of artificial AE source localisation are reported and discussed in this chapter, which shows the validity of the proposed proof-of-concept. The material of this chapter is the basis of a paper submitted to the Journal of Structural Health Monitoring [J4 in Section 1.7].

Chapter 6 also presents the experimental evaluation of both the developed wireless SHM system and from low sampled data extracted AE features in providing a robust SHM system for WTBs under field environment. This has been shown by the consideration of the localisation and classification of different AE events emulated as well as changes of environmental conditions e.g., impact damage and rain respectively. Time and time-frequency feature extraction algorithms in addition to PCA method have been used to extract the most relevant information, which in turn are used to classify or recognise a testing condition that is represented by the response signals.

## Chapter 1

---

Chapter 7 summarizes the research work conducted so far with its limitations and provides suggestions for the directions of further work based on the current investigation. The chapter ends with the practical implications of this research.

# CHAPTER 2: LITERATURE REVIEW ON WTB HEALTH MONITORING

The results of an extensive literature review are presented in this chapter, beginning with an introduction to wind power systems. This includes descriptions of the main parts of the system with particular emphasis on the blade of the wind turbine. The chapter also considers failure models for WTB which cause audible stress waves, and then the state-of-the-art techniques used for monitoring the structural health of this component are described. Evaluations of the strengths and weaknesses of these techniques are offered, and a comparison is made of the selection criteria used to decide which techniques are able to passively detect defects and show potential ability for integration with WSNs. Attention is also given to the finer details of WSNs and the major challenges faced in the application of this technology associated with SHM for OWTBs, with special attention paid to a combination of AE techniques with WSNs. In addition, the use of low sampling rates approach is described, which can make WSNs more valuable and efficient in the intended SHM application.

The chapter is organised as follows. Section 2.1 presents a brief background to wind power system along with a description to main parts. Section 2.2 reviews some common failure models for WTBs. State-of-the-art techniques for the SHM for WTBs are discussed in Section 2.3 along with a detailed comparison. Section 2.4 introduces WSNs in conjunction with relevant data acquisition approaches. Finally, the conclusions and problem identification are drawn in section 2.5.

## 2.1 Background to Wind Power Systems

Wind turbines are typically used to convert wind power into a useful form of energy, electricity. Figure 7 shows the main components of this system, including the nacelle, tower, rotor, and blades. Other parts are required for delivering usable electricity, in-

cluding batteries, charge-controllers, inverters, and cabling. Some of these components are discussed below.

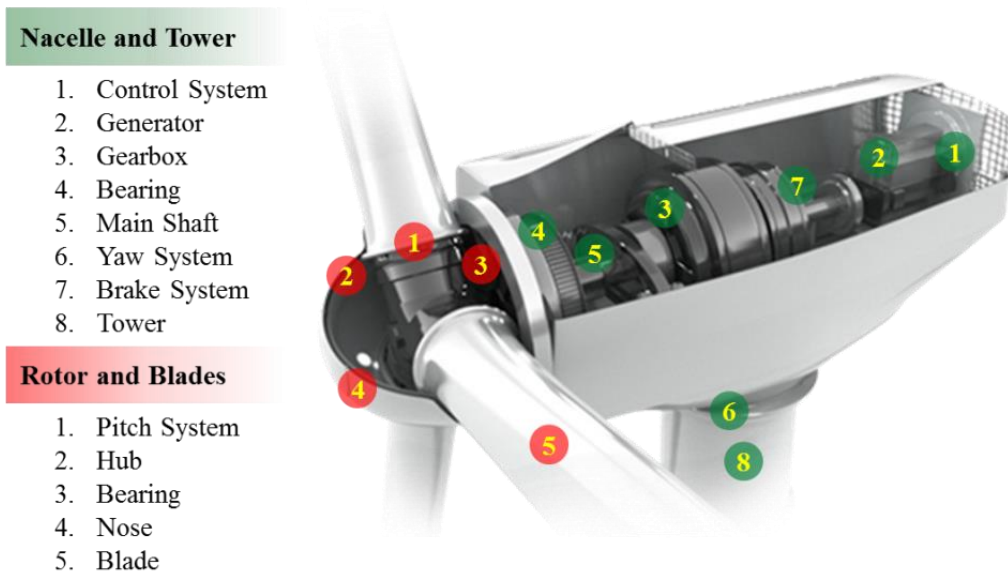


Figure 7: Key parts of a wind turbine [40].

### 2.1.1 Nacelle and Tower

The nacelle is the large covered housing which contains the key components of the wind turbine generator. These components include a control system, a generator, gearbox, bearing, rotor shaft, yaw, and brake systems. The rotor shaft transfers the motion into the gearbox which greatly increases the speed of the rotational shaft. This shaft is connected to the generator and converts the mechanical, rotational movement into electricity. The control system is employed to balance and optimise the operation of the wind turbine and its energy productions as well as providing a means for monitoring the wind turbine unit. The main function of the yaw system is to ensure that the rotor of the wind turbine faces the wind as its direction changes, so that the amount of electric energy generated is maximised at all times. The braking system is utilised to slow the rotor speed either electrically or mechanically. The main shaft bearing system has the function of supporting and carrying the main shaft.

The abovementioned components are carried and supported by an essential, usually tubular, part called the tower. This raises the wind turbine high into the air at between 10m to 100m above the ground and surrounding obstacles in order to increase energy production, since at this height the air flows are stronger and more reliable as well as less

turbulent, particularly if the wind speed is low. In addition, having naturally faster and more consistent wind speeds prolongs the life of the wind turbine components and therefore decreases maintenance costs.

### **2.1.2 Rotor and Blades**

Energy is collected from the wind through a rotor which usually consists of two or more blades. These blades are attached to a hub and adjusted by pitch systems to regulate the angle of the blades so that they can take the maximum advantage of wind speed. At the same time, the pitch systems function as a brake by adjusting the blade angle to slow-down the movement of the blade. The blade face bearings are used to support the rotor or other moving parts and to allow the blade to pitch about a span-wise axis. These blades rotate about an axis which could be horizontal or vertical, at a rate determined by the wind speed and the shape of the blades. Once the blades are forced to move by any significant rotational speed, they spin the generator through the main shaft to produce power. This results in the kinetic energy of the wind being converted into electricity.

Most wind turbines have three blades, and their length varies generally between 30 to 60m (in the future blades are expected to reach 100m long). The weight of blades depends on the size and the design material of the blades. Current WTBs are of specific interest from an engineering point of view, due to the complexity of their structures. They are typically fabricated from glass/carbon fibre reinforced plastics (G/CFRP) supported by lightweight materials such as wood or plastic foam. This is due to cost and weight issues as well as the high strength, stiffness, modulus, corrosion resistance, and excellent fatigue performance of G/CFRP in contrast to other materials [41, 42]. This makes the WTB a complicated and non-homogeneous structure, resulting in variable thickness, a multi-layered structure, and arbitrary curved surfaces (of the spar cap, and leading and trailing edges and so on) [43] as illustrated in Figure 8.

WTBs are essential components of wind power systems and one of the most expensive components to maintain, representing 15-20% of the overall cost [1, 44]. They also require long time to repair in particular OWTBs. These blades are complex in section and rotate in extreme environments and under varying wind loading conditions, for example icy condition, bird and lightning strikes, and wind gusts. Such environments may lead to changes in the structure of the blades' materials or their structural geometric properties,



which can cause failure and adversely affect performance. Failure of the blade can cause damage to the overall wind turbine structure as a result of rotational imbalance [1, 18, 19]. Therefore, the detection and identification of abnormal changes in the structure of the blade, preferably in early stages, allows necessary repairs to take place promptly before the blade breaks.

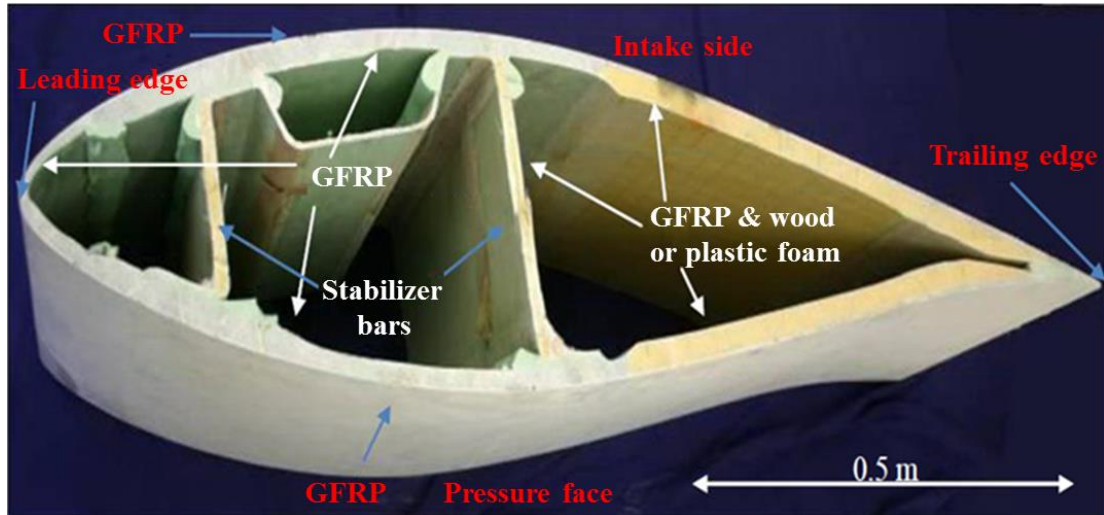


Figure 8: Cross section of a WTB showing its main parts and their variable thicknesses [43].

## 2.2 Failure Models for Wind Turbine Blades

Changes in the structure of WTB materials or geometric structural properties are defined as damage, which represents changes in boundary conditions and system connectivities [1]. Such damage can be caused by different factors. For instance, in engineering systems, most materials have some inherent initial flaws or defects which tend to grow if these materials are continuously used under environmental and operational loading. Such damage can negatively affect blade performance rather than system functionality and, as the damage increases, it will reach a point at which system operation is affected, so that results which no longer acceptable are obtained. This point is referred to as a failure [45].

Failures of WTB can also be caused by other reasons as depicted in Figure 9. These include icy condition, lightning strikes, fatigue cycles, wind gusts, thermal stress, moisture absorption, and bird strikes [1, 46, 47]. In wind farms, the interaction of aerodynamic factors between groups of wind turbines may lead to unpredictable and excessive loads on the blades. In addition, major failures of composite blades, such as GFRP and

CFRP, are caused by impact damage [48]. Such harsh environment and loads can also result in the production of different failure models, as shown in Figure 9. In the following sections, some of the common types of failure of WTBs are discussed briefly. These are related to stress waves which cause audible sound.

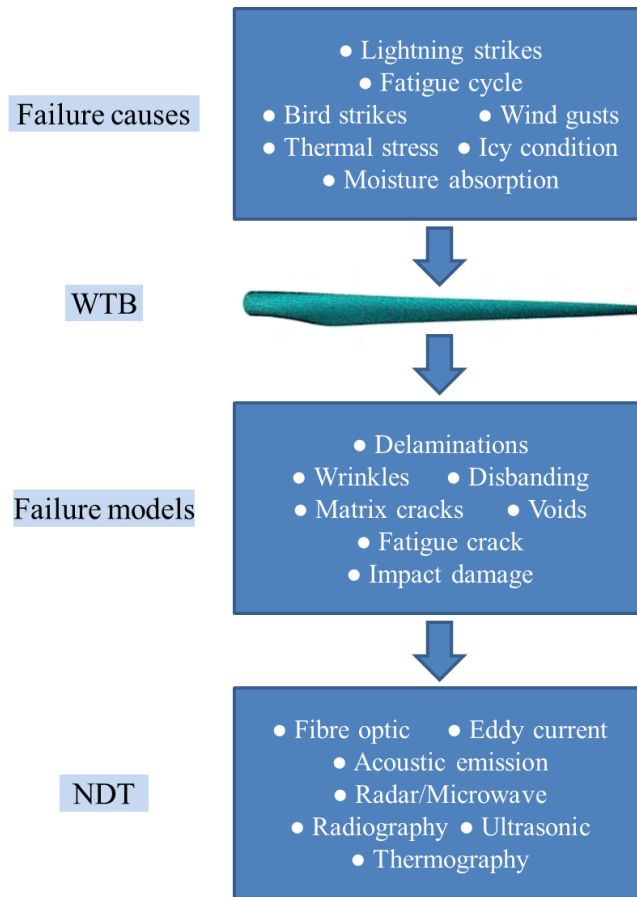


Figure 9: Failure causes and models of WTB and inspection techniques.

### 2.2.1 Impact Damage

Current WTBs are typically manufactured from fibre-reinforced composite material. These blades are placed in outdoor environments, which make them subject to accidental impact by different objects, such as tools, bird strikes, or strong hail. The effects of such causes might not be visible; however, they may lead to minor subsurface damage, including delamination, fibre breakage, debonding, and matrix micro-cracking, which may then lead to significant reductions in the compressive strength and stiffness of the composites [49]. These types of failure may increase and becomes serious as the blades are placed under load [50]. Figure 10 shows scanning electron microscopy (SEM) images of failure modes during tensile tests on twelve-layer GFRPs laminates

[51]. These failure modes might have different shapes according to the thickness and type of composite materials, as shown in Figure 11.

Composite materials have also been studied for the effects of different velocities of impact, which are classified into low-velocity, high-velocity, and hyper velocity [49]. Due to the extensive use of these materials in different areas, such as blade manufacture, aerospace, and others, many researchers have investigated the effect of impacts on such materials [49, 50, 52, 53]. To assess and inspect impact damage, different NDT techniques are available, for instance ultrasonic [54], AE [55], and X-ray radiography [56]. For more information about impact damage and NDT techniques used refer to Abrate [52].

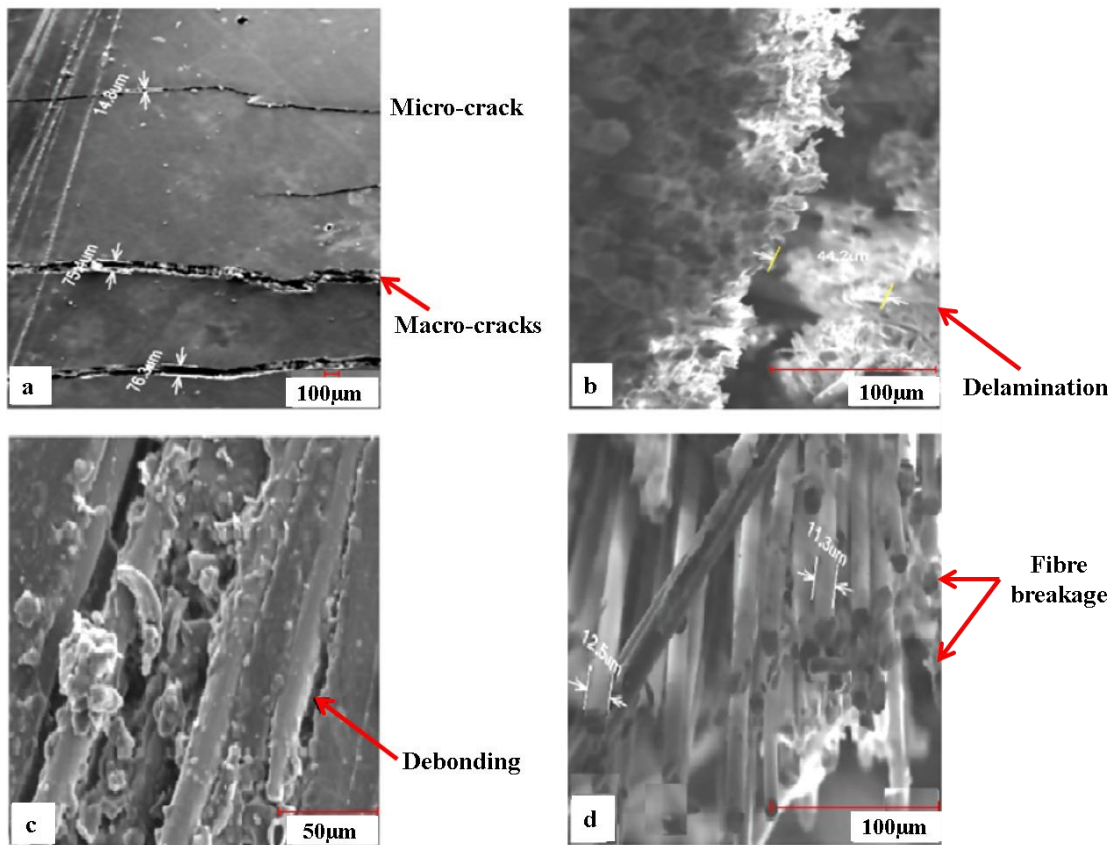


Figure 10: SEM images of failure modes on twelve-layer GFRPs laminates: (a) Matrix micro-cracking and macro-cracking, (b) Delamination (c) Fibre-matrix interface debonding (d) Fibre breakage [51].

### 2.2.2 Delamination

Delamination is a separation between plies and one of the most serious failure issues in WTB structures [57, 58]. This type of failure is undetectable through visual inspection

as it is sub-surface damage as shown in Figure 10 and Figure 11. It can also occur at several interfaces of the composite material, causing multiple delaminations. This type of failure can take place in several situations as a result either of manufacturing inconsistencies, maintenance and repair, or as a consequence of accidental impacts of foreign objects or due to severe loads, and the size of the delaminated area is proportional to the energy produced by these causes.

Such types of failures can also lead to a significant degradation in the compressive strength and stiffness of the composite component [48, 59]. Thus, robust NDT techniques are required to detect and characterise them during both: the manufacturing and employment of the composite components so that their safe operation will be ensured.

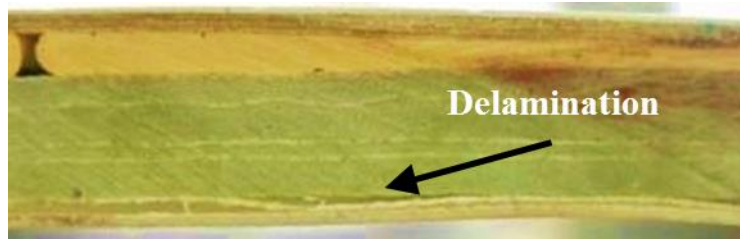


Figure 11: Delamination damage to WTG driven by a buckling load [21].

A range of specific techniques are utilised or are under development which can be used to detect or study the effect of such failures [42, 60]. Other methods are also used for the detection of delamination, such as those based on AE [61] and pulsed eddy current (PEC) thermography [48].

### 2.2.3 *Fatigue Crack*

WTBs are placed in outdoor environments which leads them to be regularly subject to varying wind loads. In particular, wind gusts and wind shear cause variations in load which may result in breaking the blade. This type of damage is known as fatigue crack and it is usually expressed as the number of repeated loading cycles needed to initiate a fatigue crack which then grows until reaching a critical size [62].

Therefore, careful blade fatigue tests are conducted by several national laboratories, for instance, the National Renewable Energy Laboratory (NREL); USA, the National Renewable Energy Centre (NAREC); UK, and others as mentioned in Section 2.3, in order to help validate and enhance the design and manufacturing of the blades [63, 64], so that the fatigue lifetime extended. Such tests are performed by applying a number of load

cycles and in each time the load is increased until the blade fails. The collected data is plotted in an S-N curve, which is defined as stress (S) against the number of cycles to failure (N).

During fatigue tests, SHM and relevant NDT techniques are utilised to assess the blade structure [65, 66]. The electrical potential technique is also used to characterise impact damage in carbon fibre composite materials [67]. In the following sections, the state-of-the-art approaches employed for blade health assessment and monitoring are discussed.

### **2.3 State-of-the-Art Techniques for SHM of WTBs**

Generally, the SHM is a recent developed technology that is defined as a method to reduce O&M costs and improve the safety and reliability of structures. This is performed by incorporating distributed sensors into the structure in order to provide continuous health monitoring, and detection of damage in this structure with minimal human interaction. Figure 12 shows the main parts of a smart SHM system. The first part involves the utilised smart materials and sensors which can be, for instance, either AE, ultrasonic, fibre optic, vibration or any other combinations. Such sensors are used to sense the structural health of the structure and need be connected with a suitable data acquisition (DAQ) system. Acquired data are then transferred to a collection point via a sensor network which can be either wired or wireless based on the nature of the sensor technique used. Data are collected at the central unit in order to be processed and analysed either off-line or online. Finally, based on the results of these analyses a decision for Go/No-Go will be taken.

Such an emerging technology has worldwide attracted a considerable number of scientific institutions and national laboratories in different areas. For instance, civil infrastructure such as bridge, dam, and building [68] and in aerospace vehicles [69]. The Structures and Composites Laboratory in Stanford's department of Aeronautics and Astronautics [70] as well as Key Lab for Smart Materials and Structures in Nanjing University of Aeronautics and Astronautics which give their attention to aerospace application.

The SHM systems have also an important role for WTBs in terms of reducing O&M costs and increasing reliability of wind turbines, particularly in the offshore industry [3,

14, 71]. Thus, SHM become an active research field since the appropriate methods could also provide critical *in-situ* information about faults in WTBs at the early stage as well as predicting the future failure of subcomponents and also providing information about the causes, types, and the locations of failure [72]. The overall significance of SHM for the OWT industry has been discussed above in Chapter 1.

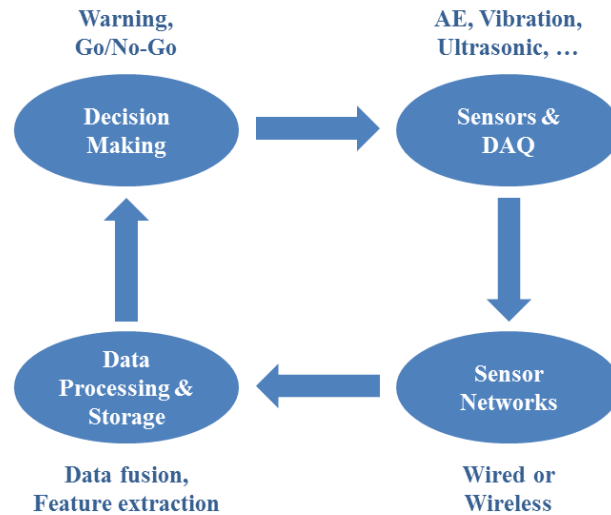


Figure 12: A block-diagram of a smart structural health monitoring system.

A large number of SHM methods are used in wind power systems [1, 3, 15, 19-21]. The SCADA (Supervisory Control And Data Acquisition) system is one of these approaches which is utilised as a global technique since it is based on the general parameters of the wind turbine system available in the control system [73]. It also provides full remote control and supervision of both the wind farm as a whole and individual wind turbines, as shown in Figure 13. The advantage of the SCADA approach is that no additional hardware is required. However, the information obtained is general and does not reflect the exact condition of specific wind turbine components.

In contrast, subsystems or components approaches are based on monitoring the health of the individual components of wind turbines and are able to provide more accurate information about the condition of each component. However, such approaches require more sensors and generate enormous amounts of data, both of which add complexity to the monitoring system. The majority of these methods are classified as certification tests and they are conducted by scientific institutions and wind turbine manufacturers as well as national laboratories, including the NREL, Sandia National Laboratory (SNL); USA, NASA Kennedy Space Centre; USA, Purdue University; USA, Virginia Tech; USA;

USA and NAREC. In particular, the Danish wind turbine industry is a world leader in the commercialisation of this technology.

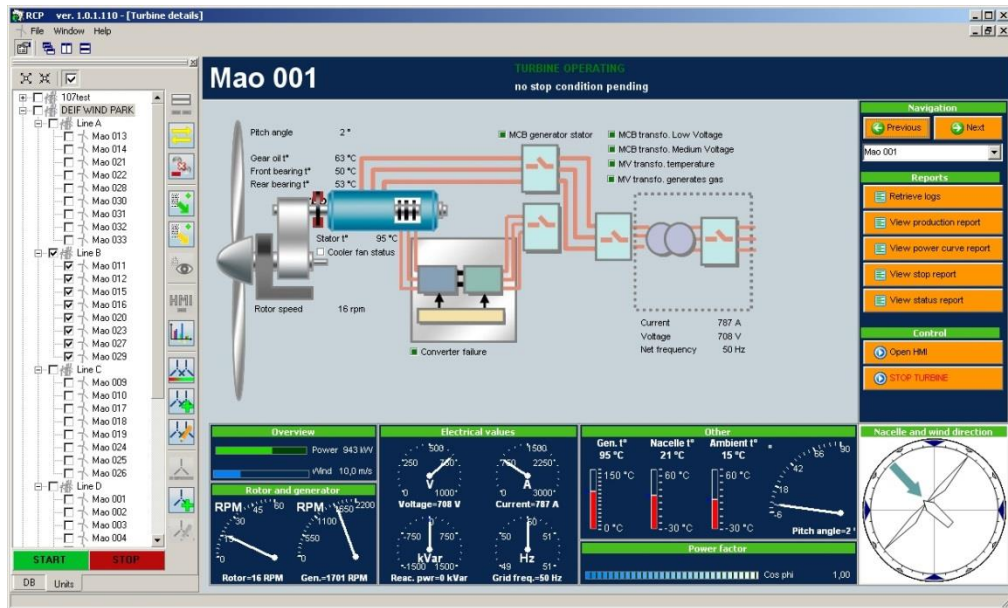


Figure 13: Wind farm SCADA system [74].

These techniques can be grouped into active or passive methods depending on the operational strategy used, as illustrated in Figure 14. In active inspection systems, the sensors first require external excitation to be applied to the structure and a response caused by this event is then measured and evaluated [75, 76]. In contrast, passive inspection approaches differ from active systems in the sense that no external excitation is needed and relevant events are usually caused by changes within the material due to, for example, external loads or incipient damage, as AE based SHM [65].

In the use of such techniques it is specified that laboratory testing must be conducted for the purpose of postproduction inspection prior to blade fitting [1, 3, 15, 19-21, 77]. A recent review [78, 79] surveys the current technologies used for testing, inspecting, and monitoring WTBs and composite materials. These include mechanical property testing, NDT, full-scale testing, SHM and condition monitoring. In the following sections, summaries are presented of SHM and relevant NDT techniques which may have promising application to WTBs. These include ultrasonic, AE, fibre optic, thermography and X-ray CT techniques. To date, the first two of these methods have been extensively used in SHM applications and, according to many literature reviews, they have the potential to perform well for online or off-line inspection techniques [78]. Due to the small vol-

ume of fibre optic sensors, it is possible to integrate them within the blade structure in order to construct ‘smart blades’. Thermography and radiography, meanwhile, have the advantage of enabling inspection of large areas in a short time. A more detailed comparison of these methods is given in Section 2.3.7.

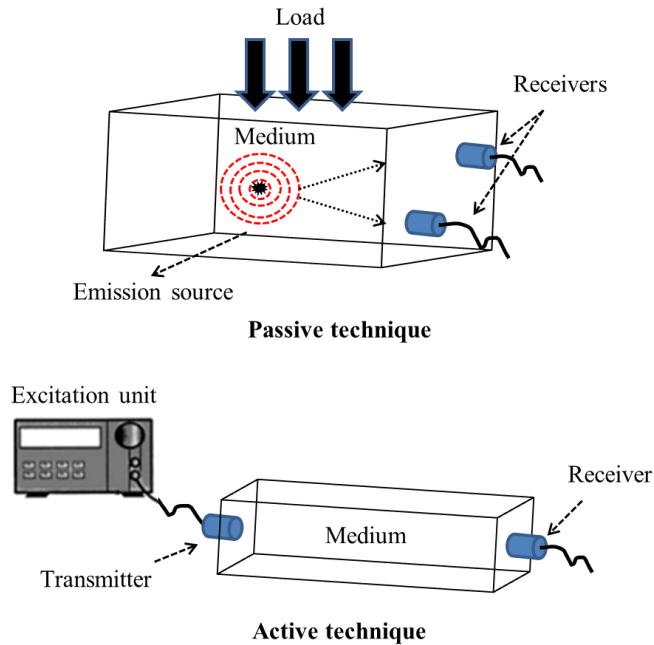


Figure 14: Active and passive techniques.

### 2.3.1 Ultrasonic Technique

The ultrasonic technique (UT) is an active approach used to inspect different solid objects. The main principle of this method is based on sending an excitation signal into a test specimen through a couplant, which is usually liquid or air, using an ultrasonic transmitter. The signal generated will propagate in the material and it be reflected at the back wall of the object or at any discontinuity of an acoustic property of the material inspected, such as flaws.

There are two different modes which can be used to pick up the reflected waveforms; reflection (or pulse-echo) and attenuation (or pitch-catch). In the former mode, the reflected waves are recorded using the same transmitter; whereas in the latter, a separate transducer known as a receiver is utilised to detect the propagated waves that have reached it. Imperfections or other conditions existing in the specimen affect the propagated waves, thus revealing their presence. The pulse echo method is limited to a penetration range from the outer surface, since only a single side access is available, whereas



this is not the case with the pitch-catch method and hence it is more sensitive to the waves propagated.

Since 1999, low frequency ultrasound NDE based on guided wave propagation has become a successful technique in commercial and industrial environments [80]. In this method, mechanical stress waves are guided by its boundaries and propagated along an elongated structure. This has the advantage that the waves travel a long distance with little loss in energy due to the employment of very low ultrasonic frequencies compared to the traditional UT. This is performed by using a single ultrasonic transducer or the deployment of transducers in the form of arrays to transmit and receive guided waves in rail and pipeline applications [81, 82]. This has the advantages of the rapid screening of these objects and allows them to be inspected even with limited access points [83]. However, the interpretation of ultrasonic collected data is highly operator dependent. The ultrasonic guided wave has also become a widespread approach used in most oil-gas companies [84] and the rail [85] and the aviation sectors [86], among others.

Recently, the ultrasonic guided wave has been applied to SHM where ultrasonic transducers can be permanently attached to a structure and the health monitoring process achieved either on demand or continuously [87]. The wind turbine industry is an example of a sector where ultrasonic guided wave is utilised, particularly for the towers and blades of wind turbines. TWI [88] is one of the leading UK companies which has worked in this area along with universities and other industrial partners to develop new approaches for SHM based on ultrasonic guided wave, such as in the IINSIGHT project [89] and HEMOW [7].

In addition, many academic institutions have used this technology for development and research purposes. For instance, Jasiūnienė et al. [90] employed a pulse-echo immersion technique to inspect a GFRP wind turbine blade. Dr. Drinkwater from Bristol University, UK, and his team have used ultrasonic arrays for the imaging of composite material in order to detect small defects in thick sections of such material [91]. Satito and Kimpara [92] have used both ultrasonic scanning devices and optical cross-sectional observations to reconstruct impact damage within CFRP laminates. Ultrasonic guided wave beam-forming has also been utilised to monitor the health of the structure of composite laminates [93].

Nevertheless, the UT is challenged by the high attenuation of sound waves in composite materials. The use of couplant-based transducers may increase the efficiency of the UT system. This coupling is in most cases water as in [94], but also it causes a challenge in field tests, particularly for WTBs. Air-coupled ultrasonic transducers could solve this problem [95]. However, this is strictly dependent on setting the correct incident angle in order to control mode purity, which is specifically required for composite materials in order to improve the signal to noise ratio (SNR) and simplify data processing compared to signals obtained with mixed mode excitation. Moreover, a large impedance mismatch between air/solid couplings may cause a poor coupling of energy from the transmitter to the sample. Finally, having a conventional excitation unit as, in the above mentioned studies is uneconomical and impractical for use in SHM systems for WTBs due to their large size and mass as well as complex geometry.

A another variation of the ultrasonic method known as acoustic wave-field imaging (AWI) has been proposed [96], in which a sparse array of ultrasonic transmitters is embedded within the component. The acoustic waves generated by exciting these transducers travel through the structure. An air-coupled receiver is employed to scan the overall surface of the sample in order to image it. In an alternative to this scheme which overcomes the limitations of air-coupling, a laser interferometric sensor can be used to perform the scan process. If the ultrasonic receivers are embedded in the structure, then laser ultrasonics will have the potential to realise the ultrasonic pitch-catch mode [97-99].

However, the techniques discussed above still face challenges if they are intended to be applied to OWTs. This is due to the harsh environment of offshore wind farms as well as the rotation of the WTBs which will make the employment of the laser ultrasonic or the laser interferometric sensors in the *in-situ* SHM systems difficult. In addition, the wind itself provides inconvenient conditions. Such techniques also require scanning the overall structure which will generate huge amounts of data. This is far from ideal in such monitoring systems. Furthermore, the inspection process would take a long time and would be limited to surface defects which may be affected by the purity of the surface. Therefore, the UT is not selected in this research for the implementation of the *in-situ* SHM system where sources of ambient excitation are needed.

### 2.3.2 *Acoustic Emission*

AE is a passive method and one of the most common and sensitive NDT methods used in SHM systems. In this technique the radiation of mechanical stress waves within the material generated due to flaws or the degradation of material is used to detect and identify the fingerprints of the main possible sources [31, 79]. The radiation of these stress waves can be caused either by applying an external load or by ambient loading. More discussion concerning the principles of this technique can be found in Chapter 5.

AE is a well-established method which has been utilised in several applications, particularly research into NDT and SHM methods [100]. These include monitoring engine oil viscosity [101], failure identification and characterisation in composite materials [51, 61] and in WTBs [102], and conducting the qualification testing of WTBs [24]. AE has also been used to study the damage mechanisms occurring in self-reinforced polyethylene composites [103]. Tests have revealed that the AE technique is able to identify cracks which generate audible sound, provided that pattern recognition software is used to evaluate this type of damage. AE techniques have also been applied in damage localisation not only in metallic or, concrete structures but also in composites [104, 105]. AE has also been combined with ultrasonic transmission in order to track information about the location and the structural health of composite materials [106]. It has also been shown that the AE method can be used to monitor the health structural of bridges [107].

The widespread use of this technique in different applications is most likely due to the following advantages. Based on a material's structure the AE method can provide a monitoring technique for large structures with limited access and only a few AE sensors, which is a significant advantage for field tests. However, for complex structures such as WTBs more AE sensors may be required [104]. AE methods also possess the advantage of locating the source of AE-related defects on the structure without the need to scan the whole structure [108].

Compared to other NDT methods, this technique offers potential sensitivity and its effectiveness depends less on the orientation of the defect [79]. It can also be used to discriminate between different AE events occurring during the inspection process. Since AE is a passive approach, it is possible to develop a long-term field inspection system running under ambient loading which can also provide the time and place of event oc-

currence. Other strengths of AE methods are discussed in Chapter 5.

However, the major challenge faced when using AE techniques is that sound waves are highly attenuated in composite materials. This challenge could be overcome by deploying more AE sensors in locations likely to suffer damage and fewer sensors in other locations. In addition, the AE source is a non-repeatable event and such an event is not generated unless an external load is applied to the structure. This means that the averaging method, which is usually applied to eliminate incoherent noise in the data, is inapplicable in this case [80]. However, for applications such as the monitoring of the health of OWTB structure these challenges would be uncritical, because WTBs run under various different environment loads such as those caused by wind which lead AE events to be repeatable and therefore the effect of noise can be minimised. AE sensors are large; however, using micro-electro-mechanical systems (MEMS) technology may reduce the size and weight of these sensors.

It is also claimed that the AE approach cannot operate on-demand or continuously. Nevertheless, this can be seen as an advantage for SHM systems for OWTBs. The reason for this is that leaving the SHM system to run continuously will produce huge amounts of data which will overload the storage and processing mechanisms of the monitoring system. Finally, the AE technique is very costly due to the high sampling rates required to capture AE events, and therefore the overall cost of the SHM system will increase [39, 109]. The last two challenges have been identified as a research problem and are taken into the consideration in this research during the implementation of the proposed SHM system for OWTBs.

### ***2.3.3 Fibre Optic Method***

Fibre optic methods are extensively used in communications technology and have recently been utilised in SHM applications in various forms. The main principle of this technique is based on the embedding or attaching of fibre optic sensors within or on the structure without the need to embed electrical devices. Then the optical fibre will act as a waveguide through which the optical power of a light source propagates. The propagation of such light is linearly affected by the load applied to the structure. By increasing this load the structure may encounter a sudden break. In this case, the light will be dramatically destroyed. Thus, such techniques can be used as an indicator to reflect the

condition of the structure [1, 110].

Fibre optic techniques have been demonstrated in a variety of applications using the different forms of optical fibres which have been developed over time [1, 111]. These include SHM in civil infrastructure such as bridges, offshore platforms [112], and marine structures [113], the dynamic and static testing of WTB performance under load [114], and blade tip deflection [115]. The fibre optic approach has been also used to study the influence of delamination on the resonance frequencies of composite material [116] as well as in damage detection [117]. The widespread employment of fiber optic methods is due to their many advantages such as flexibility and small sensor size, high multiplexing capabilities, immunity to electromagnetic interference, the fact that no signal attenuation occurs over long distances, and high sensitivity [118, 119].

However, fiber optic sensors are limited due to their susceptibility to physical damage, special test equipment is often required, and they are as yet unavailable as highly cost effective systems [120]. The fiber optic method cannot provide extra information about flaws.

### ***2.3.4 Thermography Technique***

Thermography or thermal imaging method is a non-contact NDT technique. The main principles of this method are based on capturing the thermal radiation emitted, which its amount increases with temperature, by all objects above absolute zero [121]. It has the advantage of the possible coverage of large areas in one scan without the need of interaction with the sample, and therefore inspection time is significantly minimised [122]. This makes thermography an interesting technique in the NDT and SHM fields, particularly for composite materials in which multi-layer structures exist and classic NDT techniques cannot be used to inspect them. This is because variations in the thermodynamic properties of the object due to internal or external stimuli generate surface temperature patterns which can be imaged using an infrared imaging system.

Thermography methods fall generally into two categories. In passive methods the material inspected emits infrared radiation due to the broadband sources of ambient excitation applied, whereas in active methods an external stimulus is required in order to produce a thermal gradient [79, 121]. Typical applications of both types of thermography can be found not only in NDT but also in medical, security, and military sectors, in in-

dustry such as chemicals manufacture, and in civil and mechanical engineering, and many other areas [123]. It has also been applied in damage monitoring in composites [124] as well as for the detection of cracks in objects with complex shaped such as WTBs [25].

In active thermography, different methods can be used to provide an external stimulus in order to produce a temperature flow, such as laser, flash lights, ultrasonic waves, and eddy current. Therefore, different types of thermography have been developed that can also be used to inspect composite materials; namely, flash thermography [125], sonic thermography [126], laser thermography [127], and eddy current pulsed thermography [128].

Such techniques have the advantage that they can be used in remote sensing techniques where inspection can be done metres away from the objects. They also provide full coverage of large areas in a short time. However, the lightning protection mesh present in some composite materials may mask the radiation emitted. These techniques are also more sensitive to defects on or near surface [79]. In addition, these methods are mostly applied for in-house inspection rather than in the field due to portability and cost issues which make them impractical for OWTBs.

### ***2.3.5 Radiographic Inspection***

Radiography is another NDT remote sensing technique that provides the possibility of the inspection and evaluation of objects without requiring physical contact. This is achieved by bombarding the object under test with X-rays or gamma rays, which are the most common forms of radiation [79]. The basic principle of this technique is the fact that materials have different radiation absorption properties and once a sample is penetrated by a beam, an image can be constructed by a detector which identifies the properties of this sample [129]. This will also reflect changes in either the density or thickness of the sample as well as signs of flaws.

However, the radiography method is sensitive to the orientation of flaws and cannot provide additional depth information. Such limitations have been overcome by using computed radiography (CR). This is similar to traditional radiography; however, it allows 2D and 3D cross-sectional images of an object to be generated from traditional X-ray images by rotating the sample around one axis [130]. The resulting data are then

used to construct 2D and 3D images of the object, thus delivering the additional information which would otherwise be missed.

Both techniques have been applied in several applications, including in the medical [131] and military [132] fields, in SHM for WTBs [133] and NDT as well as for composites [79, 134]. The widespread application of radiography approaches is due to the following advantages. They can inspect different types of material and thicker sections as well as produce better resolution in comparison to the ultrasonic technique because the wave-length of X-rays is significantly shorter [79, 129]. Furthermore, they require the minimum of preparation of the surface.

On the other hand, the radiography method cannot provide extra information about flaws unless CR is used, which increases the total cost both in terms of time and money. These techniques require access to both sides of the object, which may be impossible in field applications, particularly for OWTs. The next section surveys and discusses the most relevant *in-situ* SHM systems developed for WTBs.

### **2.3.6 Relevant Work on *in-situ* SHM Systems for WTBs**

Most of the above-mentioned NDT methods are well established and are suitable when conducting laboratory tests or qualification blade inspections. However, few attempts have been made to utilise them in field monitoring of the structural health of WTBs. Since the main topic of this research is the implementation of an *in-situ* SHM technique for OWTBs, this section briefly surveys the most recent and relevant SHM techniques employed for such an intention.

In-field (*in-situ*) SHM approaches for OWTBs play an important role, since they can detect faults at the time of occurrence, while wind turbines are in operation and therefore appropriate action can be taken in time to prevent the occurrence of any further damage or failure. These techniques are either stationary or dynamic in-service methods. Stationary testing means that the inspection process is completed while the blades are static, whereas in dynamic testing the inspection process is realised as the blades rotate while in-service.

Recently, there have been some attempts to extend laboratory methods to be realised as *in-situ* monitoring systems for both static and dynamic tests. One such attempt [24] is

illustrated in Figure 15-a. In this approach, an AE technique (AET) in conjunction with a “load and hold” principle was applied to a WTB. The results show the possibility of applying this method to static in-field inspection. However, it is time-consuming, difficult to implement for OWTs, and it alters the components since it needs to be repeated many times.

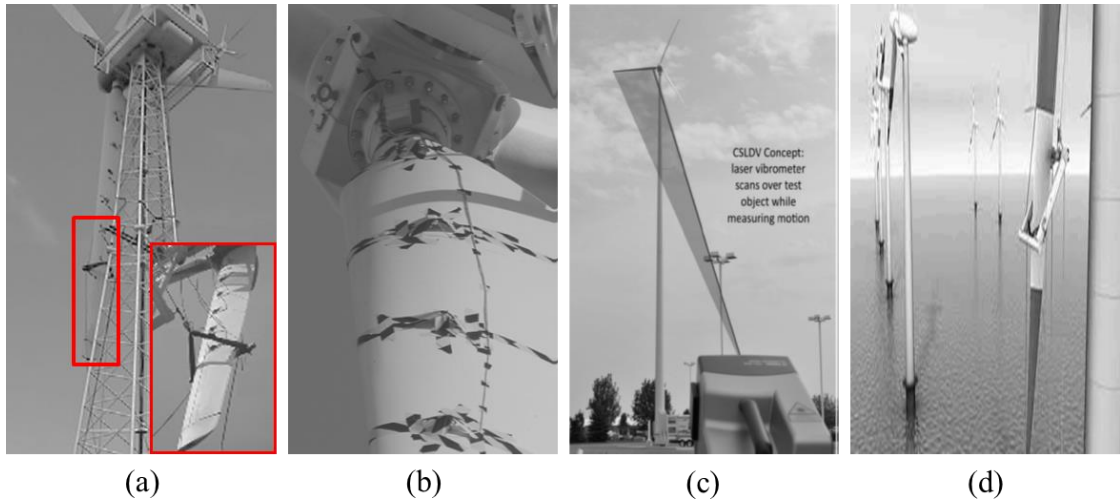


Figure 15: *In-situ* tests: a, b) AET [24], c) Laser vibrometer [5] and d) Robot inspector [29].

To overcome the drawback of overloading the wind turbine components, the authors proposed the use of AET in conjunction with WSNs, as shown in Figure 15-b. AE sensors were employed in this prototype mounted span-wise along the blade which was left under wind load during its rotation. The effectiveness of the prototype; however, was affected by noise produced due to the way the sensor was attached to the external surface of the blade.

More recently, a continuous-scan laser Doppler vibrometry (CSLDV) method has been proposed for the static inspection of WTBs [5]. Figure 15-c shows the idea behind this approach, which employs a laser vibrometer to measure the natural frequencies and mode shapes of the first several modes of the WTB. The WTB was excited by ambient wind.. In this method, a retro-reflective tape was applied on the blades in order to enhance the SNR; however, the blade’s curvature and movement affect the reflectivity at some points [46, 135].

A long distance laser ultrasonic propagation imaging system has been proposed [22] to mitigate the challenges of applying the CSLDV method via the integration of AET and



laser ultrasonic. AE sensors and ultrasonic receivers are embedded in locations likely to suffer damage. Once the AE sensor detects a failure event, a laser beam generated by a portable long distance ultrasonic propagation imaging system installed in the wind turbine tower is directed to that position for further scanning. However, the proposed wired embedded sensors and the portability of the laser ultrasonic system are still challenges, especially for offshore applications.

The same author then conducted a feasibility study [135] using a laser displacement sensor (LDS) for *in-situ* blade deflection monitoring. Another approach proposed for remotely monitoring the dynamics of WTBs uses laser interferometry [136]. However, although these proposed techniques tackle important problems in wind turbines, they are still incapable of delivering enough information about the overall structural health of the blades. In addition, these techniques require the surface of the blade to be clean and thus it would be a challenge to apply them to OWTBs, especially in extreme weather conditions, since they need to be supervised by operators.

An advanced climbing robot shown in Figure 15–d has also been proposed [29]. This approach has the advantage that it involves advanced techniques for more precise inspections. However, the cost is high and the inspection procedures must be conducted at regular intervals as well as taking a long time. Passive and active thermography technique have also been applied to inspect WTB, in the field [25], and the results show potentially effective performance in the detection of different defects. Another advanced approach for a dynamic WTB field inspection system is based on a frequency modulated continuous wave (FRCW) radar system [30]. This system uses a novel approach; however, it is still far from being a commercially viable system and it will be an expensive and time-consuming approach if it is intended to be applied to OWTBs.

So far, some of the *in-situ* techniques discussed above show clear potential for WTB inspection. Nevertheless, these techniques may be costly, time-consuming, rely on regular inspection intervals or their performance is degraded by poor SNRs. Most importantly, they also need to be supervised by an operator. Therefore, these approaches are impractical for OWTBs.

In addition, remote sensing or wireless inspection techniques would seem to be the optimum solution for such applications in order to provide online testing and inspection.

The main reasons for this are that a greater number of wind farms are being placed in more remote areas, and the size of OWTs has become physically larger. These factors make their transport and reaching them for inspection very difficult. Thus, the selection of suitable techniques and the integration of several different technologies are nowadays very important in order to develop a robust continuous online SHM system [19].

**2.3.7 Comparison of NDT Methods used in SHM for WTBs**

This section provides a short summary of the strengths and weaknesses of the NDT techniques discussed above and as shown in Table 2.

Table 2: Comparison of NDT techniques used in SHM for WTBs [1, 3, 15, 19-21, 77, 115, 119, 120].

NDT technique	Advantage	Disadvantage
Ultrasonic	<ul style="list-style-type: none"> <li>• High sensitivity</li> <li>• Detection of surface and subseries flaws</li> <li>• Depth information</li> <li>• Reproducible of flaw detection</li> <li>• Possibility of mode purity</li> <li>• Low complexity of signals</li> <li>• On-demand inspection</li> </ul>	<ul style="list-style-type: none"> <li>• Couplants are needed</li> <li>• Extensive technical knowledge is required</li> <li>• Surface preparation</li> <li>• Difficulties in inspecting irregular shapes</li> <li>• High penetrating power</li> <li>• Baseline</li> <li>• Relies on regular inspection intervals</li> <li>• Time consuming</li> <li>• Short-term field inspection</li> <li>• Supervision is needed</li> <li>• High signal attenuation</li> </ul>
Acoustic Emission	<ul style="list-style-type: none"> <li>• High sensitivity</li> <li>• Real time detection and high SNR</li> <li>• Defect localisation</li> <li>• Able to detect at an early-stage faults</li> <li>• Passive and in service inspection</li> <li>• Capable of portable or highly automated operation</li> <li>• No Couplants are required</li> <li>• Adaptable with WSN</li> <li>• No supervision is needed</li> <li>• Frequency range far from load perturbation</li> <li>• Long-term field inspection</li> <li>• No need to disassemble and clean a specimen</li> <li>• Few access points are required</li> </ul>	<ul style="list-style-type: none"> <li>• Non-repeatable event</li> <li>• Event based</li> <li>• Very high sampling rate required</li> <li>• No quantitative results about size and depth</li> <li>• High signal attenuation</li> </ul>
Fibre optics	<ul style="list-style-type: none"> <li>• High sensitivity</li> <li>• No attenuation over long distances</li> </ul>	<ul style="list-style-type: none"> <li>• Impractical for large wind farms</li> <li>• Requires extreme care for safe</li> </ul>

	<ul style="list-style-type: none"> <li>• Small size and light weight</li> <li>• High multiplexing capabilities</li> <li>• Immunity to electromagnetic interference</li> </ul>	<ul style="list-style-type: none"> <li>• installation</li> <li>• Susceptibility to physical damage</li> <li>• Thermal sensitivity</li> </ul>
Thermography	<ul style="list-style-type: none"> <li>• Large scale inspection</li> <li>• Full-coverage in short time</li> <li>• Can be used for inaccessible areas</li> <li>• Single side access is required</li> <li>• No specific safety required</li> </ul>	<ul style="list-style-type: none"> <li>• Limited to on or near surface flaws</li> <li>• Manual operation and expensive</li> <li>• Difficult to use on rotating blades</li> <li>• Difficult to detect interior damage</li> <li>• Relies on regular inspection intervals</li> <li>• Short-term field inspection</li> <li>• Supervision is needed</li> <li>• CR is a high computational cost method</li> </ul>
Radiography	<ul style="list-style-type: none"> <li>• Depth information</li> <li>• Suitable for complex structures and different material</li> <li>• Large scale inspection</li> <li>• Full-coverage in short time</li> <li>• 2D and 3D images</li> <li>• Good contrast sensitivity</li> </ul>	<ul style="list-style-type: none"> <li>• Manual operation</li> <li>• Double sides access are required</li> <li>• Expensive</li> <li>• Difficult to use on rotating blades</li> <li>• Health risks</li> <li>• Rely on regular inspection intervals</li> <li>• Short-term field inspection</li> <li>• Supervision is needed</li> </ul>

### 2.3.8 Choice of Appropriate NDT Technique for SHM for OWTBs

SHM systems for OWTBs play a pivotal role not only in the prevention of serious accidents and catastrophes but also in minimising the cost of O&M [15]. To achieve these objectives, an NDT technique should be appropriately selected in order to provide an efficient and reliable fault prediction system which gives early warnings of blade defects and may prevent major component failures. This is particularly important for OWTBs where prompt repair means that breakdown is avoided, minimising both downtime and maintenance costs as well as prolonging the lifetime of OWTs [77].

This section therefore provides guidelines for the choice or development of a suitable SHM method for OWTBs. Nevertheless, the significant challenges which face the implementation as well as the integration of any existing or future development of SHM methods for OWTBs are first reviewed.

#### 2.3.8.1 Challenges Faced by SHM Techniques for OWTBs

Placing wind farms in remote areas such as offshore environments leads to several challenges in the development of a suitable SHM technique for OWTBs. Some of these challenges have been listed in Chapter 1. Nonetheless, they are briefly reviewed here in

order to assist in providing criteria for the selection of the most appropriate inspection and monitoring technique for SHM application, as discussed in the next section.

Offshore wind farms are located in remote areas where enormous expense may be involved in reaching them, particularly in harsh environments with for example extreme weather conditions, wind gusts, and lightning. Besides that, the large scale and structural complexity of WTBs as well as their rotation under dynamic loads make the adoption of existing wired SHM approaches in such structure impossible. Offshore wind farms normally comprise of several wind turbines, which makes the possibility of inspecting them regularly and under the supervision of operators or inspectors very time-consuming and expensive. Furthermore, the existence of several wind turbines per farm necessitates the use of low cost SHM techniques with hierarchical communication, signal processing and robust data management techniques for the purpose of data minimisation.

These factors guide the choices made in the development of an appropriate SHM technique for offshore wind turbines, as shown next.

### **2.3.8.2 Selection Criteria of an NDT Method for SHM**

In general, the development of a good SHM method for OWTBs depends on the sensor technology, the data acquisition technology, signal analysis and interpretation, and the hierarchical communication between the wind farm and the remote control room [1]. Understanding and optimising these concerns will help in tackling some of the challenges mentioned above. For example, the deployment of a large number of sensors results in immense amounts of data; therefore, special ways are required to pre-process such data, and to extract only the most meaningful information for delivering to the remote control room.

Therefore, based on the above discussion, an inspection method is required to continuously monitor the structural health of the blades and to warn of possible failure at an early stage. Based on the extensive literature review of NDT methods conducted above, the method employed or that developed in the future should satisfy the following conditions:

- The method should not be based on regular inspection intervals. This is because

the condition of blades between these intervals would remain unknown.

- Faults should be detected at an early stage. This is required to take prompt repair action before a catastrophic failure occurs.
- A passive technique should be used. This is due to the difficulties in employing excitation units due to the rotation of the blades. Besides, it is unnecessary to use such units, since the blades work under wind loads which are themselves enough to excite the structure.
- The development and installation costs of the method should be low, since it will need to be integrated into a large number of wind turbines.
- The method should have the ability to be integrated with WSNs, because wired solutions are impractical for such applications.
- The method should work as a stand-alone technique without any human-machine interaction (supervision) if possible. This is due to access costs and difficulties, particularly in extreme weather conditions.

Table 3: Important selection criteria of NDT method for SHM for OWTBs.

NDT technique	Selection criteria					
	Irregular intervals	Early detection	Low Cost	Passive mode	Adaptable with WSN	No supervision
AE	✓	✓	✓	✓	✓	✓
Ultrasonic	✗	✗	✓	✗	✗*	✗
Fibre optics	✓	✓	✗	✗	✗	✓
Radiography	✗	✗	✗	✗	✗	✗
Thermography	✗	✗	✗	✓	✗	✗

\*Challenge with excitation unit,

Table 3 summarises these criteria in relation to the above-discussed NDT methods. It is worth mentioning that the cost criterion is not specified here in terms of a specific value; but based on a comparison between the cost of an UT or AE system and a radiography system. The UT system may also be adaptable with WSNs; nevertheless, difficulties will occur with excitation units. Finally, as is clear from this table, the AE technique satisfies most of the requirements of SHM systems for OWTBs. Thus, the AE technique is selected in conjunction with WSNs in the development of a wireless SHM technique

to monitor the structural health of OWTBs. The rest of this literature survey pays attention to this type of integration and the challenges which emerge.

### **2.4 WSNs and Data Acquisition Techniques**

Based on the previous discussion, the AE technique can play a pivotal role in the design of an SHM system for OWTBs since it satisfies most of the criteria required for the development of such monitoring systems in offshore environments. One of these criteria was the possibility of the integration of this technology with WSNs which will open up new horizons for transforming wired SHM systems into wireless systems. However, the combination of the two technologies encounters various issues which need to be tackled first. These challenges are out of the scope of this chapter, having been discussed in Section 1.3 in conjunction with the definition of the WSN as well as in the studies which have been published [35-38].

In the context of the challenges highlighted so far, wireless sensor nodes are resource-constrained in terms of power supply, storage capacity, and processing capability. Thus, the utilisation of WSNs in SHM systems necessitates the efficient use of these resources, particularly of the power supply which is a crucial requirement for the individual sensor nodes. This can be achieved in different ways, as shown in Figure 16 [137]. Firstly, ‘duty cycling’ takes advantage of topology control or power management which focuses on putting the radio transceiver into sleep mode whenever no transmission is needed. Alternatively mobility-based techniques deploy a mobile sink or a service for message relaying, or data-driven approaches emphasise data reduction and the utilisation of efficient techniques for DAQ. The first two approaches are beyond the scope of this literature review; however, a more detailed review of these methods has been published [137].

The data-driven technique has been used in different projects which have dealt with WSNs in sensing acoustic signals. For example, Grosse et al. [138] presented a wireless SHM technique based on the detection of AE activity, where once an AE event is detected, the system starts to record and transmit whereas otherwise the acquisition process stops. In another study [139], AE signals are locally processed to estimate AE activity based on the “Hit-rate” or “Event-rate” exceeding a threshold value. Lédeczi and his team [140] also presented a wireless monitoring system for bridges based on AE

which used sleep/wake-up modes to save power and reduce data. In the following section, the data-driven technique is discussed in more details.

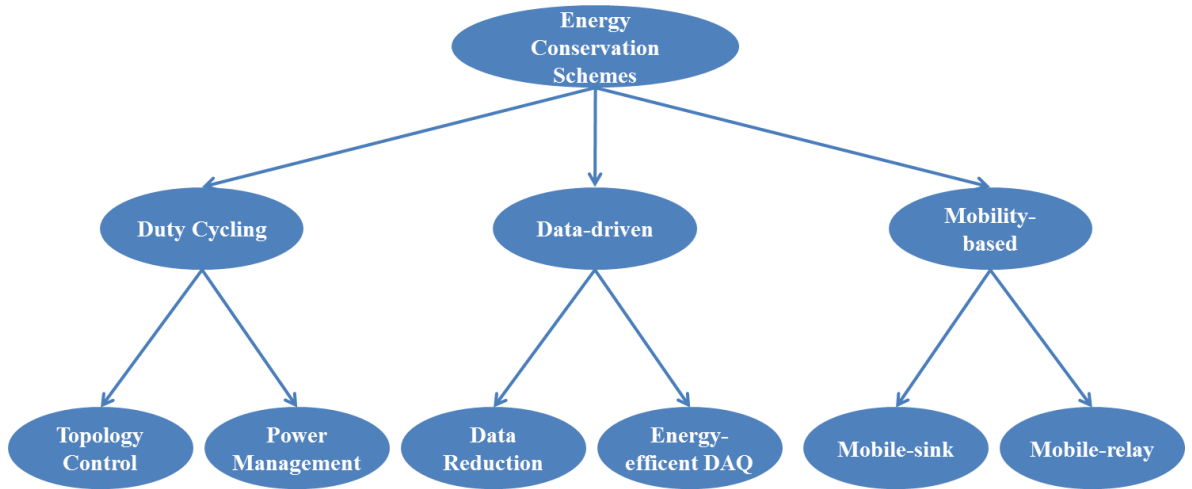


Figure 16: Taxonomy of approaches to energy saving in sensor networks [137].

#### 2.4.1 Data-driven Approaches and WSNs

Because data-driven approaches are more relevant to the topic of this study, they are considered further in this section. This type of method is categorised into two techniques which aim to reduce the amount of data transmitted by utilising two different principles, as shown in Figure 17 [137]. The first approach achieves data reduction via the local pre-processing of raw data on-board on wireless units, so that only the results of evaluation and other meaningful information are transmitted to the remote control room; these are distributed WSNs [141]. Here the radio frequency transceiver of the wireless sensor node is the most power-hungry part, whereas the local processing of data consumes much less energy [142, 143]. On the other hand, in data compression information encoded on-board is sent to the sink where it is decoded with the aim of removing redundancy in the information [144]. Finally, data prediction is based on describing the actual phenomenon sensed by a sensor node via the development of a specific model executed at the sink [145].

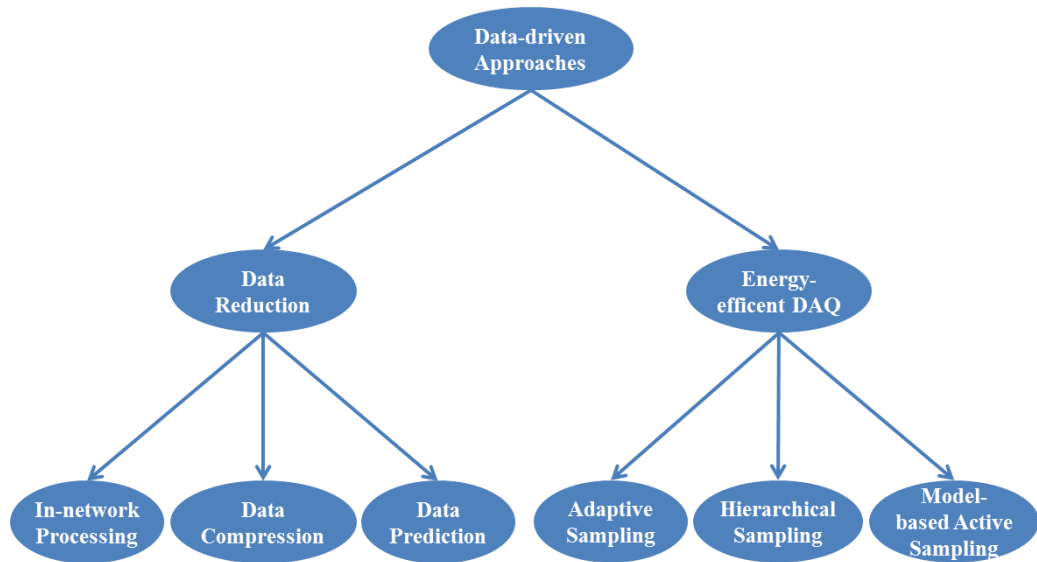


Figure 17: Taxonomy of data-driven approaches to energy conservation [137].

#### 2.4.1.1 *Energy-efficient DAQ Schemes*

In contrast, energy-efficient DAQ schemes try to tackle the problem of energy conservation from another angle, by reducing the power consumed by the sensing subsystems, such as analogue-to-digital converter (ADC) devices which may consume much more power than radio transceivers [137, 146, 147]. This may be due to the power-hungry nature of such devices, their long acquisition times, and the use of active sensors. Nevertheless, these schemes also have a direct link to data reduction and therefore the minimisation of the amounts of data transmitted.

As illustrated in Figure 17, this technique can be performed in the form of adaptive sampling, where the sampling frequency is adjusted based on a temporal analysis of the information acquired [148]. Unfortunately, this may lead to the problem of over-sampling if unnecessarily high sampling rates are set. A Kalman filter-based method is used to overcome such problems; however, this method requires the adaptive sampling to be calculated in a centralised unit which broadcasts it to the sensor nodes. Other adaptive techniques are discussed in more detail in the literature [137, 149].

Another form of energy-efficient DAQ approach is known as a hierarchical sampling routine or multi-scale sensing, in which a cluster of efficient power sensor nodes are used first to detect events; nonetheless, this process has limited resolution. Next, more advanced nodes are employed to perform a more detailed detection [150]. The level of



accuracy of this approach is the result of a trade-off between resolution and power efficiency.

Model-based active sampling predicts the future values of a sensed phenomenon based on a model which is developed using an initial set of sampled data with known levels of accuracy [151]. By doing this, energy is saved in the next sampling process. As long as the accuracy gained becomes low, a new model needs to be estimated in order to follow changes in the physical phenomenon monitored [137].

Although these methods can contribute to data reduction and therefore a preservation of the communication bandwidth as well as the optimisation of power consumption, these methods may be unsuitable for dynamic events which exhibit rapid variation over time. This is due to the significant communication overhead between the nodes and the central unit or sinks. This results in busying the wireless nodes which makes its response to other actions slow. In addition, multi-scale sensing adds more complexity to the monitoring system, particularly for SHM applications. These techniques still follow the Nyquist theorem for sampling acoustic signals which is one of the most critical challenges in WSNs. Thus, the use of sub-Nyquist sampling rates approaches is required in SHM based AE applications, which will lead to a reduction in both the amounts of data and power consumption, as discussed next.

### **2.4.1.2 Compressive Sensing Approach and WSNs**

In several WSN-based applications, due to resource limitations part of the captured data is often discarded before being stored or transmitted in order that the signal can be compressed. In addition, ADCs are power-hungry devices, particularly if high sampling rates are used. Thus, the question that is raised is why the physical phenomenon to be monitored is not sampled at lower rates in order to save cost and time, if part of the data is going to be thrown away anyway. The answer to this question represents the basic principle of the recently emerging technique of compressive sampling or sensing (CS). A recent extensive review lists the latest studies covering CS and its applications [152].

CS is an alternative theory to Nyquist criterion which is about recovering a signal or an image from a few random samples much less than what Nyquist criterion usually suggests. However, this is subject to the condition that signals or images satisfy the requirements of sparsity and compressible representation Donoho [153] and Candès et al.

[154]. The CS relaxes the Nyquist criterion and allows the employment of low sampling rates in the process of the acquisition of data from the physical phenomenon. It has attracted a considerable number of researchers in different areas ranging from medical imaging, signal processing and seismology to communications and networking. Recently, there has been a growing interest in applying the CS technique to a wider range of topics in SHM and the relevant NDT techniques in conjunction with WSNs.

Such an application has the advantages that it results in saving time and cost, since it does not work on the basis of first sensing then compressing, but instead performs compression while sensing at a lower sampling rate. Applying these principles in WSNs leads to overcoming the limited resources of WSNs, including storage, bandwidth, and power problems. This is why this approach is categorised among the energy-efficient data acquisition schemes, as shown in Figure 18.

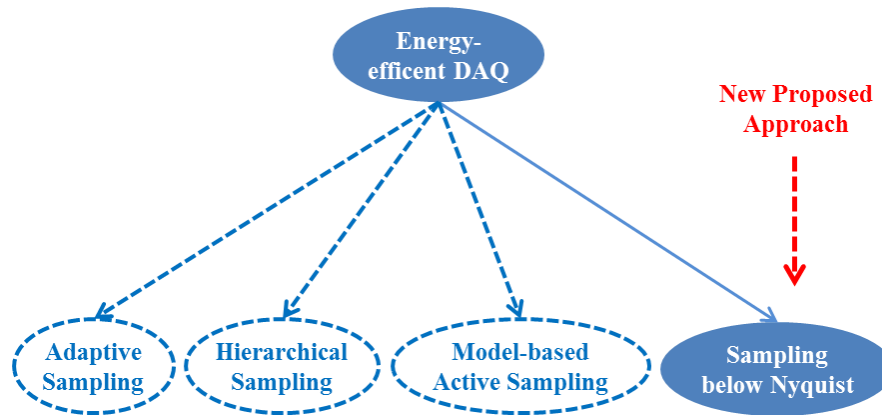


Figure 18: Taxonomy of energy-efficient DAQ approaches with the new data reduction method.

Most of the works conducted in CS [155, 156] have the intention to perfectly recover the monitored physical phenomena from a small number of random projections sent over the wireless link, as will be discussed in Chapter 3. However, the reconstruction of these phenomena at the sink may lead to a degradation in quality of the recovering process due to variations in the data gathered if it is not manipulated appropriately [157]. Also, sending a number of random vectors to the central unit is still a challenge and makes the recovery process severe [158]. This is true for applications such as SHM, in which the recovery of the original signal or image may be unnecessary if data are locally processed and main features are extracted under the use of low sampling rates. In this case, these challenges can be overcome, as shown next.

### 2.4.2 *Feature Extraction under the Use of Low Sampling Rates*

Working with the CS dates back to the research of Hsu et al. 1983 [159], where targets were recognised automatically from compressed images. Since then, it has found application in different areas, such as the detection of moving objects by surveillance systems [160]. In this application the moving objects are determined from compressed video data without the need to recover the original image, which has led to the development of computationally efficient surveillance systems.

Nagesh and Li [161] have shown that the low-dimensional random projection of original images can offer sufficient information for feature extraction, which can provide good classification. Therefore, it is also possible to extract features when CS is involved [162]. Zhang et al. [163] have used a very sparse measurement matrix which allowed them to efficiently extract features to be used for a tracking task. This enabled them to execute the tracking algorithm on a real-time basis due to computational energy savings while still performing well in terms of accuracy and robustness. In another study [164], the features of lines were directly extracted from the compressed images rather than from reconstructed images.

The same principle has been also applied in compressive wireless sensing. Shoaib et al. [158] presented a seizure-detection processor which is able to extract locally on-board features from compressively-sensed electroencephalograms (EEGs), which reduces the communication and energy costs. Dang et al. [165] presented an interesting example of running a light-weight animal classification algorithm on resource-constrained wireless nodes (MICAz) based on the extraction of a shape feature or envelope from randomly-sampled data at much lower rate than the Nyquist rate would require, where the analysis is performed using the compressed data.

The integration of CS with wireless sensor technology enables this technology to overcome to a certain degree the challenges of resource-constraints in terms of saving power, reducing communication bandwidth load, and relaxing storage capability. However, the transmission of the selected random samples to the central unit is still a challenge. According to one study [166], the power cost required to send a single bit of data is almost the same as the power required to execute a thousand instructions in a typical wireless sensor node. Therefore, the local processing of these samples for the purpose of

feature extraction can mitigate the energy conservation problem for wireless networks via the reduction in the amount of raw data transmitted. A critical discussion of these methods is presented in Chapter 3.

### 2.5 Summary and Problem Formulation

An extensive literature survey of SHM methods for WTBs is reported in this chapter. It began with an introduction to wind power systems and their most important parts, with more attention given to the blades of wind turbines, followed by a brief summary of types of failure modelling for WTBs. The state-of-the-art health inspection techniques which are promising for application to WTBs were reviewed along with a comparison of the strengths and weaknesses of these techniques. More emphasis was given to those which show potential for integration with WSNs.

In the context of this comparison and the challenges faced in applying these methods to OWTBs, the selection criteria for a suitable NDT technique to develop an SHM system for the blades were formulated. The AE technology is found to be an effective method for such applications in conjunction with WSNs. The major challenges of this combination are discussed and the use of low sampling rates is suggested to make WSNs more valuable and efficient in the intended SHM application. Thus, the literature survey ended with a review of the CS technique along with feature extraction under the use of the new proposed technique.

From the literature survey several problems arise in monitoring the structural health of OWTBs which need to be addressed especially for *in-situ* systems used for the long-term monitoring of offshore blades with continuous online feedback. These are as follows:

- Recently, wind turbines have become physically larger and more wind farms are placed in remote areas. Blades are fundamental components of wind power systems and one of the most expensive components to maintain. Faults in blades cause long downtimes which leads to high O&M costs. Early detection of potential damage and its status with the help of smart SHM techniques for condition-based O&M is now considered vital.

- The placing of wind farms in remote areas leads to access difficulties, particularly during extreme weather conditions. In addition, access to large blades requires the use of means such as ropes or other tools which may expose inspectors to risk. Limited access to the interiors of blades is also a problem. Special landing boats may even be needed to gain access to wind turbines. The inspection process may be a lengthy procedure, and for all these reasons inspection costs will increase. Visual inspections may be limited to only surface defects and not interior anomalies.
- Although many SHM and relevant NDT techniques are available, the direct adoption of traditional methods such as tap tests and ultrasonic testing to OWTBs may also be limited due to requirements of human supervision and active excitation units, which results in them not being viable for in-service or online monitoring. This necessitates the development of smart wireless sensors as well as SHM systems for OWTBs that can overcome such challenges.
- The AE technique presents the opportunity to develop a wireless, *in-situ*, and long-term monitoring system for OWTBs. Nevertheless, this method is very costly in terms of data generation due to the high sampling rates required to capture the AE events. Furthermore, the large size of OWTBs necessitates a considerable number of sensors in a complete SHM system in order to achieve full blade coverage, and online continuous monitoring increases the amount of sensing data produced.
- The heavy traffic load produced in SHM represents a challenge for wireless technology due to the limitations of data transmission over WSNs and the high latency in data collection and increased power consumption. Therefore, the reduction of the volume of the data via the use of low sampling rates in wireless technology will play a significant role in tackling such SHM problems, as shown in this thesis, particularly in Chapter 3.
- Finally, hierarchical communication and ICT tools for information fusion, decision making, and wind farm maintenance management are needed.

## Chapter 2

---

To address the problems identified, a research approach using wireless sensor networks are proposed and investigated in the next several chapters. In the following chapter, the systematic approach and the investigation of sampling rate requirements for wireless ASL are presented.

# CHAPTER 3: SYSTEMATIC APPROACH AND SAMPLING RATE REQUIREMENTS FOR WIRELESS SENSOR NETWORKS

The comprehensive literature survey carried out in Chapter 2 suggests to develop an *in-situ* SHM system based on the use of low sampling rates in wireless acoustic sensor technology in order to overcome the limitations of data transmission over WSNs, this chapter discusses the theoretical background of CS, in an effort to demonstrate the fundamental change achieved with the proposed concept of lowering the sampling rate in the acquisition operation of acoustic signals. The chapter also investigates the effect of employing the new data reduction method on the accuracy of time delay estimation (TDE) using different algorithms in the time, frequency, and time-frequency (content-based features) domains. These include basic cross correlation (BCC), generalised phase spectrum (GPS), and envelope-GPS (EGPS). It also attempts to specify methods which will effectively analyse the acoustic signals acquired at low sampling rates so that any drawbacks associated with lowering sampling rates, such as information loss and low spatial sampling, are overcome.

The chapter is organised as follows. Section 3.1 presents the systematic approach to this work. Section 3.2 reviews the CS approach in conjunction with WSNs. The TDE algorithms which are widely used for sound localisation are discussed in Section 3.3. Section 3.4 describes the experimental setup that was built to capture different acoustic signals at different sampling rates. In Section 3.5, the results of comparisons of the TDE algorithms and their impact on WSN design and development for ASL are discussed. Finally, the conclusions are drawn in section 3.6.

### 3.1 Research Methodology

To address the problems identified in the literature review, the systematic approach for a wireless *in-situ* SHM system proposed in this research is outlined in this chapter and as shown in Figure 19, which involves five main tasks. Each task is covered in one chapter of this thesis and has its own function and output that contributes to the next task as well as to the overall research. These tasks are described below:

- Task 1: Undertaking a comprehensive literature review in order to explore the state-of-the-art inspection techniques for SHM and to choose an appropriate approach for the inspection of the structural health of OWTBs in conjunction with WSNs. A proposal is also outlined for tackling the challenges identified with the selected technique, as discussed in Chapter 2.
- Task 2: Following the recommendations arising from Task 1 and due to the limitations of data transmission over WSNs, the sampling rate requirements for ASL using WSNs are investigated in this chapter. The analysis is carried out by testing different time delay estimation (TDE) algorithms in the time, frequency, and time-frequency domains based on content-based features extracted from the aliased versions of the sound signals used.
- Task 3: Based on the conclusions drawn from the previous task, which were based on the use of a wired localisation system, a wireless setup for ASL is built in order to validate the findings of the previous task using data received from a centralised AWSN. The completion of this task is the basis of the work discussed in Chapter 4 and is realised by continual experimental assessments of system performance by conducting several kinds of measurements of the centralised wireless ASL using low sampling rates. The underlying theory behind the technique developed is also studied.
- Task 4: The experiments discussed in the previous task are lab-based experiments using a centralised AWSN where advanced signal processing techniques are used to locate a sound source. This task will extend the experience gained from Task 3 to the field environment. The completion of this task is the basis of the work discussed in Chapter 5. A case study for *in-situ* AE sensing and the localisation of emulated impact damage are also considered in this chapter, where



blade health is assessed and the emulated AE events are localised.

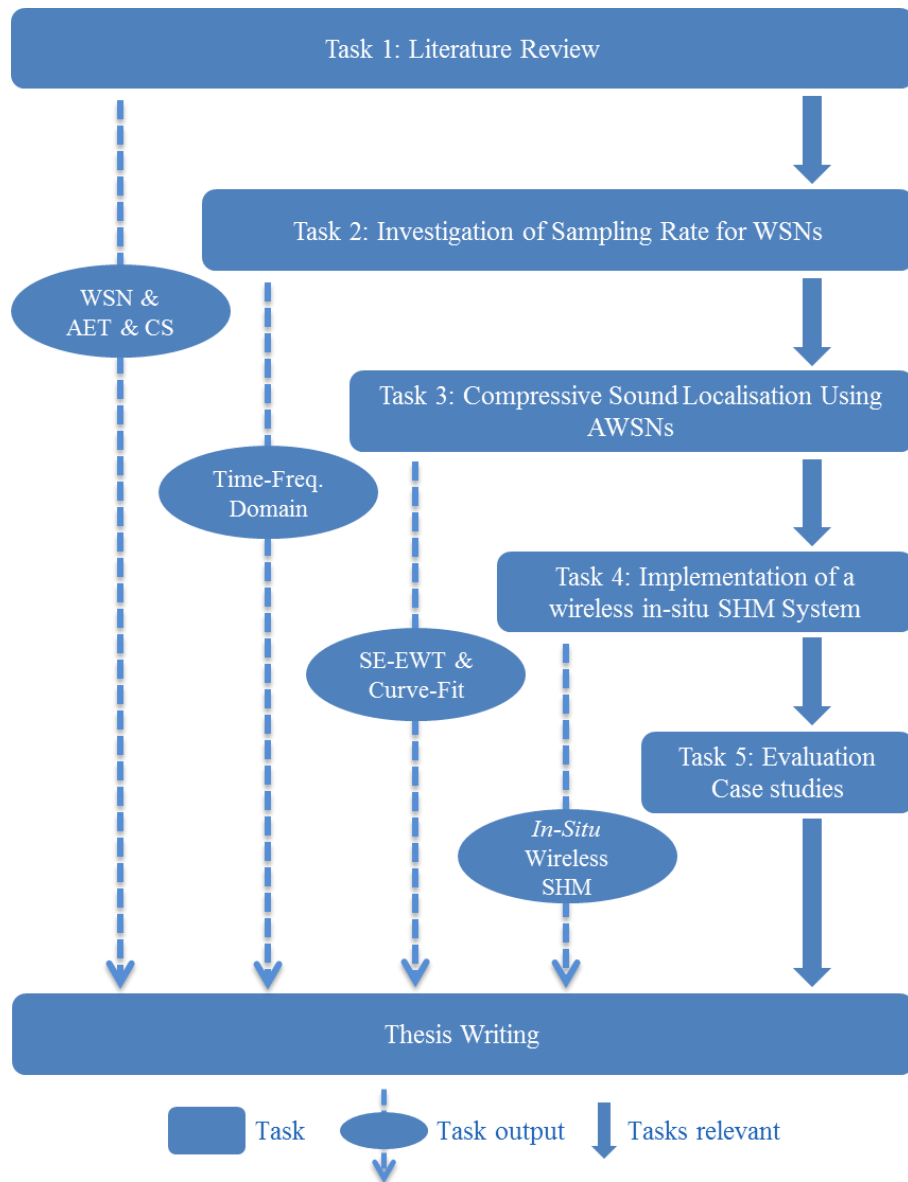


Figure 19: Block diagram of the research methodology.

- **Task 5:** In addition to the evaluation of the *in-situ* wireless SHM system implemented for the localisation of AE sources emulated on WTBs, it is of significant importance to distinguish between such emulated sources and AE events relative to environmental monitoring. Therefore, a further evaluation case study of the *in-situ* system developed is considered in this Task. The material of this task is the basis of the work discussed in Chapter 6.

The rest of this chapter reports on the completion of Task 2, whereas the rest of the the-

sis covers the material introduced in the last three tasks where a critical discussion of the results is also provided.

### 3.2 Requirements of Low Sampling Rates

The Nyquist sampling criterion states that, for a perfect reconstruction of a signal, the sampling frequency should be at least greater than or equal to double the maximum frequency of the signal being monitored. Otherwise, aliasing will occur which will cause the misinterpretation of the sampled signals (aliased versions) and ruin the reconstruction process. However, CS offers new concepts for relaxing the Nyquist-Shannon sampling theorem, where the original signals or images can be reconstructed from far fewer samples than traditional techniques necessitate [153, 167]. This opens new horizons for facilitating numerous applications in different areas, ranging from image reconstruction, medical imaging, compressive wireless sensing, and analogue-to-digital converter. Recently there has been a growing interest in applying the CS approach to a wide range of applications, such as wireless ASL, SHM and many others. In the following section, the underlying theory behind the traditional CS is discussed, followed by an explanation of the use of this approach with WSNs. Then the derived concept of utilising the low sampling rates in the WSNs is presented.

#### 3.2.1 Compressive Sensing Theory

CS is a new approach and is still being explored. The main principle of this technique is detailed in several published studies [153, 168, 169]. CS is an alternative theory to the Nyquist concept, and concerns the recovery of signal or image from a few random samples at much lower rates than what the Nyquist criterion would usually suggest, provided that the signals have a sparse or compressible representation [153, 154].

Next, a brief introduction to CS in mathematical terms is given. Assuming a discrete time signal of interest in  $\mathbb{R}$  is given by  $x(t)$  where  $t = 1, \dots, n$ . This signal can be represented as in Equation (3.1) [153, 167]:

$$x = \sum_{i=1}^n \alpha_i \psi_i, \text{ or in a matrix form as } x = \Psi \alpha \quad (3.1)$$

where  $\Psi = [\psi_1, \psi_2, \dots, \psi_n]$  is the  $n \times n$  basic matrix with basis orthonormal vectors  $\psi_i$  as columns and the vector  $x = [x(1), \dots, x(n)]^T \in \mathbb{R}^n$  of  $n$  sampled values of  $x(t)$ .  $\alpha$

represents the  $n \times 1$  column vector of coefficients and can be expressed as in Equation (3.2) [153, 167]:

$$\alpha = \Psi^T x, \text{ where } \Psi^{-1} = \Psi^T \quad (3.2)$$

Assuming  $y$  is an  $m < n$  length data vector acquired by a linear projection of  $x$  which is defined as in Equation (3.3) [153, 167]:

$$y = \phi x = \phi \Psi \alpha = \tilde{\phi} \alpha \quad (3.3)$$

where  $\tilde{\phi} = \phi \Psi$  is an  $m \times n$  matrix and  $\phi \in \mathbb{R}^{m \times n}$  is known as a measurement matrix with  $m \ll n$ . Then the aim is to recover the signal  $x$  or to find a suitable approximation of it by finding a solution to Equation (3.3). This problem is an ill-posed problem, since it is an underdetermined system, where the number of equations  $m$  is less than the number of variables. A solution to this problem exists for a case where signals or images are sparse, which is the case for most of them, which means that for a signal of length  $n$ , it is possible to represent this signal with  $k \ll n$  non-zero coefficients [170]. Under this condition, Equation (3.3) can be solved to retrieve  $\alpha$  from a small number of measurements with very high accuracy based on optimisation approaches [171, 172] from which the signal  $x$  is reconstructed using Equation (3.1).

Therefore, to reconstruct the compressible signal  $x$  from a relatively small set of random projections, a convex  $\ell_0$  norm minimisation problem needs to be solved as in Equation (3.4) [173]:

$$\min_{x \in \mathbb{R}^n} \|x\|_0 \quad \text{provided that } \phi x = y \quad (3.4)$$

where  $\|\cdot\|_0$  represents the  $\ell_0$  norm (i.e., the count of the nonzero elements in  $x$ ). However, the  $\ell_0$  norm gives unstable numerical results and it is an NP-hard problem [174]. It has been proven that the  $\ell_1$  norm is equivalent to the  $\ell_0$  norm and can be easily expressed as a linear program for providing an efficient solution to the previous convex minimisation using Equation (3.5) [154]:

$$\min_{x \in \mathbb{R}^n} \|x\|_1 \quad \text{provided that } \phi x = y \quad (3.5)$$

In reality, measurements are contaminated by a finite level of noise which needs to be taken into account while solving the optimisation problem, as in Equation (3.6) [167,

175]:

$$\min_{x \in \mathbb{R}^n} \|x\|_1 \quad \text{provided that } \|\phi x - y\|_2 \leq \varepsilon \quad (3.6)$$

where  $\|\cdot\|_2$  denotes the  $\ell_2$  norm (i.e., the Euclidean norm) and  $\varepsilon$  is a given noise level.

As seen in Equations (3.4)-(3.6), the main target of the sparse approximation problem is to find a good approximation of the original signal or image via a linear combination of a few elementary signals which are randomly chosen from a fixed set of signals. Because the present research is not based on the full reconstruction of the original information, these techniques will not be considered in the rest of this chapter. However, more details and other techniques have been presented in a comprehensive survey of most practical methods for sparse approximation [175].

### ***3.2.2 Uniform Low Sampling Rates Concept***

The aforementioned discussion focuses mainly on the principle of CS in recovering a compressible signal  $x$  from far fewer measurements  $y$  than is usually required. These measurements inherit most of the sparse salient information of the original data [163]. Such data make it possible to directly use them to extract meaningful information, if appropriate techniques are employed, without first having to reconstruct the original data. This has the advantage that it is not only computationally efficient but also reduced communication cost and balanced network load problem associated with large data transmissions [160].

On the other hand, the employment of low sampling rates in the data acquisition operation of acoustic signals is particularly relevant for applications where meaningful information can be extracted from the content-based features (envelopes) of the aliased versions (low sampled data) without the need to use the reconstructed signals. In this case, the following questions may be raised:

- Would be possible to use the aliased versions for further processing, without the need to recover the original signal? In which domain of analysis should they be processed?
- Would they be usable for locating sound sources? Would they inherit useful features for AE event detection and classification?
- By doing so, what are the conditions and guidelines for the employment of low

sampling rates to reach this goal?

- How can the drawbacks, including information loss and the low spatial resolution caused by the employment of such sampling rates, be overcome?

The answers to these questions represent the major contributions of this research which are sought in the rest of this chapter as well as the subsequent chapters.

In general, the utilisation of low sampling rates in this research differs from the principle of the traditional CS in the following important aspects and as shown in Figure 20. Firstly, this research utilises a concept of employing low sampling rates much lower than the Nyquist rate to generate aliased versions of the physical phenomenon ( $x$ ), rather than using a random projection process, as shown in Figure 20-a. The produced versions represent the raw data which can be either sent to a global central unit or processed locally in order to extract the features required and to create the AVPs. The AVPs will be then transmitted via the wireless link to the collection point where they are used for further analysis, as shown in Figure 20-b and discussed in Chapter 5.

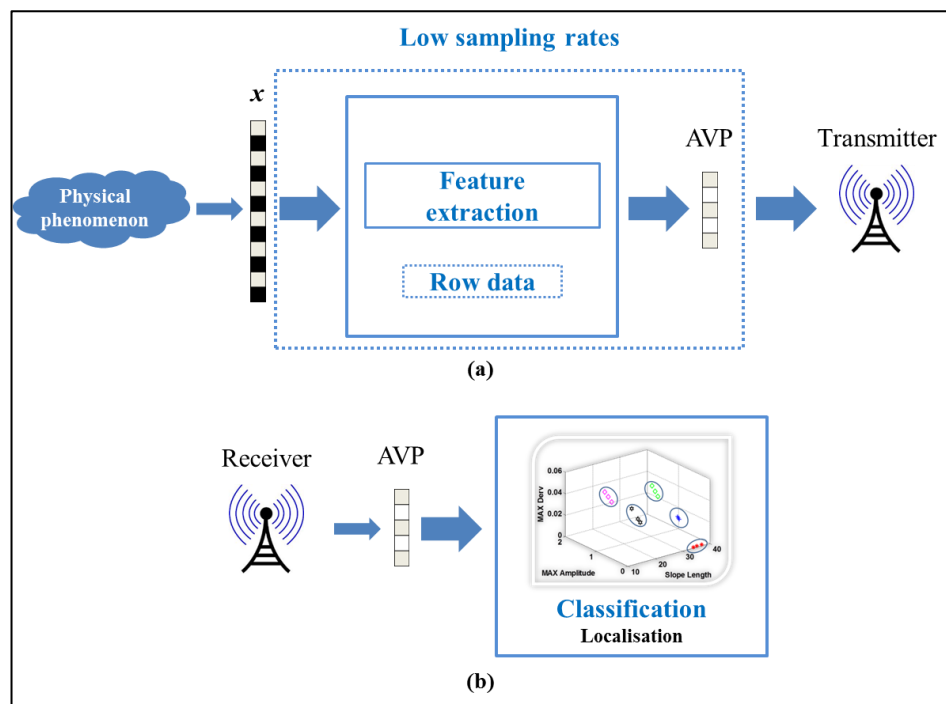


Figure 20: The principle of utilising low sampling rates at: a) wireless node, b) central unit.

The new proposed approach has the following key advantages:

- It directly utilises a low sampling rate much below the Nyquist rate which pre-

serves the resource-constrained sensors and enables them to classify high frequency signals.

- Most importantly, such a new approach also provides timing information about the occurrence of an event, which is needed for the localisation purposes.
- The utilisation of a low sampling rate leads to the sensed data being coherent among the wireless nodes. This is also useful for the purpose of TDE.
- The aliased versions of the physical phenomenon can conserve the original shape, which helps in maintaining the most salient information (features) of the original signals without the need to reconstruct them.

### ***3.2.3 Conditions for the Utilisation of Uniform Low Sampling Rates***

As stated above, the reason for applying low sampling rates much below the Nyquist rate is to preserve the resource-constrained at the wireless sensor level without the need to recover the original signals. However, this is restricted to narrow bandwidths and not periodic signals. In other words, it is limited to transient or abnormal signals, such as acoustic pulses or AE signals. These types of signals are expected to be generated in the target application of this research, which is the SHM of WTBs. This means that the acoustic signal generated should have a finite pulse duration. The following sections investigate the effect of the utilisation of such uniform low sampling rates on the time delay estimation for sound source localisation.

### **3.3 Acoustic Source Localisation Using Low Sampled Data**

The determination of the location of a sound source relative to reference points is known as acoustic source localisation (ASL). This localisation process can be achieved based on the arrival time of acoustic signals captured with at least two or more microphones and the velocity of sound in the medium in which the sound source is located. In the literature, several TDE techniques have over the years been developed with varying degrees of accuracy and computational complexity [176-178]. This section reviews the typical TDE algorithms which will be investigated in order to test their dependence on the sampling frequency using different domains such as time, frequency, and time-frequency (content-based features).

### 3.3.1 Time Delay Estimation Using Microphone Arrays

Before describing the typical TDE algorithms, a simple mathematical model for the acoustic signal received at any microphone shown in Figure 21 is presented. Such a model shows how the relative TDE between the microphone outputs is used to investigate the relationship between the sampling rate and estimation accuracy under the three domains. From Figure 21, if  $x_i(t)$ ,  $i = 1, \dots, 3$  denotes the  $i$ -th signal of the  $i$ -th microphone which can be modelled as Equation (3.7):

$$x_i(t) = \alpha_i s(t - \tau_i) + \eta_i(t) \quad (3.7)$$

where  $\alpha_i$  represents an attenuation factor due to propagation effects;  $\tau_i$  is the propagation time from the unknown source  $S(t)$  to the  $i$ -th microphone;  $\eta_i(t)$  is assumed as an uncorrelated additive noise signal at the  $i$ -th microphone. Then the time delay between any two microphone signals, for example,  $M_1$  and  $M_2$ , can be expressed as Equation (3.8):

$$\tau_n = |\tau_2 - \tau_1| \quad (3.8)$$

$\tau_n$  can be estimated by applying TDE algorithms to the two signals  $x_1(t)$  and  $x_2(t)$ , as shown in the following sections.

Once the time delay is estimated, the location of the acoustic source can be computed using the triangulation method between the three microphones and the sound source, as shown in Figure 21 and Equations (3.9) and (3.10). More details about the use of this method are given in Atmoko et al. [179].

$$d_n = c \cdot \tau_n \quad (3.9)$$

$$d_m = c \cdot \tau_m \quad (3.10)$$

where  $c$  is the propagation speed of sound in air which is assumed to be  $340 \text{ ms}^{-1}$ .

The time delays  $\tau_n$  and  $\tau_m$  can now be estimated using the above mentioned algorithms in order to quantify the estimation accuracy for each domain, as shown in the next section. As a result, the acoustic source location can be estimated as reported next.

The following derivation of sound source location is in 2-D space. From the two triangles  $SM_2M_1$  and  $SM_2M_3$ , it is possible to derive the cosine relations for both angles  $\varphi_n$  and  $\varphi_m$  which are azimuths for microphones one and three as in Equations (3.11) and (3.12) respectively.

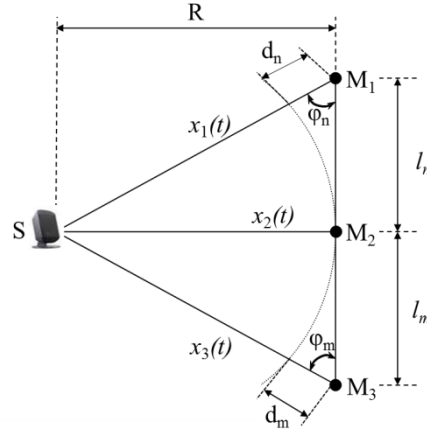


Figure 21: Geometrical relationship of three microphones and a sound source.  $R$  is the shortest path between sound source  $S$  and  $M_2$ .

$$\cos \varphi_n = \frac{l_n^2 + (R + d_n)^2 - R^2}{2l_n(R + d_n)} \quad (3.11)$$

$$\cos \varphi_m = \frac{l_m^2 + (R + d_m)^2 - R^2}{2l_m(R + d_m)} \quad (3.12)$$

where  $l_n$  and  $l_m$  represent the known separation distances between the microphones, as shown in Figure 21.  $R$  is the shortest path between the sound source and the reference microphone  $M_2$ . Similarly, from the triangle  $SM_1M_3$ , it is possible to develop the expression in Equation (3.13):

$$\cos(\varphi_m + \varphi_n) = \frac{(l_m + l_n)^2 - (R + d_m)^2 - (R + d_n)^2}{2(R + d_m)(R + d_n)} \quad (3.13)$$

Using Equations (3.11)-(3.13) it is now possible to calculate, via appropriate substitutions, the three variables  $R$ ,  $\varphi_n$ , and  $\varphi_m$  as in Equations (3.14)-(3.16):

$$R = \frac{l_n(l_m^2 - d_m^2) - l_m(l_n^2 - d_n^2)}{2(d_m l_n + d_n l_m)} \quad (3.14)$$

$$\varphi_m = \cos^{-1} \frac{l_m^2 + (R + d_m)^2 - R^2}{2l_m(R + d_m)} \quad (3.15)$$

$$\varphi_n = \cos^{-1} \frac{l_n^2 + (R + d_n)^2 - R^2}{2l_n(R + d_n)} \quad (3.16)$$

As is seen in Equations (3.14)-(3.16), by knowing the variables  $R$ ,  $\varphi_m$ , and  $\varphi_n$  it is possible to estimate the sound source location in 2D. Moreover, the propagation path differ-



ences  $d_n$  and  $d_m$  play an important role in the estimation of these parameters. The more accurate  $d_n$  and  $d_m$  are, the better the localisation results become. These two parameters will be used to evaluate the performance of the TDE methods under the use of low sampling rates to study the requirements of the ASL at rates much below the Nyquist rate, as shown in the following sections.

### ***3.3.2 Selection of Appropriate Analysis Method for Low Sampled Data***

The employment of sampling rates much below those usually considered necessary in the acquisition process necessitates new knowledge about the selection of an appropriate analysis technique which will be used to process the aliased versions of the acoustic signals. This is done by the investigation of different TDE algorithms in the time, frequency, and time-frequency (content-based features) domains under the use of low sampling rates. The reason behind this is to find new ways to overcoming the challenges faced when lowering the sampling rate. Such knowledge is useful for specifying a suitable domain of analysis for the use of WSNs in ASL and SHM applications.

#### ***3.3.2.1 Time Domain Analysis for TDE***

Several TDE procedures have been proposed and implemented in the time domain over the years. The basic idea of most of these techniques is based on locating the absolute extremum of the cross-correlation, cross-correlation coefficient function or some other statistic associated with the observed signals. For example, basic cross-correlation (BCC) [180] and generalised cross-correlation (GCC) algorithms [181] search for coherence among the captured acoustic signals in order to determine the lag at which the cross-correlation function (CCF) has its maximum. This lag then represents the time delay between the two signals, as shown in Table 4. The main difference between the two algorithms is that GCC uses weighting functions (filtering the captured signals) to improve the performance of the TDE approach [181, 182].

As shown in Table 4, the GCC is defined as the inverse Fourier transform of the cross-spectrum of the input signals,  $X_1(\omega)X_2'(\omega)$ , scaled by a weighting function  $W(\omega)$  which is summarised in Table 5 for several common GCC methods.

The BCC and GCC approaches have been widely used in different applications, such as sonar, displacement or velocity determination and pattern recognition [183]. Further-

more, they can be applied in flow or strain determination from sequences of images [184]. Time domain approaches have the advantages that they are simple, and therefore not computationally expensive, and more suitable for real-world applications. However, they depend strongly on the coherence among the signals received, which is likely to impact upon their accuracy in precisely estimating the time delay [185], particularly if low sampling rates are used.

Table 4: Basic mathematical expressions for BCC and GCC.

TDE algorithm	Mathematical expression	Estimated time delay
BCC	$R_{x_1x_2}(\tau) = \frac{1}{T-\tau} \int_{\tau}^T x_1(t) x_2(t-\tau) dt$	$\tau_{12} = \operatorname{argmax}_{\tau} R_{x_1x_2}(\tau)$
GCC	$R_{x_1x_2}(\tau) = \int_{-\infty}^{\infty} W(\omega) X_1(\omega) X_2'(\omega) e^{j\omega\tau} d\omega$	$\tau_{12} = \operatorname{argmax}_{\tau} R_{x_1x_2}(\tau)$

Table 5: Commonly used weighting functions in the GCC method [181].

Method Name	Weighting Function $W(\omega)$
Cross Correlation	1
Roth Impulse Response	$1/G_{x_1x_1}(f)$
Phase Transform (PHAT)	$1/ G_{x_1x_2}(f) $
Smoothed Coherence Transform (SCOT)	$1/\sqrt{G_{x_1x_1}(f)G_{x_1x_1}(f)}$
Eckart Filter	$G_{s_1s_1}(f)/[G_{n_1n_1}(f)G_{n_2n_2}(f)]$
Hannon and Thomson (HT)	$ \gamma_{12}(f) ^2/( G_{x_1x_2}(f) [1- \gamma_{12}(f) ^2])$

### 3.3.2.2 Frequency Domain Analysis for TDE

Frequency domain algorithms are based on examining the phase spectrum of two signals. For instance, the GPS is used to compute the time delay between two signals  $x_1(t)$  and  $x_2(t)$  by estimating the cross-power spectral density (CPSD) of the two signals and

then computing the phase slope of the CPSD as a function of frequency [185]. Figure 22 shows a typical measured phase spectrum from the test signals, discussed below, in conjunction with an estimate of the actual phase spectrum. As seen in this figure, the signal used is dominated by ambient noise at frequencies below  $\omega_0$  and greater than  $\omega_1$ . Thus, the GPS uses the frequency band  $\Delta\omega$  to weight the phase in order to improve the TDE which can be described as follows,

Let  $\beta_i$  represent the estimated phase at the frequency  $\omega_i$  from two sensors  $x_1(t)$  and  $x_2(t)$  with a number of points  $N$ ; then the time delay is defined as in Equation (3.17) [186]:

$$\tau_{12} = -\frac{\sum_{i=1}^{N/2} W_i \beta_i \omega_i}{\sum_{i=1}^{N/2} W_i \omega_i^2} \quad (3.17)$$

where  $W_i$  is a frequency dependent weighting function at frequency  $\omega_i$ .

In this equation, only the frequency band  $\Delta\omega$  which corresponds to the linear phase gradient of CPSD shown in Figure 22 is selected to calculate the time delay.

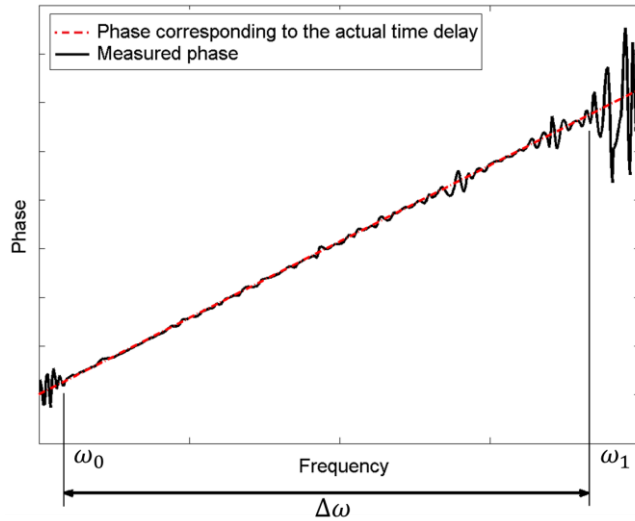


Figure 22: Selection of the cut-off frequencies  $\omega_0$ ,  $\omega_1$ , and frequency bandwidth  $\Delta\omega$ .

This GPS algorithm has potential application in radar, sonar and optical imaging systems [187]. It has the advantages over the time domain algorithms that in the frequency domain the time delay is directly estimated, which makes it easier to use filters [188]. This leads to improving the speed of estimation of time delays and simplifying the signal processing algorithms. Furthermore, as shown in Equation (3.17), only a selected frequency range is used in this calculation [185]. This makes the localisation process more robust in a noisy environment, since the CPSD will be weighted according to this

range [186].

### 3.3.2.3 *Time-Frequency Domain Analysis for TDE*

Content-based feature data analysis algorithms, such as envelope GPS (EGPS) algorithm rely on the analysis of the actual contents of the signal, such as the shape or any other information that can be derived from it. This concept has been successfully applied in research fields such as image retrieval applications [189]. In this investigation, this concept will be adopted for the estimation of the time delay between two signals  $x_1(t)$  and  $x_2(t)$  by first extracting the envelopes or shape of both signals using the Hilbert function [190] and then, as in frequency domain algorithms, the GPS method is applied to calculate the time delay using the signal envelopes. The reason behind the use of the signal envelope is to smooth the signal shape and to overcome the loss of information due to the employment of low sampling rates.

## 3.4 Experimental Setup for TDE at Low Sampling Rates

In order to investigate the influence of sampling frequency on the accuracy of TDE for ASL, so that an appropriate domain of analysis for an accurate ASL algorithm can be specified, a wired experimental setup was built as shown in Figure 23. The experiments were conducted in an ordinary indoor laboratory environment which contains objects such as tables, PCs and lab equipment which are normally found in a typical laboratory.

The geometrical limitations of  $l_n$ ,  $l_m$ ,  $R$  and  $S$  directivity have not been discussed for the reliable localisation of the source, which is out of the scope of this study. As shown in Figure 23, three omni-directional mini electret condenser microphones were positioned to face a sound source and used to simultaneously capture acoustic signals generated from the sound source. They were positioned so that the acoustic signals reached them at different instants of time.

The acoustic signals were pulses and male speech signals, as illustrated in Figure 24-a and were generated for the test using professional audio software and played through a PC speaker. Figure 24-b shows the frequency spectrum of these signals, were acquired at a sampling frequency of 48kHz for a recording period of 8s. A computing system was used to save and process the received data off-line. The time delay was then estimated using the above mentioned algorithms under the same structure at different sampling

frequencies ranging from 1kHz to 48kHz.

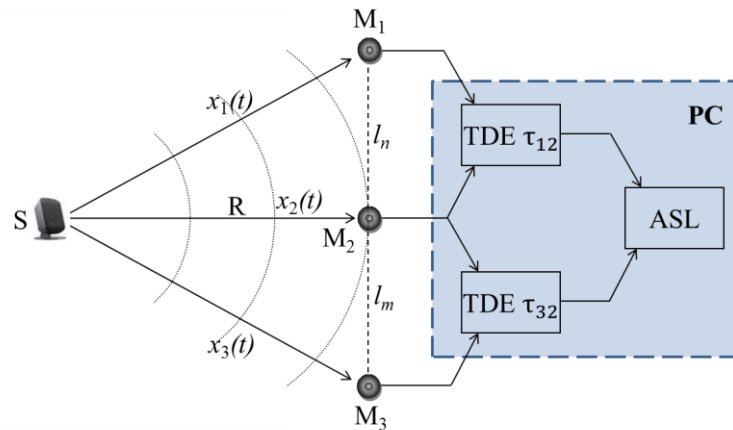


Figure 23: Schematic representation of the wired experimental setup for the ASL.

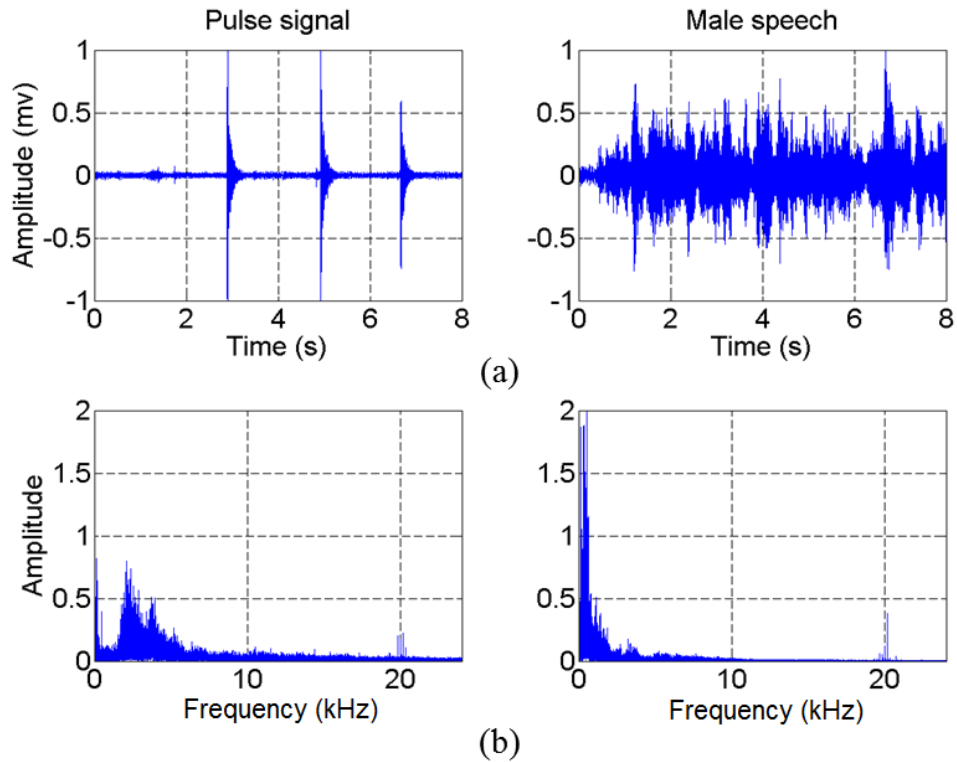


Figure 24: Wave forms of sound sources and their spectrum used as test signals: left, pulse signal, and right male speech ‘acoustic camera’.

### 3.5 Results and Discussion

Traditional sampling frequencies, which comply with the Nyquist criterion for proper sound signal reconstruction in wired solutions, present problems when employing

WSNs in ASL or SHM applications. For this reason, the experiments were conducted here in order to investigate the effect of sampling frequency on the accuracy of the TDE process using the BCC, envelope BCC (EBCC), GPS and EGPS algorithms, so that a valuable technique could be specified for processing the acquired sound signals using lower sampling frequencies in ASL and SHM applications. In these experiments, different acoustic signals were generated, as mentioned in Section 3.4, and were captured by three microphones which acquired data at a sampling frequency of 48kHz under the same structure. A down-sampling process was then applied to the captured signals in order to reduce the sampling rate of these signals. This process was utilised by reducing the sampling rate of the signal acquired by an integer factor  $M$ , so that if  $x(n)$  represents the data sequence then the down-sampled sequence  $y(m)$  is represented by  $x(nM)$ .

Theoretically, based on the Nyquist sampling theorem, this process can introduce aliasing effects to the down-sampled data due to the decreased sampling rate. This problem can be overcome with the right signal processing technique to extract TDEs since the reconstruction process of the original signal is unnecessary in this application. After each down-sampling process the time delay among these signals was estimated using the above mentioned algorithms and errors in the TDE process were computed using the following Equation (3.18):

$$TDE_{Error} = (Expected\ time\ delay - Computed\ time\ delay) \quad (3.18)$$

where the expected time delay denotes the known distance  $d$  divided by the speed of sound  $c$ , and the computed time delay is the delay estimated by the TDE algorithms.

Figure 25 shows the results of this process where errors in the TDE are plotted against the sampling frequency. In this figure, the actual delay is 833 $\mu$ s, which corresponds to 40 samples. As is seen in this figure, the trend of the error in the time domain shows large deviations at lower sampling frequencies, whereas as the sampling rate becomes higher these deviations tend towards zero. This is because the cross-correlation algorithms depend on finding the highest value of CCF to estimate the time delay between two signals, which can be missed due to the low time resolution of the time axis if low sampling frequencies are used. This conforms to what is expected, since time domain algorithms for ASL are strongly affected by the sampling frequency used.

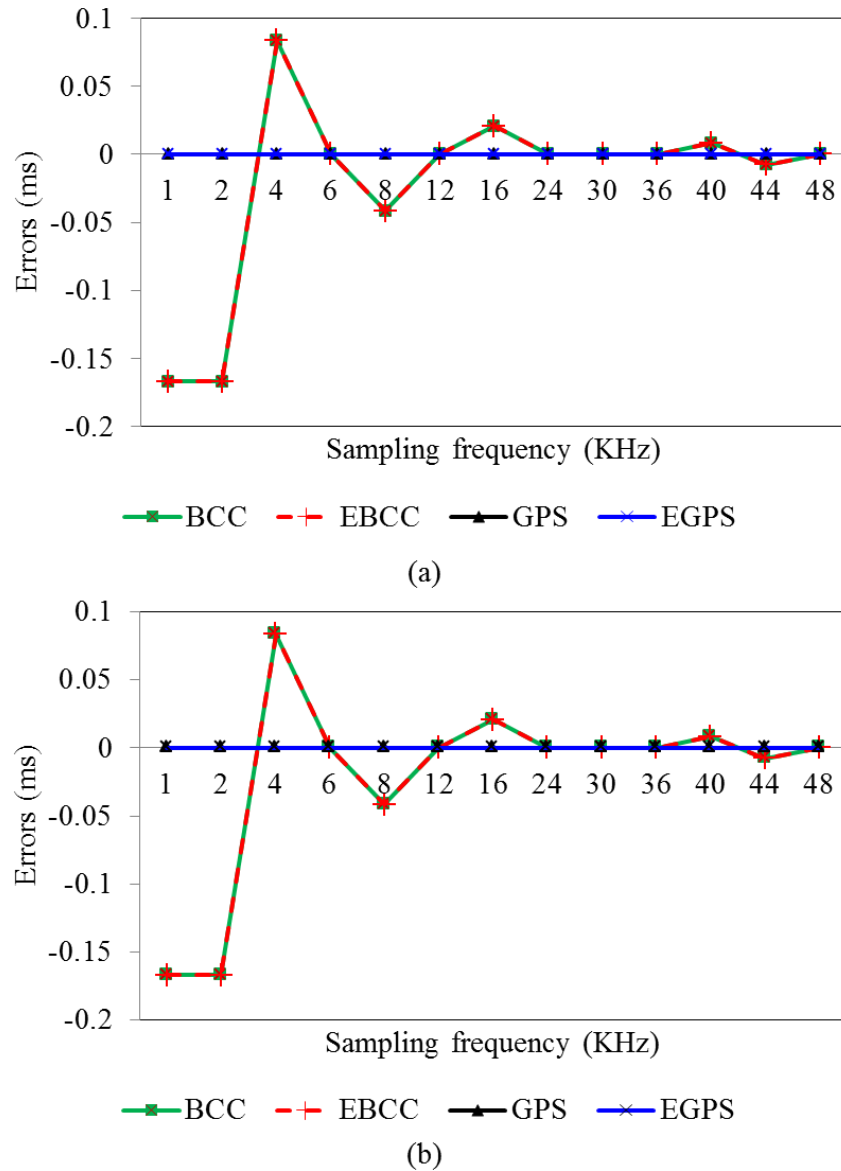


Figure 25: Comparison results of TDE algorithms using: a) pulse, b) speech signals, for a delay of 40 samples.

In contrast to time domain analysis, it can be clearly seen in the ASL algorithms based on the frequency and time-frequency domains, i.e., GPS and EGPS, as shown in Figure 25, those errors in the TDE are less than  $0.3\mu\text{s}$ . This is because these algorithms estimate the time delay through information contained in the frequency and time-frequency domains. This can be clarified by seeing Figure 22 where only the frequency band  $\Delta\omega$  is used to weight the phase of used aliased signals which leads to the improvement gained in these TDE calculations. This means that the use of the linear part of the computed phase spectrum makes the calculation of TDE not affected and the errors in TDE are not

sensitive to the sampling frequencies in the range used in the experimental studies from 1 to 48kHz. From these results it can be concluded that, for sound localisation and SHM applications, it is possible to use low sampling rates to capture acoustic signals in order to construct the aliased versions of acoustic signals. This gives the opportunity to process these versions to estimate the time delay between them, provided that these aliased versions are processed in the frequency or time-frequency domain.

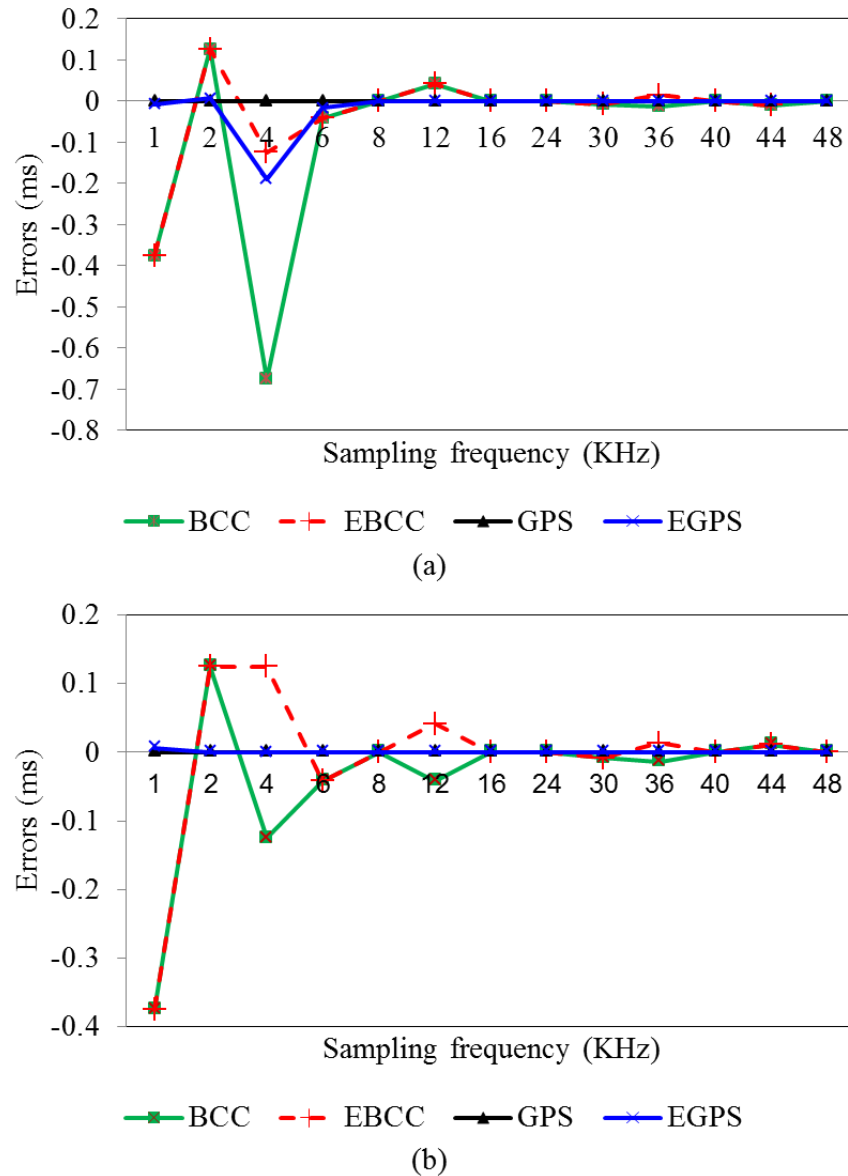


Figure 26: Comparison results of TDE algorithms using: a) pulse, b) speech signals, for a delay of 30 samples.

To confirm this finding, data with a time delay of  $625\mu\text{s}$ , corresponds to 30 samples were used in simulation of a different location of a sound source as another example of



the investigation of TDE errors under the same set of sampling frequencies. The results of this study are illustrated in Figure 26. As can be seen from this figure, the variations in error in the time domain at low sampling rates are higher than those in the other two domains, while at high sampling rates all domains exhibit steady results. It is clear that in both cases the computed errors at lower sampling frequencies using GPS or EGPS are almost the same as the results obtained at higher sampling frequencies. In contrast, the time domain algorithms exhibit unstable behaviour at lower sampling frequencies, and hence it was concluded that is more appropriate for such applications to use frequency or time-frequency domain to estimate the time delay if low sampling rates are chosen.

To illustrate the fact that the proposed method is independent of the location of the sound source, different time delays were simulated and investigated, with the results shown in Figure 25 and Figure 26. In addition to the sample delays of 40 and 30, another experiment with a delay of 10 samples was also conducted and the results are shown in Figure 27. As shown in these figures, the errors in time delay estimation tend to decrease as the sampling rate increases. This means that error variation patterns will remain similar as the time delay is changed.

Therefore, given these results, it is confirmed that data from low sampling rates below the Nyquist rate directly in the sensing process can be utilised to save data acquisition costs and time. In addition, this leads to the property of coherence among the aliased versions of the acoustic signals being preserved, which is useful for delivering the time information required for the ASL. As no signal reconstruction is required, the sparsity feature is no longer needed. To overcome drawbacks such as information loss and low spatial resolution caused by this employment, the envelopes of the aliased versions are used. In addition, these envelopes should be processed in the frequency or time-frequency domains.

However, if frequency domain algorithms are used to analyse the aliased version of the received signals, they will be unable to show the dominant spectral component at the original signal frequency in cases where surrounding noise may affect the original signals. This means that a major portion of frequency content is lost and any TDE used in this domain will lead to inaccurate results. Therefore, the time-frequency domain is proposed as an optimal domain for the processing of these aliased versions, as is discussed in the next chapter.

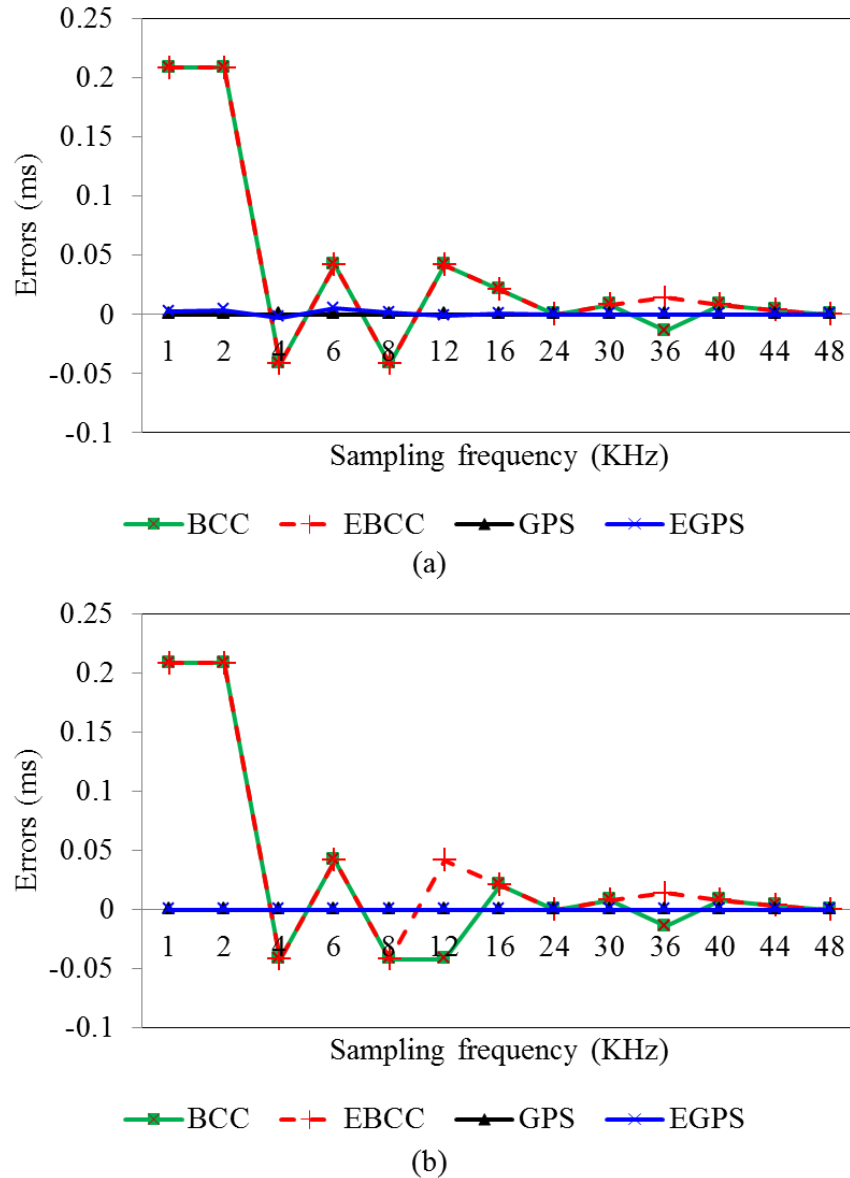


Figure 27: Comparison results of TDE algorithms using: a) pulse, b) speech signals, for a delay of 10 samples.

### 3.6 Summary

Based on the literature survey and the problems identified in Chapter 2 and due to the limitations of data transmission over WSNs, a low sampling rate method for sound localisation has been proposed in this chapter. With low rates of sampling data, acoustic source localisation using the data content in terms of time, envelope, and content-based feature domains, such as the BCC, GPS and EGPS algorithms, has been investigated. Time-frequency domain and envelope content-based features have been identified as

optimal domain for processing the aliased versions and mitigating the effect of the information loss. Such conclusions were drawn based on the use of a wired localisation system. Therefore, the next chapter extends the use of low sampling rates to the wireless ASL so that data received from the AWSN are used to validate these findings.

# CHAPTER 4: EXPERIMENTAL VALIDATION OF SOUND LOCALISATION USING AWSNs AT LOW SAMPLING RATES

In the previous chapter, it has been shown that, for wireless sound source localisation, the use of low sampling rates in data acquisition operations can be used. This depends on the utilisation of appropriate domains of analysis and the development of new time delay estimation algorithms in order to overcome the challenges associated with lowering the sampling rate. To validate these findings in a wireless system using centralised AWSNs, this chapter introduces a lab-based experimental wireless setup for ASL in conjunction with the use of low sampling rates. In addition, it proposes algorithms for centralised data processing based on the utilisation of the envelope feature and wavelet transform (WT) technique for processing data received from the wireless system globally at a central unit. Such algorithms are also required to mitigate the problems accompanying the use of AWSNs, including errors relevant to time synchronisation issues among wireless units, which affect the accuracy of TDE.

The methods proposed are also used to smooth the contents of the aliased versions received through the combination of different time-frequency contents. Enhanced versions of aliased signals are processed using cross-correlation (CC) in conjunction with a parabolic fit interpolation to accurately calculate the time delay. Shannon entropy (SE) is used to select an optimum scale index which gives the optimum spatial resolution. Such an algorithm is useful for developing precise wireless ASL without the need for any excessive sensor resources, particularly for SHM applications.

The chapter is organised as follows. Section 4.1 presents a brief background to this work. Section 4.2 discusses data processing strategy for the aliased data. The TDE algorithms proposed for sound localisation is discussed in Section 4.3. Section 4.4 describes

the Shannon entropy based TDE algorithm proposed for minimising the computational complexity of the previous method. Section 4.5 presents the experimental setup for the ASL system using AWSNs. In Section 4.6, the estimation results of sound localisation using both proposed methods are discussed and compared. Finally, the conclusions are drawn in Section 4.7.

### **4.1 Background**

The integration of acoustic sensors into WSNs opens up new horizons for transforming wired ASL systems into wireless systems [191]. This involves the utilisation of distributed wireless units which are able to realise on-board computation to achieve either distributed or centralised data manipulation. Such integration has been adopted in a large variety of applications, including vehicle identification [192], SHM [140], and military activities [193].

WSNs have been widely used in such applications due to the enormous number of advantages that are highlighted in chapters one and two as well as in Yick et al. [37]. The use of such wireless technology also faces challenges during implementation in real applications as discussed earlier and in a review and discussion published by Jangra [194] of various issues associated with WSNs, including bandwidth and computational limitations at the level of the wireless unit.

Therefore, the utilisation of low sampling rates, as discussed in Chapter 3, will help in solving such problems, since power consumption is linearly proportional to the sampling rate of an analogue-to-digital converter [146]. Recently, there has been growing interest in the use of low data acquisition sampling rates in WSNs [165] so that low-cost commercial off-the-shelf (COTS) wireless units can be implemented without the need for extra hardware resources. Nevertheless, lowering the sampling frequency below the Nyquist criterion can be detrimental due to information loss, which produces inaccurate results in sound localisation.

### **4.2 Signal Processing Strategy under the Use of Low Sampling Rates**

To the best of the present author's knowledge, no wireless ASL system has previously used low sampling rates below the Nyquist criterion to process the aliased versions to locate sound sources. Therefore, the goal of this chapter is to validate the feasibility of

using low sampling rates in AWSNs to develop a low-cost, energy-efficient, and reliable wireless ASL. At the same time, this study tries to achieve a reasonable estimation accuracy of sound location using data obtained from AWSNs and to analysis them in time-frequency domain, even if the Nyquist rule is violated.

The strategy of performing this is based on the utilisation of a signal envelope instead of amplitude values in the TDE process. This is because the envelope is a preferred method for smoothing the shape of a signal and minimising the ambiguity present around its onset. This has been used in several applications such as ultrasonic ranging measurements [195]. However, although using the envelope as defined so far instead of amplitude signal values is an essential step, it is insufficient to establish a robust localisation algorithm at low sampling rates. Further steps are needed to enhance estimation accuracy. Therefore, the WT is proposed to extract the time and spectral contents of the aliased signals, which help in facilitating further improvements in TDE accuracy. The next section will discuss this strategy in more details.

### 4.3 Proposed Localisation Method

To date, there has been no progress in the development of TDE and localisation algorithms, when the low sampled data are involved in the estimation process of the time delay based on the aliased versions of the signals captured. This section discusses a localisation technique proposed to counteract the effect of violating the Nyquist criterion as well as noise effects and to improve time resolution in order to gain feasible localisation results. There is a variety of time-frequency methods, including the short-time Fourier transform (STFT), Hilbert-Huang transform (HHT), Wigner-Ville distribution (WVD), and wavelet transform (WT). In this work, the latter approach is utilised here to overcome the challenge of using low sampling rates using AWSNs.

This technique is known as envelope-based WT cross-correlation (EWT-CC), and is a three-stage strategy, as shown in Figure 28. In the first stage, the envelopes of the aliased signals denoted by  $\tilde{x}_i(t)$ , where  $i = 1, \dots, 3$ , are extracted using the methods explained in the next section. In the second stage, the WTs of these envelopes are computed. This is achieved by the utilisation of discrete values for the scaling parameter  $s_j, j = 1, \dots, N$ . For each scale index, the CC in conjunction with a parabolic fit interpolation in the wavelet domain is applied to estimate the time delay  $\tau_{12j}$ . Finally, the aver-

age of the computed delays is calculated in order to obtain the final time delay  $\tau_{12}$ . These steps are discussed in detail in the following subsections.

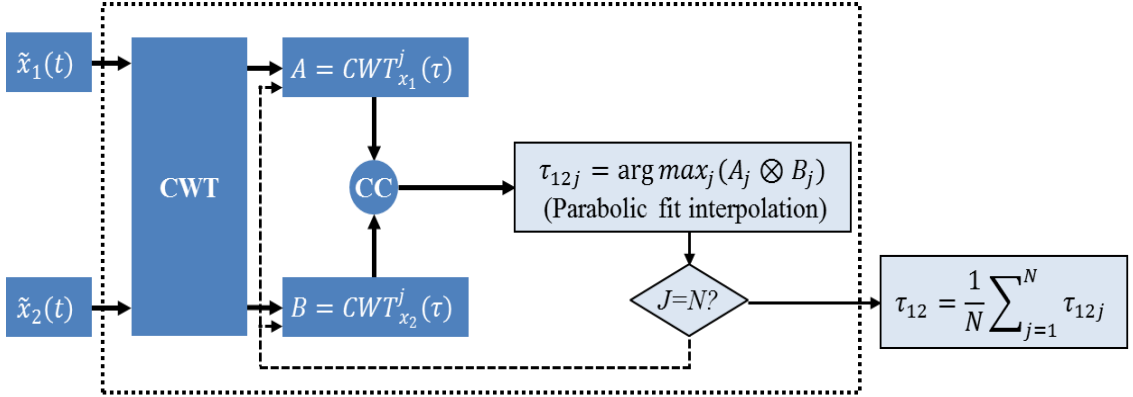


Figure 28: Detailed block diagram of the proposed TDE algorithm EWT-CC.

### 4.3.1 Envelope Fitting for Smoothing Shape Feature

In the literature, several methods can be employed to extract the envelopes of signals captured. Actually, any extraction method can be used here as long as no time delay is introduced due to its operation. Envelopes are usually extracted from band-pass filter outputs by full-wave rectification and low pass filtering. Another method, which is implemented in this work, is to use the square root of the energies of the original and the Hilbert transformed signals, as shown in Equation (4.1) [196].

$$\tilde{x}_i(t) = \sqrt{x_i(t)^2 + \hat{x}_i(t)^2} \quad (4.1)$$

where  $x_i(t)$  is the original signal,  $\hat{x}_i(t)$  is the Hilbert transformed signal,  $\tilde{x}_i(t)$  is the obtained envelope, and  $i \in (1, 2, 3)$ .

### 4.3.2 Wavelet Transform

Both the continuous wavelet transform (CWT) and discrete wavelet transform (DWT) have been found to be effective approaches in many applications, including in the signal processing field. In this study, the WT is proposed to counteract the impact of using low sampling rates on the estimation accuracy of sound source location. In mathematics, the WT is defined for a signal  $x(t)$  as in Equation (4.2):

$$WT_x^\xi(\tau, s) = |s|^{-1/2} \int x(t) \xi^*\left(\frac{t-\tau}{s}\right) dt \quad (4.2)$$

where  $\xi(t)$  is the transforming function or mother wavelet which can be expressed as in

Equation (4.3) [197]:

$$\xi_{(\tau,s)}(t) = |s|^{-1/2} \xi\left(\frac{t-\tau}{s}\right) \quad (4.3)$$

where  $\tau \in \Re$  and  $s > 0$  are the translation and scale parameters of the mother wavelet respectively. The factor  $1/\sqrt{|s|}$  is an energy normalisation factor and ‘\*’ denotes the complex conjugate [198]. Equation (4.2) is also known as the CWT, which has the ability to break up a continuous-time function into wavelets by performing an inner product between the signal and a series of daughter wavelets. These series are generated by the stretching and translation of the mother wavelet via controlling  $s$  and  $\tau$  values [199]. Such an operation provides the capability to analyse the signal at different levels of resolution and to present the processed signal in the time-frequency domain. This highly convenient property offers the possibility of good time and frequency localisation, as explained in the next section.

In addition, the WT offers several different valuable mother wavelets that can be employed in the CWT, DWT and in the signal analysis, including Haar, Meyer, Morlet, Daubechies, Mexican Hat, Gaussian and many others available in the MATLAB library [200]. Table 6 lists some popular mother wavelet families. The range of various wavelet filters, indeed, represents the strength of this transform. This means that, based on the signal features or shape, an optimum mother wavelet, which is closest to the signal under test, can be selected for the detection of those particular features. This can be achieved by the utilisation of quantitative criteria, including the maximum energy or minimum Shannon entropy (SE) [201, 202].

#### 4.3.2.1 *Optimum Mother Wavelet Selection for Signals under Analysis*

The key to the use of the WT here is to look for a set of wavelets that contain descriptions which are most close to the signal under analysis [202]. This is performed by stretching and translating the mother wavelet via varying the scale index  $s_j$ . Therefore, the more similar these wavelets are to the signal components, the larger the wavelet coefficients. This means that the wavelet coefficients will have relatively high magnitudes for the case where a high correlation between a major frequency component corresponding to a particular component exists in the signal, and in the mother wavelet.



This allows the derivation of a basic criterion in the selection of the mother wavelet for signals under investigation. To apply this criterion to the problem at hand, some arbitrary wavelet filters are selected, and then the cross correlation-coefficients between these signals and the chosen mother wavelets are computed. Finally, the optimum mother wavelet is the wavelet which maximises the cross-correlation coefficient. Figure 29 shows the normalised cross-correlation coefficient of aliased versions of acoustic signals, which are captured in three real wireless measurements, namely  $M_1$ ,  $M_2$ , and  $M_3$  as discussed in Section 4.5, with the wavelet filters listed in Table 6.

It is clear that the Mexican hat wavelet exhibits the largest cross-correlation coefficient in comparison to those from the rest of the wavelet filters. This mother wavelet is then considered as the optimal mother wavelet for the range of experiments conducted in this study. However, this may vary from one application to another based on the nature or shape of the signal and the order of the mother wavelet used. The experimental results discussed in Section 4.6 will further validate these results regarding the selection of the optimal mother wavelet.

The reason behind the maximisation of the cross-correlation coefficient when the Mexican hat wavelet is used is the large similarity between this wavelet and the envelope of the aliased versions under analysis. In addition, the noise generated is uncorrelated with the Mexican hat wavelet and thus its effects can potentially be reduced in the estimation process. As shown in Figure 29, there are also good correlations among the Daubechies order 4, Gaussian order 4, and the test signal, which is most likely due to the similarities in shape between these wavelets and Mexican hat wavelet as shown in Table 6. Although the Haar wavelet shape differs from the shape of the optimum wavelet, its correlation coefficients also show high values and this may be due to the fact that this wavelet is good at transient or discontinuity detection [203, 204].

Finally, the DWT is another form of WT which involves the use of the dyadic scheme. This is satisfied by the utilisation of discrete values of the scaling and translation  $s = 2^j, \tau = k2^j, j, k \in \mathcal{Z}$  [197], where  $\mathcal{Z}$  denotes the set of integers. In this study, CWT is applied instead of DWT [197]. This is because CWT does not require that the wavelet has to satisfy the orthogonality condition, which makes the selection of an appropriate mother wavelet for feature extraction easier. Another reason for this utilisation is that the CWT can be time-invariant which means the same phase relationship is reserved

and no additional time delay is introduced [197, 205].

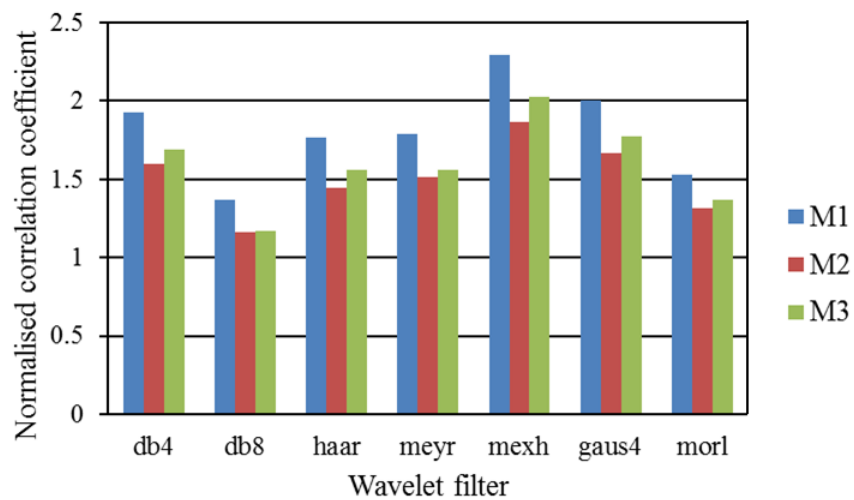
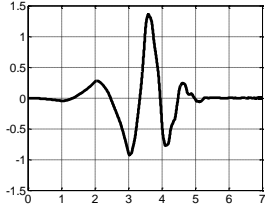
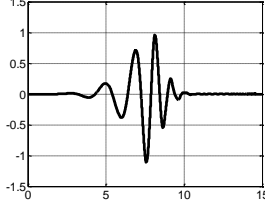
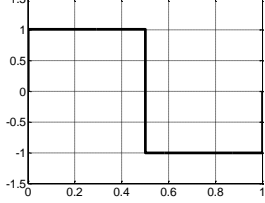
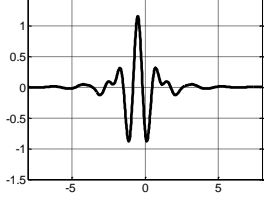
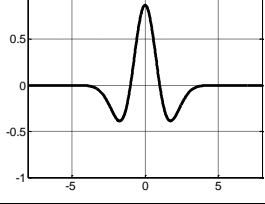
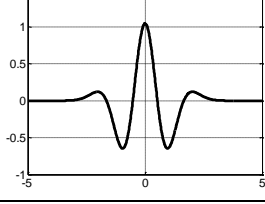



Figure 29: Comparative plot of correlation coefficients with various wavelet filters for the signals under investigation.

Table 6: Waveforms of some selected mother wavelet.

Mother wavelet	Wavelet function plot
Daubechies wavelet: 'db4'	
Daubechies wavelet: 'db8'	
Haar wavelet: 'haar'	
Meyer wavelet: 'meyr'	
Mexican hat wavelet: 'mexh'	
Gaussian wavelet: 'gaus4'	
Morlet wavelet: 'morl'	

### 4.3.2.2 Sound Localisation Using WT and CC

As mentioned previously, the proposed technique for locating a sound source wirelessly is a centralised approach known as EWT-CC. This means that this algorithm requires the aliased versions to be received at the central unit in order to localise the sound source. To estimate the time delay between any two received signals, for instance  $x_1(t)$  and  $x_2(t)$ , there are many techniques which, as explained in Chapter 3, can be applied to these signals. One of these is the conventional CC, which is expressed in Equation (4.4) [180] and used here for comparison purposes and to be combined with WT:

$$R_{x_1 x_2=1/(T-\tau)} \int_{\tau}^T x_1(t)x_2(t-\tau)dt \quad (4.4)$$

where  $T$  is the observation time interval. The aim of Equation (4.4) is to examine the coherence between the received signals in order to estimate the time lag at which the CCF has its maximum.

In the proposed algorithm, the CWT is applied to the envelopes extracted from the aliased acoustic signals received at the central unit, for example,  $\tilde{x}_1(t)$  and  $\tilde{x}_2(t)$ , just before the execution of the CC algorithm. Equations (4.5) and (4.6) represent the CWT of these envelopes.

$$CWT_{x_1}^j(\tau) = \int \tilde{x}_1(t)\xi^*\left(\frac{t-\tau}{s_j}\right)dt \quad (4.5)$$

$$CWT_{x_2}^j(\tau) = \int \tilde{x}_2(t)\xi^*\left(\frac{t-\tau}{s_j}\right)dt \quad (4.6)$$

As stated above, varying the  $s$  parameter in the mother wavelet in Equations (4.5) and (4.6) leads to the dilation or compression of the signals, which allows to search for the similarity in terms of frequency contents between the series of daughter wavelets and  $\tilde{x}_i(t)$  at each scale index:  $s_j, j = 1, \dots, N$  where  $N$  is the number of variations and  $\tau$  is assumed to be equal to the sampling period [197]. The process of dilating or compressing the signal via scale variation allows us to analyse the signal and to compute the wavelet coefficients at different resolutions (i.e., in multi-resolution analysis). The CWT coefficients here represent a measure of the cohesion between the signal and the mother wavelet, at that particular scale index. If the frequency components of the signal correspond to the scale of the mother wavelet, then the computed coefficients at this time instant in the timescale are comparatively large [197].

As a result of this process, two 2D wavelet coefficient matrices are generated for Equations (4.5) and (4.6); namely,  $A$  and  $B$  respectively, as shown in Figure 28. Each row in  $A$  and  $B$  corresponds to the  $j^{\text{th}}$  wavelet coefficients. The size of these matrices is  $(N \times M)$  where  $M$  is the length of the processed signal. At each level of resolution the time delay is estimated. As seen in Figure 28, after obtaining the  $j^{\text{th}}$  wavelet coefficient matrices, the CC algorithm in conjunction with curve-fitting interpolation is applied to the individual rows  $A_j$  and  $B_j$  in order to estimate the delay under the  $j^{\text{th}}$  scale, as in Equation (4.7):

$$\tau_{12j} = \arg \max_j (A_j * B_j) \quad (4.7)$$

where “\*” denotes the conventional CC. This process is repeated until  $j = N$  and then the actual time delay  $\tau_{12}$  between  $x_1(t)$  and  $x_2(t)$  can be calculated by taking the average of  $\tau_{12j}$  as given in Equation (4.8):

$$\tau_{12} = \frac{1}{N} \sum_{j=1}^N \tau_{12j} \quad (4.8)$$

Once the time delays are estimated, as shown in the previous paragraph, using the last equation, the propagation path differences (PPDs) as well as the sound location can be computed as explained in Chapter 3.

The method discussed above uses a multi-scale averaging technique to estimate the delays among received signals. This represents a drawback of this algorithm, since it is time-consuming. To counteract this, a Shannon entropy (SE) criterion is applied in Section 4.4 to optimise the selection of the best scale index that gives the best estimation accuracy without the need to perform multi-scale averaging. Next, the use of parabolic fit interpolation is discussed.

#### 4.3.2.3 *Parabolic Fit Interpolation for Improvement of Spatial Resolution*

In the classical time delay estimation measurements, the discrete cross-correlation is only calculated at integer indices. This means that inaccurate estimation is given if the true delay between two signals is a non-integral multiple of the sample period. There are several techniques that can be used to optimise this time resolution, such as a parabolic interpolation [206] where the position of the peak is located at its centre. Theoretically, fitting a parabola requires at least three points, as shown in Figure 30: the maximum

peak of correlation coefficients ( $I_0$ ), its preceding ( $I_{0-1}$ ), and subsequent ( $I_{0+1}$ ) neighbours. The three points are needed in order to calculate the coefficients  $a$ ,  $b$ , and  $c$  in Equation (4.9) which represents the applied parabola [206]. In Figure 30, the blue dotted curve represents the curve fitted to the red dashed curve of the cross-correlation output.

$$y = ax^2 + bx + c \quad (4.9)$$

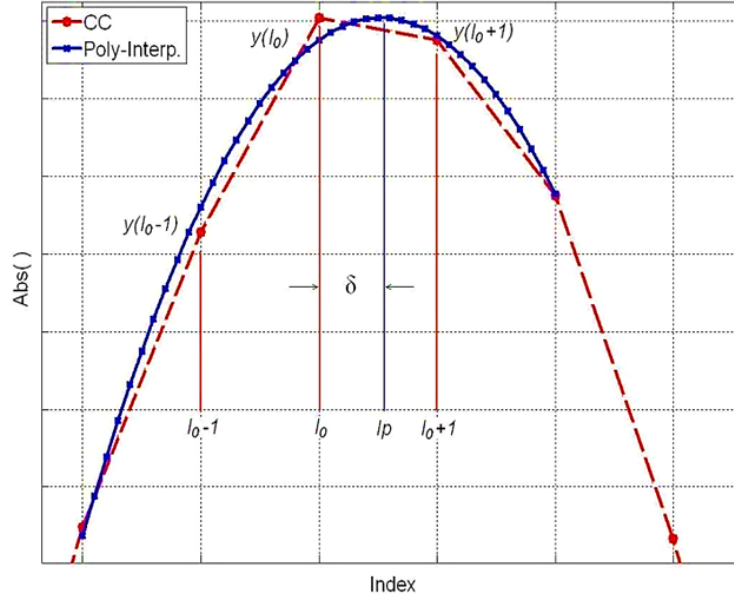


Figure 30: Curve-fitting interpolation using three points.

The coefficients  $a$ ,  $b$ , and  $c$  in Equation (4.9) are calculated by substituting the three sample points and their corresponding indices in the parabola equation, which yields the following Equations (4.10a-c):

$$y(I_0 - 1) = aI_{0-1}^2 + bI_{0-1} + c \quad (4.10a)$$

$$y(I_0) = aI_0^2 + bI_0 + c \quad (4.10b)$$

$$y(I_0 + 1) = aI_{0+1}^2 + bI_{0+1} + c \quad (4.10c)$$

Once the coefficients  $a$ ,  $b$  and  $c$  are calculated, the derivative of Equation (4.9) can be taken. This equals zero when the peak is maximum; therefore, the interpolated peak,  $I_p$ , is computed, as illustrated in Equation (4.11).

$$I_p = -b/2a \quad (4.11)$$

A series of experiments have been conducted in order to estimate the propagation path differences, as discussed in Section 4.6, which show the performance of the proposed

parabolic fit interpolation. Based on the current setting of the sample frequency used in these experiments (4807Hz), the minimum distance resolution was improved in these experiments in average from 7.07cm to 1.50cm, which is almost five times better. Such an improvement resolution will contribute to increasing the estimation accuracy of sound source localisation using the AWSNs at low sampling rates, as illustrated in Section 4.6.

#### 4.4 Shannon Entropy based EWT for TDE

The modified technique, Shannon entropy-based EWT (SE-EWT), is also a three-stage strategy, as shown in Figure 31. In the first stage, the envelopes of the received signals  $\tilde{x}_i(t)$  are extracted, as mentioned in Section 4.3.1. The second stage applies CWT to the envelopes extracted, as explained in the previous section. In the last stage, the SE of the wavelet coefficients (SEWCs) is computed and the best scale value for the TDE is specified, as discussed in the following subsection.

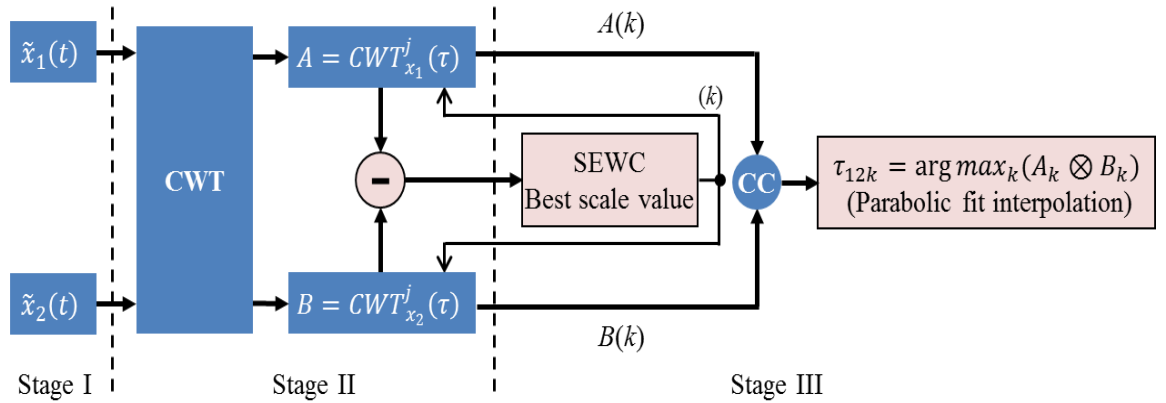


Figure 31: Detailed block diagram of the modified TDE algorithm, SE-EWT.

##### 4.4.1 Shannon Entropy Criterion for Optimum Scale Selection

SE measures the degree of similarity between different segments of signals and gives an excellent indicator of energy concentration [207]. In other words, the energy distribution of the wavelet coefficients can be described by this criterion. This is why the SE has been utilised in different applications for the selection of a suitable and optimal mother wavelet-based CWT. This is required in order to obtain the best performance in the application used [208, 209].

In this research, the SE is adopted in the proposed TDE algorithm in order to select the

most appropriate CWT scale index which gives the best TDE accuracy. This is because varying the scale value within the CWT will produce the local minima in the wavelet domain if SE is applied. In this case and at that particular scale, the similarity in terms of frequency contents between the series of daughter wavelets and signals processed will be high. This means that the more similar the mother wavelet is to the signal components, the larger the wavelet coefficients [202]. This criterion will then yield the best scale value that gives the maximum resolution.

Below, a mathematical definition of SE is first given, and then its use in the choice of the optimum scale is explained. For any discrete probability distribution,  $P$ , where  $P = (p_1, p_2, \dots, p_M)$ , the SE is defined as in Equation (4.12) [202].

$$SE(P) = \sum_{i=1}^M p_i \cdot \ln(p_i) \quad (4.12)$$

Assuming that the wavelet coefficients of an input signal  $x(t)$  calculated at a scale index,  $a$ , are denoted by  $C_a = (c_{a,1}, c_{a,2}, \dots, c_{a,M})$ , then the normalised SEWC of the computed CWT coefficients at the scale  $a$  is given by Equation (4.13):

$$SEWC(a) = \sum_{i=1}^M \left( \frac{c_{a,i}^2}{C} \cdot \ln\left(\frac{c_{a,i}^2}{C}\right) \right) \quad (4.13)$$

where  $C$  is a normalisation factor calculated using Equation (4.14):

$$C = \sum_{a=1}^M \sum_{i=1}^N c_{a,i}^2 \quad (4.14)$$

To find the most appropriate CWT scale for the best resolution, the SEWCs are computed using Equation (4.13) for all scale values. Then the best scale is equal to the minimum index of the SEWCs, as in Equation (4.15). The reason behind selecting the minimum value is that the higher energy concentration is, the lower the SEWC will be.

$$Optimum\ Scale = \arg \min_s (SEWC_s) \quad (4.15)$$

#### 4.4.2 Problem of Applying SE and CWT

As mentioned previously, the aim of using the SE here is to select the best scale index which leads to the best TDE accuracy. However, due to the properties of time-frequency algorithms such as WT, the generated wavelet coefficients for both envelopes  $\tilde{x}_1(t)$  and  $\tilde{x}_2(t)$ , represented by matrices  $A$  and  $B$  respectively in Figure 28, include large amounts of redundant data. This redundancy is caused by the redundant information generated for the same time point due to the change in the scale index during the calculation of the



CWT [210].

Therefore, applying the SE directly to such redundant data may lead to miscalculation of both the local minima as well as the optimum scale value. An example showing this redundancy is illustrated in Figure 32-a and -b. These figures show the coefficients for real aliased acoustic signals captured at low sampling rates using the system setup discussed in the next section. These coefficients are displayed as images for the scale range 1 to 200. The WT shows the occurrence of a single, short duration acoustic pulse around index 125.

To overcome this problem and in order to make SE work efficiently, the redundant data were filtered out via subtracting the wavelet coefficients of matrix  $B$  from those of matrix  $A$ . The result of this subtraction is depicted in Figure 32-c which displays the difference between the previous two images. The advantage of this step is that it removes the ambiguity in finding the local minima and therefore the optimum scale value can be accurately computed.

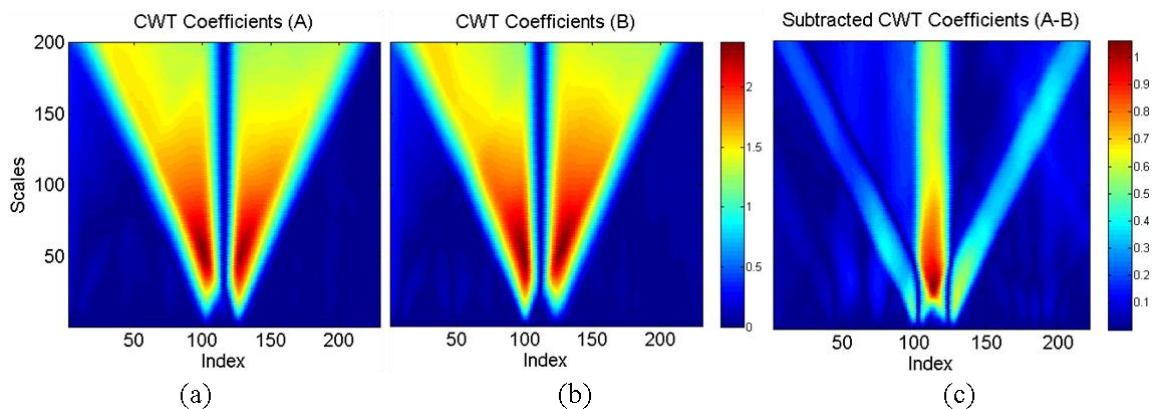


Figure 32: Redundancy of CWT coefficient (Zoom-In) of an acoustic pulse: a) matrix  $A$ , b) matrix  $B$  and c) difference  $(A-B)$ .

Figure 33 shows the computed SEWCs vs. scales as a consequence of applying SE to  $A$ ,  $B$ , and the difference  $A-B$  for real data. As is clear from this figure, there are no minima in either the  $A$  or  $B$  curves for the range of scales shown. On the other hand, the SEWCs of the difference  $A-B$ , the dashed curve, obviously have a minimum which helps in the determination of the optimum scale index that gives the most accurate TDE results according to Equation (4.15) and as discussed in Section 4.6.2.

The major advantage of the new SE-based envelope WT algorithm over the proposed

algorithm discussed in Section 4.3 is that the computational complexity of the former approach is much lower. In the SE-based envelope WT method, there is no longer a need to estimate the delay at each scale index using the CC in conjunction with a parabolic fit interpolation in the wavelet domain. Instead the SE-EWT applies the CC only once, at the selected optimum scale index, to estimate the time delay  $\tau_{12}$ . This leads to a reduction in the computational complexity by a factor of  $N$ . Table 7 summarises the approximate computational complexity of both algorithms which shows the degree of reduction in complexity.

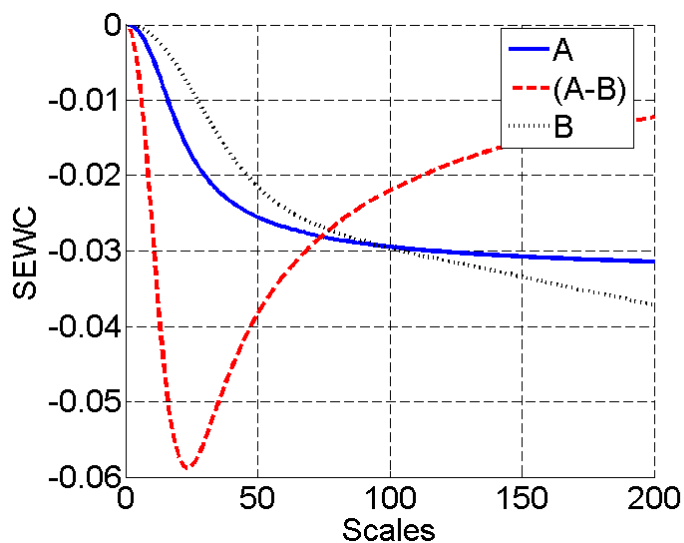


Figure 33: Shannon entropy of wavelet coefficients, SEWCs, vs. scales.

The calculation in Table 7 is based simply on the evaluation of the most important parts in both algorithms and on the assumption that the number of samples is  $M$ , the number of scales is  $N$ , and the number of lags is  $n$  for which the CC is computed. It also does not take into account the computational complexity of CWT because this is the same for both algorithms. As a next step, both algorithms are tested and evaluated using the experimental wireless work presented below.

#### 4.5 Experimental Setup for ASL Using AWSNs

The abovementioned low sampled TDE algorithms are intended to be utilised in a wireless ASL application. Thus, before the performance of the proposed algorithm is validated and discussed, it is most important to explain the wireless system setup used in

the experimental work. In addition, problems with the realisation of synchronised sensing in this wireless ASL system are also discussed.

**Table 7: Computational complexity comparison of both TDE algorithms.**

Method	Summation			Multiplication		
	CC	AVG	SE	CC	AVG	SE
EWT-CC	$2N^2 \sum_{n=0}^{M-1} (M-n)$	N	-	$2N^2 \sum_{n=0}^{M-1} (M-n)^2$	-	-
SE-EWT	$2N \sum_{n=0}^{M-1} (M-n)$	-	N	$2N \sum_{n=0}^{M-1} (M-n)^2$	-	N

#### 4.5.1 Configuration of the Experimental AWSNs

The principle of WSNs discussed in Chapter 1 is proposed here for implementing a wireless ASL system which is then used to test and validate the TDE and ASL algorithms proposed based on the use of low sampling rates. The system was employed to study the utilisation of a single-hop WSN for sound source localisation at uniform low sampling frequencies with more attention is given in this study to the sensing process. Thus, this work can be easily extended to multi-hop WSNs for data collection from multiple sources by integrating multi-hop data collection protocols such as CTP [211].

This section discusses the system configuration designed and implemented as a proof-of-concept model for the wireless ASL system. The hardware prototype for the designed single-hop WSN comprises hardware components such as wireless sensing units, a base station (gateway) and a central control unit (PC). Each wireless sensing unit consists of a wireless node, a signal conditioning, and a microphone and takes charge of capturing acoustic signals independently. Each unit is programmed with a unique identification number to prevent data chaos in data transmission.

The schematic structure of the wireless sensing unit is depicted in Figure 34. This structure mainly consists of signal conversion, processing core, data storage and wireless communication components as well as signal conditioning part. Some of the key components which make up single-hop WSNs are discussed in this section.

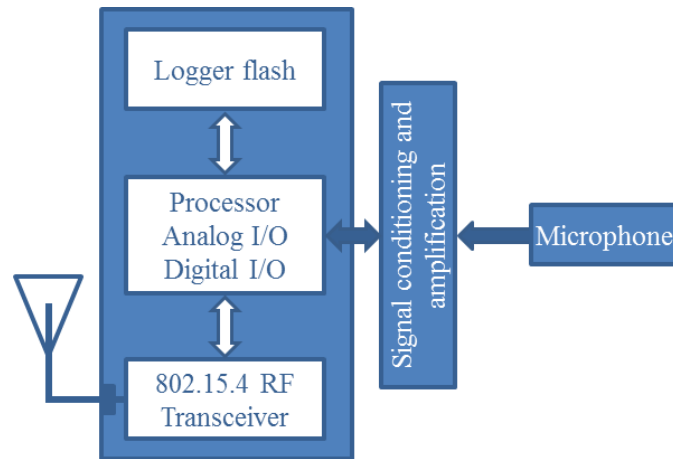


Figure 34: The schematic structure of a wireless sensing unit.

#### 4.5.1.1 *Signal Conditioning*

Generally, the outputs of microphone sensors have to be pre-processed through signal conditioning and amplification circuit boards. This is required in order to filter and adjust the acoustic waveforms to the ADC inputs of a wireless node used. For this purpose, MTS310 sensor board has been used as low-cost current state-of-the-art sensor technologies that provide capabilities to use different sensor modalities [212]. One of these modalities is an omni-directional microphone sensor which is used in these experiments to collect the acoustic signals generated.

#### 4.5.1.2 *Wireless Node of AWSNs*

MICAz motes represent one of the low-cost current state-of-the-art sensor technologies that provide capabilities to build wireless networks [37]. The MICAz is 2.4GHz, IEEE/ZigBee 802.15.4 boards equipped with 4KB of RAM. At the centre of the mote is the processing core which contains function modules for data collection, processing and communication control. The MPR2400 is based on the Atmel ATmega128L and capable of running at speeds up to 7.3MHz [213]. This mote also supports a 10 bit analogue to digital converter with 8 channel and 0-3V input range, refer to Appendix A for more specification details. All the motes used are programmed under the TinyOS environment which is an operating system which has been widely used for WSN design [214].

#### 4.5.1.3 *Wireless Setup of ASL System*

The experimental wireless sensing setup is shown in Figure 35. The figure also illus-

trates the triangular configuration which is composed of three wireless units and a sound source used for this purpose. The wireless units are placed in a straight line at different positions ( $P_0$ - $P_4$ ) in order to construct a sensor array with a known geometry and to give different test configurations.

One of these wireless units acts as a reference node and is positioned at  $P_2$ . The locations of the two other wireless units vary between points  $P_0$  and  $P_4$  and, accordingly, the PPDs  $d_n$  and  $d_m$  also vary. The PPDs are the extra distances that the acoustic signals generated from  $S$  travel in order to reach the two wireless units with respect to the reference node. For simplicity, it is assumed that these nodes are located at points  $P_0$  and  $P_4$ .

The mathematical model for the acoustic signals received at any wireless unit is described in Section 3.3. Next, the process of the TDE using EWT-CC is explained. These units sense simultaneously via the omni-directional microphone sensor and send the data to a base station. All the sensing units communicate with the base station via a radio frequency (RF) interface. An MIB520 gateway board incorporating a MICAz mote is used to forward the captured aliased signals to the central unit where they are processed off-line using MATLAB. The sound source is then located using the approaches explained above. In the following, both acoustic sensing and RF transmission strategies are discussed in more detail. After that, issues regarding the realisation of a synchronised data acquisition process among wireless units are discussed.

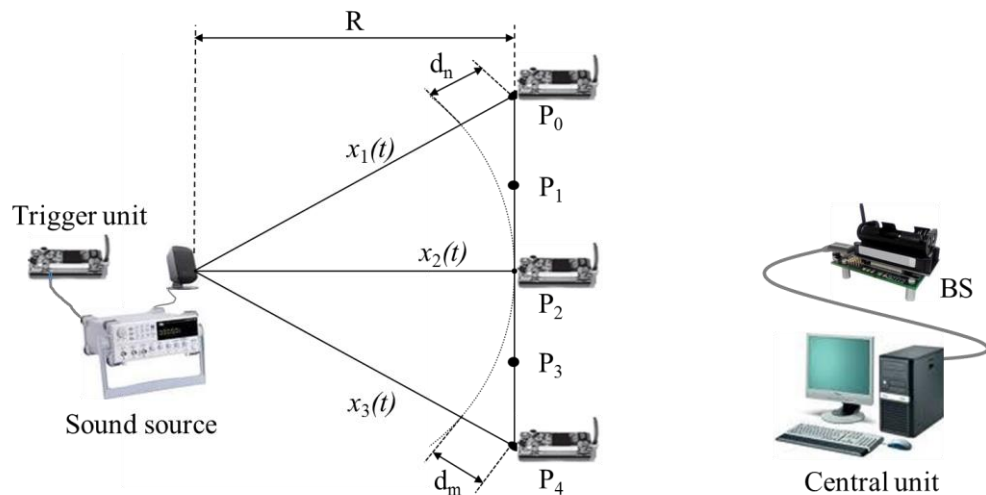


Figure 35: Wireless experimental setup and the triangular configuration of wireless units-sound source for the localisation where  $P_i$  represents wireless unit position and  $R$  is the shortest path between sound source  $S$  and the wireless unit located at  $P_2$ .  $R$  varies between 1 and 2.5m.

The experiments were conducted in an ordinary indoor laboratory environment which contains objects such as tables, PCs and lab equipment. Street traffic and people talking contributed to the background noise where the experiments were being conducted.

#### 4.5.1.4 Acoustic Sensing Strategy

The acoustic sensing process within the single-hop WSN commences with the receipt of a start command which is broadcast by the base station. For the purpose of testing and validation of the proposed algorithms, an additional wireless unit is used to trigger the KEITHLEY 3390 function generator, as shown in Figure 36. This is needed in order to generate the acoustic test signal within the sampling period of the wireless units employed in order to make the detection process easier. (In a real SHM system where acoustic emission events are random, a simple threshold crossing is used to ensure that such events will be captured by the wireless units, as discussed in Chapter 5). This wireless unit is programmed so that one of the LEDs turns on once it receives the start command. This LED (Pin 1) is connected to the trigger input of the function generator in order to trigger it during the acquisition process of wireless units.

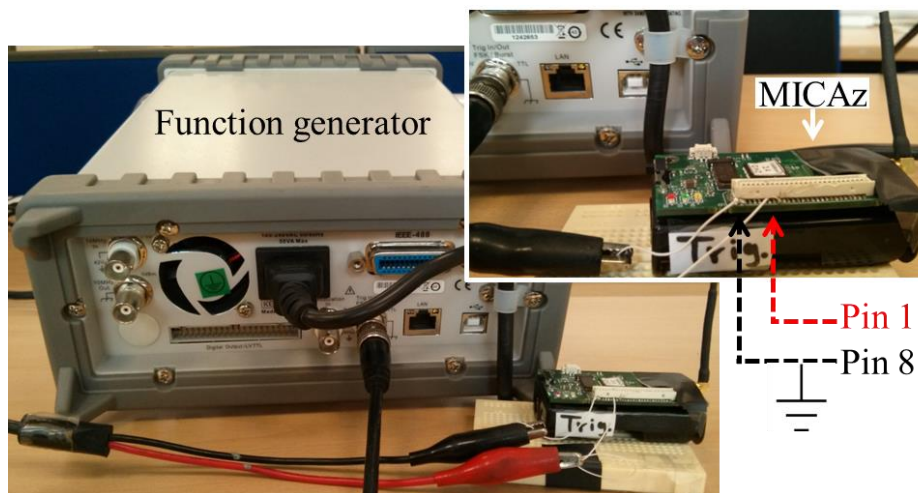


Figure 36: Connection of KEITHLEY 3390 function generator with MICAz as a trigger node.

The test signal used in these experiments was produced using the function generator and simulated through generating a tone burst of 50-sinusoidal cycles of frequency 10kHz which was played via a PC speaker. These values were selected experimentally in order to generate a reasonable acoustic pulse shape used for the experiments conducted.

It is worth mentioning that the TinyOS operating system running on MICAz motes has two modes; namely, the task and hardware event handler (HEH) modes [214]. Both modes can be utilised in performing data acquisition operations, and more discussion of this is presented in Section 4.5.2. In the task mode, the acoustic test signals were acquired at a 4096Hz sampling frequency for a recording period of 0.3s. This sampling rate is almost the maximum sampling rate that the MICAz mote can achieve using such a mode. While in the latter, the generated acoustic signals are acquired at the minimum sampling rate that the MICAz mote can achieve using this mode which is 4807Hz for the same recording period. Note that in Chapter 3, it has nevertheless been shown that lower sampling rates than these can be used.

### **4.5.1.5 RF Transmission Strategy**

As this research focuses more on the sensing process rather than network protocols, it is crucial that data collisions among transmitted data are avoided. To achieve this, the transmission operation is conducted according to the following strategy. The wireless units were given three different levels of priority to start the sending operation. The wireless unit with the highest priority transfers its raw data, in packets with a length of ten samples each, to the control unit once it fills its local buffer, whereas the other two units wait until the first one finishes the transmission process. The second and third levels of priorities are given to the other wireless units. The wireless units with first and second priorities will also not commence a new sensing process until the wireless unit with third priority finishes transferring its collected data.

Having the transmission process in a sequence, as mentioned earlier, can avoid data collisions among transmitted data and ensure that all packets are received correctly. It also ensures to a certain degree that the sensing process amongst the wireless units is synchronised. However, a scheme with higher synchronisation can be utilised by incorporating existing time synchronisation protocols [215, 216], which is left for future work.

### **4.5.2 Realisation of Synchronised Data Acquisition in AWSNs**

As mentioned above, WSNs are composed from multiple acoustic wireless units deployed at different locations. These units should work collaboratively in order to achieve a robust wireless localisation system. Time synchronisation among these units

is likely to be an important factor in helping to satisfy such requirements. Detailed comprehensive reviews of different time synchronisation protocols along with relevant techniques in the decomposition of time delays over a wireless link have been published [217].

Collected signals can be coherent if the wireless units of the WSNs are properly time-synchronised [191, 218]. In addition, WSNs which work depending on high precision clock synchronisation seem to exhibit consistency of collected data, which is likely to help in solving the problem of the redundant detection of the same event and coordination [219]. A further reason why appropriate time synchronisation is an important factor in WSNs is that communication among the sensors can then be more effectively utilised [218].

These reasons and others [219] do indeed require that time synchronisation protocols should be designed and implemented so that WSNs can be robust and beneficial in the intended applications. This leads to the major concern of designing time synchronisation protocols for WSNs which: (a) achieve high precision in time synchronisation, especially in applications such as sound localisation, SHM and tracking moving targets; (b) have the capability of overcoming node and link failures [218]; (c) are robust in situations of dynamic topology change [219]; and (d) require lower communication bandwidth and power consumption [220].

However, from previous studies in the area [221] and the preliminary experimental results using MICAzs in this research, it is noticeable that the use of time-synchronised wireless units based on global time does not guarantee that the acquired acoustic signals or the acquisition operations among wireless units are perfectly synchronised with each other. This is because most time synchronisation protocols consider delays in the radio message delivery in WSNs rather than delays caused by the nature of the operating system which runs on the motes used in that particular application. This nature can generally be deterministic or non-deterministic.

The former means that the start and end of the execution of data acquisition operations can be predicted with a high degree of certainty; whereas in the latter, this execution can occur in an unpredictable order and at unpredictable times, and the execution time of the same code varies at each repeated execution, especially if it is performed on different



microcontrollers, as is the case in WSNs. In real time measurements, this is a very important factor which also needs to be considered in order to perform synchronised sensing measurements in particular when MICAz is used, as discussed next.

To investigate this problem, the TinyOS employed in this research and many others [222] should first be analysed. This operating system has two modes of execution threads: task and HEH modes [214]. The former mode has a non-deterministic nature, which means that the execution time for the same code varies at each repeated execution. This introduces unpredictability into waiting times during the acquisition operation due to the TinyOS scheduler executing posted tasks. This results in unequal intervals, which leads the acoustic sensing tasks of all wireless units unsynchronised, and synchronisation sensing errors (SSEs) thus increase. It also has the disadvantage that it does not allow the users to either control the execution procedures of their measurement process or set priorities among the steps of the measurements.

One attempt to overcome this synchronisation problem has been published [15]. A resampling solution based on a combination of interpolation, filtering, and decimation processes is applied to the acquired signals in order to compensate for SSEs. However, the resampling process is a considerable challenge, since perfect filtering is hard to achieve due to the infinite number of filter coefficients required. Furthermore, the proposed solution increases computational costs which make it impractical in real applications.

In contrast, the HEH mode is a deterministic mode which allows the user to control the execution process by forcing the controller to execute the data acquisition operation via assigning a priority to this operation. This leads the measurement to run with precise timing and a high degree of reliability. Thus, the use of this mode is proposed in this research to realise synchronised data acquisition among acoustic wireless units, since asynchronous commands are immediately executed.

To show the efficiency of the selected HEH mode compared to the task mode in the development of a suitable data acquisition system for the wireless acoustic source localisation system, both modes of the TinyOS were implemented and tested using MICAz motes and the results are discussed in Section 4.6.1.

## 4.6 Results and Discussion

The main aim of this chapter is to develop and evaluate novel time delay estimation algorithms in order to overcome the challenges associated with lowering the sampling rate below than the Nyquist rate in AWSNs. This section introduces and discusses the results of applying both EWT-CC and SE-EWT in order to accurately calculate the time delay from the aliased acoustic signals captured by the wireless ASL system discussed in Section 4.5. To begin with, the results gained for overcoming the synchronisation problem in the sensing operation via considering the HEH mode rather than the task mode are considered. After that, results for both proposed algorithms in conjunction with the parabolic fit interpolation and SE are presented.

### 4.6.1 Synchronised Data Acquisition Process

In order to test the efficiency of the HEH mode in comparison to the other mode, wireless units were positioned at the same points and at the same distances from the sound source. Such a setup should introduce no time delays among the collected aliased acoustic signals, which gives the opportunity to measure levels of SSE caused by the two modes.

Figure 37 shows the first 200 samples of an example of the envelopes extracted from the aliased acoustic signals captured using the wireless units one, two, and three, as they were positioned at the point  $P_2$  in Figure 35. Figure 37-a illustrates the effect of using HEH mode in minimising the SSEs during the acquisition process. Figure 37-b depicts, in contrast, the result of using the task mode where errors in the acquisition process are obviously higher with respect to the onset of these signals.

Theoretically, the onset of the curves shown in Figure 37-b should start at the same time instant because the wireless units were located at the same point. However, this is not the case. This is mainly due to the SSEs introduced by the task mode. To show the random variations in repeated measurements of the task mode in comparison to the HEH mode, the SSEs of 30 experimental measurements are plotted in Figure 38. The time delays were estimated by applying the EWT-CC algorithm to the acquired aliased signals as described in Section 4.3.4.

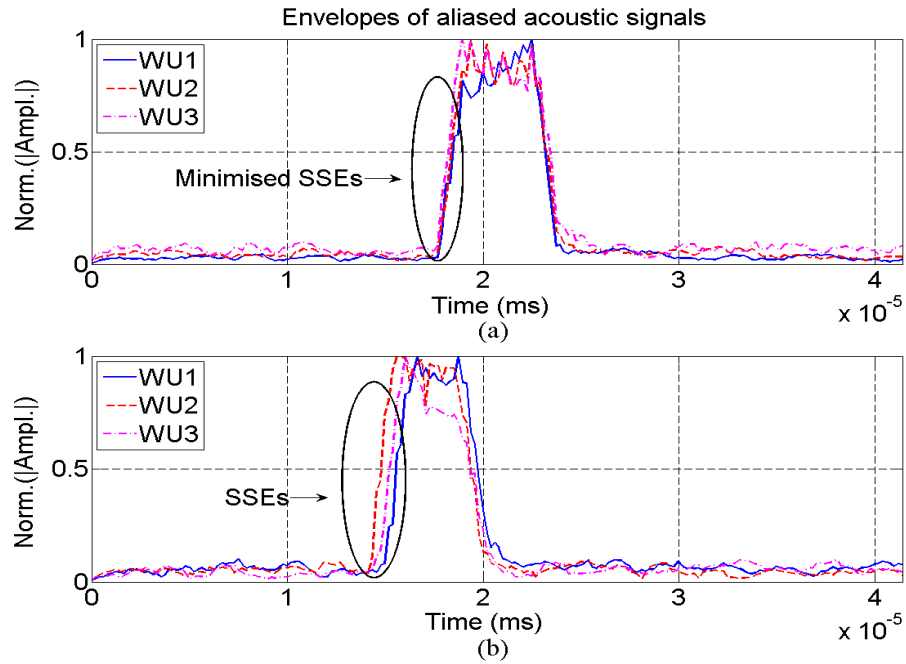


Figure 37: The first 200 envelope samples of captured acoustic signals using a) HEH mode and b) task mode.

From Figure 38, it is clear that the task mode exhibits unstable results due to the non-deterministic nature of this mode, where the average of the calculated SSEs is 1.1ms with a standard deviation of 0.6 which represents a poor repeatability indicator. Such errors yield an estimation error in the PPD around 1m, based on the maximum SSEs and assuming a sound velocity of  $340\text{ms}^{-1}$ , which would represent a massive error if the experiments were considered as a near-field measurement.

In contrast, the HEH mode yields a good repeatability and is able to achieve a sufficient level of accuracy for the TDE which shows an average of 0.06ms with a standard deviation of 0.1. This means the SSEs of HEH mode are much lower than the task mode errors where the RMS errors of the estimated time delays in both modes are 0.1ms and 1.2ms respectively.

To conclude this section, the cause of the SSEs is mainly due to the unsynchronised data acquisition operation, which is caused by the task mode. In contrast, the HEH mode exhibits a significant improvement in delivering synchronised data acquisition operations, since the SSEs of wireless units are minimised due to the deterministic nature of this mode. Such a conclusion is very important for realising synchronised data acquisition operations and designing a robust wireless sound localisation system using low sam-

pling rates and MICAz notes. This is because the minimisation of SSEs contributes to the enhancement of the TDE among the received signals, as seen in the next section.

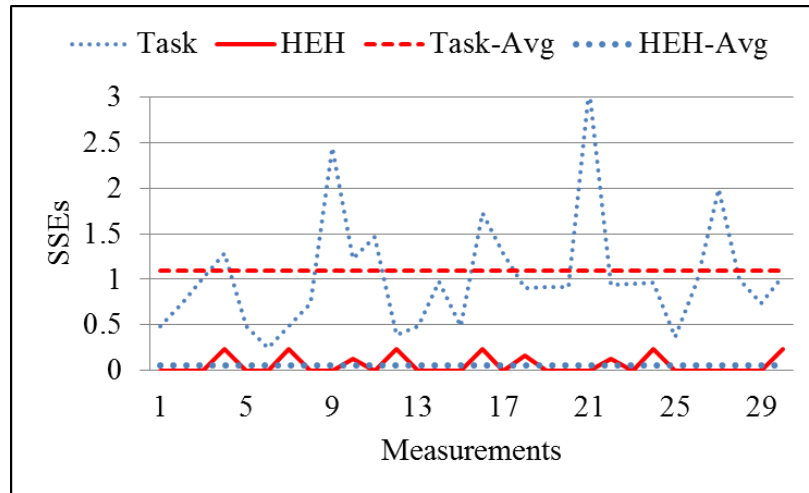


Figure 38: Repeatability measurements of Task and HEH modes.

#### 4.6.2 Wireless ASL at Low Sampling Rates

To evaluate and compare the proposed algorithms experimentally, several measurements have been conducted using the wireless setup shown in Figure 35. In each measurement, the three wireless units simultaneously receive a start sample command from the base station in order to commence the sensing process. The experiments were again conducted in an ordinary indoor laboratory environment as explained in Section 4.5.1. A tone burst of 50-sinusoidal cycles of frequency 10kHz is used as an acoustic test signal played through a PC speaker representing a sound source. This acoustic signal is propagated in the air medium in order to reach the acoustic wireless units. Based on the previous discussion, the HEH mode was selected to program the wireless units in order to minimise the SSEs. The sampling rate was set to 4.8KHz and the sample duration was around 0.3s.

Figure 39-a shows an example of aliased versions of the acoustic signals captured by wireless units one, two, and three, as they were positioned at  $P_0$ ,  $P_2$ , and  $P_4$  in Figure 35 respectively. In contrast, Figure 39-b depicts the envelopes extracted from these aliased versions which preserve the original shape of the test signal used as discussed in Chapter 3. This salient information represents a very important feature of the developed TDE algorithms, as seen below. In both figures, the solid curves represent the signals

received at wireless unit one and the dashed curves show the signals received at wireless unit three, while the dotted curves illustrate the signals received at the reference wireless unit two.

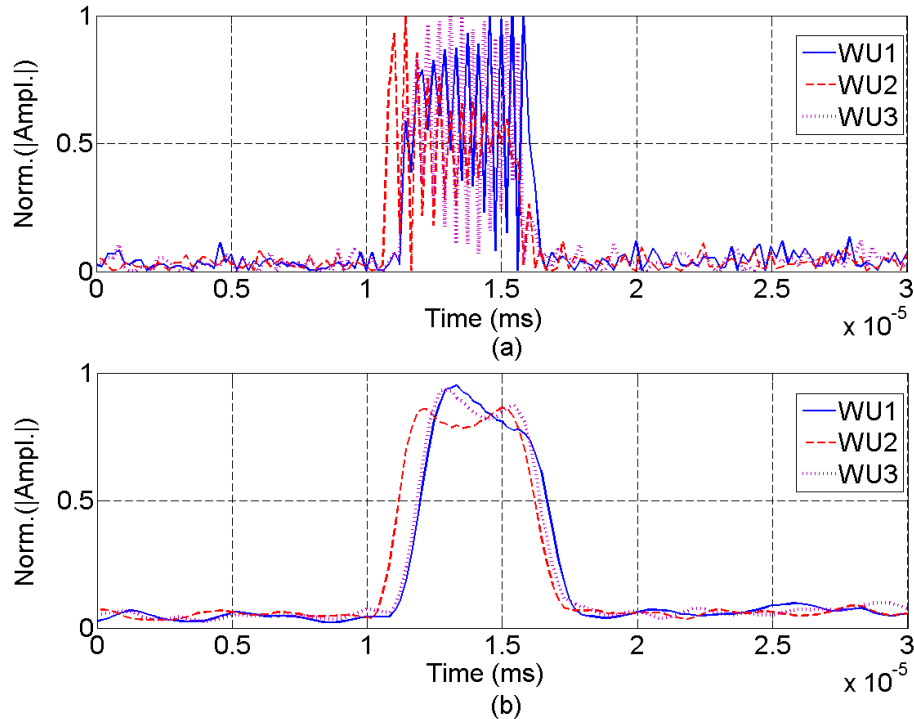


Figure 39: The first 200 samples of captured signals by wireless units one, two, and three at 4.8KHz: a) Aliased acoustic signals b) Their envelopes.

As is seen in Figure 39-b, since the distance between the reference wireless unit and the sound source represents the shortest path, the signal received from this wireless unit appears first in this figure. Whereas the two other wireless units were located at equal distances from the reference node, and their received signals appear second and at almost the same time. Therefore, feeding these envelopes, instead of the original signals, to the WT is an important step towards improving localisation accuracy.

Before the results of this processing are discussed in this section, and for the purpose of showing the functionality of the proposed approaches, as well as explaining how they improve the spatial resolution of the sound source localisation, it is useful to illustrate the advantage of applying the EWT-CC with curve fitting interpolation in improving localisation accuracy.

Figure 40 explains the results of the individual steps of the proposed technique. As

shown in this figure, due to the low time resolution caused by the utilisation of low sampling rates, the output of CCF gives a false maximum index. On the other hand, the WT improves the shapes of the aliased signals and the SNR due to the high correlation between these envelopes and the Mexican hat mother wavelet used. This results in the hidden characteristics of both envelopes being revealed and therefore the output of the EWT-CC becomes narrow, as shown in this figure. This makes the identification of the index of the maximum output much easier. As a final step towards detecting the most accurate index, curve fitting interpolation is applied to the output of EWT-CC as explained in Section 4.3.1.

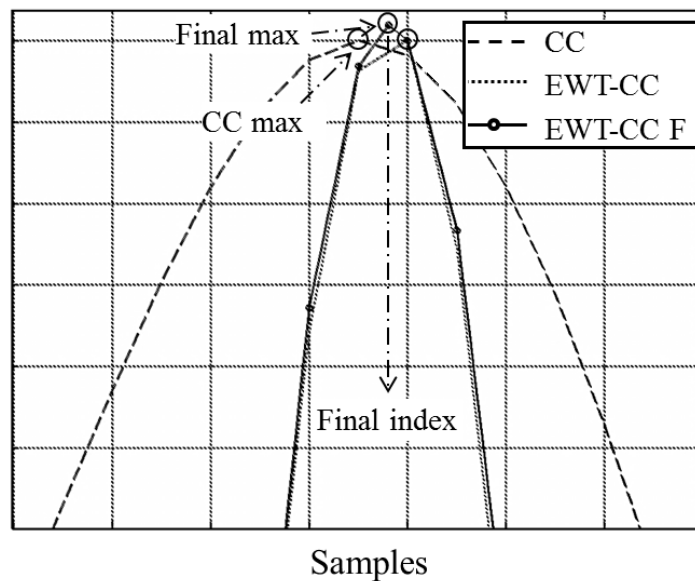


Figure 40: Zoom-In output of CC and EWTCC with and without parabolic fit interpolation.

#### 4.6.2.1 Results of the EWT-CC Algorithm

The results of EWT-CC are validated by conducting several wireless experiments for sound localisation where different values for  $d_m$  and  $d_n$  shown in Figure 35 were estimated. These values result from varying the positions of wireless units one and three between  $P_0$  and  $P_4$ . The results of these experiments are reported in Table 8. This table summarises the  $d_n$  and  $d_m$  estimation results obtained by the developed wireless localisation system using both conventional CC and the proposed EWT-CC with and without curve fitting interpolation approaches. The table also reports the averages and standard deviations of these results gained from 15 experiments in order to show the

robustness of the proposed algorithm in the estimation of these PPDs under the use of low sampling rates discussed in Chapter 3. The results also show that replicated measurements can provide closely similar results.

It is apparent from this table that results when applying EWT-CC with curve fitting interpolation are much more highly correlated with the real values of  $d_n$  and  $d_m$  than the other results. A good example of this is the case where  $d_n = 15\text{cm}$ . The average of the estimated result using EWT-CC with fitting is 15.62cm, while it is 12.26cm using CC and 16.51cm using EWT-CC without fitting. Again, the standard deviation of the EWT-CC with fitting for this example is lower than that of the CC and EWT-CC without fitting. This means that the errors in the estimation of  $d_n$  and  $d_m$  using EWT-CC with curve fitting interpolation are much lower than those with the CC method due to the multiresolution analysis possible with CWT and curve interpolation. Consequently, the use of such a method in the estimation of PPDs exhibits better performance than employing the CC method as shown in Figure 41.

Table 8: AVGs and STDs of estimated PPDs for 15 experiments using CC, EWT-CC, and EWT-CC Fitting.

Configuration of $SN_1$ $SN_2$ $SN_3$	PPDs (cm)		Estimated PPDs (cm)					
			CC		EWT-CC		EWT-CC Fitting	
			AVG	STD	AVG	STD	AVG	STD
$P_2$ $P_2$ $P_2$	$d_m$	00.00	6.14	3.07	1.80	1.14	1.12	0.80
	$d_n$	00.00	2.56	4.58	1.91	1.85	1.23	1.01
$P_0$ $P_2$ $P_3$	$d_m$	15.00	12.26	5.65	14.20	3.43	15.19	2.60
	$d_n$	36.00	26.41	20.62	37.01	3.90	36.47	3.73
$P_1$ $P_2$ $P_3$	$d_m$	21.00	23.11	9.44	22.93	5.00	21.41	4.10
	$d_n$	15.00	12.26	10.51	16.51	5.62	15.62	4.50

Figure 41 illustrates the RMS errors computed for the three configurations shown in Table 8. As seen from this figure the maximum RMS error in the estimation of  $d_n$  and  $d_m$  using EWT-CC with curve fitting interpolation is 1.70cm, while it is 2.68cm using just EWT-CC and 9.97cm using CC. In addition, the trend of the RMS error using the

proposed method is shown to decline with the increase in PPDs.

Such an enhancement in the estimation accuracy of sound localisation has two causes. Firstly, employing the envelopes of acquired signals reduces the ambiguity present around the peak indices of CC; and secondly processing these envelopes in the time-frequency domain using WT integrates both time and spectral contents in the estimation process. Thus, the EWT-CC algorithm in conjunction with curve fitting interpolation is able to achieve a sufficient level of estimation accuracy for the wireless ASL at low sampling rates, as compared to the time domain methods, as shown in Chapter 3.

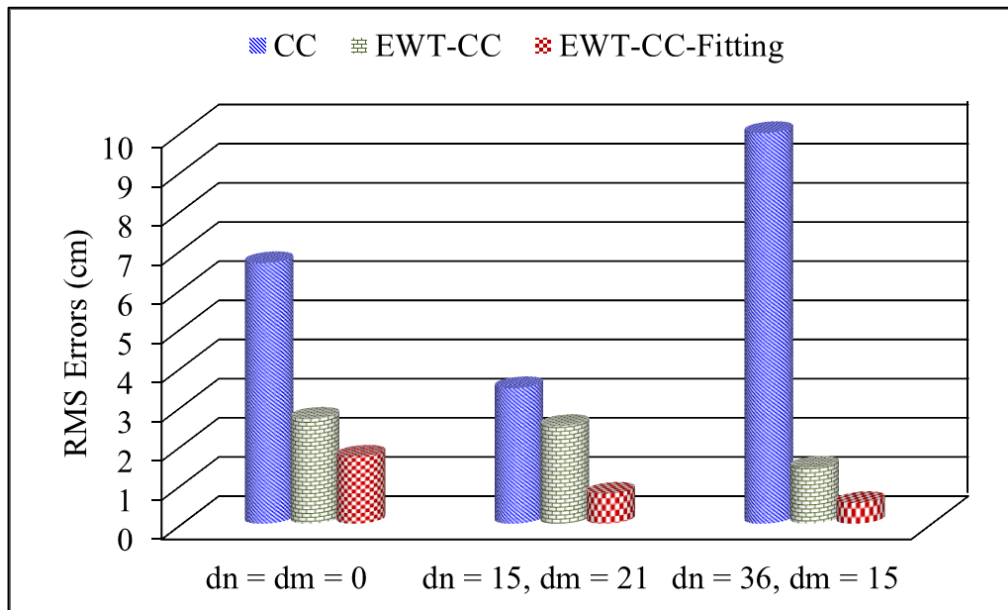


Figure 41: RMS errors for CC, EWT-CC and EWT-CC-Fitting algorithm.

Although the EWT-CC delivers more accurate localisation results in comparison to the CC, the multi-scale averaging technique still represents a drawback in this algorithm since it is time-consuming as explained in 4.4. Next, the results for the modified algorithm, SE-EWT, are reported and compared with those for the EWT-CC.

#### 4.6.2.2 Results of the SE-EWT Algorithm

The results of this algorithm are based on the use of the SE to estimate the optimum scale index that gives the best estimation results, as discussed in Section 4.4. To show the functionality of this modified method, two examples of the estimation of the PPDs are demonstrated in Figure 42 and Figure 43. These figures show the estimated PPDs and Shannon entropy of wavelet coefficients (SEWCs) vs. scales in one plot. In both



figures, the scale range was 1 to 100, where increasing the number of scales significantly increases the computational time of the WT.

The figures also explain the strategy of the employment of the SE to determine the PPDs, which is as follows. In the first, the SE is calculated for all WT coefficients, which results in SEWCs. In the second, the index of the minimum value of the SEWCs is selected, which represents the optimum scale index. Finally, the WT coefficients which correspond to this index are then selected and used in the estimation process by applying CC in conjunction with the curve fitting interpolation to these coefficients.

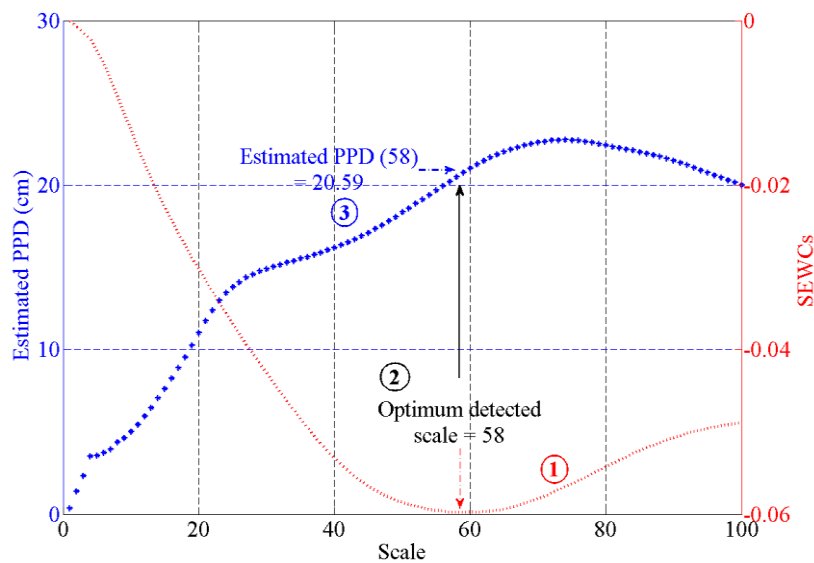


Figure 42: First example for using the SEWCs to select the optimum scale value (58) which delivers the PPD (20.59cm), where the actual PPD 21cm was.

In addition, the two examples illustrate the difference between the EWT-CC approach and the modified one. In the former, the PPDs were estimated at each scale value, represented by the thick blue dots curves in both figures, and then the EWT-CC algorithm takes the average of these, whereas the latter only estimated the PPDs at the optimum scale value. In Figure 42, the estimated PPD using the modified method is 20.59cm while for multi-scale averaging it was around 22cm for the same example. Furthermore, in Figure 43, the SE-EWT delivered a value of 35.50cm in comparison to 36.82cm from the EWT-CC technique.

To conclude, both approaches provide almost the same results with respect to the actual PPDs which are 21cm and 36cm, and more examples are summarised in Table 9. How-

ever, according to Table 7 the computational complexity of the EWT-CC method is higher than that of SE-EWT. This makes the latter approach more suitable to be employed in wireless ASL applications if the time delays are intended to be extracted from the aliased versions of the acoustic signals captured at low sampling rates.

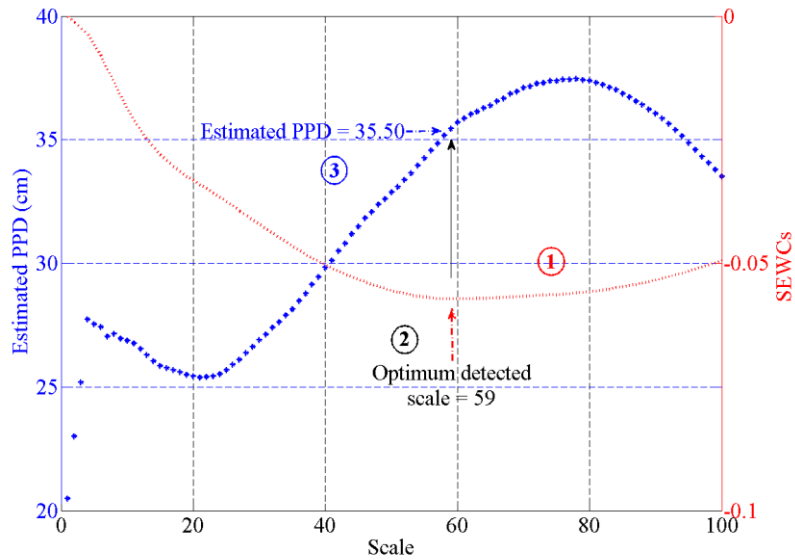


Figure 43: Second example for using the SEWCs to select the optimum scale value (59) which delivers the PPD (35.50cm), where the actual PPD 36cm was.

Table 9: Comparison between EWT-CC and SE-EWT algorithms.

Configuration of WU <sub>1</sub> WU <sub>2</sub> WU <sub>3</sub>	PPDs (cm)		Estimated PPDs (cm)			
			EWT-CC		SE-EWT	
			AVG	STD	AVG	STD
P <sub>2</sub> P <sub>2</sub> P <sub>2</sub>	d <sub>m</sub>	00.00	1.12	0.80	1.00	0.78
	d <sub>n</sub>	00.00	1.23	1.01	1.12	0.90
P <sub>0</sub> P <sub>2</sub> P <sub>3</sub>	d <sub>m</sub>	15.00	15.19	2.60	14.99	3.01
	d <sub>n</sub>	36.00	36.47	3.73	36.13	2.89
P <sub>1</sub> P <sub>2</sub> P <sub>3</sub>	d <sub>m</sub>	21.00	21.41	4.10	21.40	3.50
	d <sub>n</sub>	15.00	15.62	4.50	15.03	3.91

### 4.7 Summary

Working with low sampling rates and localising a sound source using a centralised AWSN as well as from acoustic signals acquired at low sampling rates much below the Nyquist rate have been investigated. This includes the development of a new signal processing algorithm to be used for sound source localisation. The new technique has been implemented using an envelope-based wavelet transform cross-correlation (EWT-CC) in conjunction with a parabolic fit interpolation method. The intention of this technique is to globally extract the time delays from the aliased acoustic signals captured by the AWSN and received at a centralised collection point.

The proposed algorithm, offers a multi-resolution domain of analysis which shows potentially good performance in counteracting the ambiguity of peaks due to the low time resolution. The proposed approach enhances the spatial resolution of the localisation process in the following respects. Firstly, via the employment of the WT, it was possible to extract the characteristics hidden in the envelopes of the aliased versions looking for the closeness between them and the mother wavelet. Secondly, by applying the Shannon entropy, it was possible to select an optimum scale index that gives the best spatial resolution. Furthermore, the utilisation of curve-fitting interpolation enhances spatial resolution by a factor of almost five based on the current setting of the developed wireless system. Finally, the use of the HEH mode in the MICAz platforms makes the data acquisition operation among acoustic wireless units more synchronised.

The approaches presented are proposed for the centralisation of data processing, which means that the individual wireless units are required to send the raw data to the central unit to be processed and analysed. This was performed for global off-line data processing, which still can overload the data transmission over WSNs if continuous online monitoring is involved. Therefore, the use of wireless sensing systems is obviously required, which involves approaches for decentralised data processing in order to extract meaningful information or important features from content-based features with the use of low sampling rates. This provides the framework of the next chapter in conjunction with the implementation of a wireless *in-situ* SHM system on the top of WTBs for continuous monitoring and further field study evaluations of the use of low sampling rates approach.

# CHAPTER 5: WIRELESS SHM CASE STUDY I: SOUND LOCALISATION ON WTBs AT LOW SAMPLING RATES

In the previous chapter, the experimental validation of TDE algorithms based on the utilisation of acoustic data received from lab-based centralised AWSNs has been discussed. Building upon the experience gained, this chapter introduces a proof-of-concept distributed sensor network implementation proposed for an *in-situ* wireless SHM system for WTBs. It also discusses the challenges facing the SHM system developed by utilising AWSNs based on AE. This system is then used for the field study validation of the proposed reduction technique. The validation is based on the extraction of meaningful information from the content-based features on-board the wireless units to form the AVPs and to send only these to the control unit. The AVPs are then utilised in the remote control unit to locate AE events occurring during a test phase with the intention to preserve the communication bandwidth, since only AVPs are transferred.

The chapter is organised as follows. The *in-situ* wireless SHM system setup is discussed in Section 5.1 along with a review of the AE technique and common AE parameters. Section 5.2 presents the software setup and the considerations taken into account when performing field studies. In Section 5.3, considerations relating to the localisation of artificial AE sources are discussed. In Section 5.4, the estimation results for AE source localisation are presented. Finally, the conclusions are drawn in Section 5.5.

### 5.1 *In-situ* Wireless SHM System Setup for WTBs

The implementation of the proposed wireless sensing technique on the top of WTBs is based on the utilisation of a single-hop WSN, since attention is given in this work to the sensing process rather than network protocols. Thus, this work can be extended to mul-

ti-hop WSNs for data collection from multiple sources by integrating multi-hop data collection protocols such as CTP [211]. This section discusses the system configuration which is implemented as a proof-of-concept model for the WTB SHM system.

### **5.1.1 AWSN Model and Hardware Requirements**

The development of the *in-situ* SHM system takes advantage of wireless technology to form a monitoring network. Figure 44 illustrates the deployment of the proposed model of a sensor network prototype on the WTBs. This system is a single-hop WSN which is comprised of hardware components such as wireless sensing units and a base station (gateway). Each wireless sensing unit consists of a wireless node and an AE sensor and takes charge of one blade of the wind turbine structure and records the AE events independently. Every unit is programmed with a unique identification to prevent data chaos in data transmission.

As shown in Figure 45, the MICAz motes equipped with the sensor board (MTS310) are used in developing the wireless system. The schematic structure of these wireless sensing units is discussed in Chapter 4. The omni-directional microphone sensor of the MTS310 board is replaced by a BNC connector for AE sensors. The AE sensor is the BII-7070 from ‘Benthowave Instrument Inc.’ ([www.benthowave.com](http://www.benthowave.com)) and operates at a usable frequency range of 0.1Hz to 400kHz with a size of  $\phi \times L = 18.6 \times 20\text{mm}$ . It is characterised by relatively small mass and low cost. This wireless prototype system is applied to a 300W wind turbine which is installed on the roof of the School of Electrical and Electronic Engineering (EEE). This wind turbine has three blades made of carbon with a diameter of 1.5m (see Appendix B for more details of specifications).

All of the sensing units communicate with a PC base station via an RF interface and are programmed in a TinyOS environment [222]. The PC base station includes an MIB510 gateway board incorporating a MICAz mote which is used to forward the extracted features or the raw data to the PC for monitoring and processing. The PC runs a software package which consists of a Java application and MATLAB scripts to provide a user-friendly graphical user interface (GUI) which allows operators to control the monitoring process, as explained in Section 5.2.

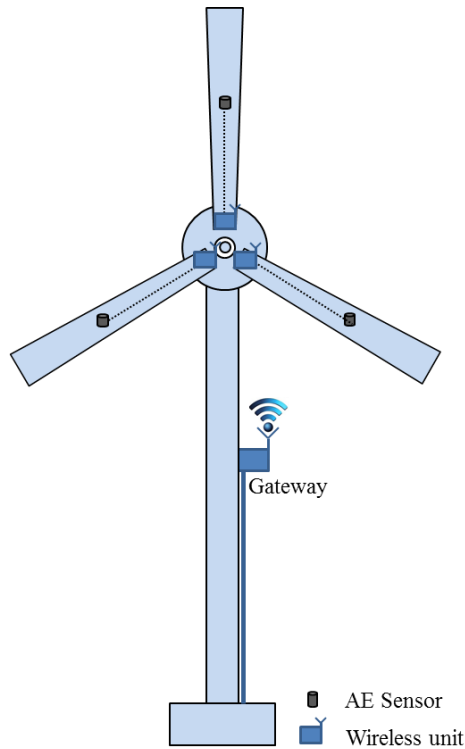


Figure 44: a) Illustration of a monitoring network with the wind turbine.

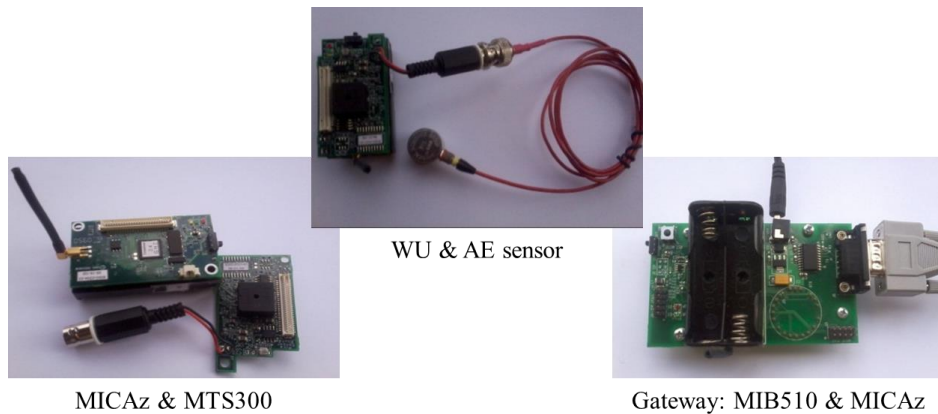


Figure 45: Hardware components: wireless unit (WU) and gateway.

### 5.1.2 Integration of Wireless System and AE Technique

Bringing together the entire component subsystems into one system which is integrated into the wind turbine unit for *in-situ* monitoring requires that it can be ensured that the attachment of sensing units to the WTBs will last for a long time. This is achieved by placing the wireless units in waterproofed plastic secured by cable tidy-ties in the wind turbine nose, as shown in Figure 46-a. This has the advantage that it makes the radius of rotation of the wireless units very small, so that the rotation of the WTBs has no effect

on the data transmitted. This is because the path loss is proportional to rotating radius [223].

Figure 46-b and -c illustrates the attachments of AE sensors and their cables to the WTBs. A diagram showing the attachment configuration is given in Figure 46-c, where a portion of a protection tube of 18.7mm diameter and 24mm in length is fixed by an Araldite adhesive to the WTB. The AE sensor is positioned in the tube and secured by a screw, and its cable is held by a cable holder which is fastened to the blade using the Araldite adhesive. The reason for this attachment is that it gives the system the flexibility to allow changes to be made to the AE sensor at any time, and also minimises the noise generated compared to the use of tabs [24]. The AE sensor is attached to the WTB at an equal distance of 300mm, which is almost 30% along the length of the blade from the root section. This is because it has been found by both simulation and experimental methods for WTBs that this area is more prone to damage [1].

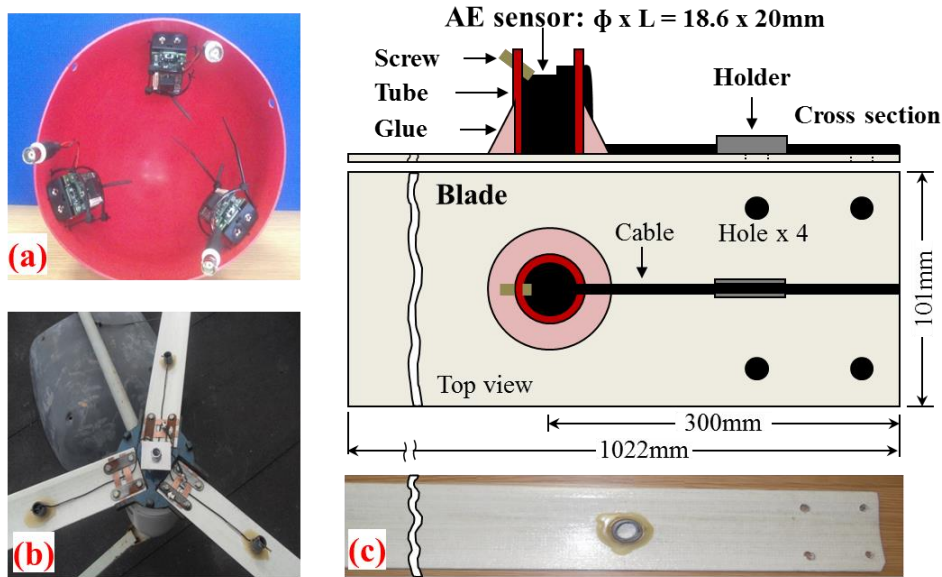


Figure 46: Wireless unit installation: a) photograph of WSN node inside the nose, b) photograph of AE sensors fixed on the blades, c) Diagram of AE sensors fixed on the blades.

The AE data captured from the rotating blades are wirelessly sent to the MIB510 serial gateway which is attached to the wind turbine tower, as shown in Figure 48-b. This data can then be transferred to the remote control unit via wired or wireless communication, such as using Wi-Fi or any other wireless techniques. In this application, the gateway

used forwards the data collected to the PC base station in the lab via a serial cable which is also used to power the serial gateway. Since the proposed system is based on the integration of WSNs and AE technique, the following section gives more attention to the AE approach.

### *5.1.3 Acoustic Emission Technique*

The AET is one of the most commonly used and sensitive NDT methods for SHM systems, and shows potential capabilities for providing information on the degradation in structural health of materials under mechanical load. This technique is defined as the radiation of mechanical stress waves generated due to sudden changes in the internal structure of a material [31]. This can be due to overloading beyond or near to the material's yield stress. Other possible AE sources include impacts, the origination and growth of cracks, fatigue cracks, delamination, matrix cracking, and fibre breakage in composite material [224]. These sources are all failure-related and the signals generated propagate in the material. Therefore, the AE technique has been found to be an effective method for the detection of such failures and, by using suitable signal processing algorithms, these failures can be localised, identified, and classified [51].

AE waves are abnormal and transient activities which are affected by the characteristics of the induced stress field. These waves can be converted into a number of useful AE parameters or features, as shown in Figure 47, which can then be used to identify these events. Some of these are as follows [140]:

- Amplitude,  $A$ , is the maximum amplitude which is usually measured in decibels (dB).
- Rise time,  $R$ , is the time interval between the first threshold crossing and the time when the AE signal reaches its  $A$ .
- Duration,  $D$ , represents the time difference between the first and the last crossings of the threshold value.
- Counts,  $N$ , refer to the number of times the signal crosses the threshold value.
- Power,  $P$ , is the area under the curve or the summation of the squared sample values.
- Arrival time,  $T$ , is the time of the first threshold crossing.



- Root mean square, RMS, is a statistical average parameter used for comparatively long transients.

Such AE features can be used to separate and identify different AE sources, such as crack growth, impact, friction and others, provided that pattern recognition software is used to evaluate these sources [225, 226]. However, not all of the common AE features can be extracted from the aliased versions. Counts are one such exception. The reason for this is that this feature represents the number of threshold crossings along the timespan between the initial and the last crossings of the threshold value. These in-between crossings are in most cases unavailable when envelopes are utilised in the extraction process. However, the duration feature which represents the timespan between these two points is still valid in this domain, since the threshold crossings occur at these points, as shown in Figure 47.

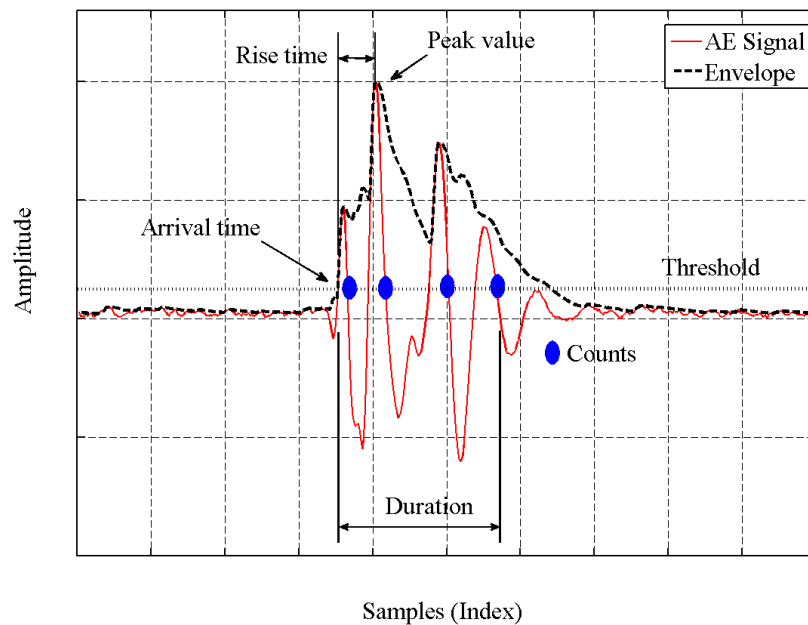


Figure 47: Key features of an aliased AE signal.

Comparing to the vibration technique, which needs data from multi-axes, AE is non-directional and a single AE sensor is enough to conduct measurement [227, 228]. Furthermore, the former technique records the local motion of a component, whereas the latter listens to the component and registers its response [15, 21]. This technology is therefore selected in this study because it is a passive technique and can be applied to structures with limited access without any supervision. It also allows the investigation

of defects in the structure under real loading conditions, such as a wind load in the intended application of this study.

The AE technique also plays an important role in the inspection of many civil engineering structures [229]. This is due to its high sensitivity to sound events generated from inside and on the surface of material structures if they are stressed and at earlier stages of beginning to fail [230]. It also has the advantage that the localisation of AE sources is possible by utilising multiple AE sensors. Structural resonances and usual mechanical background noise have no effect on the AE signal due to differences in the detection of frequency ranges [231]. However, the AE technique is very costly due to the high sampling rates required [39], which was taken into consideration in the implementation of the proposed wireless SHM system for WTBs.

### ***5.1.4 System Setup and Implementation***

The entire wind turbine unit has been installed with the wireless SHM system on the School's roof, as shown in Figure 48-a and -b. The gateway is placed in a waterproof case and attached next to the wind turbine tower. This gateway is basically used for sending a start sensing command, and setting the threshold value of the sensing process as well as switching between the AVP and raw data modes. These commands are initiated by the control unit which is located in the School's lab (Figure 48-c), as discussed below.

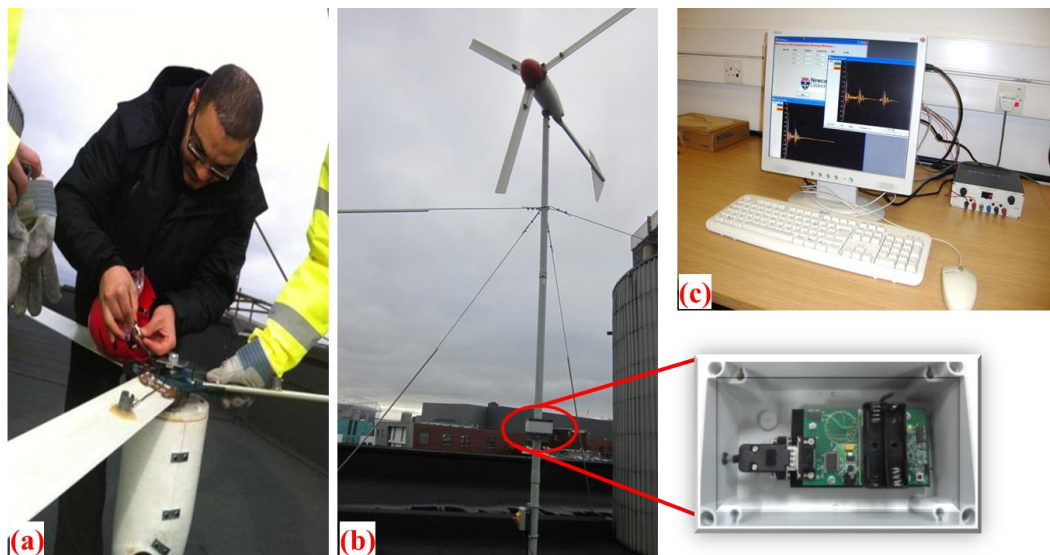


Figure 48: System installation: a) WT installation on the school's roof, b) Gateway fixed to the WT tower, c) Control unit.

## 5.2 Software Setup and Sensing Considerations

To make communication between the control unit and the wireless sensing units easier, and to control the wireless monitoring system, a software package for this system is designed. This package consists of an operating package and a Java application GUI. The former package is executed by the TinyOS operating system installed on the MICAz hardware platform, and its main function is to perform the operations of sensing and the transmission of AE data. The GUI is used to interact with the developed wireless monitoring system.

The main functions of this GUI are to provide an interface for controlling the monitoring process and to fuse the collected features and to perform data analysis which helps in the assessment of WTB condition. Figure 49 shows samples of screenshots of this GUI. This prototype also offers to the user the ability to switch between two transmission modes: ‘AVP’ mode or ‘Raw Data’ mode. The latter mode is needed for the cases where the actual raw data needs to be used, as discussed in Chapter 4, or for the user to conduct more signal analysis, as shown in Chapter 6. To transfer the raw data to the control unit, a request raw data command should be broadcast to all sensing units via the GUI. This results the raw data being displayed in the ‘Raw Data Windows’ as well as saving them in MATLAB script files.

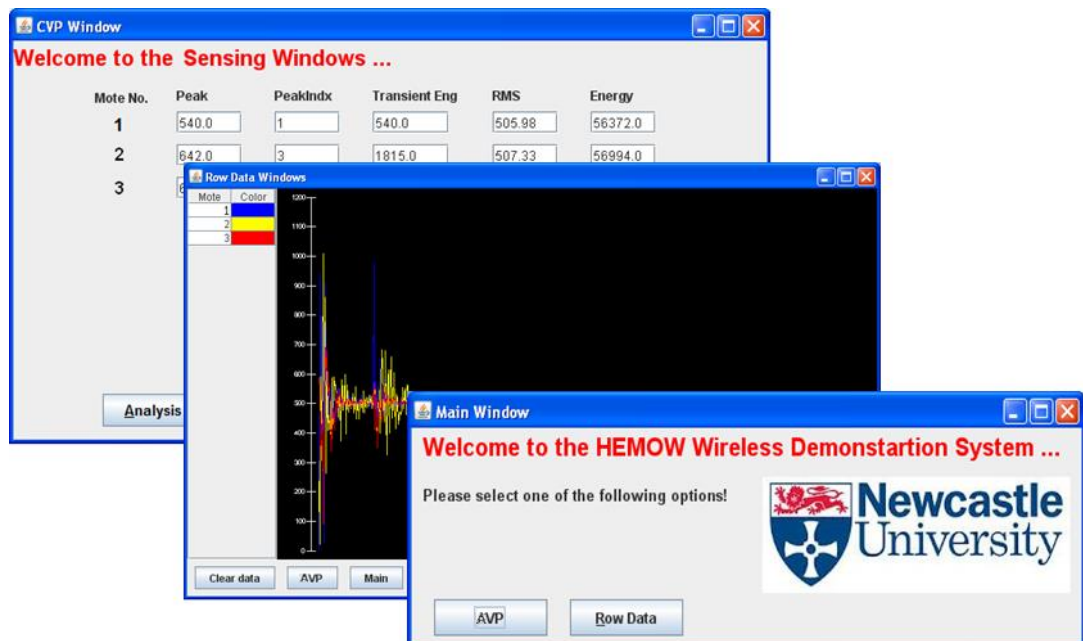


Figure 49: Screenshot of the GUI of the wireless demonstration system.

**5.2.1 AE Sensing for Field Study**

The sensing of the AE events, in this application, differs slightly from that explained in Chapter 4. This process commences in all wireless sensing units with the receipt of a start command, indicated by ‘SC’ in Figure 50. This command is broadcast by the base station and forces the wireless units to enter into a listening mode which makes them wait for AE events to occur which are above a pre-set threshold value, indicated by ‘ED’. Once the wireless units detect such events they start acquiring AE signals at a sampling rate of almost 4.8KHz for a sampling period of 0.11s.

After finishing the sensing operation, the sensing units start to execute the sending operation based on the transmission mode as discussed in the next section. As soon as they complete the sending operations, they enter again into the listening mode and a similar procedure is repeated in the same sequence.

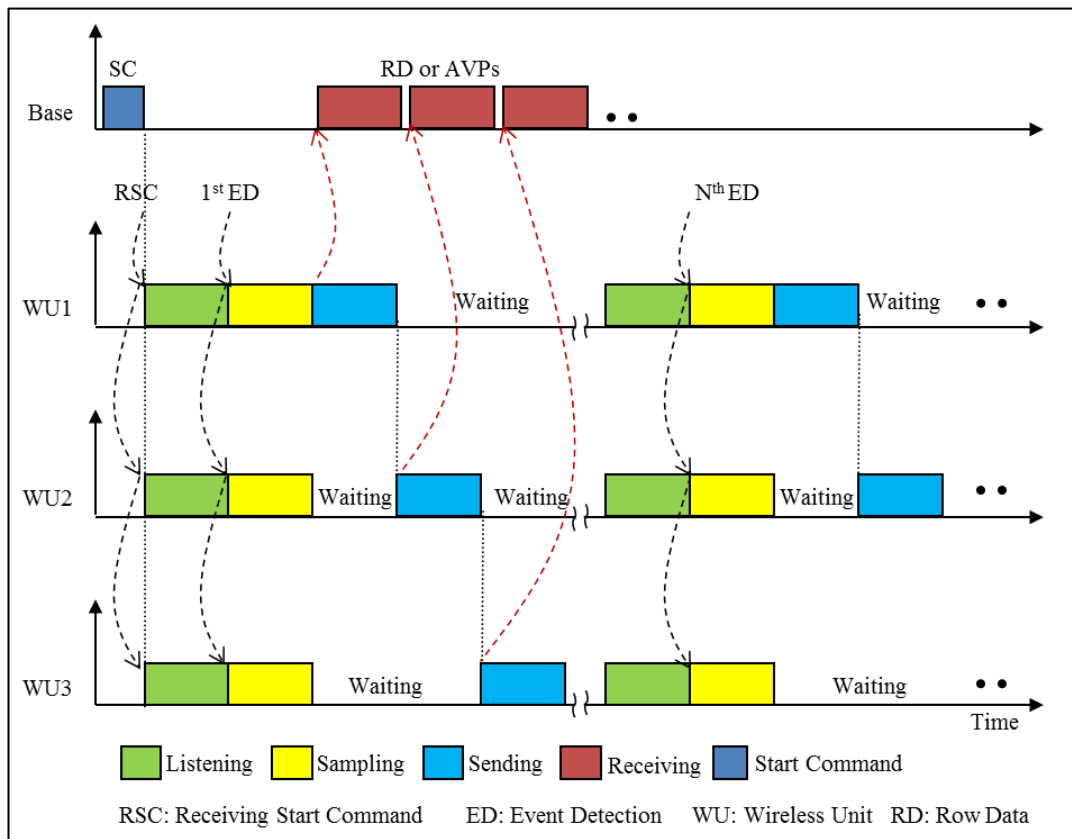


Figure 50: Schematic diagram of synchronised sensing and transmission operations.

**5.2.2 Event Based Transmission Strategy for Field Study**

In the proposed wireless system, the transmission operation is an event-based process,

which means that wireless units will not send any data unless an AE event is detected. Once the AE event is detected, these units will transfer their data after the sampling process is completed and according to the strategy explained in Chapter 4 and shown in Figure 50. It is worth mentioning here that the waiting period for each wireless unit is very small, due to the short time required for the transmission process and particularly for the transmission of AVPs, since this is the default transmission option as explained below and in Chapter 6. Thus, data loss will be rare.

Moreover, depending on the transmission mode, the wireless units will send either raw data or the constructed AVPs to the control unit. The default setting of this mode is set to AVP mode. In this case, the wireless units process the raw data in order to extract meaningful AE information or important features from the aliased versions; and only those in the form of AVPs, instead of the aliased versions, will be sent to the remote control unit. For cases where the transmission mode is set to raw data, the wireless units will follow the same sending strategy as explained in Chapter 4. Irrespective of transmission mode, data are collected from various wireless units and aggregated into the control unit for further analysis.

### ***5.2.3 On-Board AE Feature Extraction Algorithm for Field Study***

For field study and continuous monitoring, the relevant AE aliased signals captured should be locally pre-processed on-board the wireless units, so that only the results of evaluation and other meaningful features are transmitted to the remote control room, which reduce the amounts of data captured. These features are essential for the further analysis and classification of AE events. However, as the wireless system developed here is based on the use of MICAz platforms, which have limited power resources and memory size as well as low processing capabilities, computationally expensive algorithms which are based on spectral and statistical approaches [232] cannot be considered. Therefore, relatively simple signal processing algorithms need to be considered for on-board AE feature extraction.

In addition, for better analysis and classification results, content-based features should be extracted from the envelope of the received AE aliased versions rather than from the amplitude values of the time domain signal, since the envelope optimises the signal shape and minimises the ambiguity in the signal caused by lowering the sampling rate.

Figure 51 summarises the steps of the proposed feature extraction algorithm utilised in this wireless SHM system, which are discussed next.

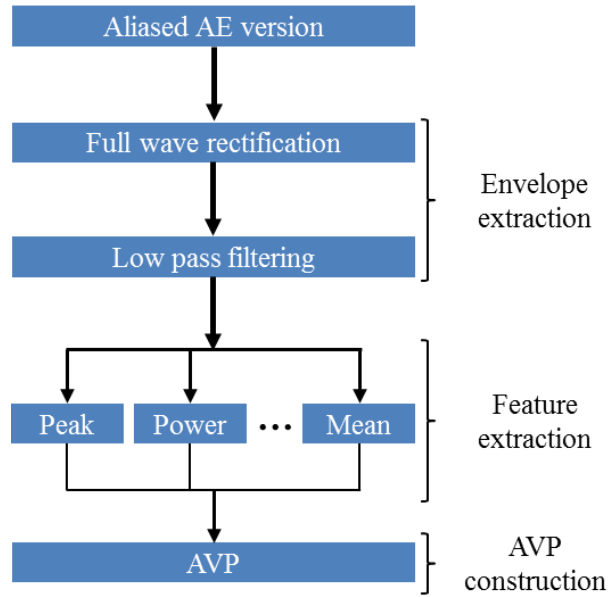


Figure 51: On-board feature extraction algorithm.

### 5.2.3.1 On-Board Envelope Extraction of Aliased AE Signal

As pointed out previously, the envelope of the aliased AE signal is extracted on-board; thus, the extraction method differs from that explained in Chapter 4 in the sense that it is relatively simple and not computationally complex. In this algorithm, the envelope is extracted from band-pass filter outputs by full-wave rectification and low pass filtering, as shown in Figure 51. To do this, a one-pole filter with a smoothing parameter  $\beta$  is applied to the full rectified AE aliased version shown in Equations (5.1) and (5.2) [233].

$$y(t) = |x(t)| \quad (5.1)$$

$$y(t) = (1 - \beta)x(t) + \beta y(t - 1) \quad (5.2)$$

where  $x(t)$  is the aliased AE signal,  $t = 1, 2, \dots, N$  where  $N$  is the number of samples. This method is implemented in a streaming manner, where each sample is fully processed and saved before the next sample arrives without having a specific loop for running the filter code. Figure 52 shows an example of an aliased AE version with the envelope extracted using the one-pole filter. The aliased version was captured using the developed in-suit SHM system.

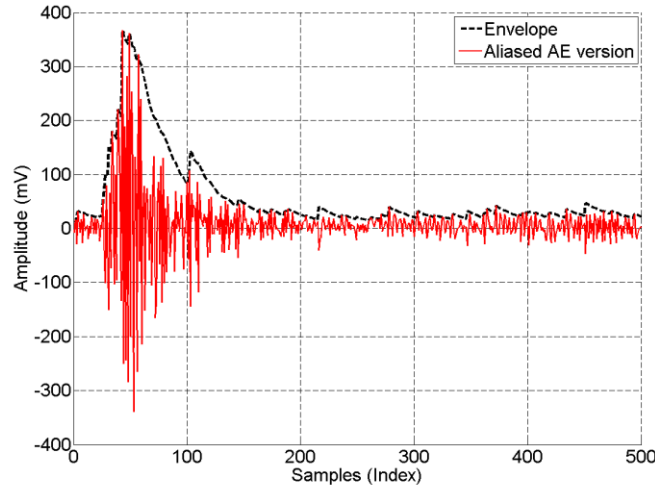


Figure 52: Aliased AE signals with its envelope.

### 5.2.3.2 Extraction of AE Features of Aliased AE Signal

As mentioned in Chapter 3, the advantage of the utilisation of low sampling rates is that the original shape can be conserved, which helps in maintaining the most salient information or features of the original AE signals without the need to reconstruct them. This means that the most relevant AE event parameters, discussed in Section 5.1.3, will be retained if the aliased versions of acoustic signals are used. Fortunately, most of them are time-domain features, as shown in Figure 47. This simplifies the process of on-board feature extraction.

AE features, including peak value, arrival time, mean value, and power value, are extracted from the envelopes of the aliased AE signals. These features have the advantage that they can be computed while the sensing process is in progress without the need to have acquired the whole signal first. The extracted features are assembled in vectors named ‘acoustic vector properties’ (AVPs) which are transferred to the control unit where they are characterised and used to distinguish different AE events.

In the previous sections, the main concepts and considerations of the proposed wireless SHM monitoring system are explained. The following sections concentrate more on showing the functionality of this system in terms of the localisation of AE events on the WTBs caused by artificial AE sources via hitting the blades with a plastic stick which has a diameter and length of 15mm and 500mm respectively. Such sources could emulate impact damage or audible cracks caused by different objects, such as tools, bird strikes, or strong hail, all of which represent abrupt AE events.

### 5.3 Validation of AE Source Localisation on WTBs

For SHM applications, AE source localisation is very important for large structures such as WTBs in which active regions where damage in material structure is expected can be identified and therefore a more precise investigation using other NDTs can be undertaken. To locate the AE sources on WTBs there are different techniques of source localisation: line-of-sight location, zonal location, and constraint geometrical point location [234]. In the following subsections, these techniques are detailed. Here, it is important to mention that the calculation of localisation features such as arrival time and peak amplitude are locally extracted by the individual acoustic wireless units. These features are then transferred to the control unit where they are assembled and utilised to estimate the location of the AE event.

#### 5.3.1 Line-of-Sight AE Source Localisation on WTB

Line-of-sight localisation basically depends on the calculation of the arrival time of AE events and the velocity of AE signals in the medium in which they propagate. This type of localisation is conducted here in order to verify the possibility of locating AE events based on their arrival times measured by the individual wireless units. The velocity with which AE signals propagate in the WTB, which is made of carbon fibre is also measured. Figure 53 depicts the setup used to conduct these wireless measurements. An artificial AE sound is generated by hitting the blade with a metallic ball, which has a diameter of 9mm and a mass of 3g, at known positions in order to conduct the velocity measurements.

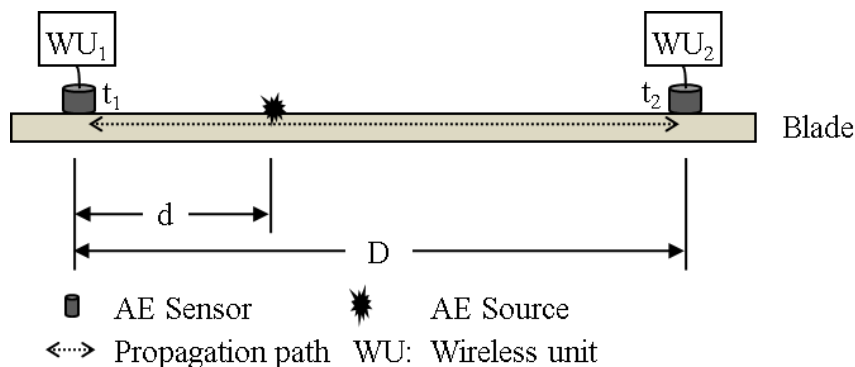


Figure 53: Linear localisation of AE events.



### 5.3.1.1 *Measurement of Arrival Time Features*

The arrival time features of aliased AE signals are calculated using the first threshold crossing. This method is applied in conjunction with low pass filtering to overcome the ambiguity caused by utilising low sampling rates, which leads to enhancing the detection accuracy of the arrival times of the captured aliased AE versions. These times are measured based on the local time of the individual wireless units, which affects the measurement precision of the arrival times of these events due to the drift in the clocks of these units.

To overcome this problem, a simple time synchronisation procedure is applied in which the wireless units time-stamp the arrival of the start sample command ‘SC’ (see Figure 50), which is denoted by  $t_{bi}$ , and then they use these timestamps to convert the arrival time to a global time according to the relation: *global arrival time* =  $(t_i - t_{bi})$ , where  $t_i$  is the arrival time of the detected AE signal at each wireless unit and  $i \in (1, 2, 3)$ . A sequence of measurements has been conducted in order to test the robustness of this method, in which the arrival times were calculated with and without using the global arrival time relation.

In these measurements, the wireless units were located at equal distances from a sound source, which means that the AE signals should arrive at the individual units at the same time instant. By comparing the results obtained from both cases, it has been found that using the global time reduces the time synchronisation errors from  $46.33\mu\text{s}$  to  $1.55\mu\text{s}$  which represents an average improvement of 96.65% according to the setting of the experiments conducted. Such an improvement will have a positive impact on both velocity and localisation measurements, as shown next.

### 5.3.1.2 *Measurement of Propagation Velocity*

Based on detected arrival times  $t_1$  and  $t_2$  (Figure 53), a calibration method is used to measure the velocity of wave propagation ( $v$ ) using the relation:  $v = D/(t_2 - t_1)$ , where  $D$  is the known distance between the two AE sensors (i.e., wireless units). Due to the short length of the blade used, only a small number of measurements are conducted. However, to show the robustness and repeatability of these measurements, each one is repeated a number of times and the results are discussed in Section 5.4.

### 5.3.2 *Zonal Localisation for Active Blade Identification*

It is important for the experiments conducted that AE events are traced in order to specify the active zone or blade (i.e., the damaged blade). This is useful in order that more attention can be given to that particular zone or blade. This can be done by zonal localisation, where each blade is assigned to an AE wireless unit and, via a comparison between the maximum amplitudes ( $A$ ) of the AE signal received at the wireless units, the active blade can be specified. In contrast, to trace the active region within a large blade, AE wireless units can be spaced apart on the blade and AE source can be assumed to be within a region and less than halfway between AE wireless units.

In this study, zonal localisation is used to specify the active blade, and the results of this localisation are presented in Section 5.4.2. However, additional precise localisation techniques are required to determine the exact location of the AE source, as shown next.

### 5.3.3 *Constraint Geometrical Point Localisation of AE Sources*

The constraint geometrical point location technique is used to pinpoint precisely the AE source based on the arrival time and signal strength features as well as the predetermined sound velocity ( $v$ ). For large scale WTBs where multiple AE wireless units are deployed, this technique can also be combined with zonal location to provide more precise source localisation results. This can be achieved by clustering the wireless units deployed on the blade into areas, where active areas are specified based on the principle of zonal location i.e., signal strength. Then constraint geometrical point location is applied to precisely pinpoint the AE source, as explained next.

Due to the small size of the wind turbine used in this study, a combination of zonal and constraint geometrical point localisation is implemented as shown in Figure 54. To apply this localisation technique to the WTBs, a model of 2D localisation needs first to be developed. To achieve this, AE sensors are assumed to be configured as shown in Figure 54. In this configuration, it is also assumed that the AE sensors are located in a 2D plane and the AE signals generated propagate in constrained paths along the blades. In Figure 54,  $D_1$  and  $D_2$  represent the shortest paths which will be taken by the AE signals in order to reach the AE sensors  $S_1$  and  $S_2$  respectively.

Based on the configuration shown in Figure 54 and these assumptions, a 2D model can

be derived as shown in Figure 55 where the shortest paths  $D_1$  and  $D_2$  are approximated by  $\check{D}_1$  and  $\check{D}_2$  respectively. In this case, the Equations (5.3)-(5.5) [234] are valid and can be used to estimate the unknown coordinates of the AE source,  $x$  and  $y$ , which are indicated by the intersection of hyperbolas which are not shown in this figure.

$$d = \sqrt{(l_{13} - y)^2 + x^2} = \check{D}_2 - v \cdot \Delta t_{31} \quad (5.3)$$

$$\check{D}_2 = \sqrt{(l_{12} - x)^2 + y^2} = \check{D}_1 - v \cdot \Delta t_{21} \quad (5.4)$$

$$\check{D}_1 = \sqrt{x^2 + y^2} \quad (5.5)$$

where  $d$  is the distance between  $S_3$  and the AE source,  $l_{1,3}$  and  $l_{1,2}$  are the distances between  $S_1$  and  $S_3$  and  $S_1$  and  $S_2$  respectively, which are equal in this configuration.  $\Delta t_{21}$  and  $\Delta t_{31}$  are the differences in arrival times between AE sensors  $S_1$  and  $S_2$  as well as between AE sensors  $S_1$  and  $S_3$ .

The proposed approach is examined by conducting several experiments to locate AE sources produced at a known location on blades by artificial AE events produced via hitting the blades with the same plastic stick discussed in Section 5.2. The results of these experiments are discussed in Section 5.4.3.

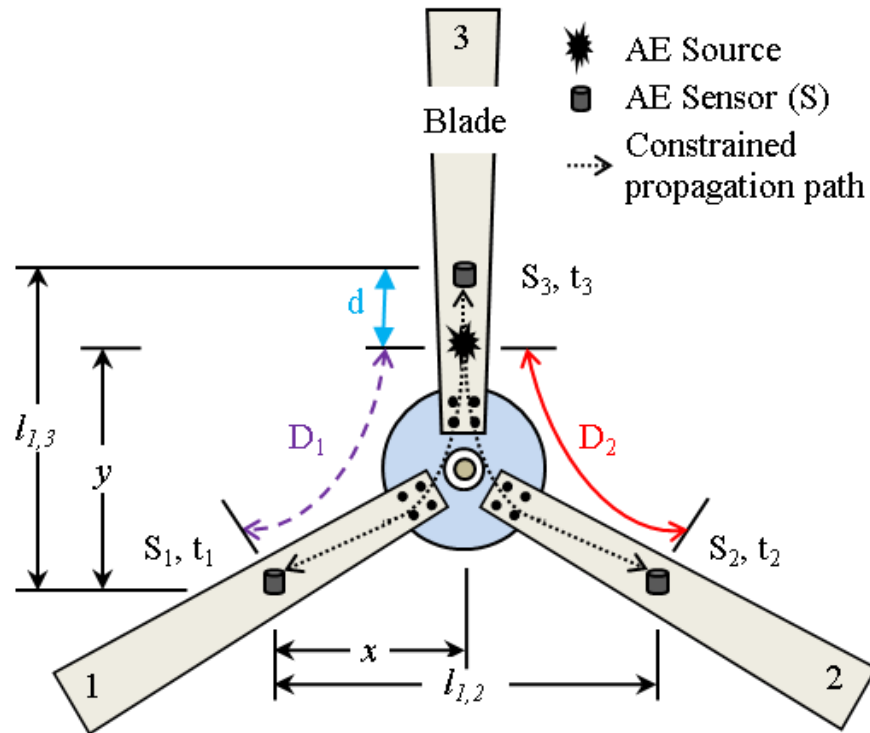


Figure 54: Proposed configuration of acoustic wireless units,  $x$  and  $y$  are the unknown coordinates of AE source,  $t_i$  is the arrival time of AE signal at AE sensor  $S_i$ .

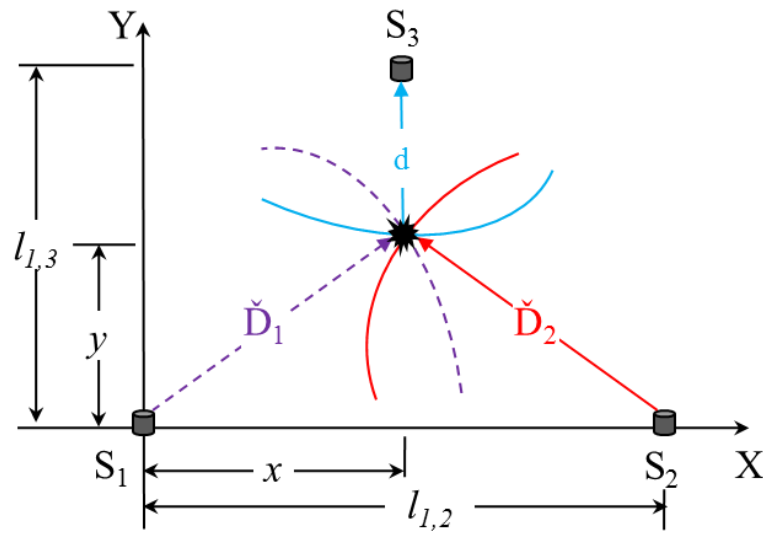


Figure 55: Proposed 2D localisation model.

## 5.4 Results and Discussion

The aim of this chapter is to develop and evaluate a proof-of-concept model for the *in-situ* wireless SHM of OWTBs. This system is also used to evaluate the use of low sampling rates technique proposed in this study for field test studies. The system has been used and tested for the localisation of AE events on WTBs released during a test phase and in *in-suit* environmental conditions.

These AE events were captured at a sampling rate of 4.8KHz, which is much below Nyquist requirements. The arrival times of these events have been detected as discussed in Section 5.4.1 and used to estimate the delays among the AE aliased signals captured. These signals were processed locally at the wireless units used in order to extract AE features and to construct the AVPs. These AVPs were received at the control unit for further analysis. This section presents and discusses the results of the above-mentioned experiments.

### 5.4.1 Line-of-Sight Localisation of AE Events

Different artificial AE events were generated at known positions and localised using line-of-sight localisation on a single WTB. The results show the potential of the AE source localisation at low sampling rate based on the arrival time feature. These experiments were conducted using the setup shown in Figure 53. The relation  $d = 0.5 \cdot$

$(D - v \cdot \Delta t_{21})$  is used to localise the sound source, where  $v$  is the velocity measured and  $\Delta t_{21}$  is the difference in arrival times between AE sensors  $S_1$  and  $S_2$ . The results gained from six experiments are summarised in Table 10.

From the results shown in Table 10, the actual and estimated results are closely matched giving an overall error of 4.13% based on the measurement setting. The percentage error was calculated according to Equation (5.6).

$$Error_{\%} = \frac{|measured\ value - actual\ value|}{actual\ value} \cdot 100\% \quad (5.6)$$

As seen in Table 10, the rate of estimated error decreases as the distance  $d$  increases. This is because the use of low sampling rates led to decreasing spatial resolution, which in contrast increases the error in the detection of arrival times of the signals as  $d$  becomes smaller. Next, the results of active blade identification and constraint geometrical point localisation are reported.

**Table 10: Line-of-sight results of AE events localisation based on AVPs.**

Exp. #	D (cm)	d (cm)	Average of estimated d (cm) from 6 readings	Error (%)
1	82	35	35.52	1.49
2		20	19.65	1.75
3		15	13.47	10.20
4	88	40	40.03	0.08
5		30	31.52	5.07
6		21	22.30	6.19

#### 5.4.2 Active Blade Identification

Active (damaged) blade identification has a significant importance in the application in SHM of OWTBs. This is because it can restrict the inspection process to that particular blade, which saves cost and time. Abnormal AE signals can be caused by different failure sources. Thus, locating their sources can be used to specify the most likely damaged

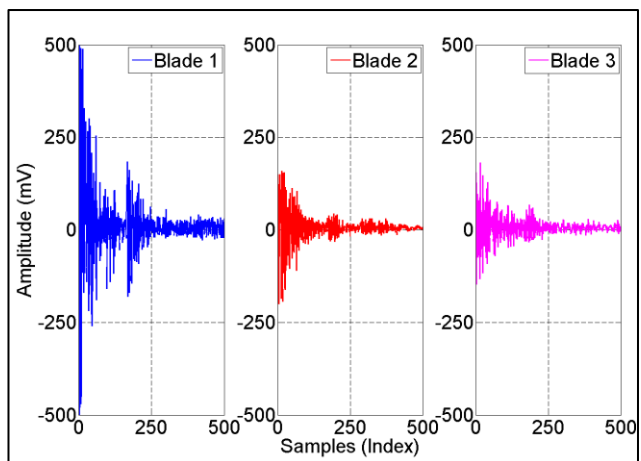
blade. To emulate these sources, WTBs were individually subject to several hits, as discussed above.

Figure 56 shows the AE aliased signals received as a consequence of hitting the three blades individually while they were static. Each reading consists of 500 samples and all of them are initiated by a simple threshold crossing condition (100mv) which was chosen experimentally to be above noise level. Figure 56-a illustrates the results of hitting blade number one. It is clear that a strong AE event was occurring at this blade, which needs to be taken into account in event detection and localisation as discussed next. The other two plots show the results of the propagation of this event to blades two and three.

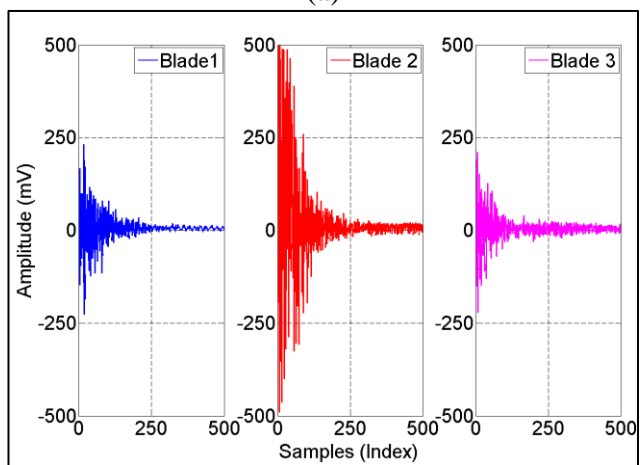
In contrast Figure 56-b and -c depicts the consequence of hitting blades two and three respectively. In both cases, the strongest aliased AE signal can be used to specify which blade was subject to the hit, whereas weak signals were obtained in each case as a result of the propagation of both strongest aliased AE signals to the other blades. In addition, it can be observed in Figure 56-a that there is a slight difference between the waveforms shown in this figure and those in Figure 56-b and -c in which the first shows that there is a minor hit result following the main hit result.

These aliased signals shown in Figure 56 also demonstrate that applying uniform sampling rates lower than Nyquist requirements in the acquisition process can still preserve the shape or contents of the AE signals. This is because the shape and common AE features of these aliased versions are correlated with the AE signals captured at high sampling rates [140]. This is a very important criterion in the extraction of AE features in SHM applications, which is not satisfied in techniques previously applied [153, 167] where a set of random projected samples was used, as discussed in Chapter 3.

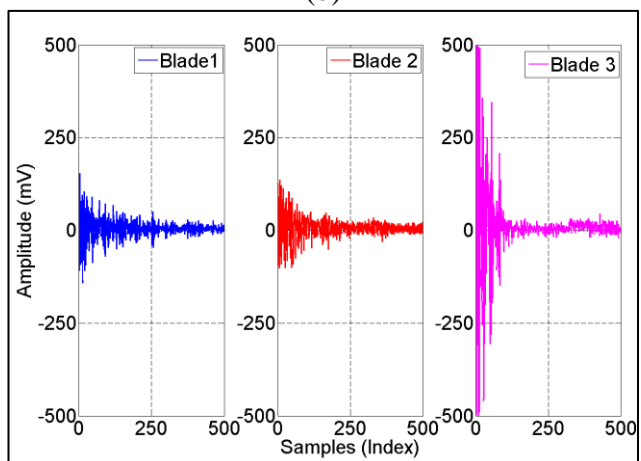
The determination of the active blade can also be achieved based on the AVPs received, as depicted in Figure 57 which summarises the results illustrated in Figure 56. For each test, the maximum peak values indicate the active blade which was hit. This means that, from Figure 57 and based on the peak values, the first test shows that the AE event occurred on blade number one, whereas they occurred on blades two and three in the second and third tests respectively. The results gained here can be combined with those of the constraint geometrical point location technique to provide more precise source localisation results for large scale WTBs, as discussed next.



(a)



(b)



(c)

Figure 56: Aliased AE signals received from the wireless units as a consequence of hitting the three blades individually a) one, b) two, and c) three.

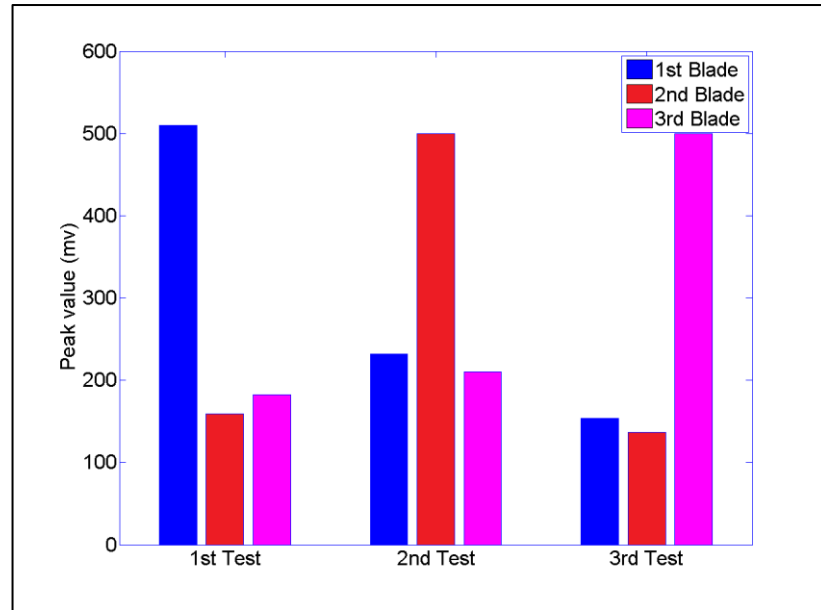


Figure 57: Active blade identification based on peak value features of AE events shown in Figure 56.

#### 5.4.3 Constraint Geometrical Point Localisation of AE Events

Due to the symmetry of sensor configuration in Figure 54, the distance  $x$  is known and equals  $l_{1,2}/2$  and the arrival times at  $S_1$  and  $S_2$  are equal, which means that  $\Delta t_{21} = 0$ . Thus, any two sensors located on the propagation path are sufficient to estimate the distance  $d$  and consequently the coordinate  $y$ . In addition, once the active blade is specified based on zonal location, as explained in Section 5.3, then the proposed model in Figure 55 can be adjusted accordingly.

The proposed approach is examined by conducting several experiments to locate AE sources produced at known locations on blades by artificial AE events. For this purpose, the locations of AE sensors were changed to 50cm instead of 30cm on each blade, in order to provide more scope for changing the value of  $d$ . In these measurements, a calibration method as discussed in Section 5.3 is used to measure the velocity of wave propagation from the measured time difference between the different AE sensors on the blades, and it is found to be around  $2 \times 10^4$  m/s on average. It is worth mentioning that as the distance between the two AE sensors decreases the measured velocity becomes inaccurate. The reason behind this is that the velocity measurement will be dominant by the small distance between the two sensors which is dominant by the complex structure of the wind turbine at hub. Whereas as this distance increases, it will be dominant by the simple one-dimensional structures of the blades.



Based on the velocity calculated, several experiments were conducted to locate the AE sources using the wireless setup discussed in Section 5.1 and based on the model shown in Figure 55. The results obtained are summarised in Table 11. From the results shown in this table, the actual and the estimated results are closely matched. They give an overall error of 7.98%, which shows the feasibility of the proposed model for AE source localisation at sampling rates much lower than the Nyquist rate for the specific wind turbine structure. The percentage error was calculated according to Equation (5.6). It is noticeable that the percentage error also increases with a decrease in  $d$ . In addition, the results obtained here although for a small wind turbine system, show significant potential to be extended to large-scale OWTBs.

**Table 11: Estimation results of constraint geometrical point localisation.**

Exp. #	$l_{1,2}, l_{1,3}$ (cm)	$\check{D}_1, \check{D}_2$ (cm)	$d$ (cm)	Average of estimated $d$ (cm) from 6 readings	Error (%)
1	92	103	15	17.58	17.20
2			20	21.70	8.50
3			25	23.19	7.24
4			30	31.90	6.33
5			35	36.60	4.57
6			40	41.61	4.02

### 5.5 Summary

In this chapter, the implementation of an *in-situ* SHM monitoring system for WTBs has been introduced and described based on the integration of the AE technique and wireless technology. The developed system was integrated onto a 300W wind turbine installed on the roof. The technique proposed in Chapter 3 has been applied to this wireless system for field test study and validation. A case study of sound localisation at low sampling rates has been investigated and discussed.

As elaborated in this chapter, the artificial AE events were generated on WTBs and used to test the robustness of the system in terms of localising AE sources based on the con-

tent-based features extracted from the aliased AE versions on-board the wireless units. These features formed the AVPs which were received and fused in the central unit to estimate the location of AE sources. This has been achieved for the complementary aspects of the line-of-sight, zonal, and constraint geometrical point localisation techniques. A localisation model for the latter technique in conjunction with the zonal approach has been developed and applied to the three WTBs. Several wireless localisation tests have been carried out to assess the localisation capabilities of the proposed model on the WTBs. The results illustrate the feasibility of the proposed model for AE source localisation at sampling rates much lower than the Nyquist rate in this specific wind turbine structure.

These results were obtained for a small wind turbine system. However they represent a proof of the concept of developing the *in-situ* SHM system based on the integration of the AE technology and WSNs with the utilisation of low sampling rates discussed throughout this research. In addition, such conclusions are important for the further design and development of wireless SHM systems and their application in developing continuous *in-situ* offshore large scale WTB condition monitoring systems. In the next chapter, further field validation of the proposed system is considered by conducting subsequent *in-situ* experiments in which AE events and environmental monitoring are taken into account under different environmental conditions and artificial AE sources.

# CHAPTER 6: WIRELESS SHM CASE STUDY II: AE EVENT AND ENVIRONMENTAL MONITORING

In the previous chapter, an *in-situ* wireless inspection system proposed for monitoring the structural health of the WTBs in conjunction with the localisation of AE sources has been presented. The work presented in this chapter conducts field test studies for the validation of both the developed wireless SHM system and AE features in providing a robust SHM system for WTBs. This is shown by conducting further *in-situ* experiments in which AE events are detected and discriminated amongst in different environmental conditions in conjunction with artificial AE sources. The intention of using such sound sources is to emulate impact damage or audible cracks caused by different objects such as tools, bird strikes, or strong hail. Time and time-frequency feature extraction algorithms, in addition to the PCA method, are used to extract the most relevant information, which in turn can be used to classify or recognise a testing condition that is represented by the response signals.

The layout of this chapter is as follows. Section 6.1 presents a general introduction to the proposed feature extraction and classification plan for system validation. Section 6.2 discusses the feature extraction techniques proposed in this study to extract AE parameters. System validation procedures are discussed in Section 6.3. In Section 6.4, the validation results of AE events and environmental monitoring conditions are presented. Finally, the conclusions are drawn in Section 6.5.

## 6.1 Introduction

As explained in Chapter 2, AE WSNs are large collections of resource-limited wireless units, densely deployed to collectively monitor an area or execute a certain task. The limited resources necessitate that only small amounts of data gathered by these units should be used to detect and discriminate different AE events. This should be performed

by extracting the most important AE parameters locally on-board from the aliased versions collected at the central unit. Figure 58 below illustrates the proposed feature extraction and classification strategy for the detection and classification of AE events.

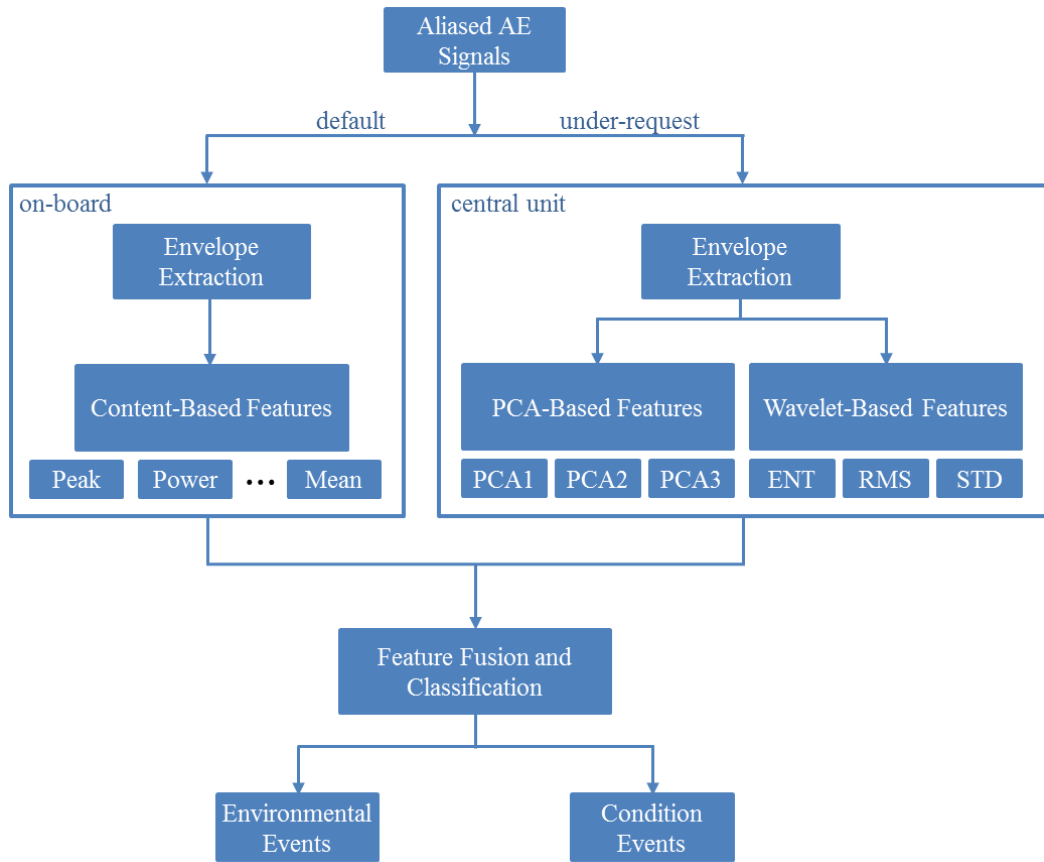


Figure 58: AE events detection and classification strategy.

As seen in Figure 58, the proposed strategy provides two possible options for the extraction of AE features: either on-board the wireless units or in the central unit. The former option represents the default case and it is implemented for a continuous monitoring approach where a simple content-based feature algorithm is applied; whereas the latter is used for off-line techniques or for cases where more investigation is requested, using advanced feature extraction approaches, including principal component analysis (PCA) and WT.

The on-board feature extraction method was discussed in the previous chapter. However, in the following sections, a brief background of feature extraction techniques proposed for centralised processing is presented along with the motivation behind their use. The effectiveness of individual features is then tested and discussed. Based on the re-

sults obtained, only features that perform well are selected for feature fusion and then for AE event classification.

### **6.2 Extraction and Fusion of AE Features**

The key to a successful *in-situ* SHM system for WTBs is an effective monitoring system with the highly reliable ability to detect and discriminate different AE events and environmental conditions. This can be achieved by extracting the most relevant AE features, which in turn can be used to classify or recognise a testing condition that is represented by the response signals [235].

Feature extraction can be seen as a process of transforming a set of data into a set of features which are then used for further analysis and classification [235]. Such a process has the advantage that it allows the representation and classification of different AE events using a small number of features compared to the size of the original data, which saves memory space and speeds up the monitoring process. Therefore, extracting distinctive and distinguishable features from aliased AE signals is imperative for their proper classification. To achieve an optimal SHM system it is extremely important that the feature extraction process is accompanied by appropriate feature selection and optimisation, which are considered to be complementary steps in improving performance and identifying the most relevant features of a particular AE event.

#### **6.2.1 Pre-processing of Aliased AE Signals**

Work under the use of low sampling rates to extract meaningful information requires the use of envelopes of aliased signals instead of amplitude values in the extraction process, in order to mitigate the problems associated with employing low sampling rates below the Nyquist requirements such as the loss of information. Therefore, the first step in the extraction process is to fit or extract the envelope of the aliased acoustic versions. This can be performed as discussed in Sections 4.3 and 5.3.

#### **6.2.2 Principal Component Analysis-Based Features**

PCA is a multivariate statistical signal processing technique extensively used for feature extraction to reduce the dimensionality of the original data, thus allowing a simpler analysis process. This is achieved by transforming the data linearly into a smaller num-

ber of uncorrelated (i.e., independent) and orthogonal to all other principal components (PCs) which correspond to the maximum possible amount of variation within the data. Each PC is a linear combination of the original data and the first principal component explains most of the variation in the data and each succeeding component accounts most of the remaining variance and so on. The number of significant components to use is user-defined. However, in most cases, the first, second, and third components provide a good summary of all of the possible variation.

PCA has been used in diverse applications, including the analysis of PEC response from corrosion in mild steel [236], the detection of metal loss [237], the analysis of acoustic emission signals from landing gear components to detect fatigue fractures [238], the automatic classification of acoustic emission patterns [226], face recognition [239], and biomedical engineering [240, 241]. The widespread use of this technique in different applications is most likely due to the following advantages. In addition to its simplicity, the PCA is a non-parametric method which allows the extraction of the most important or hidden information from confusing data sets. It also provides a tool to explain a large percentage of the total variance with only a few components, which can reduce a complex data set to a lower dimension set [242]. Therefore, PCA can be used to provide the features of any such data sets.

In this study, PCA-based signal processing is applied to extract dominant AE features from the aliased AE signals. Thus, diverse AE events and environmental conditions can accurately be discriminated and classified. The approach suggested in this study uses the envelope of the aliased AE time-series signals acquired from various different impact and environmental conditions. To obtain the PCs each data set from a wireless measurement is transformed into a column vector,  $\Gamma_n$ , whose length  $N$  is specified by the number of variables used. For  $M$  measurements, an array matrix  $\Gamma$  with the size of  $M \times N$  will be obtained, as in Equation (6.1) [237]:

$$\Gamma = [\Gamma_1, \Gamma_2, \dots, \Gamma_M] \quad (6.1)$$

As a next step and to ensure that the first principal component accounts for the direction of maximum variance, the mean is calculated and subtracted along each dimension, as in Equations (6.2) and (6.3) respectively. This leads to a mean of zero which helps in finding a basis that minimises the mean square error of the approximation of the data

[243].

$$\bar{\Gamma} = \frac{1}{M} \cdot \sum_{n=1}^M \Gamma_n \quad (6.2)$$

$$\gamma_i = \Gamma_i - \bar{\Gamma} \quad (6.3)$$

The orthogonal Eigen-signals are then calculated by working out the covariance matrix  $C$ , as shown in Equation (6.4):

$$C = \frac{1}{M} \cdot \sum_{n=1}^M \gamma_n \cdot \gamma_n^T = \frac{1}{M} \cdot A \cdot A^T \quad (6.4)$$

where  $A = [\gamma_1, \gamma_2, \dots, \gamma_M]$ .

After calculating the eigenvectors and eigenvalues of the covariance matrix, the eigenvector with the largest corresponding eigenvalue is seen as the direction of the first PC. Similarly, the eigenvector with the second largest eigenvalue represents the direction of the second PC and so on. In this study, the aliased AE time-series signals are characterised as projections of the first three principal component scores of the aliased AE signal i.e., the first three normalised principal components PCA1, PCA2, and PCA3 of the  $i$ -th AE signal,  $x_i$ , as illustrated in Equation (6.5) [236]:

$$PCA_i = \frac{x_i^{PC_i}}{|PC_i|}, i = 1, 2, 3 \quad (6.5)$$

The AE projection space contains the new features that are used for classification purposes, as shown in Section 6.4.

### 6.2.3 Wavelet Transform-Based Features

WT offers simultaneous time domain and frequency analysis for de-noising and smoothing data in a natural and integrated way [244]. This allows the pre-processing of data in order to better locate and identify significant features. Following the discussion in Section 4.3, the WT decomposes the data into orthogonal subspaces, each of which contains information about details at a given resolution. This resolution is high in the frequency domain while it is low in the time domain; or when the resolution is low in the frequency domain it is high in the time domain. This leads to the de-noising of the signal being processed [245].

Various types of WT are available in the wavelet analysis toolbox provided by MATLAB. For the purpose of de-noising and smoothing the aliased AE signals, sta-

tionary wavelet transformation (SWT) [246] is used in this part of the study. The SWT is a shift-invariant transform compared to, for instance, the classical DWT. This is achieved as a result of upsampling the coefficients of the filter by a factor of  $2^{j-1}$  in the  $j^{\text{th}}$  level of DWT instead of using the downsamplers and upsamplers in this technique [247]. This means that a translated version of a signal  $x$  is the same as the SWT of the original signal, which is important in various applications, including de-noising, pattern recognition, feature extraction, and change detection.

Figure 59 illustrates the block diagram of the SWT. In this figure, for a given signal  $S$  of length  $N$ , the first step of the SWT algorithm starts with decomposing it into two sets of coefficients; namely, the approximation coefficients  $cA_j$  and detail coefficients  $cD_j$ . Both vectors are generated via the convolution of  $S$  with low-pass (Lo\_D) and high-pass (Hi\_D) filter respectively. In the next step, the  $cA_j$  and  $cD_j$  coefficients are again split into two parts using the same scheme. However, the filters used in this step are obtained by up-sampling the filters employed in the previous step. As a result,  $cA_2$  and  $cD_2$  are generated. More generally, these can be expressed in the following Equations (6.6) and (6.7) [245]:

$$cA_{j,k} = \sum_n h_0^{\uparrow 2j}(n-2k) \cdot cA_{j-1,n} \quad (6.6)$$

$$cD_{j,k} = \sum_n h_1^{\uparrow 2j}(n-2k) \cdot cD_{j-1,n} \quad (6.7)$$

where  $h_0^{\uparrow 2j}$  and  $h_1^{\uparrow 2j}$  denote inserting  $2j-1$  number of zeros between two points of  $h_0$  and  $h_1$ ; and  $h_0(n) = \langle \emptyset, \emptyset_{-1,n} \rangle$ ,  $h_1(n) = \langle \xi, \emptyset_{-1,n} \rangle$ ;  $\emptyset$  is a scale function;  $\xi$  is a wavelet function; and  $n = 0, 1, \dots, N-1$ .

Two resolution levels of wavelet decomposition have been implemented in order to preserve most of the significant wavelet behaviour, and to minimise the significant wavelet behaviour which corresponds to noise in the aliased AE signal. Three types of statistical measurements were applied to the wavelet approximation coefficients as unique features for each aliased AE signal. Wavelet entropy (ENT) is a measure of the energy dispersion among wavelet coefficients. The entropy of a signal  $x_i$ ,  $i = 1, 2, \dots, N$  is given as in Equation (6.8) [232]:

$$ENT = -\sum_{i=1}^N x_i^2 \cdot \log(x_i^2) \quad (6.8)$$

Another statistical measure is the root mean square (RMS) which is the sum of squares



of the difference between the amplitudes and mean value of the signal  $\bar{x}$ , and it is measured as in Equation (6.9) [248]. In addition to the standard deviation (STD) feature, these features are used for classification purposes, as discussed in Section 6.4.

$$RMS = \sum_{i=1}^N (x_i - \bar{x})^2 \quad (6.9)$$

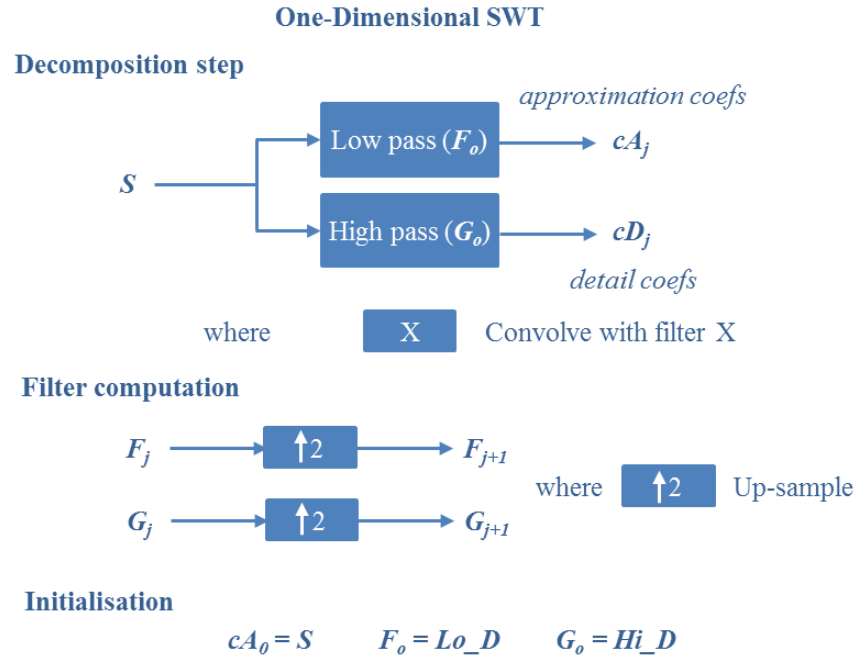


Figure 59: Block diagram of SWT.

#### 6.2.4 Wavelet Transform-Principal Component Analysis Based Features

As mentioned in the previous section, the pre-processing of data with WT leads to the smoothing of the aliased AE signal and better identification of significant features. Thus, the fusion of this type of data pre-processing with multivariate statistics (PCA) facilitates the extraction of the hidden information in these signals for data analysis and interpretation. The integration of WT and PCA has found application in defect classification and quantification for pulsed eddy current NDT [249], and in condition monitoring to detect faults in an automobile engine using AE [248] as well as in face recognition [250, 251]. This promising type of integration is adopted in this work for better feature extraction via the application of PCA to the wavelet coefficients of aliased AE signals captured wirelessly using low sampling rates lower than the Nyquist rate in the data acquisition operations. The results of this integration are presented in Section 6.4.

### **6.3 System Validation Using Emulated Impact Damage and Environmental Monitoring**

The proof-of-concept hardware implementation of an *in-situ* wireless SHM system for WTBs proposed in Chapter 5 is experimentally evaluated in this chapter. This is accomplished by detecting and classifying different AE events as well as changes in environmental conditions. As mentioned in Section 6.1, two complementary options were available to perform this validation: firstly, by fusing the AVPs received from the individual wireless units at the remote control unit; or, secondly, by collecting the raw data of the aliased AE signals at the remote control unit in order to extract the AE features using the aforementioned advanced feature extraction techniques.

For the validation process, it is important that AE events relevant to environmental conditions are recorded and separated from those relevant to the health condition of WTBs. Thus, different case studies are considered, including those with AE events and environmental monitoring under different environment conditions. Artificial AE sources are generated to emulate impact damage or audible cracks caused by different objects such as tools, bird strikes, or strong hail in order to validate the system. These cases represent abrupt signals and continuous monitoring for the detection of sudden changes under wind and rain loads. The validation of AE event localisation has been discussed in Chapter 5, and therefore this chapter gives more attention to the validation of the environmental monitoring and classification of emulated impact damage based on the features extracted using the abovementioned algorithms, as discussed next.

### **6.4 Validation Results and Discussion**

Leaving the WTB system to rotate under different environment conditions is likely to result in different AE events based on these conditions as well as on the structural health of the blades. Therefore, for a robust SHM system it is very important to be able to distinguish and characterise these events in order to specify the main causes of such events. This section discusses the experimental results of the system validation based on these variables. The experiments were conducted using the wireless experimental setup discussed in Chapter 5 in order to collect the AE signals generated.

### 6.4.1 AE Event and Environmental Monitoring

Continuously *in-situ* sensing the structural health of the three blades leads to the monitoring of the AE events under different environmental conditions. This results in different AE events based on the health condition of the blades as well as climate conditions. The waveforms of various relevant environmental conditions were recorded during this type of *in-situ* experiment under wind and rain conditions. The experiments were conducted while the wind turbine was installed on the School roof with the wireless monitoring system on top of it. As explained in Chapter 5, each reading consists of 500 samples, all of which were initiated by a simple threshold crossing condition which was below 100mv in order to allow the wireless units to detect such waveforms even if they were weak.

#### 6.4.1.1 AE Event and Environmental Waveforms

Figure 60 depicts an example of waveforms detected while the blades rotated due to the wind i.e., the *Wind condition*. Such types of waveforms are caused by the sound produced as a result of blade rotation. These signals are characterised as noisy signals whose variance and power increase with wind speed. However, raising the detection threshold value of the wireless units will lead to the filtering of these signals.

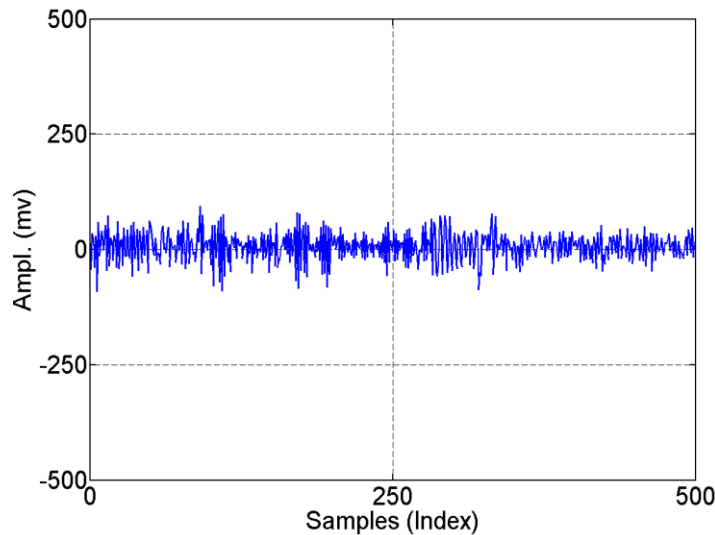


Figure 60: Wind condition waveform detected.

The second environmental condition waveforms were signals caused during the *rainfall condition*. These signals were recorded while the blades were stationary and then when

the blades were rotating. Figure 61 shows an example of the waveform recorded in the former case. This type of signals is characterised by a random sequence of repetitive AE pulses whose peak and repetition values depend on the density and speed of the rainfall.

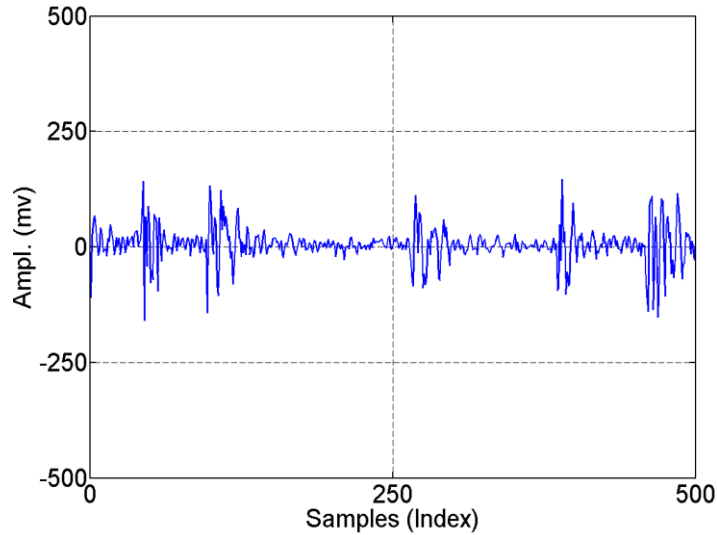


Figure 61: *Rainfall condition waveform detected.*

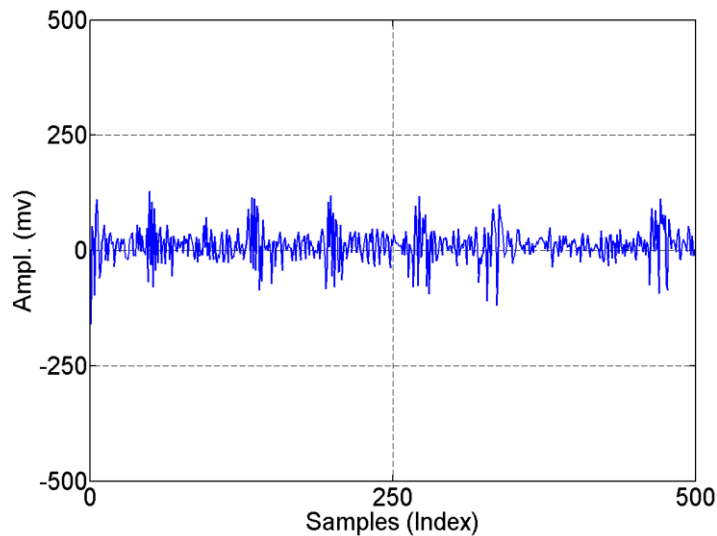


Figure 62: *Rainfall and wind condition waveform detected.*

In contrast, a waveform of a *rain and wind condition* is shown in Figure 62. This type of waveforms was recorded during light rainfall while the blades were spinning under the wind load. As a result of blade rotation the collected rain waveform was contaminated with the noise caused by the spinning of the blades. This type of waveform appears as a sum of the two waveforms of the *rain* and *wind conditions*.

In addition, the blades were also hit with a plastic stick while the blades were stationary and then during the rain test in order to capture both an abnormal signal and a *rainfall condition* waveform. Figure 63 and Figure 64 show an example of waveforms obtained from such experiments for impact as well as rain and impact conditions respectively. Based on the results of the experiments conducted, these types of signals can be usually characterised by the differences in amplitude and shape between the hit event and the rainfall signals. It is worth mentioning that the AE signal received as shown in Figure 63 was captured while the threshold crossing value was low, which allows the capture of the signal onset in comparison to the signals shown in Figure 56.

Furthermore, by comparing the signals received from all wireless units for the measurements in the *rainfall condition*, it is noticeable that there is a high correlation between these signals in terms of the amplitude and width of the individual pulses, as shown in Figure 65-a. This is because they were caused by the same condition, i.e., *rainfall*. This makes the features extracted from such signals among wireless units almost the same. In contrast, if one of the blades encountered a hit during the *rainfall condition*, the received signals will be similar to the signals shown in Figure 65-b. In addition to the rain condition waveforms, this figure shows the signals caused by the emulated impact damage of blade number one. As discussed in Chapter 5, the impact signal propagated from this blade to the other two blades, which are then captured by wireless units two and three, can be clearly seen in the last two plots in Figure 65-b.

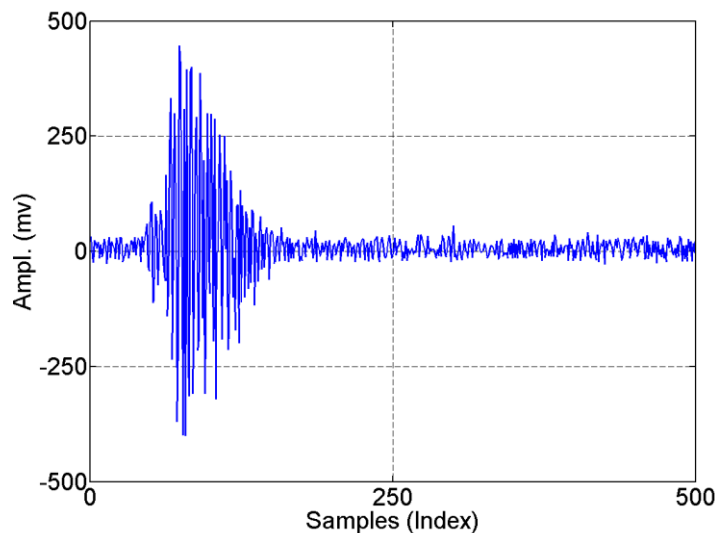


Figure 63: Emulated impact damage waveform.

The above mentioned *in-situ* wireless experiments were conducted several times and a sequence of AE aliased waveforms was recorded under the aforementioned conditions. In addition, waveforms of the *steady case* at a very low wind speed were also recorded. These waveforms were further analysed and classified as discussed next.

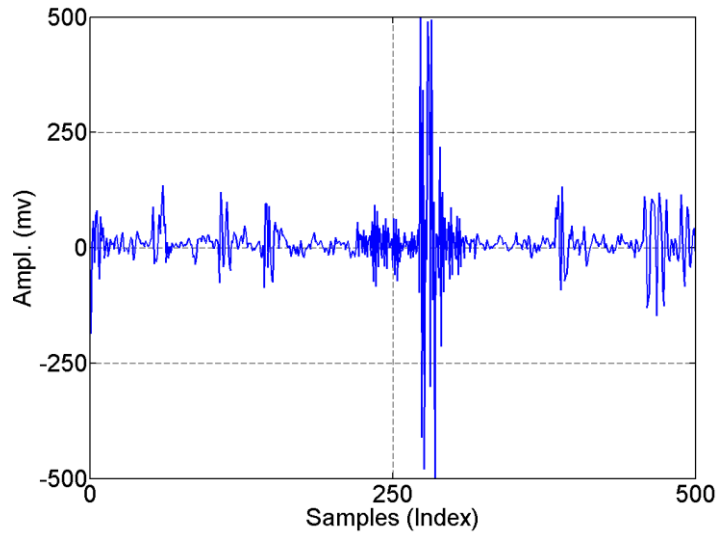


Figure 64: Emulated impact damage and rain condition waveform detected.

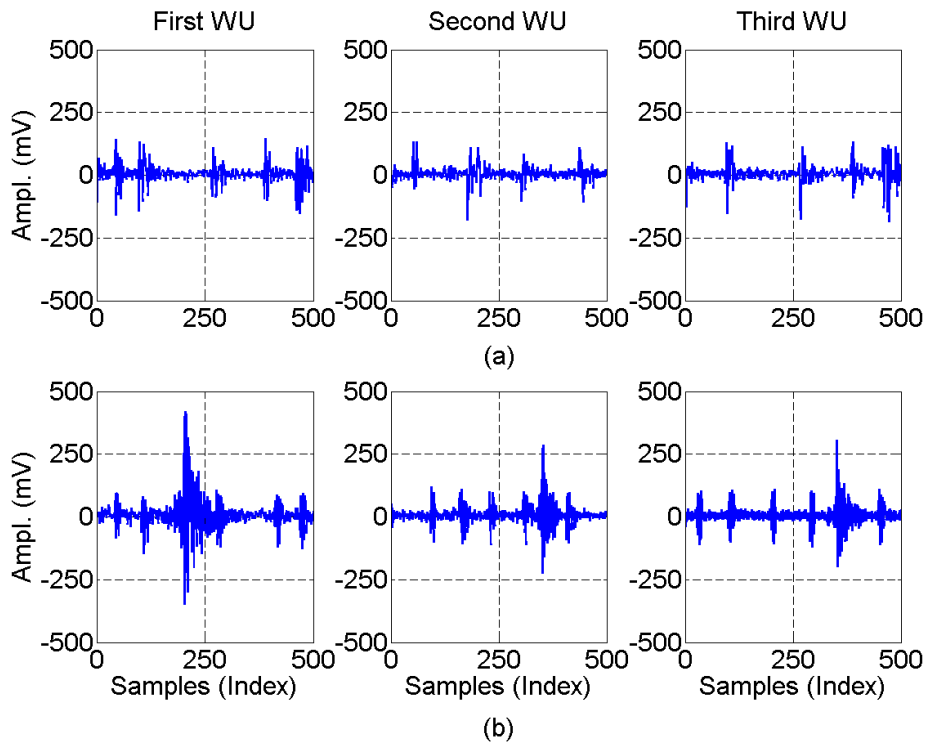


Figure 65: AE events received at three wireless units (WU), a) for rain, b) rain and hit measurements.

### 6.4.1.2 Classification of AE Event and Environmental Monitoring

As discussed above, the AE event and environmental experiments were repeated several times, and in each case the AE parameters or features discussed in Sections 5.4 and 6.2 were extracted on-board the wireless unit and at the remote control unit respectively. In both cases, these features were used at the control unit to discriminate between the waveforms captured during these experiments.

Figure 66 illustrates the results using peak value and RMS features as a combination to lead to the signals recorded being distinguished. From the captured waveforms discussed above, it is noticeable that those relevant only to the *wind condition* have values of RMS greater than those in waveforms for the *steady condition* case. This difference was increased by increasing the speed of rotation of the WTBs. In contrast, the difference in peak values due to raindrops hitting the blades between the waveforms of the former condition and the *rainfall condition* led to the two cases being distinguishable, and as the strength of the rainfall increased this difference increased as well. In addition, the waveforms relevant to the *rain and wind condition* were distinguished by their relatively large RMS values compared to the *rainfall condition* due to the difference in noise levels.

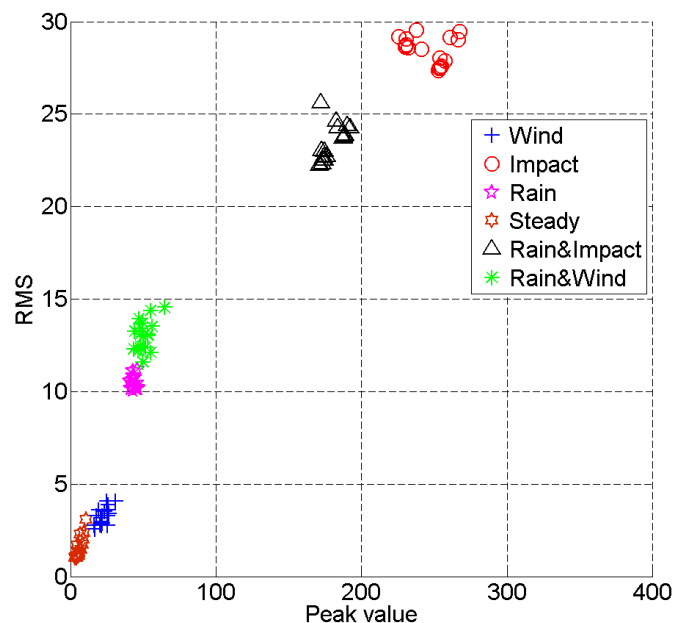


Figure 66: Classification of received events under different environment conditions using time domain features.

Finally, for the cases where the blades were manually hit, in order to generate artificial sounds which emulated audible cracks or impact damage due to different objects, the AE events produced gave the highest peak values as shown in Figure 66. These values made the discrimination of these events from the waveforms discussed above very easy. The signals resulting from the propagation of the emulated impact damage to the other blades are not considered in Figure 66 since they show the same features as the main signals, but with relatively low values.

In addition to the time domain features which were used in the above classification of AE events under different environment conditions, the PCA features have also been applied to a similar set of such events collected at the remote unit. Figure 67 illustrates the discrimination results of this process. In this figure, to ensure better representation of this classification, the first two PCs features have been integrated with the time domain features (average of peak values) of the AE events captured. As seen in this figure, it was found that this integration has the potential to discriminate between these AE events, where they are clearly classified into six non-overlapping clusters based on this combination.

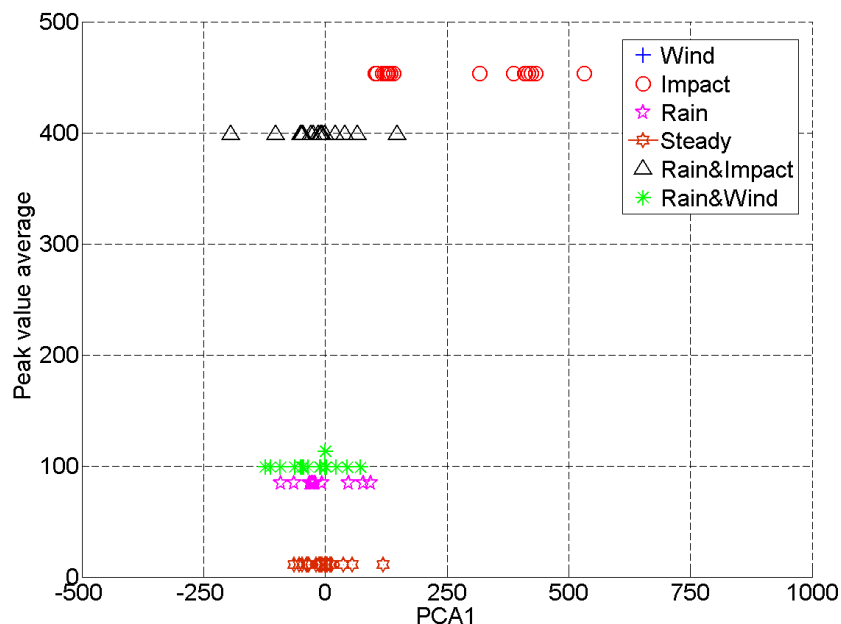


Figure 67: Classification of received events under different environment conditions using the integration of time domain and PCA features.



In the last two figures, it can be seen that waveforms relative to the impact damage emulated are obviously separated from the rest of waveforms discussed above. To obtain better identification and classification of such impact or crack AE events, more emulated impact measurements were conducted and additional feature extraction algorithms applied, as discussed in the next section.

#### 6.4.2 Discrimination and Classification of Emulated Impact Damage

Monitoring of the emulated impact damage is carried out on WTBs through the developed wireless SHM system. The impact was emulated by hitting the blades while they were static, by three metallic balls of different sizes, as shown in Figure 69. The smallest ball (SB) has a diameter and mass of 5mm and 1g respectively, whereas the medium ball (MB) is 9mm and 3g and the largest ball (LB) 13mm and 9g. The balls were thrown to the blades at the same speed and from the same height (H) and at the same distance (D) from the AE wireless units, as shown in Figure 68.

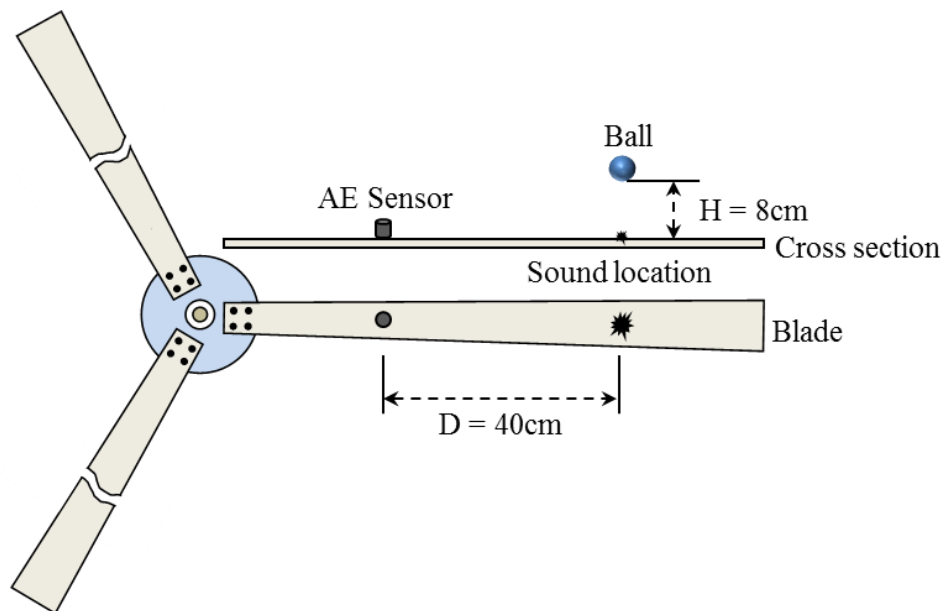


Figure 68: Emulated impact damage setup.

As a result of this emulated impact damage three different aliased AE signals were generated, as illustrated in Figure 69. It can be seen in this figure that the duration and power parameters of these signals are proportional to the size of the ball used, where the largest ball caused the longest signal duration and maximum power. These experiments were repeated several times and in each case the AE parameters or features discussed in

Section 5.4 were extracted on-board the wireless unit and sent to the control unit in the form of APVs. These APVs were used in the control unit to discriminate between the three cases.

To identify the three cases, it was found that the AE parameters such as power and duration features are sensitive to the type of impact damage emulated. These parameters were used to discriminate between the different ball impacts, as shown in Figure 70. This figure shows that the AE aliased signals caused by the smallest ball were characterised by small values of the selected parameters. These parameters increased as the size of the ball increased, leading to a clear separation between the three cases.

To confirm these results, the WT and PCA feature extraction algorithms have also been applied to the AE aliased signals collected at the remote unit for the same set of experiments. Figure 71 illustrates the discrimination results of the impact signals caused by the three balls using SWT-based features; namely, the entropy and standard deviation parameters.

As can be seen in Figure 71, the three impact cases can be easily identified as they are well separated. This technique is simply used to cluster the AE signals, using statistical information gained from the WT coefficients, into individual groups which have similar values representing the three different AE generation sources. It is also noticeable that the aliased AE waveforms produce a more linear and monotonic distribution in terms of grade classification of the acoustic signals generated.

The combination of WT and PCA has also been applied to the same set of aliased AE signals discussed above in order to confirm these results using different feature extraction algorithms. Figure 72 illustrates the results of using WT-PCA based features in distinguishing between the three cases of impact damage using the first three PCs. AE signals caused by the largest ball are separated from the others as the PCA1 values are all positive. In addition, the PCA3 values are all negative for the smallest ball which distinguishes them from the signals caused by the medium ball, whereas the PCA2 values are positive for all cases.

Despite the fact that the results show a distinct separation between these signals, the patterns shown in Figure 70 and Figure 71 are lost which showed no much improvement through combining WT and PCA based algorithms. However, the values of PCA3 are

almost linearly proportional to the strength of these signals which increased as the effect of the impact source increased.

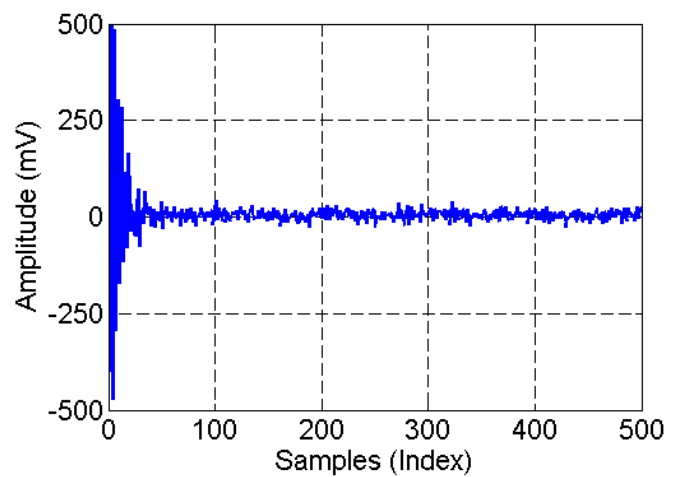
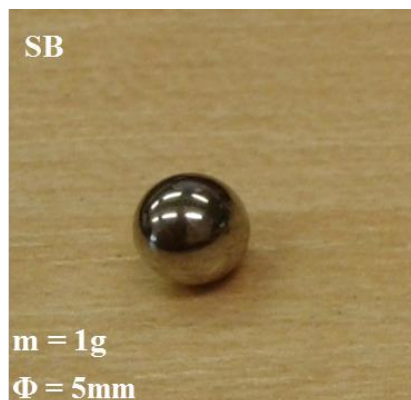
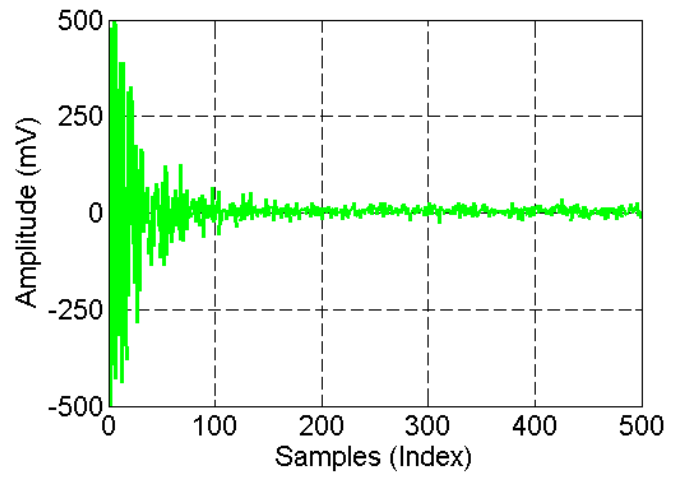
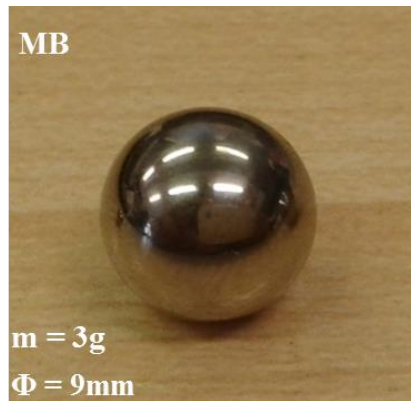
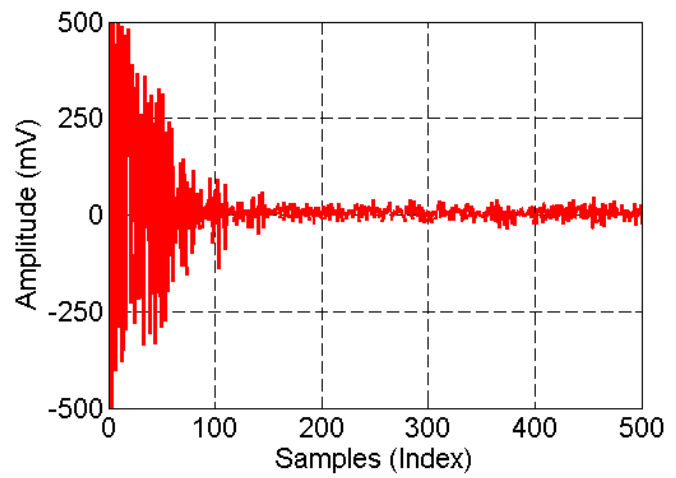
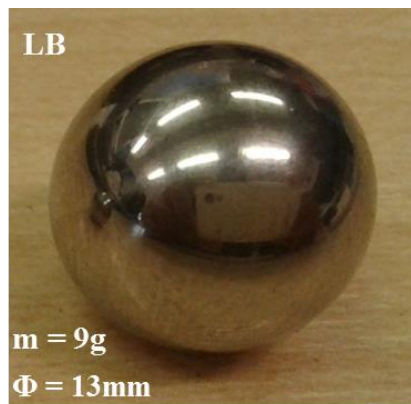


Figure 69: Aliased AE signals caused by the emulated impact damages by the three balls; a) LB, b) MB, and c) SB.

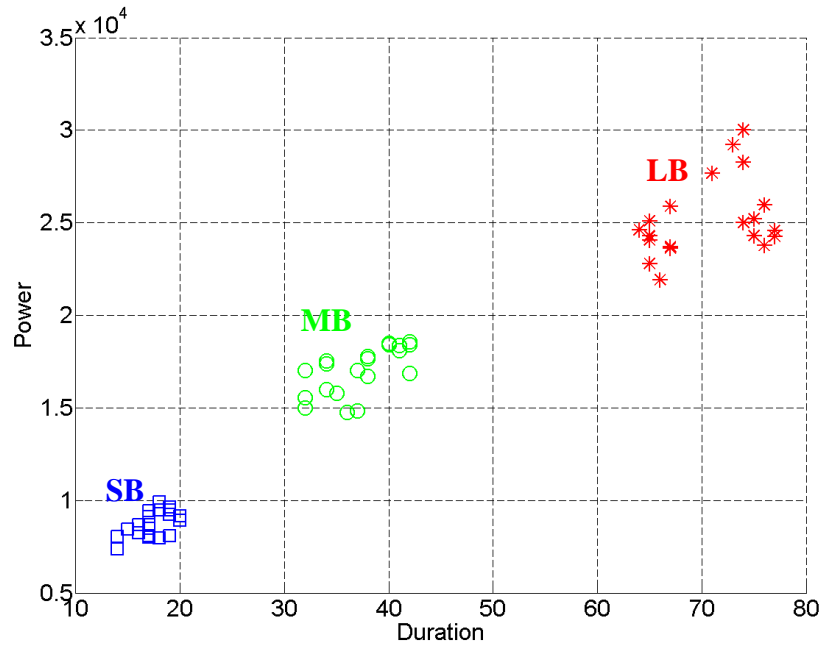


Figure 70: Discrimination between impact signals caused by the three balls.

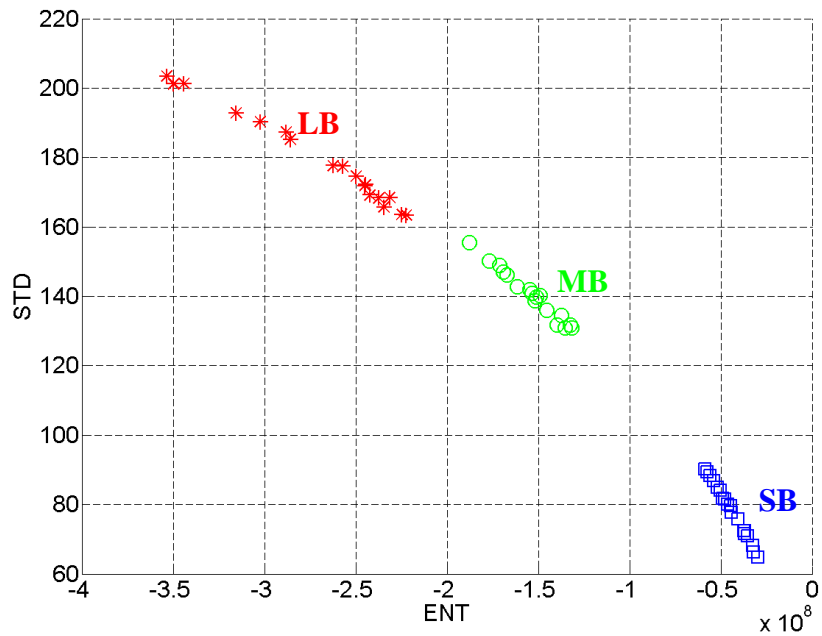


Figure 71: Discrimination between impact signals caused by the three balls using SWT-based features.

Since PCA is a purely mathematical procedure, it is useful to relate the results obtained to the time-domain features of the aliased AE waveforms in order to facilitate physical explanations. It is found that the normalised third PC for all sets of aliased AE signals correlates with the time domain feature of the normalised average power parameter of

these signals, as shown in Figure 73. Therefore, as the effect of the impact increases with increasing grades, the duration of the aliased signals increases and hence more power is accumulated by the AE sensor.

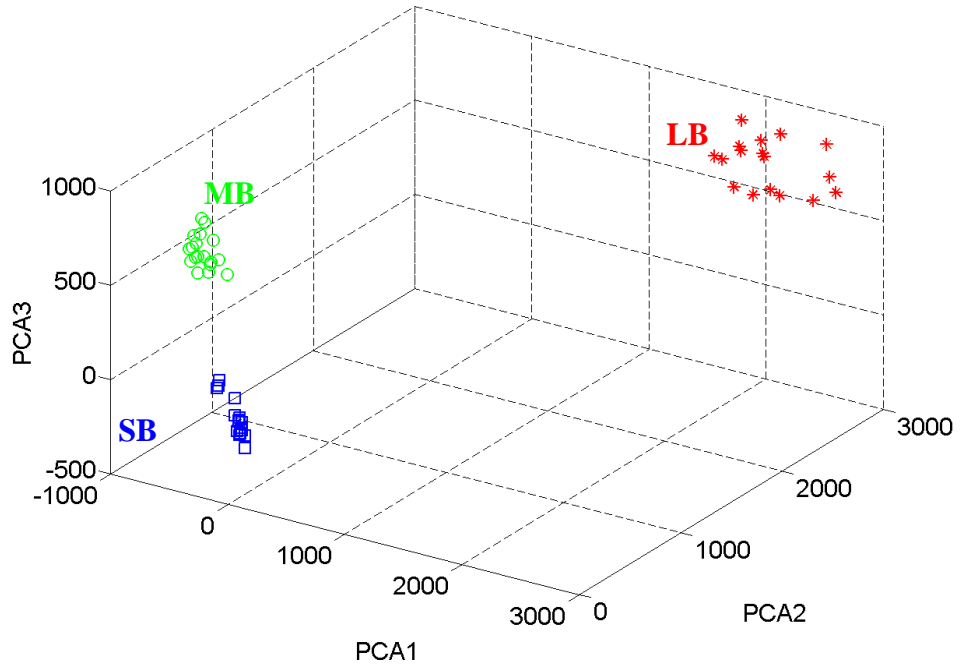


Figure 72: The principal component analysis of the WT coefficients to discrimination between impact signals caused by the three balls.

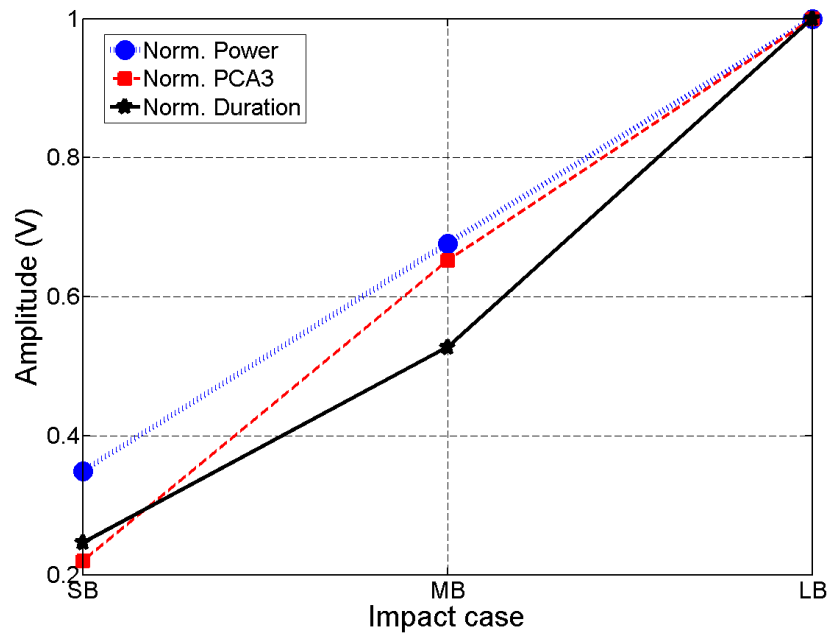


Figure 73: Third principal component correlates with normalised average power parameter of aliased AE signals for the three impact cases.

## 6.5 Summary

In order to demonstrate the validation of the wireless SHM system developed in the course of this research, AE events were captured under different environmental conditions, including wind and rain conditions. In addition, artificial AE sources were generated while the blades were static and during the rain test to emulate audible cracks or impact damage caused by different objects. A sequence of experiments was conducted and in each measurement AE aliased waveforms were captured and time and time-frequency AE features were extracted in addition to PCA features.

Based on the measurements conducted during the validation of the proposed *in-situ* wireless SHM technique with field deployment on the WTB structure, the main characteristics of the waveforms captured are summarised in Table 12. The data collected here are based on the experimental settings and environmental conditions on the days of the experiments, which may have varied from day to day, but the trends in the data are similar.

Table 12: Waveform descriptions of the AE event and environmental conditions.

AE event and environmental condition	Waveform description
Steady	A very low noisy signal.
Wind	Noisy signals whose variance and power increased with increasing wind speed.
Rain	Random sequence of repetitive AE pulses whose peak and repetition values depend on the strength of the <i>rainfall</i> .
Impact	Abnormal signals whose AE parameters such as power and duration depend on the strength of impact.
Wind and Rain	A sum of the two waveforms of the rain and wind conditions.
Impact and Rain	A sum of the two waveforms of the impact event and <i>rainfall</i> .

To check data validity, simple repeatability tests were also carried out. Each waveform was captured several times. The results of separating and clustering the individual groups based on the extracted AE features were then plotted for all groups. These re-

sults were confirmed using time and time-frequency feature extraction algorithms in addition to the PCA technique. This also showed that working under the utilisation of low sampling rates to extract AE features from aliased AE waveforms can help in fulfilling the requirements of AWSNs for SHM systems as discussed in Chapters 1 and 2.

The data samples collected were limited in terms of the number and type of measurements taken, due to the small size of the wind turbine unit used and safety issues associated with using the wind turbine on the School roof. The evaluation case studies confirm the feasibility of employing the proposed *in-situ* wireless system for SHM applications. It would be better if a wider range of real defects was considered. However, the investigation of the full range of possible defects which might occur would have been beyond the scope of this research, due to the time required to develop such defects.

# CHAPTER 7: CONCLUSIONS AND FURTHER WORK

In this chapter, the research work presented in this thesis is summarised. It starts with a summary of the research exploring the major work that has been completed throughout the journey of this research. In the subsequent section, the main scientific contributions described in the thesis are presented. After that the limitations of the study are discussed, followed by the potential directions for future research in terms of both extending the existing system to cope with multi-hop data collection and its adoption in large scale wind turbines. Finally, the practical implications of the research are described.

## 7.1 Research Summary

Interest in the integration of SHM systems into various industrial applications has been steadily growing over the last few years. This is because such systems are widely considered as efficient techniques for significantly reducing the costs of the O&M of safety-critical structures and systems. This is also true for the wind power industry where rising demand for the harvesting of wind energy means that wind turbines have become physically larger and more wind farms are placed in remote areas in order to increase efficiency and the levels of power generated. These requirements have made the development of *in-situ* SHM techniques for OWTs an important research topic.

For such an application, an SHM system can be deemed successful only if it provides good sensitivity to defects, fault prediction and the evaluation of the remaining lifetime, as well as the prevention of the early collapse of wind turbine units. This can be achieved in terms of giving warnings of the need for product replacement and maintenance in the early stages, along with defect localisation and identification. To achieve this, two relevant topics have been considered. The first is to implement an *in-situ* wireless SHM technique for OWTBs based on the integration of wireless technology and the



AE technique in conjunction with the use of low sampling rates; and the second is to develop appropriate signal processing algorithms to detect, localise, and classify different AE events under the employment of low sampling rates. The research can be categorised in terms of various tasks which are described as follows.

The subject of this research and the framework within the project was conducted as well as the main contributions of this thesis were introduced in Chapter 1. For convenience a summary of this work and the results are also presented in Chapter 1.

The contributions made in Chapter 2 are represented by providing background information on wind power systems, with special attention given to WTBs in conjunction with different types of failure model for them. State-of-the-art techniques for inspecting and monitoring the structural health of WTBs are also explored. The strengths and weaknesses of these techniques are compared, and criteria used to select the most appropriate are presented. The literature survey concluded that the AE technique has been found to be an effective method of detecting WTB failures; however, wired-based solutions make the adoption of this technology in the SHM of OWTBs is almost impossible due to, for example rotation of blades. Thus, integrating this technique with WSNs was suggested in order to develop a robust wireless SHM system. The potential and limitations of this integration are discussed. A sensing method based on the use of low sampling rates is also described with the intention to solve the limitations of power and commutation bandwidth at the level of wireless sensor. It also helps to overcome the requirement of high sampling rates in accordance with the Nyquist rate which are required for highly reliable acoustic records.

The fundamentals of the CS technique are briefly discussed in Chapter 3. A concept based on the use of low sampling rates, lower than the Nyquist rate, in data acquisition operations was proposed. The advantage of this utilisation is that it is an energy-efficient scheme for wireless technology. In addition, the shape of the original acoustic signal is preserved. This helps in retaining the most salient information, such as timing information and the coherence of aliased signals captured by the different wireless nodes, both of which are very important for ASL and classification.

The main drawbacks of working under the use of low sampling rates are discussed since it may significantly reduce the performance of the TDE algorithms due to loss of infor-

mation and low spatial resolution. Therefore, based on experimental and comparative studies of different domains of analysis for TDE, it was concluded that the employment of the time-frequency domain and envelopes of the aliased signals instead of their amplitude values would be significant in overcoming this issue and allow this utilisation while enhancing the accuracy of TDE.

These techniques were then successfully evaluated in Chapter 4 using data from AWSNs. Thus, the main contribution of this chapter is in proposing a novel TDE algorithm based on the recommendations of the previous chapter. The proposed technique takes advantage of the envelope feature to smooth the aliased acoustic versions received from the ASL system which was developed using AWSNs. The WT and CC in conjunction with parabolic fit interpolation were then employed to estimate the time delays among the aliased signals captured. However, the multi-scale averaging approach used to calculate the time delay represents a drawback of this technique, since it is time-consuming. To counteract this problem, an SE criterion is applied in order to optimise the selection of the scale index that gives the best estimation accuracy without the need to perform averaging. In addition, the experimental results have shown that, a wireless ASL system based on MICAz platforms and TinyOS HEH mode was able to realise synchronised sensing operations among the wireless units due to its deterministic nature which greatly improved the accuracy of estimation.

Building on the experience gained from the aforementioned work, an *in-situ* wireless SHM system was implemented on the top of WTBs. Thus, the main contribution of Chapter 5 was to introduce the hardware implementation of this proof-of-concept for the *in-situ* system in conjunction with a detailed discussion of the main challenges facing this implementation. The feasibility of this wireless technique with field deployment on the WTB structure was validated by experimental results for the localisation of several AE events. Both centralised and decentralised approaches were considered for the developed system in which the AE parameters were extracted from the envelope of the aliased AE signals on-board the wireless units. These parameters were used to construct only the AVPs, which were sent to the remote control room for central processing where the AE events can then be identified and classified. In this chapter, AVPs have been used in a combination of the constraint geometrical point and zonal localisation

techniques to localise the AE sources, which have shown precise source localisation results with the WTBs structure used in this study.

In Chapter 6, the potential of the proposed wireless SHM system is evaluated using different case studies. This has been performed by conducting several wireless *in-situ* measurements in which several AE events emulating impact damages as well as changes in environmental conditions were detected and monitored. The extraction of AE parameters was performed on-board the wireless units and at the remote control unit using time and time-frequency feature extraction algorithms in addition to PCA method respectively. Complementary information is identified and schemes for event monitoring with data fusion are discussed, which in turn are used to classify or recognise a testing condition that is represented by the response signals.

### **7.2 Main Contributions of the Research**

As part of Newcastle University contributions to the HEMOW-FP7 Project, the aim and objectives of this research have been met, and the following achievements have been satisfied concerning the development of a proof-of-concept SHM technique for OWTBs based on WSNs and AE techniques in conjunction with the use of low sampling rates.

- A thorough review has been undertaken of different SHM systems with relevant non-destructive testing and evaluation techniques in conjunction with WSNs as well as the potential for their integration.
- Through a comparative study in conjunction with the use of different time delay estimation algorithms, it has been shown that the utilisation of low sampling rates overcomes the challenges posed by the limitations of data transmission over WSNs for ASL. This original contribution will be important in terms of data reduction and power savings in the design and development of the proposed offshore wind turbine SHM technique based on AWSNs.
- Through the investigation of a novel combination of the wavelet transform, envelope fitting, cross-correlation and the Shannon entropy criterion, the utilisation of ASL using AWSNs with the setting of sampling frequency lower than the commonly required Nyquist frequency has been validated. These results contribute to the reduction of the amount of sensing data, level of power consump-

tion, and communication bandwidth required and is therefore beneficial for AWSN applications.

- Through the implementation of an *in-situ* SHM system on the top of a 300W wind turbine installed on the School roof composed of the developed WSN and an AE technique, the use of low sampling rates has been evaluated in a field environment. In addition, signal processing techniques for the extraction of local AE features from the aliased AE signals have been used to monitor and assess the structural health of WTBs. This contributes to solving the problems of limited power and bandwidth for data transmission in WSNs, which could enhance the performance of the developed *in-situ* wireless SHM for OWTBs.
- The *in-situ* wireless SHM has also been experimentally evaluated based on the utilisation of low sampling rates the consideration given to the detection, monitoring, and classification of different AE events emulating impact damage and audible cracks as well as changes in environmental conditions. Furthermore, through a combination of zonal and constraint geometrical point localisation techniques, a localisation model has been developed and precise source localisation results were achieved for the complex structure of WTBs. Such a model is a potential candidate for large scale WTBs to provide precise estimation results for AE source localisation.
- Several aspects of the research have been the subject of publications in refereed journals, conference papers, and posters.

### 7.3 Limitations of the Research

The research has introduced an *in-situ* wireless SHM system which has the ability to satisfy the SHM requirements for OWTB development. However, the following limitations are still there:

- In the current *in-situ* prototype system, the MICAz platforms used to develop the wireless units are resource constrained in terms of limited power supply, which represents a weakness in this system.

- Since this is one of the first wireless SHM prototypes for WTBs, its hardware implementation is limited to a small scale of wind turbines. For larger scale systems the AE sensors and wireless units would need to be fitted differently.
- Due to the resource constraints on wireless units, the on-board signal processing algorithms were relatively simple rather than advanced techniques, which may limit their performance and efficiency in AE feature extraction.
- The evaluation case study was limited in terms of the number and type of measurements taken due to the small size of wind turbine unit used and safety issues of using the wind turbine on the School roof. It would be better if a wider range of real defects was considered. However, the investigation of the full range of possible defects to occur would have been beyond the scope of this research, because many defects may take days, months or even longer to develop.

### 7.4 Suggestions for Future Work

The research presented in this thesis can significantly improve SHM practice in OWTB development and more cost effective of O&M in terms of safety-critical components and systems. This is due to the introduction of the *in-situ* wireless SHM system which was developed based on new concepts in the signal processing field and aspects of hardware implementation. However, there are several directions for further development and improvement of the current work in terms of tackling the abovementioned research limitations. In the following, some opportunities which stem from this research can be investigated in future work:

- The proposed *in-situ* wireless SHM system was developed based on the utilisation of low sampling rates in acquisition operations, which may reduce the power consumption of wireless units. However, the use of a limited power supply represents a drawback in this system. To overcome this limitation, energy harvesting systems show promising approaches. There are different possible solutions which can be integrated with such systems. For example, ambient vibrations can be converted into electrical energy based on giant magnetostrictive material [252], using a new technique based on infrared solar rectennas [253], or utilising ambient RF energy to remotely power the wireless units [254].

- The current wireless system presented in this research was adapted to a small scale of wind turbines. However, its feasibility appears promising for practical large scale WTBs. Therefore, further development of this work is necessary to make this system effectively applicable to large wind power systems. This can be performed by paying more attention to the multi-hop WSN data aggregation protocols [211]. In addition, with the future improvement of sensors as well as wireless technologies, alternative low profile and low mass AE sensors based on, for example, MEMS or piezofilm technologies and wireless nodes can be used. However, the integration of these sensors with WTBs is still a challenge which is required to be tackled. This may be performed by mounting them inside the blades or even integrated into their structure during the manufacturing process.
- AE source localisation is very important for large structures such as WTBs in identifying active regions where damage in the material structure is expected. To achieve this by extending the work in this study, the large scale WTB can be divided into regions each of which is assigned to a wireless AE unit or a group of units. Then, by applying the combination of zonal and constraint geometrical point localisation techniques, active regions can be specified, as discussed in Chapter 5. This would have the advantage of excluding the inspection of inactive areas, and therefore minimising the inspection costs.
- Future work based on this research should pay more attention to the implementation of time synchronisation protocols among wireless units in order to enhance the robustness of the wireless localisation system. Furthermore, an analysis of power consumption in relation to sampling rates should be able to confirm the importance of the reduction of sampling frequencies in WSN applications.
- Although, AET can detect the generation and propagation of defects in online and *in-situ* monitoring, it is a challenge to obtain quantitative information about the defects. Therefore, it is thought for future work that a more precise investigation can be conducted by collecting more data from the sensors around that particular region or using other NDTs, as explained in next section. In addition, the investigation of different possible defects could be achieved if the proposed *in-*

*situ* wireless system will be mounted in a large scale wind turbine placed in remote area. Furthermore, the discrimination capabilities of the system could be developed to the point that training and validation data collected will be passed to automatic classification techniques, such as artificial neural network (ANN) or support vector machine (SVM) in order to provide a robust and fully automated SHM system for OWT units.

### **7.5 Research Implications for Practice**

The research is significant because it has resulted in a better understanding of the nature of SHM development and its requirements for monitoring OWTBs, specifying the strengths and weaknesses of existing NDT approaches and identifying the most suitable technique to be integrated with wireless technology in order to develop an *in-situ* wireless SHM system for such applications. This system was designed with the intention to be easy to use, simple, flexible and adaptable as well as these advantages are supported through the evaluations. Therefore, the aforementioned contributions have several significant implications for both assessing and constructing online SHM systems, particularly for OWTBs and many other applications.

Furthermore, due to the advantages of low cost and the early detection as well as localisation capabilities of the *in-situ* wireless SHM system presented in this thesis, new horizons are opened up for integrating this system in many applications, ranging from civil to engineering applications such as bridges, highways, tall buildings, and aircraft and ship structures. In addition, the system could be combined with more advanced techniques, for example, climbing vehicular robots [29, 255]. After the defect zone is localised using the *in-situ* SHM system as discussed in Chapter 5, robots can be sent to that particular zone for further precise inspection, as shown in Figure 74. This has the potential to make the inspection process using vehicular robots based on event monitoring rather than on regular inspection, which is more cost effective.

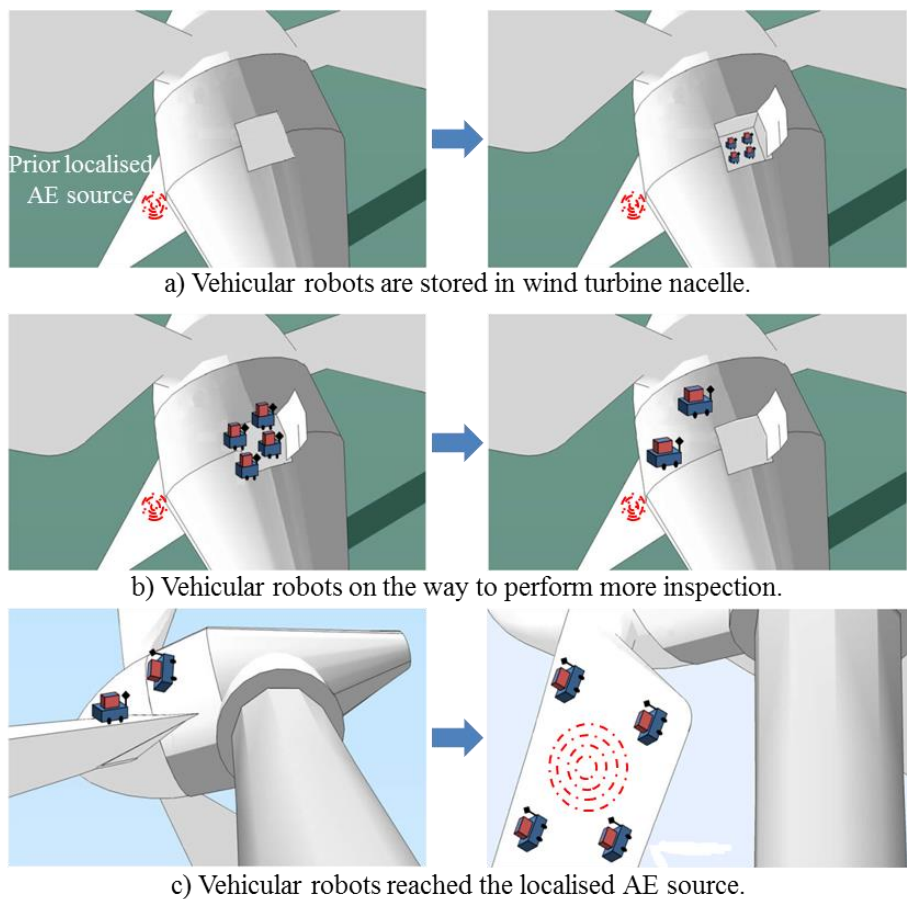


Figure 74: Combination of the proposed *in-situ* wireless SHM system and vehicular climbing robots.



## References

- [1] C. C. Ciang, J. R. Lee, and H. J. Bang, "Structural health monitoring for a wind turbine system: A review of damage detection methods," *Measurement Science and Technology*, vol. 19, pp. 1-20, 2008.
- [2] S. J. Watson, B. J. Xiang, Y. Wenxian, P. J. Tavner, and C. J. Crabtree, "Condition monitoring of the power output of wind turbine generators using wavelets," *Energy Conversion, IEEE Transactions on*, vol. 25, pp. 715-721, 2010.
- [3] P. J. Schubel, R. J. Crossley, E. K. G. Boateng, and J. R. Hutchinson, "Review of structural health and cure monitoring techniques for large wind turbine blades," *Elsevier Renewable Energy*, vol. 51, pp. 113-123, 2013.
- [4] G. R. Kirikera, V. Shinde, M. J. Schulz, M. J. Sundaresan, S. Hughes, J. van Dam, F. Nkrumah, G. Grandhi, and A. Ghoshal, "Monitoring multi-site damage growth during quasi-static testing of a wind turbine blade using a structural neural system," *Structural Health Monitoring*, vol. 7, pp. 157-173, 2008.
- [5] S. Yang and M. S. Allen, "Output-only modal analysis using continuous-scan laser doppler vibrometry and application to a 20kW wind turbine," *Mechanical Systems and Signal Processing*, vol. 31, pp. 228-245, 2012.
- [6] A. Güemes, A. Fernández-López, and B. Soller, "Optical fiber distributed sensing - physical principles and applications," *Structural Health Monitoring*, vol. 9, pp. 233-245, 2010.
- [7] HEMOW. (March 2013). *Health Monitoring of Offshore Wind Farms*. Available: <http://www.hemow.eu/>
- [8] S. Jacobsson and K. Karltorp, "Formation of competences to realize the potential of offshore wind power in the European Union," *Energy Policy*, vol. 44, pp. 374-384, 2012.
- [9] "20% Wind Energy by 2030: Increasing Wind Energy's Contribution to U.S. Electricity Supply," ed: U.S. Department of Energy, 2008, pp. 1-248.
- [10] RESCO. (March 2013). *Wind and Marine Power*. Available: <http://www.resco.org.uk/wind-and-marine-power>
- [11] S. Dyas, J. Scheidler, S. Taylor, K. Farinholt, and G. Park, "Structural health monitoring of wind turbine blades under fatigue loads," in *Topics in Experimental Dynamics Substructuring and Wind Turbine Dynamics*. vol. 27, ed: Springer New York, 2012, pp. 227-245.
- [12] CWIF. (March 2013). *Caithness Windfarm Information Forum - Accident statistics* Available: <http://www.caithnesswindfarms.co.uk/>
- [13] RenewableUK. (March 2013). *Offshore Wind Energy*. Available: <http://www.renewableuk.com/>
- [14] C. R. Farrar and H. Sohn, "Pattern recognition for structural health monitoring," presented at the Workshop on Mitigation of Earthquake Disaster by Advanced Technologies, 2000.

## References

---

- [15] Z. Hameed, Y. S. Hong, Y. M. Cho, S. H. Ahn, and C. K. Song, "Condition monitoring and fault detection of wind turbines and related algorithms: A review," *Renewable and Sustainable Energy Reviews*, vol. 13, pp. 1-39, 2009.
- [16] D. Balageas, C.-P. Fritzen, and A. Guemes, *Structural health monitoring*. London: ISTE Ltd, 2006.
- [17] S. Kerstin, E. Wolfgang, A. Jörg, L. Elfrun, and L. Gerhard, "A fibre Bragg grating sensor system monitors operational load in a wind turbine rotor blade," *Measurement Science and Technology*, vol. 17, pp. 1167-1172, 2006.
- [18] A. Light-Marquez, A. Sobin, G. Park, and K. Farinholt, "Structural damage identification in wind turbine blades using piezoelectric active sensing," vol. 10, pp. 55-65, 2011.
- [19] I. Amenabar, A. Mendikute, A. López-Arraiza, M. Lizaranzu, and J. Aurrekoetxea, "Comparison and analysis of non-destructive testing techniques suitable for delamination inspection in wind turbine blades," *Composites Part B: Engineering*, vol. 42, pp. 1298-1305, 2011.
- [20] F. P. García Márquez, A. M. Tobias, J. M. Pinar Pérez, and M. Papaelias, "Condition monitoring of wind turbines: Techniques and methods," *Elsevier Renewable Energy*, vol. 46, pp. 169-178, 2012.
- [21] R. Raišutis, E. Jasiuniene, R. Šlitteris, and A. Vladišauskas, "The review of non-destructive testing techniques suitable for inspection of the wind turbine blades," *ULTRAGARSAS (Ultrasound)*, vol. 63, pp. 26-30, 2008.
- [22] J.-R. Lee, H.-J. Shin, C. C. Chia, D. Dhital, D.-J. Yoon, and Y.-H. Huh, "Long distance laser ultrasonic propagation imaging system for damage visualization," *Optics and Lasers in Engineering*, vol. 49, pp. 1361-1371, 2011.
- [23] R. Kažys, R. Raišutis, E. Žukauskas, L. Mažeika, and A. Vladišauskas, "Air-coupled ultrasonic testing of CFRP rods by means of guided waves," *Physics Procedia*, vol. 3, pp. 185-192, 2010.
- [24] M. J. Blanch and A. G. Dutton, "Acoustic emission monitoring of field tests of an operating wind turbine," *Key Engineering Materials*, vol. 245-246, pp. 475-482, 2003.
- [25] P. Meinlschmidt and J. Aderhold, "Thermographic inspection of rotor blades," presented at the 9th European Conference on NDT, Berlin, Germany, 2006.
- [26] J. W. Newman and J. Lindberg, "Laser shearography of wind turbine blades," *Materials Evaluation*, vol. 68, pp. 828-837, 2010.
- [27] W. Steinchen and L. X. Yang, *Digital shearography; theory and application of digital speckle pattern shearing interferometry*. Bellingham, Wanshington, USA: SPIE Press, 2003.
- [28] E. Bayraktar, S. D. Antolovich, and C. Bathias, "New developments in non-destructive controls of the composite materials and applications in manufacturing engineering," *Journal of Materials Processing Technology*, vol. 206, pp. 30-44, 2008.
- [29] N. Elkmann, T. Felsch, and T. Förster, "Robot for rotor blade inspection," presented at the 1st International Conference on Applied Robotics for the Power Industry (CARPI), 2010.
- [30] N. Tralshawala and W. I. Faidi, "System and method for inspecting a wind turbine blade," United States Patent 8120522, 2011.

## References

---

- [31] M. Huang, L. Jiang, P. K. Liaw, C. R. Brooks, R. Seeley, and D. L. Klarstrom, "Using acoustic emission in fatigue and fracture materials research," *JOM*, vol. 50, pp. 1-14, 1998.
- [32] gCaptain. (March 2013). Available: <http://gcaptain.com/wartsila-aker-solutions-high/>
- [33] MOOG. (March 2013). *Offshore Expertise*. Available: <http://www.moog.com/markets/energy/wind-turbines/offshore-expertise/>
- [34] R. E. Sheppard, F. J. Puskar, and C. Waldhart, "Blade inspection guidance for offshore wind turbine facilities," 2011, pp. 976-981.
- [35] S. Jang, H. Jo, S. Cho, K. Mechitov, J. A. Rice, S. H. Sim, H. J. Jung, C. B. Yun, J. B. F. Spencer, and G. Agha, "Structural health monitoring of a cable-stayed bridge using smart sensor technology: deployment and evaluation," *Journal of Smart Structures and Systems*, vol. 6, pp. 439-459, 2010.
- [36] J. P. Lynch and K. J. Loh, "A summary review of wireless sensors and sensor networks for structural health monitoring," *Shock and Vibration Digest*, vol. 38, pp. 91-128, 2006.
- [37] J. Yick, B. Mukherjee, and D. Ghosal, "Wireless sensor network survey," *Computer Networks*, vol. 52, pp. 2292-2330, 2008.
- [38] K. Sukun, S. Pakzad, D. Culler, J. Demmel, G. Fenves, S. Glaser, and M. Turon, "Health monitoring of civil infrastructures using wireless sensor networks," presented at the 6th International Symposium on Information Processing in Sensor Networks, IPSN, 2007.
- [39] G. C. McLaskey, S. D. Glaser, and C. U. Grosse, "Acoustic emission beamforming for enhanced damage detection," in *SPIE, Sensors and Smart Structures Technologies for Civil, Mechanical, and Aerospace Systems*, 2008, pp. 693239-1 – 693239-9.
- [40] W. Wallonia. (March 2013). *Wind industry in Wallonia Belgium* Available: <http://www.windturbinewallonia.be/>
- [41] S. Abrate, *Impact on composite structures*: Cambridge university press, 2005.
- [42] C. Ramadas, M. Janardhan Padiyar, K. Balasubramaniam, M. Joshi, and C. V. Krishnamurthy, "Delamination size detection using time of flight of anti-symmetric (Ao) and mode converted Ao mode of guided Lamb waves," *Journal of Intelligent Material Systems and Structures*, vol. 21, pp. 817-825, 2010.
- [43] A. Jüngert, "Damage Detection in wind turbine blades using two different acoustic techniques," *The NDT Database & Journal (NDT)*, 2008.
- [44] F. M. Larsen and T. Sorensen, "New lightning qualification test procedure for large wind turbine blades," in *Proceedings of International Conference on Lightning and Static Electricity*, Blackpool, UK, 2003, pp. 36.1–10.
- [45] C. R. Farrar and K. Worden, "An introduction to structural health monitoring," *Philosophical Transactions of the Royal Society A: Mathematical, Physical and Engineering Sciences*, vol. 365, pp. 303-315, 2007.
- [46] A. Ghoshal, M. J. Sundaresan, M. J. Schulz, and P. Frank Pai, "Structural health monitoring techniques for wind turbine blades," *Journal of Wind Engineering and Industrial Aerodynamics*, vol. 85, pp. 309-324, 2000.
- [47] G. Y. Tian, F. Abugchem, L. Cheng, and O. M. Bouzid, "Health monitoring of offshore wind farms," presented at the International Conference on Engineering Structural Integrity Assessment, ESIA11, Manchester, UK, 2011.

## References

---

- [48] C. Liang and T. Gui Yun, "Pulsed electromagnetic NDE for defect detection and characterisation in composites," in *Instrumentation and Measurement Technology Conference (I2MTC), 2012 IEEE International*, 2012, pp. 1902-1907.
- [49] P. Kumar and B. Rai, "Impact damage on single interface GFRP laminates - An experimental study," *Composite Structures*, vol. 18, pp. 1-10, 1991.
- [50] S. Agrawal, K. K. Singh, and P. K. Sarkar, "Impact damage on fibre-reinforced polymer matrix composite - A review," *Journal of Composite Materials*, vol. 0, pp. 1-16, 2013.
- [51] V. Arumugam, C. S. Kumar, C. Santulli, F. Sarasini, and A. J. Stanley, "Identification of failure modes in composites from clustered acoustic emission data using pattern recognition and wavelet transformation," *Arabian Journal for Science and Engineering*, pp. 1-16, 2012.
- [52] S. Abrate, *Impact engineering of composite structures* vol. 526: Springer, 2011.
- [53] F. J. Yang and W. J. Cantwell, "Impact damage initiation in composite materials," *Composites Science and Technology*, vol. 70, pp. 336-342, 2010.
- [54] F. Aymerich and S. Meili, "Ultrasonic evaluation of matrix damage in impacted composite laminates," *Composites Part B: Engineering*, vol. 31, pp. 1-6, 2000.
- [55] A. K. Mal, F. Shih, and S. Banerjee, "Acoustic emission waveforms in composite laminates under low velocity impact," in *Smart Nondestructive Evaluation and Health Monitoring of Structural and Biological Systems II*, San Diego, CA 2003, pp. 1-12.
- [56] K. T. Tan, N. Watanabe, and Y. Iwahori, "X-ray radiography and micro-computed tomography examination of damage characteristics in stitched composites subjected to impact loading," *Composites Part B: Engineering*, vol. 42, pp. 874-884, 2011.
- [57] H. Ghasemnejad and N. Ghafari-Namini, "Protection of offshore wind turbine blades against extreme conditions," in *Environment Friendly Energies and Applications (EFEA), 2012 2nd International Symposium on*, 2012, pp. 371-375.
- [58] B. F. Sørensen, E. Jørgensen, C. P. Debel, F. M. Jensen, H. M. Jensen, T. K. Jacobsen, and K. Halling, "Improved design of large wind turbine blade of fibre composites based on studies of scale effects (Phase 1), Summary report," 8755031765, 2004.
- [59] R. Grimberg, A. Savin, R. Steigmann, A. Bruma, and P. Barsanescu, "Ultrasound and eddy current data fusion for evaluation of carbon-epoxy composite delaminations," *Insight - Non-Destructive Testing and Condition Monitoring*, vol. 51, pp. 25-31, 2009.
- [60] R. Grimberg and G.-Y. Tian, "High-frequency electromagnetic non-destructive evaluation for high spatial resolution, using metamaterials," *Proceedings of the Royal Society A: Mathematical, Physical and Engineering Science*, vol. 468, pp. 3080-3099, 2012.
- [61] J. J. Scholey, P. D. Wilcox, M. R. Wisnom, and M. I. Friswell, "Quantitative experimental measurements of matrix cracking and delamination using acoustic emission," *Composites Part A: Applied Science and Manufacturing*, vol. 41, pp. 612-623, 2010.
- [62] C. Kong, J. Bang, and Y. Sugiyama, "Structural investigation of composite wind turbine blade considering various load cases and fatigue life," *Energy*, vol. 30, pp. 2101-2114, 2005.

## References

---

- [63] J. Paquette, J. Van Dam, and S. Hughes, "Structural testing of 9 m carbon fiber wind turbine research blades," in *AIAA 2007 Wind Energy Symposium*, 2007, pp. 8-11.
- [64] D. T. Griffith, J. A. Paquette, and T. G. Carne, "Development of validated blade structural models," presented at the 46th AIAA Aerospace Sciences Meeting and Exhibit, 2008.
- [65] M. A. Rumsey, J. R. White, R. J. Werlink, A. G. Beattie, C. W. Pitchford, and J. van Dam, "Experimental results of structural health monitoring of wind turbine blades," presented at the 46th AIAA Aerospace Sciences Meeting and Exhibit, 2008.
- [66] S. Taylor, G. Park, K. Farinholt, and M. D. Todd, "Fatigue crack detection performance comparison in a composite wind turbine rotor blade," *Structural Health Monitoring*, vol. 0, pp. 1-12, 2013.
- [67] P. E. Irving and C. Thiagarajan, "Fatigue damage characterization in carbon fibre composite materials using an electrical potential technique," *Smart Materials and Structures*, vol. 7, pp. 456-466, 1998.
- [68] A. S. Kiremidjian, G. Kiremidjian, and P. Sarabandi, "A wireless structural monitoring system with embedded damage algorithms and decision support system," *Structure and Infrastructure Engineering*, vol. 7, pp. 881-894, 2009.
- [69] L. E. Mujica, J. Vehí, W. Staszewski, and K. Worden, "Impact damage detection in aircraft composites using knowledge-based reasoning," *Structural Health Monitoring*, vol. 7, pp. 215-230, 2008.
- [70] SACL. (April 2013). *Structures And Composites Laboratory, Department of Aeronautics & Astronautics at Stanford University*. Available: <http://structure.stanford.edu/#>
- [71] E. J. Wiggelinkhuizen, L. Rademakers, T. W. Verbruggen, S. J. Watson, J. Xiang, G. Giebel, E. Norton, M. C. Tipluica, A. J. Christensen, and E. Becker, "CONMOW Final Report," 2007.
- [72] Z. Hameed, S. H. Ahn, and Y. M. Cho, "Practical aspects of a condition monitoring system for a wind turbine with emphasis on its design, system architecture, testing and installation," *Elsevier Renewable Energy*, vol. 35, pp. 879-894, 2010.
- [73] M. Schlechtingen, I. F. Santos, and S. Achiche, "Wind turbine condition monitoring based on SCADA data using normal behavior models. Part 1: System description," *Applied Soft Computing*, vol. 13, pp. 259-270, 2013.
- [74] DEIF. (March 2013). *SCADA for remote supervision and control of wind turbines and wind parks*. Available: <http://www.deifwindpower.com/default.aspx?id=8097>
- [75] X. P. Qing, H.-L. Chan, S. J. Beard, and A. Kumar, "An active diagnostic system for structural health monitoring of rocket engines," *Journal of Intelligent Material Systems and Structures*, vol. 17, pp. 619-628, 2006.
- [76] V. Giurgiutiu and G. Santoni-Bottai, "Structural health monitoring of composite structures with piezoelectric-wafer active sensors," *AIAA journal*, vol. 49, pp. 565-581, 2011.
- [77] B. Lu, Y. Li, X. Wu, and Z. Yang, "A review of recent advances in wind turbine condition monitoring and fault diagnosis," in *Power Electronics and Machines in Wind Applications, IEEE*, 2009, pp. 1-7.

## References

---

- [78] B. Yang and D. Sun, "Testing, inspecting and monitoring technologies for wind turbine blades: A survey," *Renewable and Sustainable Energy Reviews*, vol. 22, pp. 515-526, 2013.
- [79] NCN. (March 2013). *Non-destructive testing of composite materials - National Composites Network (NCN) best practice guide*. Available: <http://www.ncn-uk.co.uk/DesktopDefault.aspx?tabindex=108&tabid=421>
- [80] T. Clarke, "Guided wave health monitoring of complex structures," PhD Thesis, Mechanical Engineering Department, Imperial College, London, 2009.
- [81] P. Wilcox, M. Evans, B. Pavlakovic, D. Alleyne, K. Vine, P. Cawley, and M. Lowe, "Guided wave testing of rail," *Insight-Non-Destructive Testing and Condition Monitoring*, vol. 45, pp. 413-420, 2003.
- [82] M. H. S. Siqueira, C. E. N. Gatts, R. R. Da Silva, and J. M. A. Rebello, "The use of ultrasonic guided waves and wavelets analysis in pipe inspection," *Ultrasonics*, vol. 41, pp. 785-797, 2004.
- [83] M. J. S. Lowe and P. Cawley, "Long range guided wave inspection usage—current commercial capabilities and research directions," Imperial College London, 2006.
- [84] W. Wang, Z. Feng, J. Chen, H. Dong, and C. Zhao, "Ultrasonic guided wave system developed by PetroChina," *Pipeline and Gas Journal*, vol. 238, pp. 101-102, 2011.
- [85] S. Coccia, I. Bartoli, S. Salamone, R. Phillips, F. L. di Scalea, M. Fateh, and G. Carr, "Noncontact ultrasonic guided wave detection of rail defects," *Transportation Research Record: Journal of the Transportation Research Board*, vol. 2117, pp. 77-84, 2009.
- [86] J.-B. Ihn and F.-K. Chang, "Pitch-catch active sensing methods in structural health monitoring for aircraft structures," *Structural Health Monitoring*, vol. 7, pp. 5-19, 2008.
- [87] A. Raghavan and C. E. S. Cesnik, "Review of guided-wave structural health monitoring," *Shock and Vibration Digest*, vol. 39, pp. 91-116, 2007.
- [88] TWI. (March 2013). *TWI*. Available: [http://www.twi.co.uk/content/power\\_renew\\_wind\\_index.html](http://www.twi.co.uk/content/power_renew_wind_index.html).
- [89] IINSIGHT. (March 2013). *In-situ Wireless Monitoring of Offshore Wind Towers and Blades (INSIGHT)*. Available: <http://www.insightproject.co.uk/>
- [90] E. Jasiniene, R. Raiutis, R. Iiteris, A. Voleiis, A. Vladiauskas, D. Mitchard, and M. Amos, "NDT of wind turbine blades using adapted ultrasonic and radiographic techniques," *Insight - Non-Destructive Testing and Condition Monitoring*, vol. 51, pp. 477-483, 2009.
- [91] C. Li, D. Pain, P. D. Wilcox, and B. W. Drinkwater, "Imaging composite material using ultrasonic arrays," *NDT & E International*, vol. 53, pp. 8-17, 2013.
- [92] H. Saito and I. Kimpara, "Evaluation of impact damage mechanism of multi-axial stitched CFRP laminate," *Composites Part A: Applied Science and Manufacturing*, vol. 37, pp. 2226-2235, 2006.
- [93] C. J. Lissenden and J. L. Rose, "Structural health monitoring of composite laminates through ultrasonic guided wave beamforming," in *NATO Applied Vehilce Technology Symposium on Military Platform Ensured Availability Proceedings*, 2008.

## References

---

- [94] E. Jasiūnienė, R. Raišutis, R. Šlitteris, A. Voleišis, and M. Jakas, "Ultrasonic NDT of wind turbine blades using contact pulse-echo immersion testing with moving water container," *Ultrasound*, vol. 63, pp. 28-32, 2008.
- [95] D. Tuzzeo and F. L. di Scalea, "Noncontact air-coupled guided wave ultrasonics for detection of thinning defects in aluminum plates," *Journal of Research in Nondestructive Evaluation*, vol. 13, pp. 61-77, 2001.
- [96] T. E. Michaels and J. E. Michaels, "Application of acoustic wavefield imaging to non-contact ultrasonic inspection of bonded components," in *AIP Conference Proceedings*, 2006, pp. 1484-91.
- [97] Y. Sohn and S. Krishnaswamy, "Interaction of a scanning laser-generated ultrasonic line source with a surface-breaking flaw," *The Journal of the Acoustical Society of America*, vol. 115, p. 172, 2004.
- [98] W. Gao, C. Glorieux, and J. Thoen, "Laser ultrasonic study of Lamb waves: determination of the thickness and velocities of a thin plate," *International journal of engineering science*, vol. 41, pp. 219-228, 2003.
- [99] J.-R. Lee, J. Takatsubo, N. Toyama, and D.-H. Kang, "Health monitoring of complex curved structures using an ultrasonic wavefield propagation imaging system," *Measurement Science and Technology*, vol. 18, pp. 3816-3824, 2007.
- [100] B. Ji and W. Qu, "The research of acoustic emission techniques for non destructive testing and health monitoring on civil engineering structures," in *International Conference on Condition Monitoring and Diagnosis*, 2007, pp. 782-785.
- [101] O. Inayatullah, A. Ali, N. Jamaludin, and M. J. Mohd Nor, "Application of acoustic emission technique to observe the engine oil's viscosity," in *Instrumentation Control and Automation (ICA), 2011 2nd International Conference on*, 2011, pp. 344-348.
- [102] A. G. Dutton, "Thermoelastic stress measurement and acoustic emission monitoring in wind turbine blade testing," in *European Wind Energy Conference* London, UK, 2004.
- [103] X. Zhuang and X. Yan, "Investigation of damage mechanisms in self-reinforced polyethylene composites by acoustic emission," *Composites Science and Technology*, vol. 66, pp. 444-449, 2006.
- [104] G. R. Kirikera, V. Shinde, M. J. Schulz, A. Ghoshal, M. Sundaresan, and R. Allemang, "Damage localisation in composite and metallic structures using a structural neural system and simulated acoustic emissions," *Mechanical Systems and Signal Processing*, vol. 21, pp. 280-297, 2007.
- [105] D. Aljets, A. Chong, S. Wilcox, and K. Holford, "Acoustic emission source location on large plate-like structures using a local triangular sensor array," *Mechanical Systems and Signal Processing*, vol. 30, pp. 91-102, 2012.
- [106] D. G. Aggelis, N. M. Barkoula, T. E. Matikas, and A. S. Paipetis, "Acoustic structural health monitoring of composite materials : Damage identification and evaluation in cross ply laminates using acoustic emission and ultrasonics," *Composites Science and Technology*, vol. 72, pp. 1127-1133, 2012.
- [107] S. De Santis and A. K. Tomor, "Laboratory and field studies on the use of acoustic emission for masonry bridges," *NDT & E International*, vol. 55, pp. 64-74, 2013.

## References

---

- [108] G. C. McLaskey, S. D. Glaser, and C. U. Grosse, "Beamforming array techniques for acoustic emission monitoring of large concrete structures," *Journal of Sound and Vibration*, vol. 329, pp. 2384-2394, 2010.
- [109] G. R. Kirikera, M. Sundaresan, F. Nkrumah, G. Grandhi, A. Bashir, L. Sai, V. Shanov, and M. Schulz, "Wind Turbines," in *Encyclopedia of Structural Health Monitoring*, ed: John Wiley & Sons, Ltd., 2009.
- [110] N. Takeda, "Characterization of microscopic damage in composite laminates and real-time monitoring by embedded optical fiber sensors," *International Journal of Fatigue*, vol. 24, pp. 281-289, 2002.
- [111] H. Guo, G. Xiao, N. Mrad, and J. Yao, "Fiber optic sensors for structural health monitoring of air platforms," *Sensors*, vol. 11, pp. 3687-3705, 2011.
- [112] Z. Zhou and J. Ou, "Development of FBG sensors for structural health monitoring in civil infrastructures," in *Sensing Issues in Civil Structural Health Monitoring*, ed: Springer, 2005, pp. 197-207.
- [113] J. S. Kiddy, C. S. Baldwin, and T. J. Salter, "Hydrostatic testing of a manned underwater vehicle using fiber optic sensors," in *OCEANS, 2005. Proceedings of MTS/IEEE, 2005*, pp. 1876-1881.
- [114] L.-H. Kang, D.-K. Kim, and J.-H. Han, "Estimation of dynamic structural displacements using fiber Bragg grating strain sensors," *Journal of Sound and Vibration*, vol. 305, pp. 534-542, 2007.
- [115] C. Ki-Sun, H. Yong-Hak, K. Il-Bum, and Y. Dong-Jin, "A tip deflection calculation method for a wind turbine blade using temperature compensated FBG sensors," *Smart Materials and Structures*, vol. 21, p. 025008, 2012.
- [116] W. J. B. Grouve, L. Warnet, A. De Boer, R. Akkerman, and J. Vlekken, "Delamination detection with fibre Bragg gratings based on dynamic behaviour," *Composites Science and Technology*, vol. 68, pp. 2418-2424, 2008.
- [117] R. Ian, F. Peter, and M. Stuart, "Optical fibre acoustic emission sensor for damage detection in carbon fibre composite structures," *Measurement Science and Technology*, vol. 13, pp. N5-9, 2002.
- [118] E. Udd and B. Spillman, "Fiber optic sensors: an introduction for engineers and scientists," in *Fiber Optic Sensors*, ed: John Wiley & Sons, Inc., 1991.
- [119] M. Mieloszyk, L. Skarbek, M. Krawczuk, W. Ostachowicz, and A. Zak, "Application of fibre Bragg grating sensors for structural health monitoring of an adaptive wing," *Smart Materials and Structures*, vol. 20, p. 125014, 2011.
- [120] T. W. Verbruggen, "Wind turbine operation & maintenance based on condition monitoring WT- $\Omega$ ," (ECN, Energy research Center of the Netherlands) Final report, ECN-C-03-047, 2003.
- [121] M. Jönsson, B. Rendahl, and I. Annergren, "The use of infrared thermography in the corrosion science area," *Materials and Corrosion*, vol. 61, pp. 961-965, 2010.
- [122] N. P. Avdelidis, D. P. Almond, C. Ibarra-Castanedo, A. Bendada, S. Kenny, and X. Maldague, "Structural integrity assessment of materials by thermography," presented at the Conference on Damage in Composite Materials, Stuttgart, Germany, 2006.
- [123] D. J. Titman, "Applications of thermography in non-destructive testing of structures," *NDT & E International*, vol. 34, pp. 149-154, 2001.
- [124] J. M. Roche, D. Balageas, B. Lamboul, G. Bai, F. Passilly, A. Mavel, and G. Grail, "Passive and active thermography for in situ damage monitoring in woven



## References

---

- composites during mechanical testing," in *American Institute of Physics Conference Series*, 2013, pp. 555-562.
- [125] L. Cheng and G. Y. Tian, "Comparison of nondestructive testing methods on detection of delaminations in composites," *Journal of Sensors*, vol. 2012, 2012.
- [126] X. Han, L. D. Favro, and R. L. Thomas, "Sonic IR imaging of delaminations and disbonds in composites," *Journal of Physics D: Applied Physics*, vol. 44, pp. 034013-034017, 2011.
- [127] R. F. Anastasi, J. N. Zalameda, and E. I. Madaras, "Damage detection in rotorcraft composite structures using thermography and Laser-based ultrasound," in *SEM X International Congress and Exposition on Experimental and Applied Mechanics*, 2004.
- [128] J. Wilson, G. Y. Tian, I. Z. Abidin, S. X. Yang, and D. Almond, "Pulsed eddy current thermography: system development and evaluation," *Insight: Non-Destructive Testing and Condition Monitoring*, vol. 52, pp. 87-90, 2010.
- [129] IPRT. (2013, March 2013). *Radiographic Inspection*, Institute for Physical Research and Technology, Iowa State University. Available: <http://www.iprt.iastate.edu/nde/radiographic.html>
- [130] G. T. Herman, *Fundamentals of computerized tomography: image reconstruction from projections*: Springer, 2009.
- [131] J. P. Schloraka, A. Harding, G. Harding, U. Van Stevendaal, and M. Grass, "Coherent scatter X-ray computed tomography in medical applications," in *Nuclear Science Symposium Conference Record*, 2002, pp. 900-901.
- [132] W. Swiderski and V. Vavilov, "IR thermographic detection of defects in multi-layered composite materials used in military applications," in *Infrared and Millimeter Waves, 2007 and the 2007 15th International Conference on Terahertz Electronics. IRMMW-THz. Joint 32nd International Conference on*, 2007, pp. 553-556.
- [133] O. Ley and V. Godinez, "Feasibility of using line scanning thermography in NDE of wind turbine blades," in *Nondestructive Characterization for Composite Materials, Aerospace Engineering, Civil Infrastructure, and Homeland Security*, 2011, pp. 79831W-79831W.
- [134] L. G. I. Bennett, T. R. Chalovich, and W. J. Lewis, "Comparison of neutron radiography with other non-destructive techniques for the inspection of CF188 flight control surfaces," *Nuclear Science, IEEE Transactions on*, vol. 52, pp. 334-337, 2005.
- [135] L. Jung-Ryul and K. Hyeong-Cheol, "Feasibility of in situ blade deflection monitoring of a wind turbine using a laser displacement sensor within the tower," *Smart Materials and Structures*, vol. 22, pp. 027002-027009, 2013.
- [136] M. Ozbek and D. Rixen, "Optical measurements and operational modal analysis on a large wind turbine: Lessons learned," in *Rotating Machinery, Structural Health Monitoring, Shock and Vibration*. vol. 5, ed: Springer New York, 2011, pp. 257-276.
- [137] G. Anastasi, M. Conti, M. Di Francesco, and A. Passarella, "Energy conservation in wireless sensor networks: A survey," *Ad Hoc Networks*, vol. 7, pp. 537-568, 2009.
- [138] C. Grosse, G. McLaskey, S. Bachmaier, S. D. Glaser, and M. Krüger, "A hybrid wireless sensor network for acoustic emission testing in SHM," in *SPIE Sensors*

## References

---

- and Smart Structures Technology Civil, Mechanical Aerospace System*, 2008, pp. 693238-693246.
- [139] S. A. Bachmaier, "Event-based acoustic emission technique for structural health monitoring using wireless sensor networks," *NDT. net-The e-Journal of Nondestructive Testing*, 2008.
- [140] A. Ledeczki, T. Hay, P. Volgyesi, D. R. Hay, A. Nadas, and S. Jayaraman, "Wireless acoustic emission sensor network for structural monitoring," *IEEE Sensors Journal* vol. 9, pp. 1370-1377, 2009.
- [141] E. Fasolo, M. Rossi, J. Widmer, and M. Zorzi, "In-network aggregation techniques for wireless sensor networks: a survey," *Wireless Communications, IEEE*, vol. 14, pp. 70-87, 2007.
- [142] V. Raghunathan, C. Schurgers, S. Park, and M. B. Srivastava, "Energy-aware wireless microsensor networks," *Signal Processing Magazine, IEEE*, vol. 19, pp. 40-50, 2002.
- [143] G. Anastasi, M. Conti, M. Di Francesco, and A. Passarella, *How to prolong the lifetime of wireless sensor networks*, Mobile Ad Hoc and Pervasive Communications, Chapter 6, M. Denko and L. Yang, ed. Valencia, CA: American Scientific Publishers, 2006.
- [144] Z. C. Qin, Z. Zhou, and X. C. Zhao, "A distributed source coding algorithm for clustering wireless sensor networks," *Dianzi Yu Xinxu Xuebao/Journal of Electronics and Information Technology*, vol. 35, pp. 328-334, 2013.
- [145] B. Kanagal and A. Deshpande, "Online filtering, smoothing and probabilistic modeling of streaming data," in *Data Engineering, IEEE 24th International Conference on*, 2008, pp. 1160-1169.
- [146] E. Lauwers and G. Gielen, "Power estimation methods for analog circuits for architectural exploration of integrated systems," *Very Large Scale Integration (VLSI) Systems, IEEE Transactions on*, vol. 10, pp. 155-162, 2002.
- [147] B. Schott, M. Bajura, J. Czarnaski, J. Flidr, T. Tho, and L. Wang, "A modular power-aware microsensor with >1000X dynamic power range," in *Information Processing in Sensor Networks, IPSN 2005, Fourth International Symposium on*, 2005, pp. 469-474.
- [148] C. Alippi, G. Anastasi, C. Galperti, F. Mancini, and M. Roveri, "Adaptive sampling for energy conservation in wireless sensor networks for snow monitoring applications," in *Mobile Adhoc and Sensor Systems, MASS 2007, IEEE Internatonal Conference on*, 2007, pp. 1-6.
- [149] M. Y. Zhang, W. Y. Cai, and L. P. Zhou, "A Sensing data driven clustering algorithm for adaptive sampling in wireless sensor networks," *Applied Mechanics and Materials*, vol. 182, pp. 748-752, 2012.
- [150] T. Yu-Chee, W. You-Chiun, C. Kai-Yang, and H. Yao-Yu, "iMouse: An integrated mobile surveillance and wireless sensor system," *Computer*, vol. 40, pp. 60-66, 2007.
- [151] C. Alippi, R. Camplani, C. Galperti, and M. Roveri, "Effective design of WSNs: From the lab to the real world," in *Sensing Technology, ICST 2008, 3rd International Conference on*, 2008, pp. 1-9.
- [152] CS. (2013, April 2013). *Compressive Sensing Resources*. Available: <http://dsp.rice.edu/cs>
- [153] D. L. Donoho, "Compressed sensing," *Information Theory, IEEE Transactions on*, vol. 52, pp. 1289-1306, 2006.

## References

---

- [154] E. J. Candès and M. B. Wakin, "An introduction to compressive sampling," *Signal Processing Magazine, IEEE*, vol. 25, pp. 21-30, 2008.
- [155] Q. Wang and Z. Liu, "A robust and efficient algorithm for distributed compressed sensing," *Computers & Electrical Engineering*, vol. 37, pp. 916-926, 2011.
- [156] H. Mamaghanian, N. Khaled, D. Atienza, and P. Vandergheynst, "Compressed sensing for real-time energy-efficient ECG compression on wireless body sensor nodes," *Biomedical Engineering, IEEE Transactions on*, vol. 58, pp. 2456-2466, 2011.
- [157] J. Wang, S. Tang, B. Yin, and X.-Y. Li, "Data gathering in wireless sensor networks through intelligent compressive sensing," in *INFOCOM, 2012 Proceedings IEEE*, 2012, pp. 603-611.
- [158] M. Shoaib, N. K. Jha, and N. Verma, "A compressed-domain processor for seizure detection to simultaneously reduce computation and communication energy," in *Custom Integrated Circuits Conference*, 2012, pp. 1-4.
- [159] Y. S. Hsu, S. Prum, J. H. Kagel, and H. C. Andrews, "Pattern recognition experiments in the Mandala/Cosine domain," *Pattern Analysis and Machine Intelligence, IEEE Transactions on*, vol. 5, pp. 512-520, 1983.
- [160] B. U. Töreyn, A. E. Çetin, A. Aksay, and M. B. Akhan, "Moving object detection in wavelet compressed video," *Signal Processing: Image Communication*, vol. 20, pp. 255-264, 2005.
- [161] P. Nagesh and B. Li, "A compressive sensing approach for expression-invariant face recognition," in *Computer Vision and Pattern Recognition, IEEE Conference on*, 2009, pp. 1518-1525.
- [162] B. Shen and I. K. Sethi, "Direct feature extraction from compressed images," in *Electronic Imaging: Science & Technology*, 1996, pp. 404-414.
- [163] K. Zhang, L. Zhang, and M.-H. Yang, "Real-time compressive tracking," in *Computer Vision—ECCV 2012*, ed: Springer, 2012, pp. 864-877.
- [164] A. C. Gurbuz, J. H. McClellan, and W. R. Scott Jr, "Compressive sensing of underground structures using GPR," *Digital Signal Processing*, vol. 22, pp. 66-73, 2012.
- [165] D. Thanh, N. Bulusu, and H. Wen, "Lightweight acoustic classification for cane-toad monitoring," in *Signals, Systems and Computers, 42nd Asilomar Conference on*, 2008, pp. 1601-1605.
- [166] G. J. Pottie and W. J. Kaiser, "Wireless integrated network sensors," *Communications of the ACM*, vol. 43, pp. 51-58, 2000.
- [167] Y. Bao, J. L. Beck, and H. Li, "Compressive sampling for accelerometer signals in structural health monitoring," *Structural Health Monitoring*, vol. 10, pp. 235-246, 2010.
- [168] J. Romberg, "Imaging via compressive sampling," *Signal Processing Magazine, IEEE*, vol. 25, pp. 14-20, 2008.
- [169] R. G. Baraniuk, "Compressive sensing [Lecture Notes]," *Signal Processing Magazine, IEEE*, vol. 24, pp. 118-121, 2007.
- [170] R. Chartrand, R. G. Baraniuk, Y. C. Eldar, M. A. T. Figueiredo, and J. Tanner, "Introduction to the issue on compressive sensing," *Selected Topics in Signal Processing, IEEE Journal of*, vol. 4, pp. 241-243, 2010.

## References

---

- [171] E. J. Candes, J. Romberg, and T. Tao, "Robust uncertainty principles: exact signal reconstruction from highly incomplete frequency information," *Information Theory, IEEE Transactions on*, vol. 52, pp. 489-509, 2006.
- [172] H. Mohimani, M. Babaie-Zadeh, and C. Jutten, "A fast approach for overcomplete sparse decomposition based on smoothed L0 norm," *Signal Processing, IEEE Transactions on*, vol. 57, pp. 289-301, 2009.
- [173] B. Bah, "Restricted isometry property (RIP)," 2009.
- [174] D. Mascarenas, D. Hush, J. Theiler, C. Farrar, I. To, and D. Mascareñas, "The application of compressed sensing to detecting damage in structures," in *8th International Workshop on Structural Health Monitoring*, Palo Alto, CA, 2011.
- [175] J. A. Tropp and S. J. Wright, "Computational methods for sparse solution of linear inverse problems," *Proceedings of the IEEE*, vol. 98, pp. 948-958, 2010.
- [176] J. Chen, J. Benesty, and Y. Huang, "Time delay estimation in room acoustic environments: an overview," *EURASIP Journal on Advances in Signal Processing*, vol. 2006, p. 026503, 2006.
- [177] A. Brutti, M. Omologo, and P. Svaizer, "Comparison between different sound source localization techniques based on a real data collection," in *Hands-Free Speech Communication and Microphone Arrays*, 2008, pp. 69-72.
- [178] H. Khaddour, "A comparison of algorithms of sound source localization based on time delay estimation," *Electrotechnic magazine: elektrovizija*, vol. 2, pp. 31-37, 2011.
- [179] H. Atmoko, D. C. Tan, G. Y. Tian, and F. Bruno, "Accurate sound source localization in a reverberant environment using multiple acoustic sensors," *Measurement Science and Technology*, vol. 19, p. 024003, 2008.
- [180] J. P. Ianniello, "Time delay estimation via cross-correlation in the presence of large estimation errors," *IEEE Transactions on Acoustics, Speech, and Signal Processing*, vol. 30, pp. 998-1003, 1982.
- [181] C. Knapp and G. C. Carter, "The generalized correlation method for estimation of time delay," *Acoustics, Speech and Signal Processing, IEEE Transactions on*, vol. 24, pp. 320-327, 1976.
- [182] H. Atmoko, D. C. Tan, G. Y. Tian, and F. Bruno, "Accurate sound source localization in a reverberant environment using multiple acoustic sensors," *Measurement Science and Technology*, vol. 19, pp. 024003-024012, 2008.
- [183] M. R. Belmont and S. P. V. Jardon, "Generalised cross-correlation functions for engineering applications. Application to experimental data," *Experiments in Fluids*, vol. 29, pp. 461-467, 2000.
- [184] M. R. Belmont and D. Savic, "Generalised cross-correlation functions for image processing applications," in *Image Processing And Its Applications, Seventh International Conference on*, 1999, pp. 230-234.
- [185] Z. Zhao and Z.-q. Hou, "The generalized phase spectrum method for time delay estimation," in *Acoustics, Speech, and Signal Processing, IEEE International Conference on*, 1984, pp. 459-462.
- [186] M. J. Brennan, Y. Gao, and P. F. Joseph, "On the relationship between time and frequency domain methods in time delay estimation for leak detection in water distribution pipes," *Journal of Sound and Vibration*, vol. 304, pp. 213-223, 2007.
- [187] K. R. Rao and M. A. Narasimhan, "Generalized phase spectrum," *Acoustics, Speech and Signal Processing, IEEE Transactions on*, vol. 25, pp. 84-90, 1977.

## References

---

- [188] A. Piersol, "Time delay estimation using phase data," *Acoustics, Speech and Signal Processing, IEEE Transactions on*, vol. 29, pp. 471-477, 1981.
- [189] M. A. Tahoun, K. A. Nagaty, T. I. El-Arief, and M. A-Megeed, "A robust content-based image retrieval system using multiple features representations," in *Networking, Sensing and Control, IEEE Proceedings*, 2005, pp. 116-122.
- [190] B. Yegnanarayana, S. Prasanna, R. Duraiswami, and D. Zotkin, "Processing of reverberant speech for time-delay estimation," *Speech and Audio Processing, IEEE Transactions on*, vol. 13, pp. 1110-1118, 2005.
- [191] J. C. Chen, L. Yip, J. Elson, W. Hanbiao, D. Maniezzo, R. E. Hudson, K. Yao, and D. Estrin, "Coherent acoustic array processing and localization on wireless sensor networks," *Proceedings of the IEEE*, vol. 91, pp. 1154-1162, 2003.
- [192] M. F. Duarte and Y. Hen Hu, "Vehicle classification in distributed sensor networks," *Journal of Parallel and Distributed Computing*, vol. 64, pp. 826-838, 2004.
- [193] J. Sallai, W. Hedgecock, P. Volgyesi, A. Nadas, G. Balogh, and A. Ledeczki, "Weapon classification and shooter localization using distributed multichannel acoustic sensors," *Journal of Systems Architecture*, vol. 57, pp. 869-885, 2011.
- [194] A. Jangra, Swati, Richa, and Priyanka, "Wireless sensor network (WSN): architectural design issues and challenges," *International Journal on Computer Science and Engineering*, vol. 2, pp. 3089-3094, 2010.
- [195] A. Egana, F. Seco, and R. Ceres, "Processing of Ultrasonic Echo Envelopes for Object Location With Nearby Receivers," *Instrumentation and Measurement, IEEE Transactions on*, vol. 57, pp. 2751-2755, 2008.
- [196] B. Lazarov, R. Matzen, and Y. Elesin, "Topology optimization of pulse shaping filters using the Hilbert transform envelope extraction," *Structural and Multidisciplinary Optimization*, vol. 44, pp. 409-419, 2011.
- [197] J. Lin and A. Zhang, "Fault feature separation using wavelet-ICA filter," *NDT & E International*, vol. 38, pp. 421-427, 2005.
- [198] O. Rioul and P. Duhamel, "Fast algorithms for discrete and continuous wavelet transforms," *Information Theory, IEEE Transactions on*, vol. 38, pp. 569-586, 1992.
- [199] K. C. Ho and Y. T. Chan, "Optimum discrete wavelet scaling and its application to delay and Doppler estimation," *Signal Processing, IEEE Transactions on*, vol. 46, pp. 2285-2290, 1998.
- [200] MATLAB. (March 2013). *The Language of Technical Computing, The Math Works Inc*. Available: <http://www.mathworks.com/products/matlab>
- [201] B. N. Singh and A. K. Tiwari, "Optimal selection of wavelet basis function applied to ECG signal denoising," *Digital Signal Processing*, vol. 16, pp. 275-287, 2006.
- [202] T. Zoughi, R. Boostani, and M. Deypir, "A wavelet-based estimating depth of anesthesia," *Engineering Applications of Artificial Intelligence*, vol. 25, pp. 1710-1722, 2012.
- [203] A. Aballe, M. Bethencourt, F. J. Botana, M. Marcos, and R. Osuna, "En transient analysis through wavelets," in *New Trends in Electrochemical Impedance Spectroscopy (EIS) and Electrochemical Noise Analysis (ENA): The International Symposium*, 2001.
- [204] A. C. Walbran, C. P. Unsworth, A. J. Gunn, and L. Bennet, "Spike detection in the preterm fetal sheep EEG using Haar wavelet analysis," in *Engineering in*

## References

---

- Medicine and Biology Society, Annual International Conference of the IEEE*, 2011, pp. 7063-7066.
- [205] J. Lin and L. Qu, "Feature extraction based on Morlet wavelet and its application for mechanical fault diagnosis," *Journal of Sound and Vibration*, vol. 234, pp. 135-148, 2000.
- [206] N. S. M. Tamim and F. Ghani, "Techniques for optimization in time delay estimation from cross correlation function," *Int J Eng Technol*, vol. 10, pp. 69-75, 2010.
- [207] C. E. Shannon, "A mathematical theory of communication," *ACM SIGMOBILE Mobile Computing and Communications Review*, vol. 5, pp. 3-55, 2001.
- [208] J.-C. Hong and Y. Y. Kim, "The optimal selection of mother wavelet shape for the best time-frequency localization of the continuous wavelet transform," in *Smart Structures and Materials: Modeling, Signal Processing, and Control, Proceedings of the SPIE*, 2003, pp. 651-660.
- [209] D. Wang, L. Ye, Z. Su, Y. Lu, F. Li, and G. Meng, "Probabilistic damage identification based on correlation analysis using guided wave signals in aluminum plates," *Structural Health Monitoring*, vol. 9, pp. 133-144, 2010.
- [210] O. Renaud, J. L. Starck, and F. Murtagh, "Wavelet-based combined signal filtering and prediction," *Systems, Man, and Cybernetics, Part B: Cybernetics, IEEE Transactions on*, vol. 35, pp. 1241-1251, 2005.
- [211] O. Gnawali, R. Fonseca, K. Jamieson, D. Moss, and P. Levis, "Collection tree protocol," in *Proceedings of the 7th ACM Conference on Embedded Networked Sensor Systems (SenSys)*, pp. 1-14, 2009.
- [212] R. J. Tait, G. Schaefer, and A. A. Hopgood, "Intensity-based image registration using multiple distributed agents," *Knowledge-Based Systems*, vol. 21, pp. 256-264, 2008.
- [213] O. Büyüköztürk and T.-Y. Yu, "Far-field radar NDT technique for detecting GFRP debonding from concrete," *Construction and Building Materials*, vol. 23, pp. 1678-1689, 2009.
- [214] P. Levis and D. Gay, *TinyOS programming*. Cambridge University Press, 2009.
- [215] K. Apicharttrisorn, S. Choochaisri, and C. Intanagonwiwat, "Energy-efficient gradient time synchronization for wireless sensor networks," *Computational Intelligence, Communication Systems and Networks (CICSyN), Second International Conference on*, pp. 124-129, 2010.
- [216] M. Bocca, L. M. Eriksson, A. Mahmood, R. Jäntti, and J. Kullaa, "A synchronized wireless sensor network for experimental modal analysis in structural health monitoring," *Computer-Aided Civil and Infrastructure Engineering*, vol. 26, pp. 483-499, 2011.
- [217] I. K. Rhee, J. Lee, J. Kim, E. Serpedin, and Y. C. Wu, "Clock synchronization in wireless sensor networks: An overview," *Sensors*, vol. 9, pp. 56-85, 2009.
- [218] M. Maroti, B. Kusy, G. Simon, and A. Ledeczi, "Robust multi-hop time synchronization in sensor networks," in *Proceedings of the International Conference on Wireless Networks*, 2004, pp. 454-460.
- [219] M. Maróti, B. Kusy, G. Simon, and Á. Ledeczi, "The flooding time synchronization protocol," in *Proceedings of the 2nd international conference on Embedded networked sensor systems*, 2004, pp. 39-49.
- [220] S. Yoon, "Power management in wireless sensor networks," *PhD Thesis, Computer Engineering, Nort Carolina State University*, 2007.

## References

---

- [221] T. Nagayama, S. H. Sim, Y. Miyamori, and B. F. Spencer Jr, "Issues in structural health monitoring employing smart sensors," *Smart Structures and Systems*, vol. 3, pp. 299-329, 2007.
- [222] M. Galetto and B. Pralio, "Optimal sensor positioning for large scale metrology applications," *Precision Engineering*, vol. 34, pp. 563-577.
- [223] L. Yi, W. Dong, P. Shirui, G. Xiaohu, G. J. Nga, and L. Sheng, "Study on electromagnetic wave propagation characteristics in rotating environments and its application in tire pressure monitoring," *Instrumentation and Measurement, IEEE Transactions on*, vol. 61, pp. 1765-1777, 2012.
- [224] V. Lopresto, C. Leone, G. Caprino, and I. De Iorio, "Analysis of acoustic emission signals produced by different carbon fibre reinforced plastic laminates," in *ICCM International Conferences on Composite Materials*, 2009.
- [225] R. K. Elsley and L. J. Graham, "Identification of acoustic emission sources by pattern recognition techniques," in *Review of Progress in Quantitative Nondestructive Evaluation*. vol. 2A, D. Thompson and D. Chimenti, Eds., ed: Springer US, 1983, pp. 471-487.
- [226] S. Rippengill, K. Worden, K. M. Holford, and R. Pullin, "Automatic classification of acoustic emission patterns," *Strain*, vol. 39, pp. 31-41, 2003.
- [227] T. H. Loutas, G. Sotiriades, I. Kalaitzoglou, and V. Kostopoulos, "Condition monitoring of a single-stage gearbox with artificially induced gear cracks utilizing on-line vibration and acoustic emission measurements," *Applied Acoustics*, vol. 70, pp. 1148-1159, 2009.
- [228] S. M. Metwalley, N. Hammad, and S. A. Abouel-Seoud, "Vehicle gearbox fault diagnosis using noise measurements," *International Journal of Energy and Environment*, vol. 2, pp. 357-366, 2011.
- [229] S. R. Basri, N. M. Bunnori, S. A. Kudus, S. Shahidan, M. N. M. Jamil, and N. M. Noor, "Applications of acoustic emission technique associated with the fracture process zone in concrete beam - a review," *Advanced Materials Research*, vol. 626, pp. 147-151, 2013.
- [230] C. U. Grosse, S. D. Glaser, and M. Krüger, "Initial development of wireless acoustic emission sensor Motes for civil infrastructure state monitoring," *Smart Structures and Systems*, vol. 6, pp. 197-209, 2010.
- [231] T. H. Loutas, D. Roulias, E. Pauly, and V. Kostopoulos, "The combined use of vibration, acoustic emission and oil debris on-line monitoring towards a more effective condition monitoring of rotating machinery," *Mechanical Systems and Signal Processing*, vol. 25, pp. 1339-1352, 2011.
- [232] A. Swedan, A. H. El-Hag, and K. Assaleh, "Acoustic detection of partial discharge using signal processing and pattern recognition techniques," *Insight - Non-Destructive Testing and Condition Monitoring*, vol. 54, pp. 667-672, 2012.
- [233] G. Tzanetakis and P. Cook, "Musical genre classification of audio signals," *Speech and Audio Processing, IEEE Transactions on*, vol. 10, pp. 293-302, 2002.
- [234] M. Wevers and K. Lambrighs, "Applications of acoustic emission for SHM: A review," in *Encyclopedia of Structural Health Monitoring*, ed: John Wiley & Sons, Ltd, 2009.
- [235] K. Worden and G. Manson, "The application of machine learning to structural health monitoring," *Philosophical Transactions of the Royal Society A: Mathematical, Physical and Engineering Sciences*, vol. 365, pp. 515-537, 2007.

## References

---

- [236] M. Alamin, T. Gui Yun, A. Andrews, and P. Jackson, "Principal component analysis of pulsed eddy current response from corrosion in mild steel," *Sensors Journal, IEEE*, vol. 12, pp. 2548-2553, 2012.
- [237] A. Sophian, G. Y. Tian, D. Taylor, and J. Rudlin, "A feature extraction technique based on principal component analysis for pulsed Eddy current NDT," *NDT & E International*, vol. 36, pp. 37-41, 2003.
- [238] M. J. Eaton, R. Pullin, J. J. Hensman, K. M. Holford, K. Worden, and S. L. Evans, "Principal component analysis of acoustic emission signals from landing gear components: an aid to fatigue fracture detection," *Strain*, vol. 47, pp. 588-594, 2011.
- [239] Z. Haitao, Y. Pong Chi, and J. T. Kwok, "A novel incremental principal component analysis and its application for face recognition," *Systems, Man, and Cybernetics, Part B: Cybernetics, IEEE Transactions on*, vol. 36, pp. 873-886, 2006.
- [240] D. Widjaja, C. Varon, A. C. Dorado, J. A. K. Suykens, and S. Van Huffel, "Application of kernel principal component analysis for single-Lead-ECG-derived respiration," *Biomedical Engineering, IEEE Transactions on*, vol. 59, pp. 1169-1176, 2012.
- [241] P. Langley, E. J. Bowers, and A. Murray, "Principal component analysis as a tool for analyzing Beat-to-Beat changes in ECG features: application to ECG-derived respiration," *Biomedical Engineering, IEEE Transactions on*, vol. 57, pp. 821-829, 2010.
- [242] J. Shlens, "A tutorial on principal component analysis," *Systems Neurobiology Laboratory, University of California at San Diego*, 2005.
- [243] A. A. Miranda, Y. A. Le Borgne, and G. Bontempi, "New routes from minimal approximation error to principal components," *Neural Processing Letters*, vol. 27, pp. 197-207, 2008.
- [244] F. Murtagh, "Wedding the wavelet transform and multivariate data analysis," *Journal of classification*, vol. 15, pp. 161-183, 1998.
- [245] L. Liu and J. Jiang, "Using stationary wavelet transformation for signal denoising," in *Fuzzy Systems and Knowledge, Eighth International Conference on*, 2011, pp. 2203-2207.
- [246] G. P. Nason and B. W. Silverman, "The stationary wavelet transform and some statistical applications," in *Wavelets and statistics*. vol. 103, ed: Springer, 1995, pp. 281-299.
- [247] M. Shensa, "The discrete wavelet transform: wedding the a trous and Mallat algorithms," *Signal Processing, IEEE Transactions on*, vol. 40, pp. 2464-2482, 1992.
- [248] P. Kabiri and A. Makinejad, "Using PCA in acoustic emission condition monitoring to detect faults in an automobile engine," in *29th European Conference on Acoustic Emission Testing*, 2011.
- [249] G. Y. Tian, A. Sophian, D. Taylor, and J. Rudlin, "Wavelet-based PCA defect classification and quantification for pulsed eddy current NDT," in *Science, Measurement and Technology, IEE Proceedings-*, 2005, pp. 141-148.
- [250] P. C. Yuela, D. Q. Dai, and G. C. Feng, "Wavelet-based PCA for human face recognition," in *Image Analysis and Interpretation, 1998 IEEE Southwest Symposium on*, 1998, pp. 223-228.



## References

---

- [251] G. C. Feng, P. C. Yuen, and D. Q. Dai, "Human face recognition using PCA on wavelet subband," *Journal of Electronic Imaging*, vol. 9, pp. 226-233, 2000.
- [252] Y. Wu and W. Liu, "A railway running status monitoring system based on energy harvesting wireless sensor network," *International Journal of Digital Content Technology and its Applications*, vol. 6, pp. 560-569, 2012.
- [253] A. M. A. Sabaawi, C. C. Tsimenidis, and B. S. Sharif, "Analysis and Modeling of Infrared Solar Rectennas," *IEEE Journal of Selected Topics in Quantum Electronics*, vol. 19, pp. 9000208-9000208, 2013.
- [254] K. M. Farinholt, N. Miller, W. Sifuentes, J. MacDonald, G. Park, and C. R. Farrar, "Energy Harvesting and Wireless Energy Transmission for Embedded SHM Sensor Nodes," *Structural Health Monitoring*, vol. 9, pp. 269-280, 2010.
- [255] M. F. Silva and J. A. T. Machado, "A survey of technologies and applications for climbing robots locomotion and adhesion," *Climbing and Walking Robots, Miripour, B.(Ed)*, pp. 1-22, 2010.

## Appendix A: MICAz Specifications



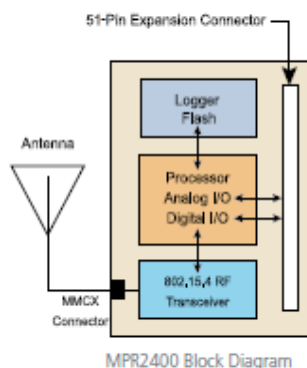
### MICAz

WIRELESS MEASUREMENT SYSTEM

- 2.4 GHz IEEE 802.15.4, Tiny Wireless Measurement System
- Designed Specifically for Deeply Embedded Sensor Networks
- 250 kbps, High Data Rate Radio
- Wireless Communications with Every Node as Router Capability
- Expansion Connector for Light, Temperature, RH, Barometric Pressure, Acceleration/Seismic, Acoustic, Magnetic and other Crossbow Sensor Boards

### Applications

- Indoor Building Monitoring and Security
- Acoustic, Video, Vibration and Other High Speed Sensor Data
- Large Scale Sensor Networks (1000+ Points)



### MICAz

The MICAz is a 2.4 GHz Mote module used for enabling low-power, wireless sensor networks.

#### Product features include:

- IEEE 802.15.4 compliant RF transceiver
- 2.4 to 2.48 GHz, a globally compatible ISM band
- Direct sequence spread spectrum radio which is resistant to RF interference and provides inherent data security
- 250 kbps data rate
- Supported by MoteWorks™ wireless sensor network platform for reliable, ad-hoc mesh networking
- Plug and play with Crossbow's sensor boards, data acquisition boards, gateways, and software

MoteWorks™ enables the development of custom sensor applications and is specifically optimized for low-power, battery-operated networks. MoteWorks is based on the open-source TinyOS operating system and provides reliable, ad-hoc mesh networking, over-the-air-programming capabilities, cross development tools, server middleware for enterprise network integration and client user interface for analysis and a configuration.

### Processor & Radio Platform (MPR2400CA)

The MPR2400 is based on the Atmel ATmega128L. The ATmega128L is a low-power microcontroller which runs MoteWorks from its internal flash memory. A single processor board (MPR2400) can be configured to run your sensor application/processing and the network/radio communications stack simultaneously. The 51-pin expansion connector supports Analog Inputs, Digital I/O, I2C, SPI and UART interfaces. These interfaces make it easy to connect to a wide variety of external peripherals. The MICAz (MPR2400) IEEE 802.15.4 radio offers both high speed (250 kbps) and hardware security (AES-128).

### Sensor Boards

Crossbow offers a variety of sensor and data acquisition boards for the MICAz Mote. All of these boards connect to the MICAz via the standard 51-pin expansion connector. Custom sensor and data acquisition boards are also available. Please contact Crossbow for additional information.

Document Part Number: 6020-0060-04 Rev A

Processor/Radio Board	MPR2400CA	Remarks
<b>Processor Performance</b>		
Program Flash Memory	128K bytes	
Measurement (Serial) Flash	512K bytes	> 100,000 Measurements
Configuration EEPROM	4K bytes	
Serial Communications	UART	0-3V transmission levels
Analog to Digital Converter	10 bit ADC	8 channel, 0-3V input
Other Interfaces	Digital I/O, I2C, SPI	
Current Draw	8 mA	Active mode
	< 15 $\mu$ A	Sleep mode
<b>RF Transceiver</b>		
Frequency band <sup>1</sup>	2400 MHz to 2483.5 MHz	ISM band, programmable in 1 MHz steps
Transmit (TX) data rate	250 kbps	
RF power	-24 dBm to 0 dBm	
Receive Sensitivity	-90 dBm (min), -94 dBm (typ)	
Adjacent channel rejection	47 dB	+ 5 MHz channel spacing
	38 dB	- 5 MHz channel spacing
Outdoor Range	75 m to 100 m	1/2 wave dipole antenna, LOS
Indoor Range	20 m to 30 m	1/2 wave dipole antenna
Current Draw	19.7 mA	Receive mode
	11 mA	TX, -10 dBm
	14 mA	TX, -5 dBm
	17.4 mA	TX, 0 dBm
	20 $\mu$ A	Idle mode, voltage regulator on
	1 $\mu$ A	Sleep mode, voltage regulator off
<b>Electromechanical</b>		
Battery	2X AA batteries	Attached pack
External Power	2.7 V - 3.3 V	Molex connector provided
User Interface	3 LEDs	Red, green and yellow
Size (in)	2.25 x 1.25 x 0.25	Excluding battery pack
(mm)	58 x 32 x 7	Excluding battery pack
Weight (oz)	0.7	Excluding batteries
(grams)	18	Excluding batteries
Expansion Connector	51-pin	All major I/O signals

## Notes

<sup>1</sup>5 MHz steps for compliance with IEEE 802.15.4D18-2003.

Specifications subject to change without notice



MIB520CB Mote Interface Board

## Base Stations

A base station allows the aggregation of sensor network data onto a PC or other computer platform. Any MICAz Mote can function as a base station when it is connected to a standard PC interface or gateway board. The MIB510 or MIB520 provides a serial/USB interface for both programming and data communications. Crossbow also offers a stand-alone gateway solution, the MIB600 for TCP/IP-based Ethernet networks.

### Ordering Information

Model	Description
MPR2400CA	2.4 GHz MICAz Processor/Radio Board
WSN-START2400CA	2.4 GHz MICAz Starter Kit
WSN-PRO2400CA	2.4 GHz MICAz Professional Kit

Document Part Number: 6020-0060-04 Rev A

## Appendix B: Wind Turbine Specifications

<b>Rated Output:</b>	300W
<b>Max Output:</b>	400W
<b>Generator:</b>	Permanent magnet generator
<b>Rated output voltage:</b>	24V
<b>Start-up wind speed:</b>	2.5m/s
<b>Rated wind speed:</b>	12m/s
<b>Security wind speed:</b>	35m/s
<b>Number of blade:</b>	3
<b>Material of blade:</b>	Carbon fibre
<b>Blade Diameter:</b>	1.5m
<b>Speed protection:</b>	Automatic leaned
<b>Rated Rotating Speed:</b>	400r/min
<b>Wind Energy Transforming Rate:</b>	0.40Cp
<b>Pole Diameter:</b>	76*2.5 steel tube
<b>Tower height:</b>	6m
<b>Work temperature:</b>	-40C° to 60C°
<b>Allocated battery:</b>	12V150AH, 2 pcs
<b>Controller:</b>	Inverter, controller, charger

Available from: **HZPRODUCT.COM, Global Wholesale Center™**

<http://www.hzproduct.com/pro/881/88281/wind-generator-300w-216318.html>